NON-LINEAR BEHAVIOUR OF REINFORCED CONCRETE FRAMES

BY

KOON WAN WONG
B.E.(Melb.), M.Eng.Sc.(Melb.), M.I.E.Aust.

A THESIS SUBMITTED FOR THE DEGREE OF
DOCTOR OF PHILOSOPHY

Department of Civil Engineering
University of Adelaide
Australia

August 1989

CORRIGENDA

Ph D Thesis
K W Wong, Feb 22, 1990

Page 2	"under static loading" to read "under proportional static loading" in line 7.
Page 3	"has been in" to read "has been observed in" in 5th last line.
Page 15	"mid-section" to read "centroid" in line 6.
Page 18	"sophisticated" to read "complex" in line 1. "obtained" to read "obtain" in lines 11,15,17.
Page 32	"iterate" to read "iteration" in line 13.
Page 34	Delete the entire sentence beginning with "The program was modified .." and replace it with "The program used does not include the material unloading path described earlier in Section 2.4." in line 2. "for beam AA3" to read "for the unbound region of beam AA3" in line 16.
Page 40	"safeguard" to read "safeguards" in line 14.
Page 41	"underestimate" to read "underestimates" in line 4. "for section" to read "for a section" in line 8. "balance" to read "balanced" in second last line.
Page 42	"squashed" to read "squash" in 7th last line.
Page 49	"are" to read "were" in lines 11,19.
Page 50	"into" to be deleted in line 8.
Page 51	"geometrical" to read "the geometrical" in line 3. "nonlinearities" to read "nonlinearity" in line 19.
Page 52	"pointed out" to read "indicated" in line 7. "used" to read "use" in line 13.
Page 53	"make" to read "makes" in line 19.
Page 54	"requiring" to read "requires" in line 7.
Page 55	"Carry out" to read "Execution of" in line 10.
Page 60	"change change" to read "change" in line 11.
Page 66	"deformed" to read "deforms" in line 9.
Page 67	"crosss" to read "cross" in the second line of the first box in Figure 3.5.
Page 68	"reinforce" to read "reinforced" in line 12.
Page 70	"plasticfication" to read "plastification" in line 3.
Page 76	"He" to read "They" in line 2. "arbitrary" to read "arbitrarily" in line 3. "earlier" to read "had earlier" in line 7.
Page 79	"refers" to read "refer" in line 2.
Page 81	"deformation" to read "the deformation" in line 13.
Page 83	"increases or decreases" to read "increase or decrease" in line 3.

Page 87 "partially" to read "a partially" in line 18.
Page 92 "He" to read "They" in line 18.
"govern" to read "governs" in the last line.
Page 93 "described" to read "describes" in line 6.
"reinforced" to read "a reinforced" in line 21.
Page 94 "solution" to read "a solution" in line 5.
"support" to read "interior support" in 6th last line.
"amount" to read "amounts" in the last line.
Page 95 "the strength of concrete" to read "different concrete strengths" in line 1.
"exist" to read "exists" in line 10.
Page 96 "load" to read "a load" in line 7.
Page 97 "limits" to read "limited" in 7th last line.
"required" to read "requiring" in 4th last line.
"concerns" to read "concerned" in 2nd last line.
"ignore" to read "ignoring" in last line.
Page 98 "literatures" to read "literature" in line 4.
"in this chapter" to read "by the author and reported in this chapter" in line 4.
"reinforced" to read " a reinforced" in line 6.
Page 99 "individual" to read "by individual" in line 7.
Page 102 After the sentence ending with "curvature" insert the following sentences: "The "key" segment is chosen by trial and error. It is likely to be one of the more highly stressed segments." in line 9.
Page 103 "gives" to read "give the" in line 13.
Page 105 "This out-of-balance forces is" to read "These out-of-balance forces are" in line 14.
Page 107 In the seventh box down from the top "$K_{unit}(1)$" to read "$K_{unit}(key)$" in Figure 4.1.
Page 112 "was" to read "were" in line 4.
Page 114 "will" in line 12 to be deleted.
Page 117 "stiffness" to read "stiffness matrix" in lines 10,11.
Page 121 "literatures" to read "literature" in line 9.
Page 122 "give" to read "gives" in line 2.
Page 130 "moment" to read "moments" in line 20.
Page 131 "curvatures" to read "curvature" in line 15.
"numerical technique" to read "a numerical technique" in line 17.
Page 136 "perfectly" to read " a perfectly" in lines 7,8.
"also difficult" to read "it is also difficult" in line 8.
"Rad, Gunnin and Furlong" to read "Gunnin, Rad and Furlong" in line 13.
Page 138 "Rad, Gunnin and Furlong" to read "Gunnin, Rad and Furlong" in 3rd last line.
Page 140 "single" to read "a single" in 4th last line.

Page 143 "moment-curvature" to read "a moment-curvature" in line 6.
"nonlinerity" to read "non-linearity" in line 19.
Page 150 "relatively" to read "a" in line 3.
"were" to read "was" in line 12.
"are" to read "were" in last line.
Page 159 "the total" to read "of the total" in 2nd last line.
Page 162 "the total" to read "of the total" in line 7.
Page 168 "end" to read "ends" in line 7.
Page 177 "quantity" to read "quantities" in line 17.
Page 185 "step" to read "steps" in line 14.
Page 188 "are" to read "is" in line 7.
"Though," to read "Though" in line 15.
Page 194 "seems is" to read "appears" in 3rd last line.
Page 195 "convenience" to read "convenient" in line 1.
"the a frame" to read "the frame" in line 10.
"was" to read "is" in lines 22,24.
Page 196 "reaches" to read "reach" in 5th last line.
Page 199 "Comparable" to read "A comparable" in line 6.
Page 200 "M_{ab} = is the moment" to read "M_{ab} = the moment" after equation 7.2.
Page 205 "Rosenbluth" to read "Rosenblueth" in line 5.
"obtain" to read "obtain the" in the last line.
Page 209 "column" to read "columns" in line 7.
Page 212 "steels" to read "steel" in line 1.
"symmetrically" to read "a symmetrically" in line 15.
"correspond" to read "corresponds" in line 16.
"constructability" to read "constructibility" in line 20.
Page 213 "is given" to be deleted in line 18.
Page 214 "higher" to read "a higher" in line 4.
Page 217 "plastic collapse" to read "a plastic collapse" in line 12.
"sway mechanism" to read "a sway mechanism" in line 17.
Page 222 "reaching peak strengths" to read "reach their peak strengths".
Page 226 "continue" to read "continued" in line 2.
Page 229 "continue" to read "continued" in line 2.
Page 234 "obtained" to read "obtained from" in line 15.
Page 236 "load" to read "loads" in 8th last line.
Page 244 "depends" to read "depend" in line 1.
Page 245 "corresponds" to read "which corresponds" in line 7.
Page 246 "has" to read "have" in 3rd last line.
Page 259 "to the same" to read "to be the same" in line 3.
Page 267 "also got rid of" to read "it also eliminated" in line 1.
"rigorous" to read "rigorous analysis" in line 21.

Page 268 "Carry out" to read "Use of" in line 4.
Page 273 Delete last line.
Page 281 "transdormation" to read "transformation" in 2nd last line.
Page 284 "then the" to read "than the" in line 11.
Page 285 "closed" to read "close" in line 5.
Page 286 "check" to read "checked" in 9th last line.
Page 287 "can now be calculated" to read "can be calculated" in line 8.
"interval" to read "intervals" in line 11.
"of unity" to read "is unity" in line 13.
"take into account" to read "take account" in 4th last line.
Page 291 "axial length due" to read "axial length change due" after equation E1.
"differentiating" to read "differentiation of" after equation E7.
Page 293 "contragrediant" to read "contragradiant" after equation E20.
Page 294 "noadal" to read "nodal" before equation E29.
"contragrediant" to read "contragradiant" after equation E31.
Page 310 "specified" to read "specifies" in the last line.
Page 312 "distant" to read "distance" in line 3.
"number of segment" to read "number of segments" in line 9.
Page 313 "specify" to read "specifies" in 8th and 10th last lines.
Page 314 "specifies" to read "specify" in line 4.
"layer" to read "layers" in 4th last line.
Page 315 "is required to specified" to read "are required to specify" in line 13.
"assign" to read "assigned" in 3rd last line.
Page 316 "element" to read "elements" in 4th last line.
Page 319 "completely" to read "complete" in 2nd last line.
Page 329 "for individual" to read "for an individual" in line 8.
"for ultimate" to read "for the ultimate" in line 10.
"for design" to read "for the design" in line 11.
Page 331 "safeguard" to read "safeguards" in line 10.
Page 334 "carry" to read "carry out" in 4th last line.
Page 337 "Proceedinds" to read "Proceedings" in Ref. 10.
Page 344 "Frish-Fay" to read "Frisch-Fay" in Ref. 74.
Page 346 "Combined and" to read "Combined Bending and" in Ref. 95.
Page 349 "Prang" to read "Pfrang" in Ref. 122.

Page 352 "Chracteristic" to read "Characteristic" in Ref. 148.
Page 353 "Porblems" to read "Problems" in Ref. 154.

Contents

List of Figures

List of Tables

ABSTRACT

An efficient computational procedure to analyse reinforced concrete skeletal plane frames taking into consideration material and geometrical nonlinearities is presented, which allows structural behaviour to be followed through the working load and overload ranges and up to ultimate load and then into the post-collapse, softening range. A computer program SAFRAME based on this procedure has been developed which is suitable for carrying out top-tier design in accordance with the new Australian concrete code, AS3600. The accuracy of the program is demonstrated by comparing analytical results obtained for columns and frames with published laboratory test results.

The program has been used to carry out a numerical study of the collapse behaviour of a wide range of portal frames and several multi-storey frames.

The results of the numerical study suggest that the final mode of collapse of a realistic portal frame is likely to be initiated by the formation of one or several hinges, which may or may not proceed into the softening stage, with final instability due to geometric non-linearity. Simple plastic collapse, with a sufficient number of hinges forming to produce a collapse mechanism, was only found to occur in relatively stocky structures.

Snapback instability, a phenomenon of softening structures, was also observed in some of the portal frames analysed.

The program was also used to evaluate the accuracy of the present Australian Standard AS3600 code-based, simplified methods for the analysis and design of slender reinforced concrete frames. Portals and multi-storey frames were included in this study. For most frames, the simplified methods give conservative results, sometimes too conservative. However, these methods may over-estimate ultimate loads in frames which fail by instability with significant lateral displacement of loaded joints. In estimating design loads, the middle-

tier method has been found to be unconservative for this type of frame.

STATEMENT OF ORIGINALITY

This thesis contains no material which has been accepted for the award of any other degree or diploma in any university and, to my knowledge and belief, the thesis contains no material previously published or written by another person, except where due reference is made in the text. I consent to the thesis being made available for photocopying and loan if accepted for the award of the degree.

K W Wong

ACKNOWLEDGEMENTS

The work described in the thesis was carried out at the University of Adelaide under the supervision of Prof. Robert F. Warner and Dr. Micheal F. Yeo. The author is deeply indebted to Prof. Warner for his excellent guidance and supervision throughout, and for his review of the thesis. The work is made possible by his interest and dedication. Dr. Yeo's contribution to the supervision of this project is gratefully acknowledged.

The author is grateful for the discussion with Dr. George Sved, Honorary Visiting Research Fellow in Civil Engineering.

The author is thankful for the valuable friendship provided by fellow postgraduates over the period of his candidature. Fellow postgraduate, Mr. Anthony Meyers proof-read part of this thesis.

The author is indebted to his parents, brothers and sisters for their love and encouragement. The author is also indebted to his wife, Lai-Yong for her continual support and encouragement.

Principal Notations

B = width of rectangular section

d = the effective depth of a cross section

H = depth of rectangular section

$EI(n)$ = the flexural stiffness of the nth segment

E_s = modulus elasticity of steel

E_c = modulus elasticity of concrete

f_{cm} = mean cylinder strength of concrete

f_{sy} = yield stress of reinforcing steel

f_s = stress in steel

f_{cmax} = peak stress of concrete in structure

F_{cu} = characteristic cylinder strength of concrete at 28 days

$ISTEP$ = typical curvature step

$[k]$ = element stiffness matrix

$[k_e]$ = first-order element stifness matrix

$[k_g]$ = second-order element stiffness matrix

$[K]$ = global or structure stiffness matrix

M^* = design bending moment

N_c = the buckling load used in column design

N_u = the ultimate strength in compression of an eccentrically loaded compression member

N_{uo} = the ultimate strength in compression of an axially loaded cross-section, without eccentricity

P = point load

$S(m)$ = the extentional stiffness of the mth element

SF = scaling factor

w = uniformly distributed load

ϕ = the strength reduction factor

ϵ_c = strain in concrete

ϵ_{cmax} = strain in concrete corresponds to f_{cmax}

γ_1, γ_2 = the column end restraint coefficients

δ_b = the moment magnifier for an unbraced column

δ_s = the system magnifier for a floor

Chapter 1

Introduction

1.1 Introduction

Collapse behaviour of reinforced concrete frames is complicated by the material and geometrical nonlinearities present in such frames. In extreme circumstances, non-linearity can even lead to the occurrence of snapback in the characteristic deflections. Snapback instability, a phenomenon described by Bažant et al(1987b), occurs when a characteristic deflection exhibits one or more local ultimate deflections, $dP/d\Delta = -\infty$, where P is a load term and Δ is the characteristic deflection. To follow such behaviour analytically, procedures have to be developed to traverse local peak load, and local peak deflections.

Much theoretical work has been carried out on the collapse behaviour of isolated reinforced concrete columns. These studies, together with limited experimental tests of structures such as simple frames and columns, enable simplified methods of design and analysis to be developed. These simplified methods,

though relatively simple to use, are based on a number of highly idealised concepts. While checks have been made on the accuracy of these methods for isolated columns, the inaccuracy when extended to more complex frames has not been adequately investigated.

1.2 Objectives and Scope

In this thesis, an investigation is made of the collapse behaviour of slender reinforced concrete frames under static loading. The investigation consists of the following:

1. development of an efficient and accurate computer program to obtain the collapse behaviour of frames with material and geometric nonlinearities.
2. development of other computer programs to assist in carrying out the prediction of strength of slender frames using the simplified methods of the Australian Standard AS3600.
3. study of the collapse behaviour of slender frames, including phenomena such as softening, snapback and instability.
4. investigations of the accuracy and adequacy of the simplified code methods of analysis and design of slender columns in frames.

The thesis is concerned primarily with the short-term collapse behaviour of slender reinforced concrete frames, with major emphasis on the predictions of the strengths of such frames.

The development of a computer program to carry out rigorous analysis, as described in item 1 of the above list, forms a major portion of the work.

Structures under investigation are assumed to be subjected only to flexural and axial forces. Deformations due to shear and torsion are not considered.

As the investigation is concerned only with short-term loading, time-dependent effects such as creep and shrinkage are outside the scope of the thesis.

1.3 Layout and Content of Thesis

A review of the methods of analysis of reinforced concrete sections is given in Chapter 2 and a review of the methods of analysis of reinforced concrete structures is given in Chapter 3.

Chapter 4 develops the underlying concept of segmental analysis and describes the computational techniques used to develop the computer program SAFRAME. The derivations for the element stiffness matrix and the fixed end moments are given in this chapter. The efficiency resulting from the use of a segmented element is illustrated.

In Chapter 5, the accuracy of results obtained from program SAFRAME is studied by comparing predictions with published test results and also with analytical results obtained by other researchers.

Non-linear behaviour of frames is studied in Chapter 6. The softening behaviour of concrete structures is described and discussed. The effects of sectional thrust and the amount of beam reinforcement are also studied in this chapter. Occasionally, snapback in characteristic deflections of frames has been observed in the analyses. Results obtained for some frames with snapback are presented and snapback behaviour in frames is described. The collapse behaviour of two 3-storey 2-bay frames is described. The order of hinge formation is traced for each of the frames.

In Chapter 7, the accuracy and adequacy of the moment magnifier method of AS3600 are investigated by analysing 144 unbraced portal frames, 36 braced portal frames and 2 multi-storey frames.

In Chapter 8, the accuracy and adequacy of the second-tier, second-order elastic method of AS3600 are investigated by re-analysing the 144 unbraced portal frames, 36 braced portal frames and 2 multi-storey frames.

Chapter 9 contains conclusions and recommendations for further work.

A user's manual for program SAFRAME is provided in Appendix H.

Chapter 2

Methods of Analysis of Reinforced Concrete Sections

2.1 Introduction

The analysis of member cross-sections to obtain moment-curvature-thrust (M-κ-N) relations forms part of most analytical techniques for the "rigorous" analysis of reinforced concrete skeletal frames.

In this chapter, computational methods to obtain M-κ-N relations for reinforced concrete sections are reviewed. The method chosen for the section analysis routine for subsequent use in Chapter 4 for the analysis of frames (program SAFRAME) is also described. Some factors affecting the M-κ-N relations are also investigated.

2.2 Moment-Curvature-Thrust Relations

2.2.1 Basic Formulation for a Beam Segment

Theoretical M-κ-N curves for reinforced concrete sections are determined on the basis of three major assumptions, the first being sections that are plane before bending remain plane after bending (also referred to as Bernoulli's principle). The second assumption is that the stress-strain curves of concrete and steel are known and the final assumption is that perfect bond exists between concrete and steel.

The curvature of a concrete segment of length dx and its relationship with the applied end moments and axial forces can be illustrated by using an initially straight segment subjected to equal end moments and axial forces. The deformed shape is shown in Figure 2.1. The assumptions that plane sections remain plane after bending and that compatibility of strain is maintained result in a linear strain distribution, as shown in Figure 2.1. For an uncracked segment with perfect bond between the concrete and the steel reinforcement, the assumption of linear strain distributions across the sections is reasonable. When cracking occurs in some sections, the behaviour of the segment is more complex. Across a primary crack, the bond between the concrete and steel is no longer perfect. This results in the strain distribution being non-linear directly at the crack. Thus, in a cracked segment, the curvature along the segment varies as a result of the fluctuation of the neutral axis caused by cracking. To simplify analysis, the average strain distribution over a segment of reasonably large gauge length is assumed to be linear. Hognestad(1951) found this to be a reasonable assumption from the strains measured over a gauge length of 150mm for laboratory tests carried out on eccentrically loaded 254mm square columns.

Hence, over a short gauge length the average curvature κ of a segment may be calculated using the expression given below:

$$\kappa = \frac{\epsilon_c}{kd} = \frac{\epsilon_s}{d(1-k)} = \frac{\epsilon_c + \epsilon_s}{d} \tag{2.1}$$

where all the basic terms are shown in Figure 2.1.

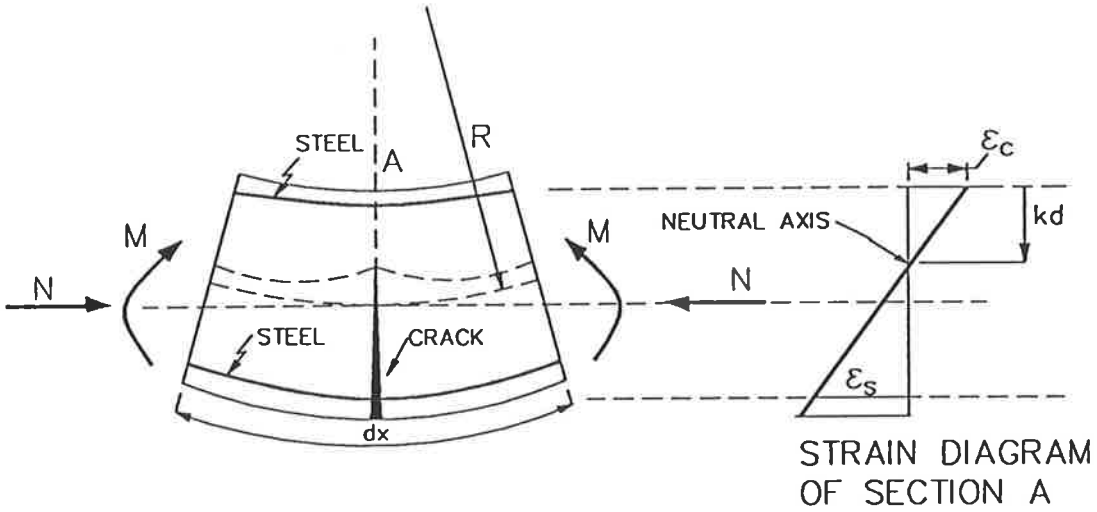

Figure 2.1: Response of concrete segment under equal end moments and axial forces

2.2.2 Methods for Determining Moment-Thrust-Curvature Relations

For a rectangular section as shown in Figure 2.2, subjected to axial force N and biaxial bending moments M_x and M_y, having a known strain distribution

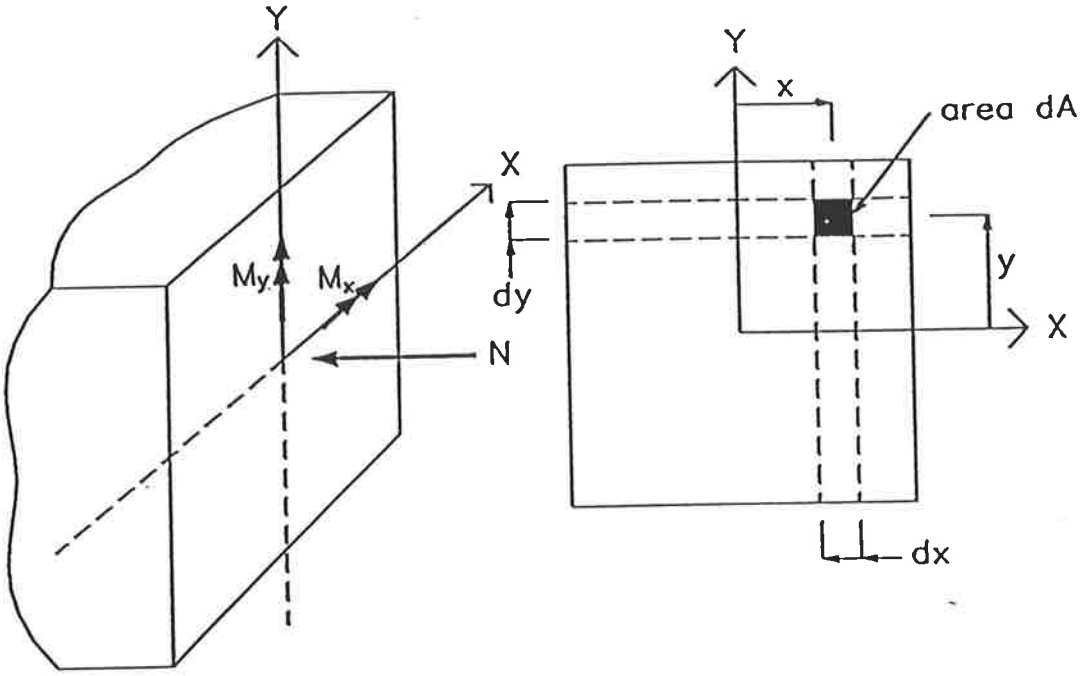

Figure 2.2: Rectangular section under forces

over the entire section, equilibrium equations relate the internal stresses to the external forces as follows:

$$N = \int_A \sigma dA \tag{2.2}$$

$$M_x = \int_A \sigma y dA \tag{2.3}$$

$$M_y = \int_A \sigma x dA \tag{2.4}$$

where

σ = average stress acting on elemental area dA.

Variables x and y are measured from the centre of the rectangular section where the axial force N acts.

Methods for determining moment-curvature relations are based on evaluating Equations 2.2 through 2.4 for known curvatures in a given section. The strain distribution is assumed to be linear about both principal axes, resulting in a skewed, planar strain distribution across the section. Moments and axial force are obtained for a given strain distribution either by integrating directly or by using numerical techniques to evaluate the equations approximately.

Methods of direct integration have been used by a number of researchers (Smith and Young, 1956; Broms and Viest, 1958; Breen, 1964; Sved, 1988);

Smith and Young(1956) derived analytical expressions to predict the moment capacity for a singly reinforced concrete section in bending about a principal axis (See Appendix A). The stress-strain relationship proposed is described by a single exponential curve which includes both the loading and unloading branch. The relationship is as follows:

$$f = f'_c \left(\frac{\epsilon}{\epsilon_o}\right) e^{1-\epsilon/\epsilon_o} \tag{2.5}$$

where

f'_c = compressive strength of a 150mm × 300mm concrete cylinder; and

ϵ_o = concrete strain corresponding to f'_c as determined from the cylinder test.

Breen(1964) used analytical expressions derived by Broms and Viest(1958) to obtain moment-thrust-curvature relations for a symmetrically reinforced rectangular section in uniaxial bending as illustrated in Figure 2.3. Hognestad's stress-strain relationship, shown in Figure 2.4, was used with the maximum flexural concrete stress f''_c assumed to be $0.85f'_c$ where f'_c is the compressive strength of a 150mm by 300mm cylinder.

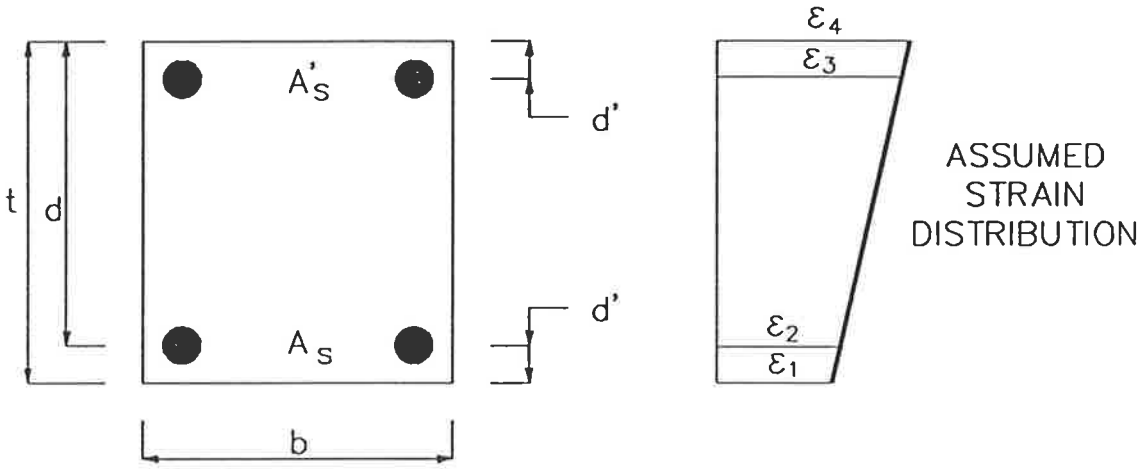

Figure 2.3: Symmetrically reinforced rectangular section

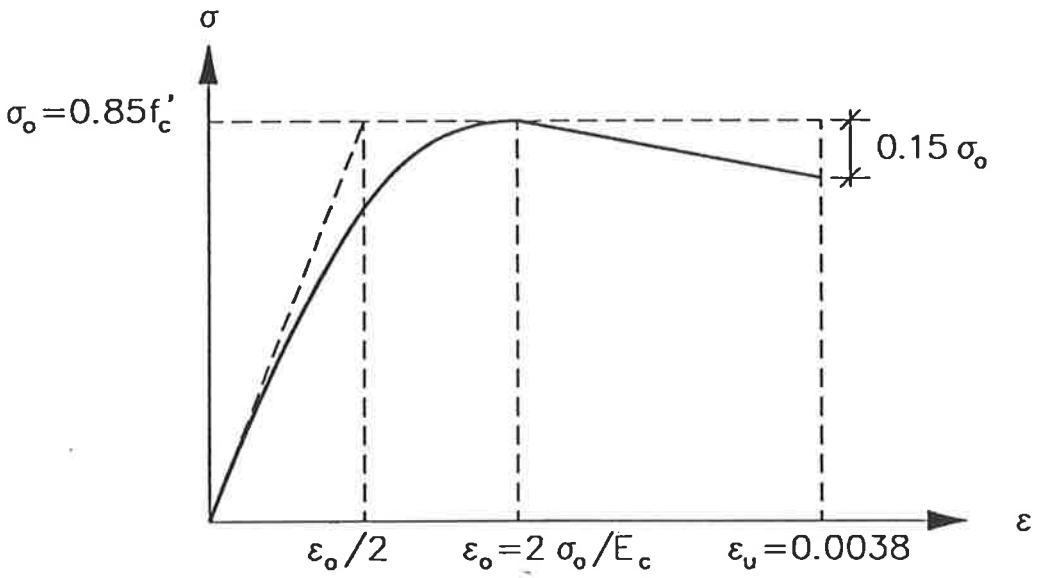

Figure 2.4: Stress-strain relationship of concrete proposed by Hognestad(1951)

The following expressions were obtained by Broms and Viest:

$$\frac{N}{f_c'' bt} = \frac{p_t\,(f_{s2} + f_{s3})}{2f_c''} + \frac{A}{\epsilon_4 - \epsilon_1} \tag{2.6}$$

$$\frac{M}{f_c'' bt^2} = \frac{p_t\,(f_{s3} - f_{s2})\,(t - 2d')}{4f_c''t} + \frac{B}{(\epsilon_4 - \epsilon_1)^2} - \frac{\epsilon_4 + \epsilon_1}{(\epsilon_4 - \epsilon_1)^2} \cdot \frac{A}{2} \tag{2.7}$$

where

N = axial load;

M = bending moment;

p_t $= A_{st}/bd$;

ϵ_1, ϵ_2, ϵ_3, ϵ_4 = strains as indicated in Figure 2.3;

f_{s2} $= E_s\epsilon_2$;

f_{s3} $= E_s\epsilon_3$;

d' = distance from the centroid of the compression reinforcement to the extreme compressive fibre;

t = depth of the section; and

f_c'' = compressive strength of the concrete in the member.

The values of A, B, f_{s2} and f_{s3} are functions of the strains ϵ_4 and ϵ_1. Owing to the discontinuities in the stress-strain relationship, different sets of equations have to be derived for four cases of strain distribution. These four cases are: (1) section in compression and maximum strain not exceeding ϵ_o, (2) section in compression and maximum strain exceeding ϵ_o, (3) part of the the section in tension and maximum compressive strain not exceeding ϵ_o and (4) part of the section in tension and maximum compressive strain exceeding ϵ_o. The values of A and B for each case have been derived by Broms and Viest.

The advantage of this approach is that it is computationally efficient, as the analytical expressions can be solved directly. One disadvantage of this method is that the idealised stress-strain relationship of the concrete has to be in a form that can be integrated easily. This limits the number of stress-strain relationships that can be used. Using a different stress-strain relationship for

concrete would require the formulation of a new set of equations. Another disadvantage of this method is that it does not take account of unloading caused by strain reversal in the concrete.

The approach proposed by Sved (1988) differs from the others in that cubic splines are used to represent the stress-strain relationship of the concrete. Sved suggested that the use of spline functions between data points allows ease of integration to obtain relations between moment, curvature and thrust. Furthermore, this approach is suitable for use in conjunction with experimental data for the stress-strain relation of concrete.

Warner(1969) pointed out that the derivation of analytical expressions ceases to be feasible in the general case of sections under biaxial bending. He proposed an alternative approach whereby the cross-section is subdivided into numerous small elements on a rectangular grid as shown in Figure 2.5. For known values of curvature ϕ, direction of the neutral axis θ and the depth of the neutral axis d_n, the strain ϵ_{ij} at the centre in the case of rectangular elements can be calculated for each ij-th element. From the strain ϵ_{ij} the stress σ_{ij} can then be calculated from any chosen stress-strain relation for the material in the element. This stress is assumed to be uniform for the element. Equilibrium Equations 2.2 through 2.4 then become:

$$N = \sum_{i=1}^{m}\sum_{j=1}^{n}\sigma_{ij}\Delta x_i \Delta y_j \tag{2.8}$$

$$M_x = \sum_{i=1}^{m}\sum_{j=1}^{n}\sigma_{ij}\bar{y}_j \Delta x_i \Delta y_j \tag{2.9}$$

$$M_y = \sum_{i=1}^{m}\sum_{j=1}^{n}\sigma_{ij}\bar{x}_i \Delta x_i \Delta y_j \tag{2.10}$$

where

σ_{ij} = stress at the centre of the ij-th element;

$\bar{y}_j$ = distance of the ij-th element from the x plastic centroidal axis;

$\bar{x}_i$ = distance of the ij-th element from the y plastic centroidal axis;

Δx_i = length of the element along the x-axis; and
Δy_j = length of the element along the y-axis.

As this method uses direct summations as an approximation to the exact integrals of Equations 2.2 through 2.4, a sufficient number of elements is required for accuracy. In analyses carried out on reinforced concrete sections, Warner found that a 10 by 10 division is usually fine enough to give acceptably small errors in the bending moments calculated. Warner also described the application of this procedure to sections with irregular shapes.

For a rectangular section of width b as shown in Figure 2.6, with bending about one axis under the influence of M_x and an axial force N, Equations 2.8 through 2.10 reduce to:

$$N = b\sum_{j=1}^{n}\sigma_j\Delta y_j \tag{2.11}$$

$$M_x = b\sum_{j=1}^{n}\sigma_j\bar{y}_j\Delta y_j \tag{2.12}$$

where

σ_j = stress at mid-level of the j-th layer;
Δy_j = thickness of the j-th layer; and
$\bar{y}_j$ = distance from the mid-point of the j-th layer to the centroidal axis.

The advantages of this method are that it is relatively easy to program and it allows the flexibility of changing the stress-strain relationship of the concrete. It also allows unloading and strain reversal to be taken into account. Another advantage of this method is that the section analysed can be of any shape. A disadvantage of the method is that an insufficient number of elements (for section under biaxial bending) or slices (for section bending about one axis)

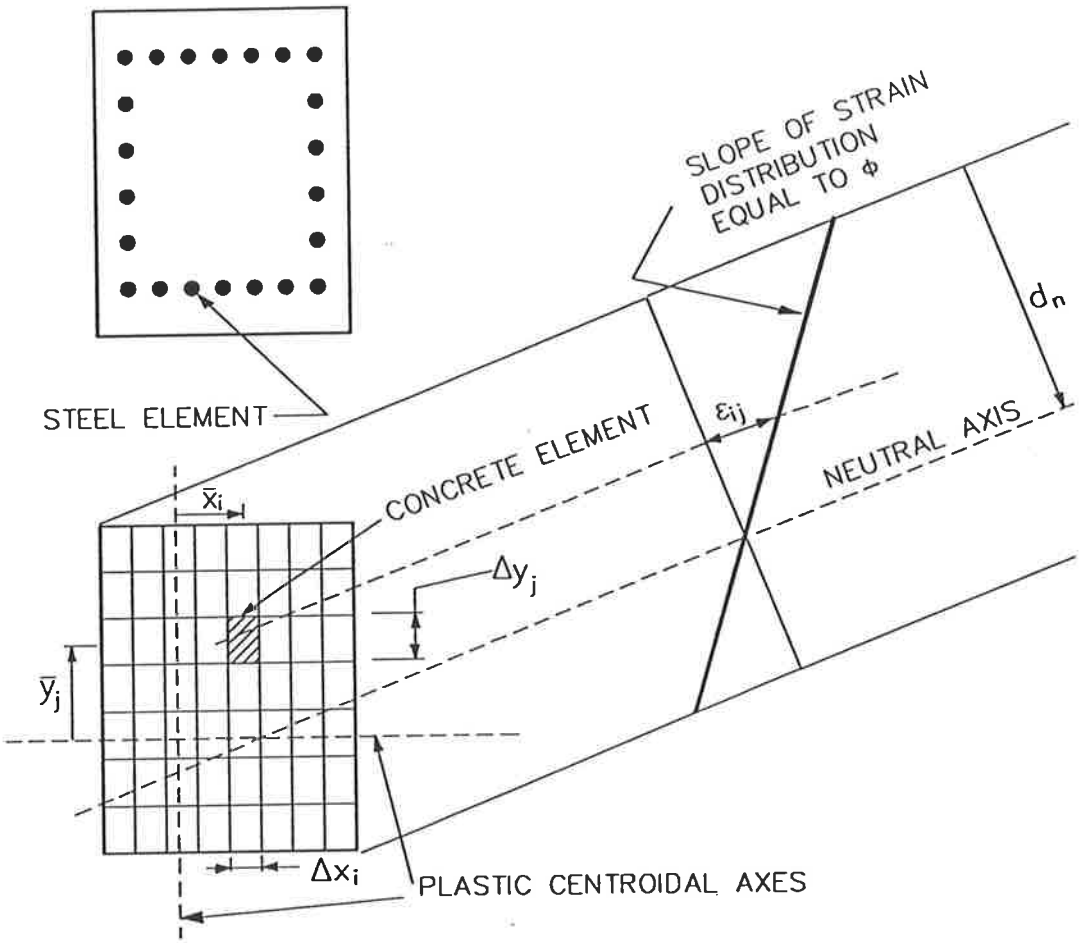

Figure 2.5: Partitioning of concrete section (Warner, 1969)

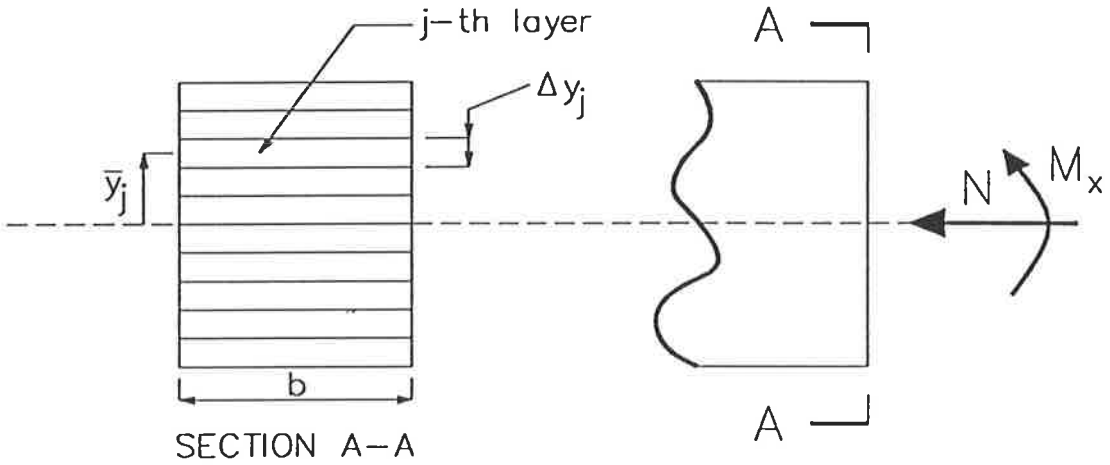

Figure 2.6: Section under bending about one axis and axial load

may give rise to inaccurate solutions, but this can be overcome by means of sensitivity analysis in which the number of elements or layers is varied to determine the number of elements or slices required.

Aas-Jakobsen and Grenacher(1974) used this method to obtain bending moment M and axial thrust N from known values of curvature κ and mid-section strain ϵ_m for a section in bending about one principal axis.

Virdi(1977) proposed a method based on numerical integration of Equations 2.2 through 2.4 using Gauss quadrature for reinforced and composite sections in biaxial bending. The Gaussian quadrature approach involves replacing a definite integral between the limits -1 and $+1$ by a weighted sum of the values of the integrand at certain specific points. The formula for a single integral is:

$$\int_{-1}^{1} f(\xi)d\xi = \sum_{i=1}^{m} H_i f(a_i) \tag{2.13}$$

where

H_i = weighting coefficients; and

ξ = a_i are the specified Gaussian points.

The integration is exact if $f(\xi)$ is a polynomial of degree up to $2m-1$. Values of H_i and a_i are available in most texts on numerical methods (Kopal, 1961; Zienkiewicz, 1967).

Double integrals can similarly be replaced by double summations:

$$\int_{-1}^{1}\int_{-1}^{1} f(\xi,\eta)d\eta d\xi = \sum_{i=1}^{m}\sum_{j=1}^{n} H_j H_i f(a_i, b_j) \tag{2.14}$$

Before the Gaussian quadrature formula can be applied to a rectangular section or quadrilateral section it is necessary to map the actual area to a corresponding square area bounded by the limits $\eta = \pm 1$ and $\xi = \pm 1$. This is achieved by devising the special co-ordinates (η, ξ) such that lines of constant η and ξ are straight and parallel to the sides of the section. This special co-ordinate system is shown in Figure 2.7 for a quadrilateral section.

The procedure involves sub-dividing the section into trapezoidal and triangular elements. In each element, stresses are calculated at a few (2 or 3) gaussian points. The integrations are replaced by weighted summations of these stresses and their moments. Virdi suggested that this method reduces the computational time by a factor of a third as compared to methods which use discrete summation as an approximation to the exact integral.

This method has the disadvantage that it involves more complicated programming when compared with the method using summation as an approximation to the exact integral.

Of the three methods described above, direct summation seems to be most suitable for the present investigation and is therefore chosen to be used in the

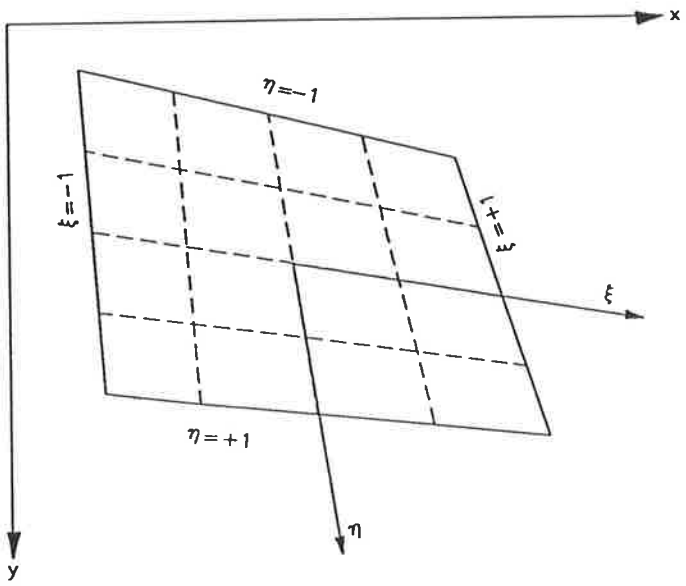

Figure 2.7: Section coordinates proposed by Virdi(1977)

program SAFRAME. It has the flexibility to allow any stress-strain relationship for the concrete to be used. In particular, material unloading needs to be considered, and this method can accommodate such effects. The disadvantage, of requiring more computational time, is largely offset by the availability of modern computing facilities.

2.2.3 Numerical Techniques to Obtain Strain Distribution for Sections Subjected to Known Forces

Up to this point, the discussion of moment-thrust-curvature calculations has involved the relatively straight forward calculation of forces from known strain distribution over the section. The reverse process, the determination of the strain distribution which corresponds to a known moment and thrust, however,

requires more sophisticated numerical techniques. In structural analysis, it is often the case that strains in the section have to be determined for a given moment and axial force.

One such technique is the Newton method, described by Harrison(1976) for solving a system of non-linear equations. This technique has also been used by Virdi and Dowling(1976) to obtain moment-thrust-curvature relations. The application of this technique to obtain a solution for mid-section strain ϵ_m and curvature κ from known moment, $M_{required}$ and known thrust, $N_{required}$ is as follows:

- assume initial values κ_o and ϵ_o, using the summation approach or the direct integration approach, obtained misclosures or boundary errors m_o and n_o, where m_o is equal to $(M_o - M_{required})$ and n_o is equal to $(N_o - N_{required})$.
- assume $\kappa_o + \delta\kappa$, ϵ_o, using the summation or the direct integration approach obtained the moment misclosure of $m_o + (\partial m_o/\partial\kappa).\delta\kappa$, and the thrust misclosure of $n_o + (\partial n_o/\partial\kappa).\delta\kappa$,
- similarly, assume κ_o, $\epsilon_o + \delta\epsilon$, hence obtained moment misclosure $m_o + (\partial m_o/\partial\epsilon).\delta\epsilon$ and thrust misclosure $n_o + (\partial n_o/\partial\epsilon).\delta\epsilon$,
- get a better approximation of κ_o and ϵ_o from the following equations:

$$\begin{bmatrix} \kappa_1 \\ \epsilon_1 \end{bmatrix} = \begin{bmatrix} \kappa_o \\ \epsilon_o \end{bmatrix} - \begin{bmatrix} \frac{\partial m_o}{\partial \kappa} & \frac{\partial m_o}{\partial \epsilon} \\ \frac{\partial n_o}{\partial \kappa} & \frac{\partial n_o}{\partial \epsilon} \end{bmatrix}^{-1} \cdot \begin{bmatrix} m_o \\ n_o \end{bmatrix} \tag{2.15}$$

- the cycle is repeated with the improved estimates κ_1 and ϵ_1 replacing κ_o and ϵ_o until misclosures m_o and n_o are within acceptable tolerances.

Another technique, based on search procedures, was proposed by Warner and Lambert(1974). The basic search technique for a nonlinear equation involves

two phases. Assume that x has to be determined for a given value of y_o, and the nonlinear equation $y = f(x)$ is defined. In the first phase, a fixed increment or decrement is applied to the unknown variable x until two values of x are obtained, x_L and x_U, which give y values that are respectively lower and higher than the required y_o value. In the second phase, iterative cycles are carried out whereby the mid-point x_M between x_L and x_U is used within the cycle. The value y_M corresponding to x_M is compared with y_o and a solution of x_o equal to x_M is accepted when y_M is sufficiently close to y_o. If this convergence check is not satisfied then x_M is used to reduce the size of the bound (by replacing either x_L or x_U depending on the value of y_M) and the whole cycle is repeated. As this technique arrives at a solution by carrying out intelligent searches, it will be referred to as the *search technique* in this thesis.

A two-dimensional nested search procedure was developed by Warner and Lambert consisting of an outer procedure to find ϵ_o and an inner procedure to find ϵ_1, where ϵ_o is the concrete strain in the extreme compressive fibre and ϵ_1 is the concrete strain in the extreme tensile fibre. Both procedures use the basic search technique described above. The nested procedure was used to obtain moment-curvature relations for reinforced concrete sections in pure bending. The equilibrium requirements under consideration are:

$$|N - N_{required}| \leq t_N \tag{2.16}$$

$$|M - M_{required}| \leq t_M \tag{2.17}$$

where

t_N and t_M = specified tolerances; and

N and M = longitudinal force and resultant moment respectively.

The flow diagram of the inner procedure SEEKE1 used by Warner and Lambert to analyse sections subjected to pure bending (where $N_{required} = 0$) is shown in Figure 2.8.

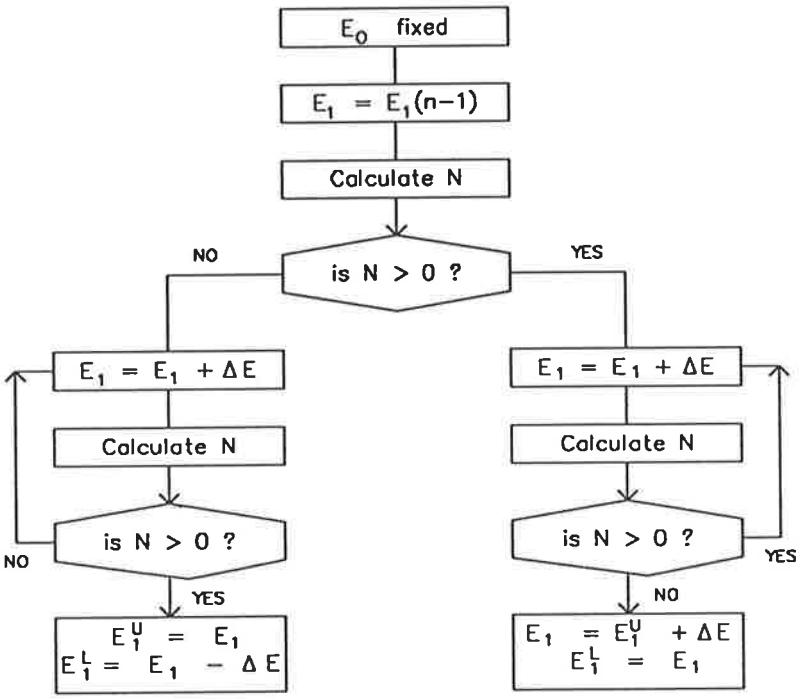

(a) Seeke1: Bounds on E_1

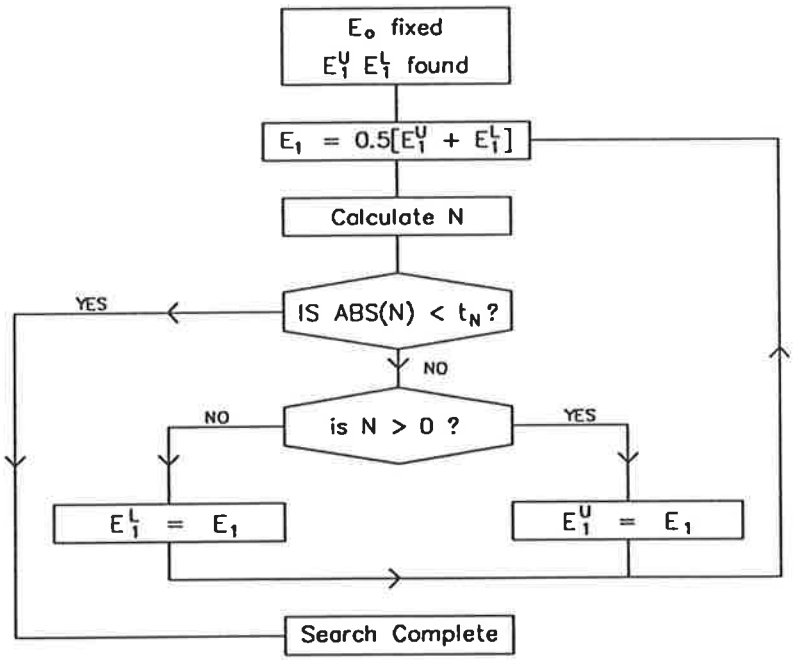

(b) Seeke1: Halving procedure

Figure 2.8: Search procedure proposed by Warner and Lambert(1974)

Warner and Lambert suggested that even though this procedure is not optimal, it has been found by them to be efficient and reliable. This technique has been used previously by Warner and Lambert(1974), Ahmad and Warner(1984), and Kgoboko(1987).

As the search procedure has been well tested by earlier researchers and found to be reliable, it is used in the section analysis routine of program SAFRAME.

2.3 Section Analysis Routines for Use in Analysis

The generation of moment-thrust-curvature relations of reinforced concrete sections has so far been discussed in isolation. We now consider the incorporation of section analysis routines into frame analysis programs.

In previous studies carried out on reinforced concrete frames, two different methods have been used to incorporate the section analysis into the frame analysis. One of these is to use a section analysis routine automatically to generate values of bending moment, curvature and thrust values, wherever required, during the analysis. The other method is to pregenerate a series of moment-curvature curves over a practical range of thrust values. An interpolating routine is then used to obtain appropriate values of bending moment, curvature and thrust as required.

2.3.1 Automatic Generation of Values of M, κ and N

In this method a built-in section analysis routine generates axial strain ϵ_m and curvature κ for given values of thrust N and moment M, as shown in the schematic diagram in Figure 2.9.

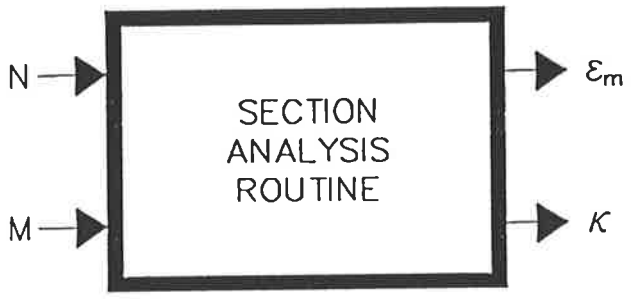

Figure 2.9: Schematic diagram of the section analysis routine

The advantage of the automatic generation method is that a minimum amount of input data needs to be fed into the main analysis program. For each section, the required input data are the shape of the section and the properties of the component materials. This reduces greatly the task of checking the accuracy of the input data.

This method was used by Aas-Jakobsen and Grenacher(1974) in their analysis of reinforced concrete structures.

2.3.2 Pre-generated M-κ-N Relations with Special Interpolation Algorithms

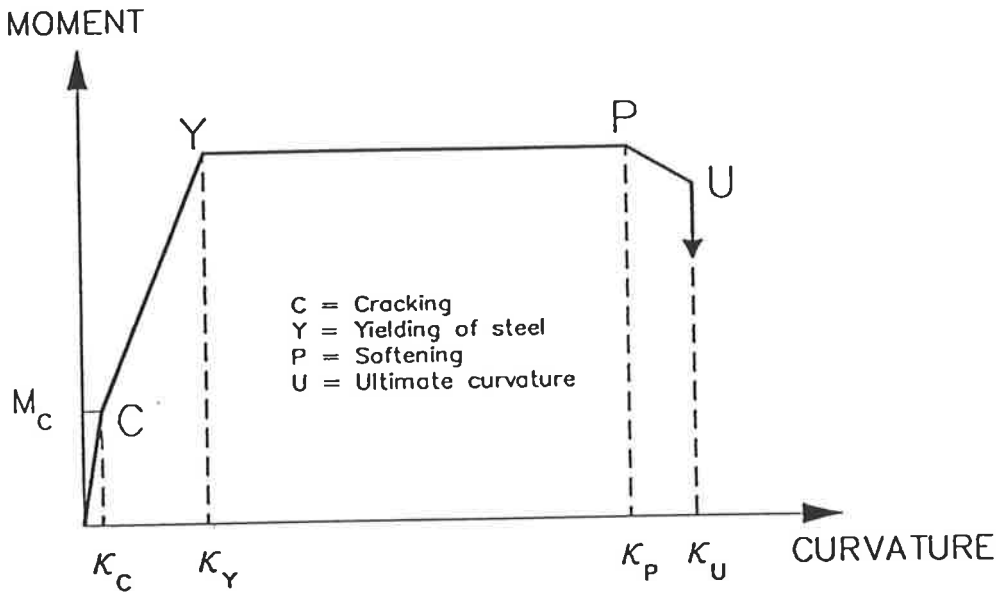

Figure 2.10: Typical linearised moment-curvature relation

In this method, a separate section analysis program is used to generate a large number of data points for a full range of M, κ, N values. The data may be directly fed into the main structural analysis program; alternatively, they can be fitted to curvilinear equations, before feeding into the main program. Another possibility is to fit the data with piecewise linear relations. The section analysis routine uses these data to generate M, κ, N data points as needed by the main program.

A typical linearised relation is shown in Figure 2.10. Key points are labelled in the figure. This may represent a piecewise linearisation of the M-κ curve for a concrete section with a particular thrust value.

Tests have been carried out by previous researchers to obtain moment curvature relations for reinforced concrete sections. From these tests, Monnier(1970) and Darvall and Mendis(1985) proposed the use of linearised M-κ relations. Monnier carried out some tests on beams to obtain moment-curvature relations using the well-known four-point bending test which gives a constant moment region. The elongations and shortenings were measured along the entire length of the constant moment region. Monnier did not include in his study the load softening behaviour of the section. From the study carried out, he concluded that the moment-curvature relation can be approximated using a trilinear relationship. Examples of idealised M-κ relations given by Monnier for four different percentages of tensile reinforcement are shown in Figure 2.11, where w_o is the percentage of tensile reinforcement ($100A_{st}/BD$). The key points in the trilinear relation are defined by the cracking moment M_r and the yield moment M_e. Monnier gave suggestions on how these values could be estimated. He concluded from his investigation that the uncracked flexural stiffness practically corresponds to the calculated flexural stiffness which includes the presence of the reinforcement. It will be noted that he did not consider the unloading, or softening, branch of the M-κ relation.

Darvall and Mendis (1985), and Tse and Darvall (1986) used a deformation-controlled testing system to obtain experimental moment-curvature relations of reinforced concrete sections, and included the softening portion of the curves. A trilinear approximation was used by Darvall and Mendis to represent the behaviour of reinforced concrete sections. The trilinear curve represents three different stages in the behaviour of the concrete section: elastic, plastic and softening. A typical trilinear moment-curvature curve is shown in Figure 2.12.

Normally only the key points of moment-curvature relations are stored. A moment-thrust-curvature point can be determined by using a simple linear interpolation between two adjacent data points for given values of thrust and

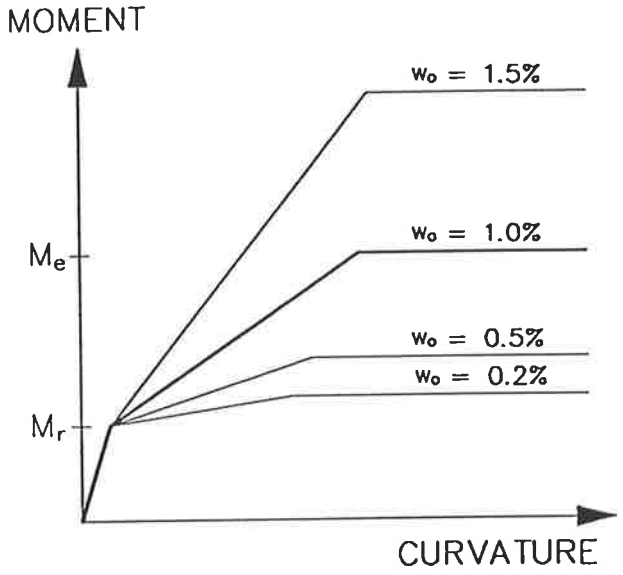

Figure 2.11: Examples of idealised M-κ relations (Monnier,1970)

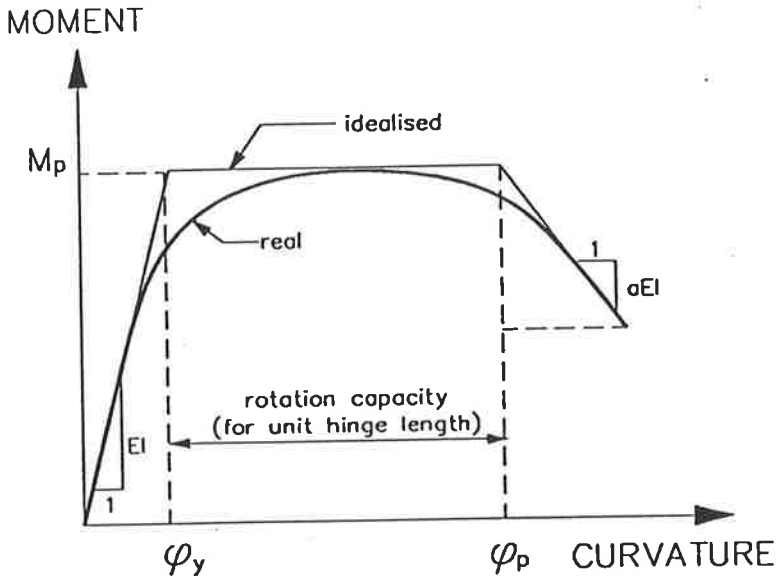

Figure 2.12: Trilinear moment-curvature relations (Darvall and Mendis,1985)

curvature if the thrust corresponds with that of one of the pregenerated curves. If the thrust value does not correspond to those of the pre-generated curves, two moment-curvature points are first determined using simple interpolation within the respective curves to give the required curvature. As these two points do not have the required thrust value, a further linear interpolation is carried out between them to obtain a solution point with the required thrust value. This process is illustrated in Figure 2.13.

The advantage of this method is that the section analysis is carried out separately, thereby reducing greatly the times required for the analysis of the structure. It also allows experimentally determined M-κ relations to be used. Furthermore, the states of the sections during loading can be easily visualised from the pregenerated curves. This assists greatly in determining the state of hinge formation at time of collapse.

The disadvantage of using this method is that linearisation and interpolation decrease the accuracy of the solution. Another disadvantage is that this method requires additional work involved in pre-generating and linearising the M-κ-N curves. If this is carried out manually and the processed data are manually fed into the routine, more time will be required to prepare input data than for those methods which automatically generate values of M, κ and N as and when required. This can be overcome by not linearising the data and programming the routine to read in directly the M-κ-N data pre-generated and previously stored onto disk files by the separate section analysis program.

2.4 Section Analysis Routine for SAFRAME

In the course of the structural analysis developed in Chapter 4 of this thesis, a section analysis routine is used to provide data points (M, κ, N) for a large number of segments.

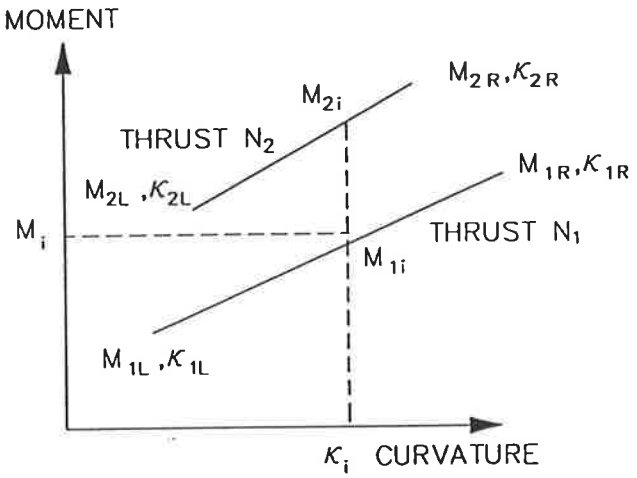

Steps to obtain M_i from known curvature κ_i and thrust N_i:

(1) Obtain (M_{2i}, κ_i) on linearised curve with thrust N_2

$$M_{2i} = M_{2L} + \left(\frac{\kappa_i - \kappa_{2L}}{\kappa_{2R} - \kappa_{2L}}\right)(M_{2R} - M_{2L})$$

(2) Obtain (M_{1i}, κ_i) on linearised curve with thrust N_1

$$M_{1i} = M_{1L} + \left(\frac{\kappa_i - \kappa_{1L}}{\kappa_{1R} - \kappa_{1L}}\right)(M_{1R} - M_{1L})$$

(3) Obtain (M_i, κ_i) with thrust N_i

$$M_i = M_{1i} + \left(\frac{N_i - N_1}{N_2 - N_1}\right)(M_{2i} - M_{1i})$$

where
M = Bending Moment
N = Thrust
κ = Curvature

Figure 2.13: Interpolation algorithm

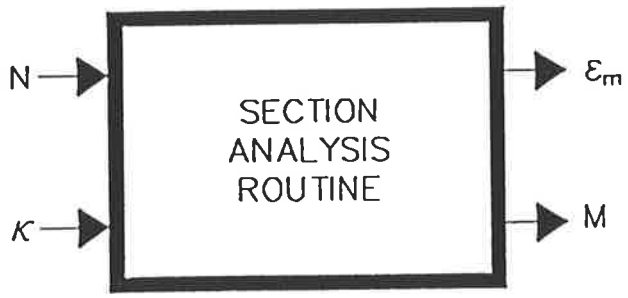

Figure 2.14: Schematic diagram of the section analysis routine

As described in Section 2.2.3, two search procedures must be used to determine unknowns ϵ_m and κ from known values of N and M. By choosing the appropriate variables as unknown when updating the flexural and extensional stiffnesses, it is possible to reduce the number of search procedures to one, hence improving the efficiency of the program. For the section analysis routine of SAFRAME, the known variables are selected to be the axial thrust N and the curvature κ, and the unknown variables are the bending moment M and the axial strain ϵ_m. This is illustrated by the schematic diagram in Figure 2.14.

The section is modelled numerically by a number of thin concrete layers and a number of reinforcing layers based on the approach of Warner(1969). In the present work it was found that 15 concrete layers were usually sufficient to provide moment-thrust-curvature relations of acceptable accuracy. Based on a trial value of the top extreme fibre strain ϵ_o and a predetermined curvature κ, the linear strain distribution across the section is specified, and so the stresses

and hence the forces in each concrete and steel layer can be determined by means of appropriate stress-strain relations. The stress-strain relationship used for concrete in the program SAFRAME is that proposed by Warner(1969), and an elastic-plastic relationship is used for the reinforcing steel. To enable realistic modelling of material behaviour, unloading paths have been included in the stress-strain relationships (Figure 2.15).

The equations defining the curvilinear stress-strain relationship are:

$$\bar{\epsilon}_c < 0.0 \quad : \quad \bar{f}_c = 0.0 \tag{2.18}$$

$$0.0 \leq \bar{\epsilon}_c < 1.0 \quad : \quad \bar{f}_c = \gamma_1 \bar{\epsilon}_c + (3 - 2\gamma_1)\bar{\epsilon}_c^2 + (\gamma_1 - 2)\bar{\epsilon}_c^3 \tag{2.19}$$

$$1.0 \leq \bar{\epsilon}_c < \gamma_2 \quad : \quad \bar{f}_c = 1 - (1 - 2\bar{\epsilon}_c + \bar{\epsilon}_c^2)/(1 - 2\gamma_2 + \gamma_2^2) \tag{2.20}$$

$$\bar{\epsilon}_c \geq \gamma_2 \quad : \quad \bar{f}_c = 0.0 \tag{2.21}$$

where

$\bar{\epsilon}_c$ = normalised strain equal to $\epsilon_c/\epsilon_{cmax}$;

$\bar{f}_c$ = normalised stress equal to f_c/f_{cmax};

$\gamma_1 = E_o \times \epsilon_{cmax}/f_{cmax}$;

E_o = modulus of elasticity of concrete;

f_{cmax} = strength of concrete; and

ϵ_{cmax} = strain corresponding to stress f_{cmax}.

The unloading paths are assumed to be parallel to the initial loading path of the stress-strain relationship. No arbitrary upper "collapse" strain is assumed for the concrete, so that the strain can increase indefinitely. The unloading effects of the concrete and steel are taken into consideration by storing the peak strains of all the layers and their corresponding stresses in an array. The values in this array are updated at the ends of the computational steps used to trace the behaviour of the structure under increasing load. In program SAFRAME, the

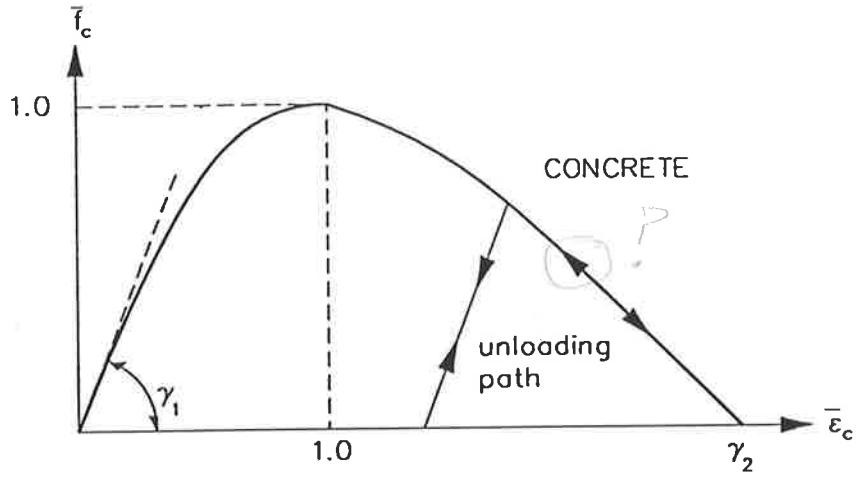

(a) Stress–strain relationship of concrete

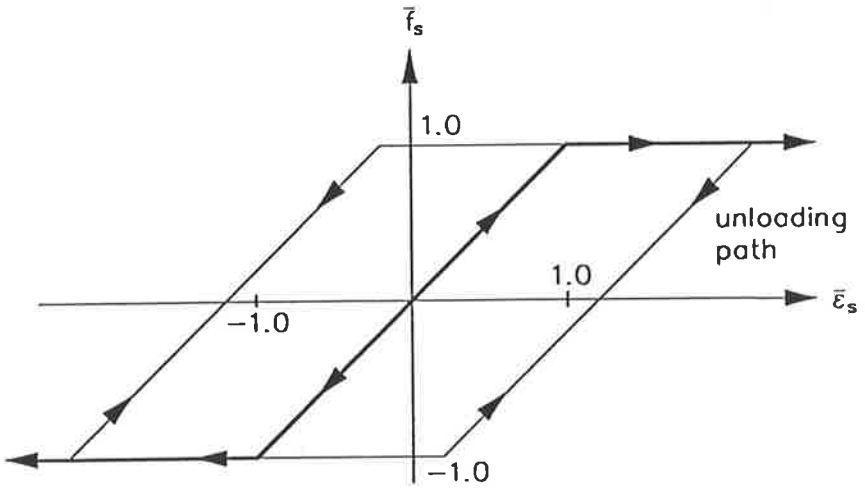

(b) Stress–strain relationship of steel

Figure 2.15: Stress-strain relationships used in program SAFRAME

computational steps represent increasing curvatures in a chosen key segment in the structure. The flow charts to calculate stresses for the concrete and steel layers, including the effect of unloading, are given in Appendix B.

Summation of the forces in the concrete and steel layers gives the thrust N (see Figure 2.16):

$$N = \sum_{i=1}^{nlayer} \sigma_{ci} A_{ci} + \sum_{j=1}^{nsteel} \sigma_{sj} A_{sj} \tag{2.22}$$

where

σ_{ci} = stress at mid-level of the i-th concrete layer;

A_{ci} = area of the i-th concrete layer;

σ_{sj} = stress at mid-level of the j-th concrete layer; and

A_{sj} = area of the j-th concrete layer.

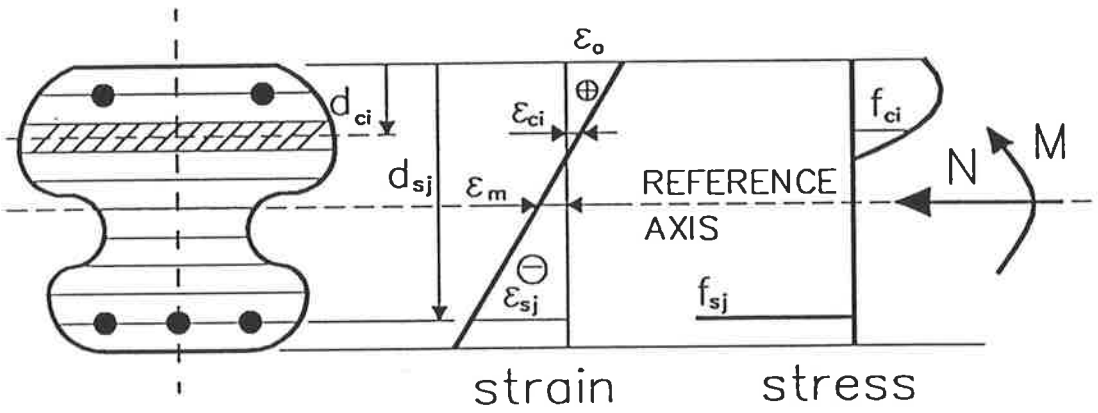

Figure 2.16: Cross section, stress and strain distribution, and forces

Adjustment of the value of ϵ_o is made using the search procedure described earlier in this chapter until the calculated thrust is equal to the desired thrust to within an acceptable tolerance.

Having obtained the required ϵ_o value, the bending moment in the section about the reference axis is calculated as :

$$M = \sum_{i=1}^{nlayer} \sigma_{ci} A_{ci} y_{ci} + \sum_{j=1}^{nsteel} \sigma_{sj} A_{sj} y_{sj} \tag{2.23}$$

where

y_{ci} = distance from the mid-level of the i-th concrete layer from the reference axis;

y_{sj} =distance from the mid-level of the j-th steel layer from the reference axis;

$nlayer$= total number of concrete layers; and

$nsteel$ = total number of steel layers.

The convergence criterion described above, which is based on the thrust values, has been found to be inefficient as it is difficult to decide on whether the present iterate is sufficiently close to the true solution. A more efficient convergence criterion based on the top strain of the section ϵ_o is therefore used. Convergence is assumed to be achieved when:

$$\left| \frac{\epsilon_o(new) - \epsilon_o(old)}{\epsilon_o(old)} \right| < tolerance \tag{2.24}$$

where

$\epsilon_o(old)$ = top fibre strain of the previous cycle; and

$\epsilon_o(new)$ = top fibre strain of the current cycle.

Table 2.1 shows the results obtained by using the two different convergence criteria described above for a reinforced concrete section shown in Figure 2.17. The use of a deformation-based criterion was found to reduce the computing time significantly. The results obtained indicate that a tolerance of 1.0×10^{-3} gives solutions of acceptable accuracy.

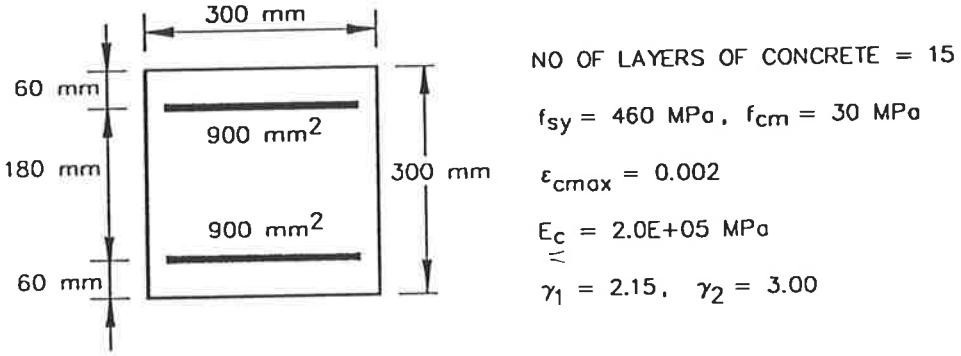

Figure 2.17: Reinforced concrete section analysed

Table 2.1: Bending moments in kNm for $N/N_{uo} = 0.30$

	force criterion	deformation criterion			
Curvature (m^{-1})	$\lvert N_{new} - N_{old} \rvert < 5 \times 10^{-3}\ kN$	tol= 5×10^{-2}	tol= 1×10^{-2}	tol= 1×10^{-3}	tol= 1×10^{-5}
0.0010	17.45	17.47	17.44	17.45	17.45
0.0050	68.32	69.14	68.52	68.34	68.32
0.0100	97.12	95.78	96.97	97.12	97.12
0.0150	117.96	117.93	118.24	117.97	117.96
0.0200	134.71	134.67	134.88	134.70	134.71

2.5 Testing of Section Analysis Routine

Two reinforced concrete sections, tested under pure flexure by Iqbal and Hatcher (1975), were analysed using the numerical procedure described here. The program was modified slightly to avoid non-linear unloading effects in the materials which were not taken into consideration.

In the tests carried out by Iqbal and Hatcher, the beams were unbound (without stirrups) at the constant moment region. Figure 2.18 shows the configuration of the beams tested. A stiff loading system was used to obtain the softening branch of the moment-curvature relation of the section.

The beams chosen for analysis are beams $AA3$ and $B2$; details of which are given in Figure 2.19. According to Iqbal and Hatcher, the reinforcing index q was chosen so that the steel would not strain harden in the post-crushing range for the concrete. Stress-strain plots for the reinforcing steel of beams $AA3$ and $B2$, shown in Figure 2.20, are reproduced from those obtained by the investigators.

Bending moment plots obtained using the section analysis program for beam $AA3$ are plotted in Figure 2.21. One of the plots is for the section with concrete strength for the structure f_{cmax} equal to f_{cm} (f_{cm} is the average cylinder strength of concrete) and the other for f_{cmax} equal to $0.85f_{cm}$. Analytical results obtained by Ahmad and Shah(1979) for the same section assuming stress-strain relationships of concrete to be those of Ahmad and Shah(1979), Desayi and Krishnan(1964), and Hognestad(1951) are also given in Figure 2.21. The stress-strain relationships proposed by Ahmad and Shah, and Desayi and Krishnan are shown in Figures 2.22 and 2.23 respectively. For the stress-strain relationship proposed by Ahmad and Shah, the four constants A, B, C and D are determined from four key points. These are the secant modulus of elasticity at 45 percent of the peak stress; the peak stress and the corresponding

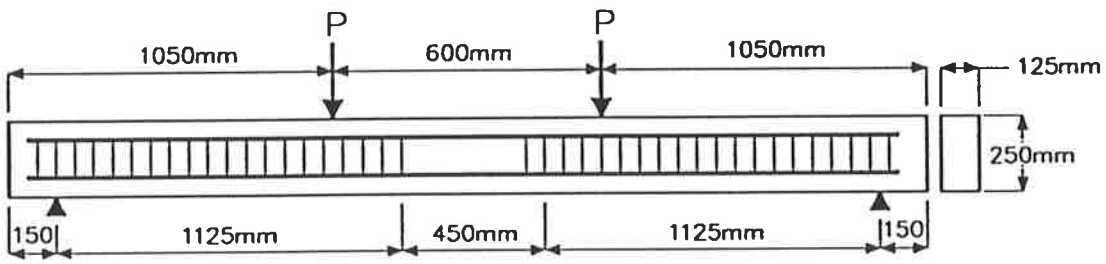

Figure 2.18: Configuration of beams tested by Iqbal and Hatcher (1975)

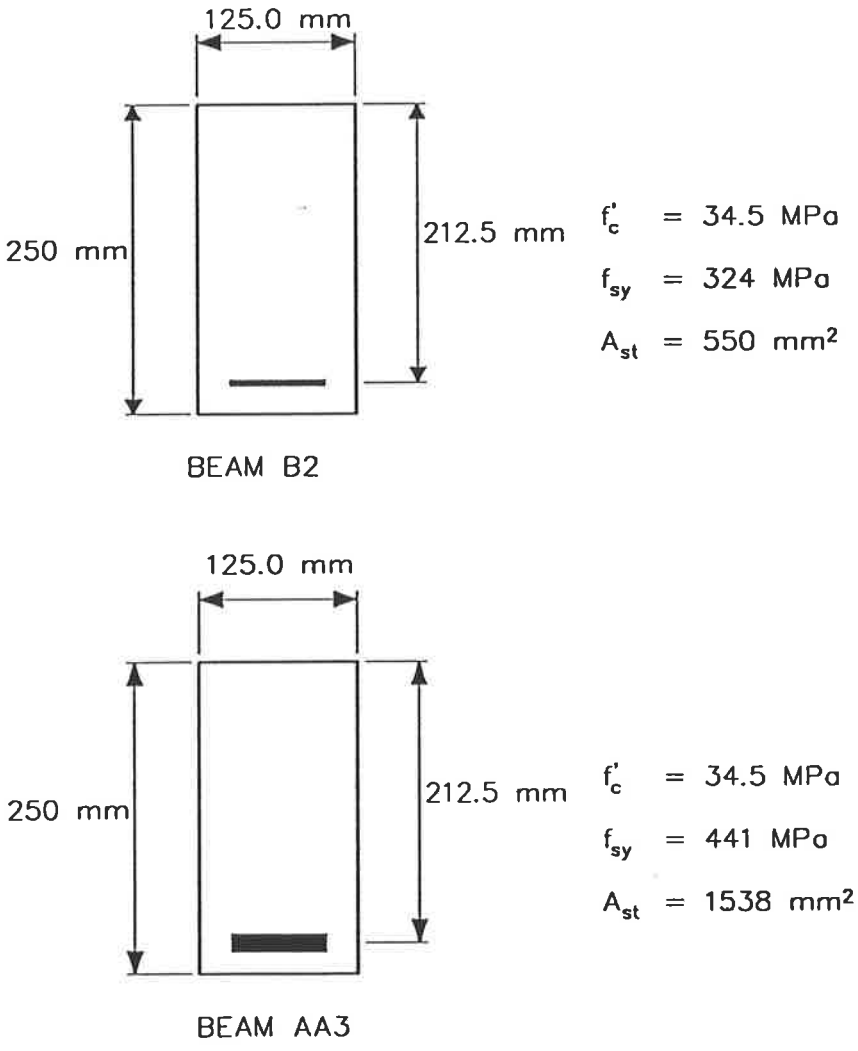

Figure 2.19: Details of beams AA3 and B2

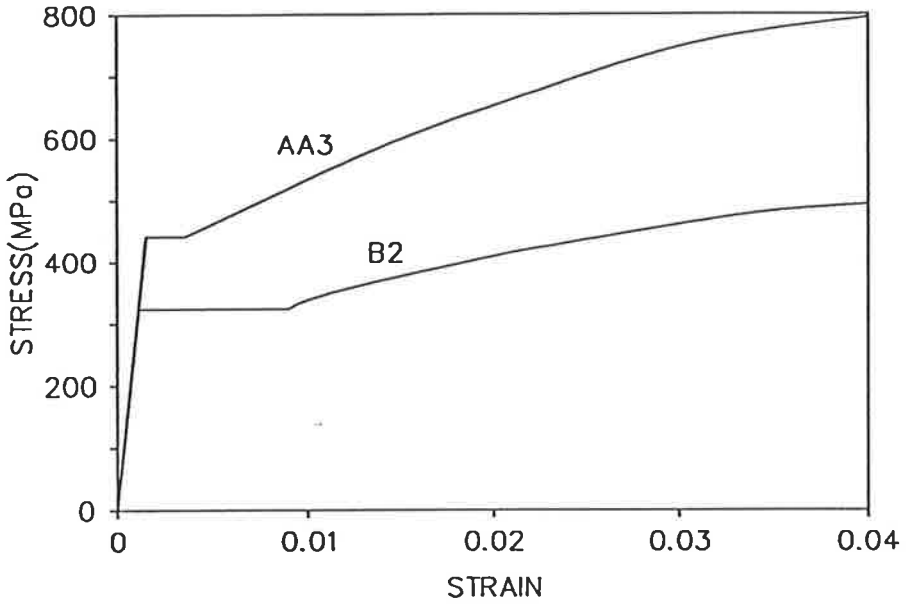

Figure 2.20: Stress-strain relationships of reinforcing bars of beams AA3 and B2

strain, the inflection point and an arbitrary point on the descending portion (Desayi and Krishnan, 1964). The peak stress was assumed to be equal to the mean cylinder strength f_{cm} in all three cases.

Similar plots were also obtained for the section of beam $B2$. These plots are shown in Figure 2.24.

Two values of peak stress for the concrete f_{cmax} were used in the analysis of the section. This is because the conversion factor between the peak strength of concrete in structural members and the mean cylinder strength depends, to a certain extent, on the placement of concrete in the structural members. This observation was pointed out by Breen(1964). Breen found that the calculated moment systematically showed less moment than that actually present. The magnitude of this error, he suggested, is caused by making the assumption

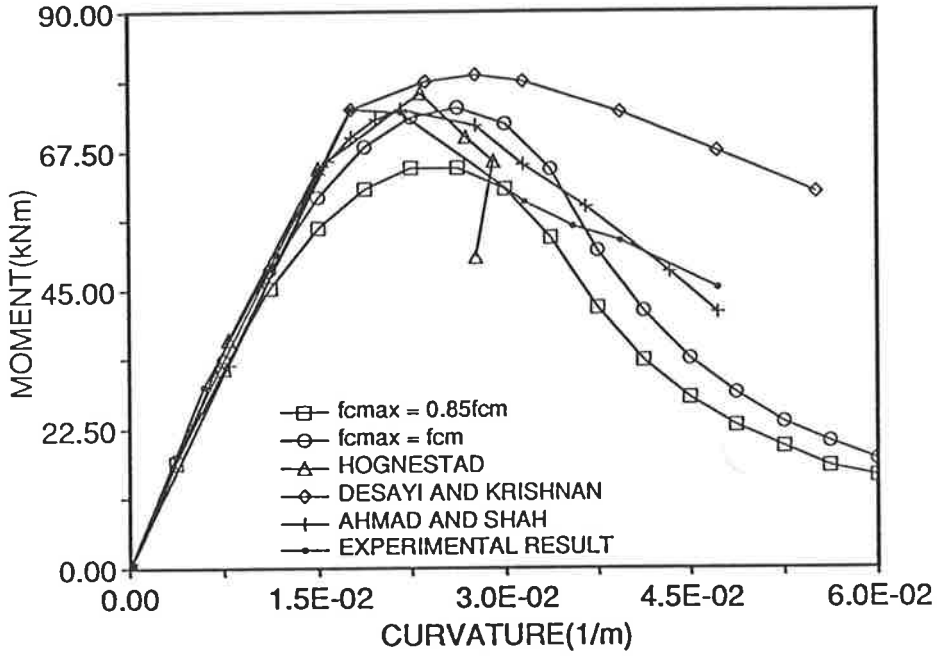

Figure 2.21: Moment curvature plots of beam AA3

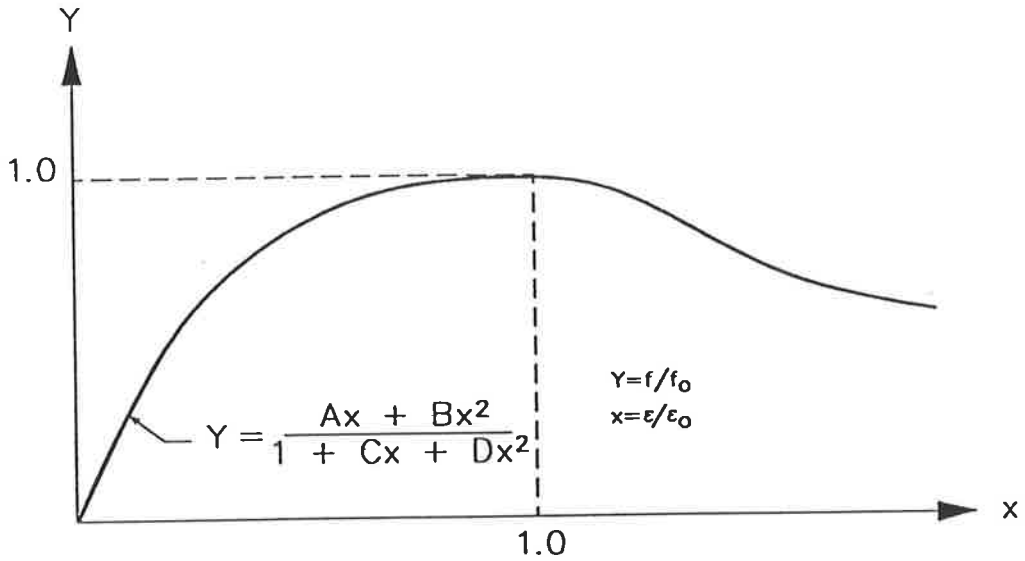

Figure 2.22: Stress-strain relationship of concrete proposed by Ahmad and Shah(1979)

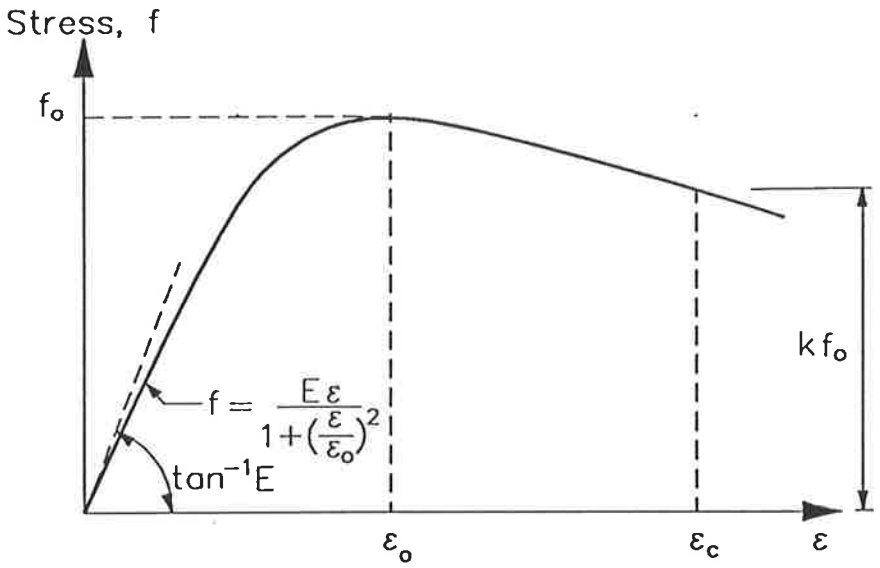

Figure 2.23: Stress-strain relationship of concrete proposed by Desayi and Krishnan(1979)

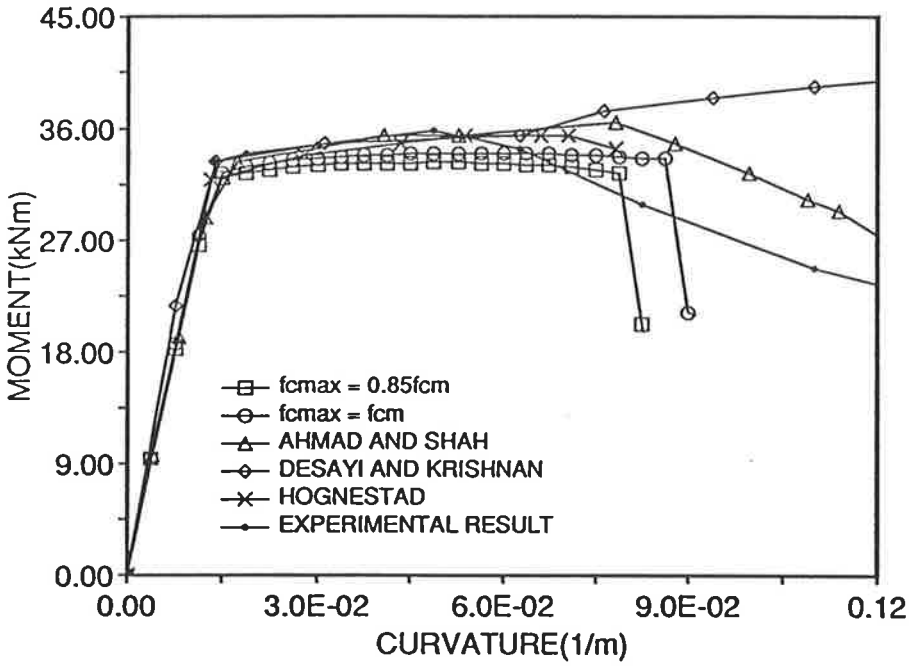

Figure 2.24: Moment curvature plots of beam B2

that f_{cmax} equals $0.85f_{cm}$ in horizontally cast members.

Results obtained from the present analysis indicate that the section analysis routine of program SAFRAME gives reasonable estimates of the behaviour of reinforced concrete sections.

2.6 Factors affecting Moment-Curvature Relations

It must be appreciated that the overall behaviour of a reinforced concrete frame is strongly dependent on the behaviour of cross-sections and segments in the high moment regions. The shape of the M-κ curve is therefore of considerable interest. One of the most important properties is ductility, or the ability to undergo large deformations under conditions of ultimate strength. Ductility governs the rotation capacity of hinging zones and hence the redistribution of moments in an indeterminate structure. This enables structures to adapt to differential foundation settlements and also safeguard structures from sudden local overloads within parts of the structure.

The ductility of a concrete section is measured by a widely accepted parameter, κ_u/κ_y, which is known as the ductility factor. The yield curvature κ_y is defined as the curvature at which the tensile steel yields. Several definitions have been used for κ_u, the ultimate curvature of a section. In most design codes, κ_u is defined by an arbitrarily chosen limiting value of the concrete strain, normally taken to be 0.003. Rüsch(1960) proposed a more satisfactory definition of κ_u based on the value of concrete strain ϵ_u corresponding to the maximum moment carrying capacity. Park and Sampson(1972) argued that many sections have considerable capacity for plastic rotation beyond the peak of the moment curvature curve and they defined κ_u as the curvature corresponding

to $0.9M_u$ along the softening branch of the M-κ diagram. Ghosh and Cohn (1972,1974) in their analytical studies chose to use the κ_u proposed by Rüsch. They found that the conventional definition based on a limiting strain of 0.003 grossly underestimate the deformability of a section. Therefore, if the conventional definition of the ultimate curvature is used, a very safe estimate of the strength of structure analysed is obtained. The conventional definition is useful for design purposes. The ratio of κ_u based on Rüsch's proposal to that based on the conventional definition was found to be as large as 4–5 for section failing in tension.

Moment-curvature relations of concrete sections are governed by the amount and type of reinforcement, the strength of concrete, the magnitude of thrust acting on the section and tension stiffening.

2.6.1 Effect of Thrust

The moment curvature relation of a section under combined bending and thrust differs significantly from that for a section under pure bending. The main difference is the reduction in ductility due to the presence of the axial load. The ductility of reinforced concrete sections subjected to combined bending and axial load has been studied by Pfrang et al(1964), Mirza and McCutcheon(1974), and Ghosh and Cohn(1974).

In all the studies mentioned, it was found that as the axial force increases, the rotation capacity of the section decreases. Pfrang et al carried out analytical studies on the effect of thrust on the ductility of rectangular sections. They found that the sections have large amounts of ductility at low axial thrust levels. As the axial thrust increases, ductility decreases markedly. They also found that at balance axial load, only a negligible amount of ductility remains for the sections.

Ghosh and Cohn(1974) carried out an extensive analytical study on the behaviour of reinforced concrete sections under combined bending and compression. In this study 405 symmetrically reinforced rectangular concrete sections of width 250mm (10in) and depth 500mm (20in) with varying concrete strengths, steel grades and reinforcement percentages were subjected to varying magnitudes of thrust. They found irregularities in the failure mode when failure was defined in terms of sectional moment capacity as compared with that defined in term of a conventional arbitrary maximum strain of 0.003. These irregularities are: (1) the moment capacities under pure bending are larger than those under bending combined with low axial loads and (2) the ultimate curvatures sometimes increase with increasing axial loads around the balanced point. Two plots illustrating these irregularities observed by Ghosh and Cohn are shown in Figure 2.25. In these plots M_u is the ultimate moment, P_u is the ultimate axial force, b is the width of the section, h is the total depth of the section and ϕ is the sectional curvature.

Mirza and McCutcheon(1974) tested 20 beams both analytically and experimentally. They found that the available rotation capacity decreased by approximately 25 per cent as the axial compressive load was increased from zero to the balanced column failure load. They also found that beyond the balance point, available hinge rotation diminished gradually, becoming zero for the case of pure axial compression.

Moment-thrust-curvature plots of a section shown in Figure 2.26 with different amounts of thrust are shown in Figure 2.27. In this figure N_{uo} is the squashed load of the section. The section was analysed using a section analysis routine described earlier in this chapter. The stress-strain relationship for concrete is assumed to be that of Warner(1969). For the concrete, mean cylinder strength value f_{cm} was assumed to be 35 MPa. Value f_{cmax} is assumed to be $0.85f_{cm}$, and value of parameter γ_2 was assumed to be 3.0. Value E_c was assumed to be $5000\sqrt{f_{cm}}$. These plots indicate the decreasing ductility of section with

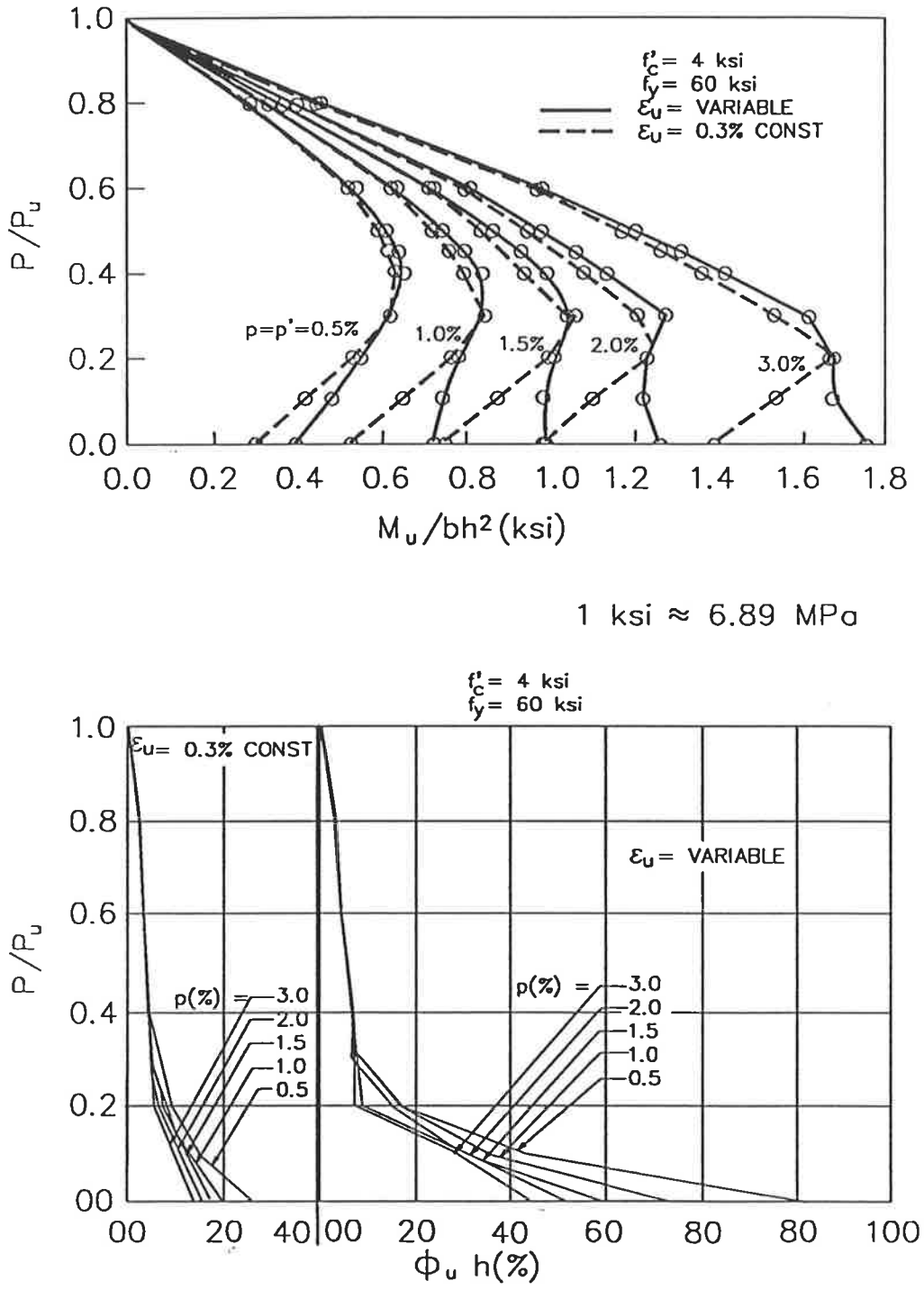

Figure 2.25: Results from analysis by Ghosh and Cohn (1974)

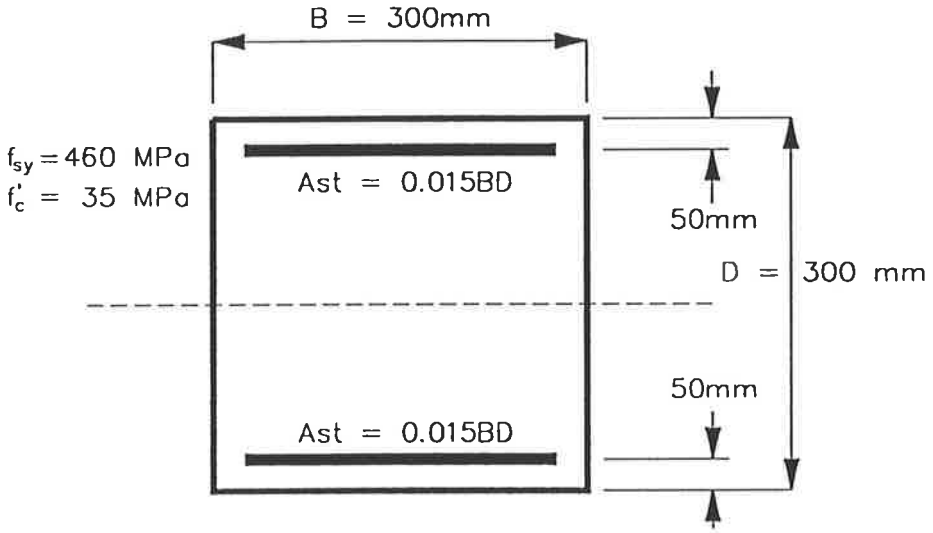

Figure 2.26: Doubly reinforced concrete section subjected to thrust

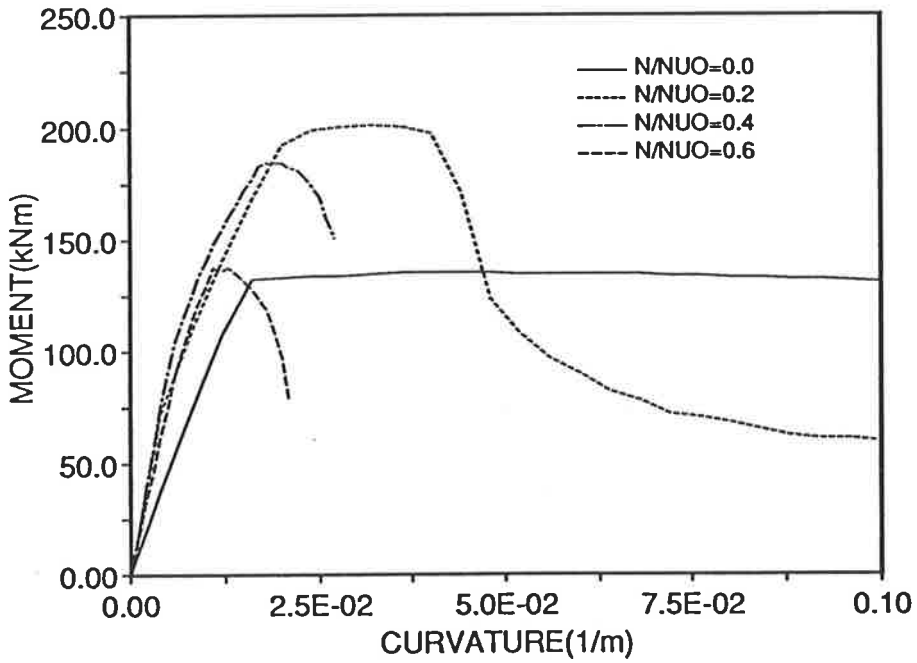

Figure 2.27: Moment-thrust-curvature plots for doubly reinforced section

increasing thrust.

2.6.2 Effect of the Amount of Reinforcement

For a singly reinforced concrete section, ductility decreases as the amount of tensile reinforcement increases. Plots of moment-curvature for the singly reinforced concrete section (Figure 2.28) are given in Figure 2.29. The analysis was carried out using the same routine as described in the earlier section. Material properties are assumed to be similar to the section analysed in the earlier section. These plots indicate the effect of the amount of tensile reinforcement on the ductility of a singly reinforced section.

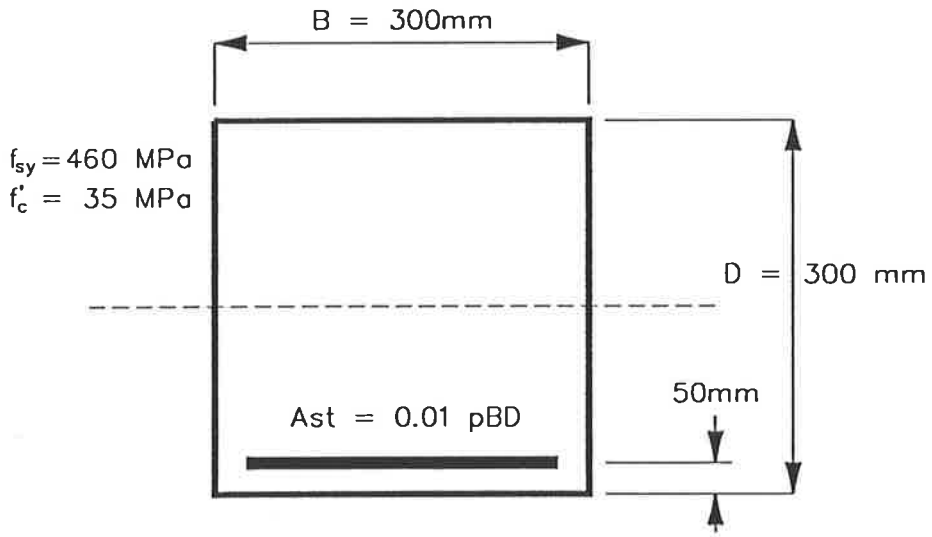

Figure 2.28: Singly reinforced section subjected to pure bending

Pfrang, Seiss and Sozen(1964) found that the general character of the M-κ relation is not markedly affected by the ratio of reinforcement for the symmetrically reinforced concrete sections analysed by them. Ductility of the sections, however, was found to be reduced by increasing the amount of reinforcement.

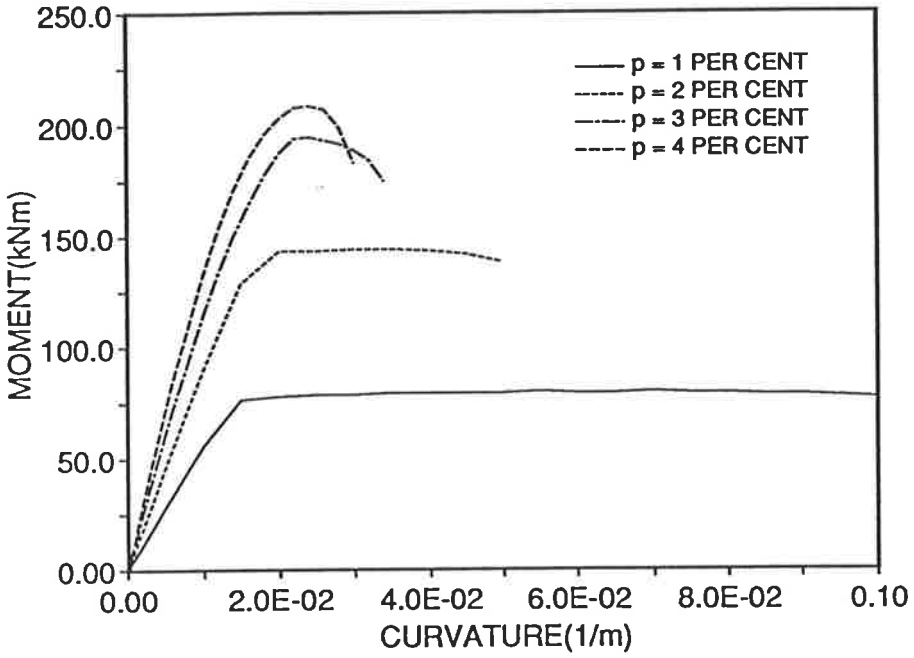

Figure 2.29: Moment-curvature relations for section with various steel proportions

Cohn and Ghosh(1972) found that section ductility can be increased by the addition of suitable amounts of compressive reinforcement.

2.6.3 Effect of Tension Stiffening

Even after the formation of cracks, it is possible for the tensile concrete to continue to carry some forces between the cracks. The contribution to flexural stiffness by the concrete in the tension zone has been observed by previous researchers(Sawyer and Stephen, 1957; Yu and Winter, 1960; Corley and Sozen, 1966) who found that the stiffness of a cracked section is greater than that calculated assuming no tensile strength in concrete.

Two commonly used techniques for modelling are: (1) to assume an average

tensile stress to act over an effective area of concrete surrounding the bars in the tension zone (Lin and Scordelis, 1975; Clark and Speirs,1978) and (2) to modify the steel stresses to include the effect of tension stiffening in the surrounding concrete (Borges and Oliveira,1963).

Gilbert and Warner(1978b) used both techniques in predicting slab deflections using a layered finite element approach. Three stress-strain relationships used for the concrete in the tension zone based on the first approach are shown in Figure 2.30. The first relationship, shown in Figure 2.30(a), has stepped diagrams similar to that proposed by Scanlon and Murray(1974), but the number and magnitude of the steps have been reduced in the once-removed and twice-removed layers. The second relationship, shown in Figure 2.30(b), has unloading curves similar to that of Lin and Scordelis, but as in the earlier case, the shapes of the unloading curves have been adjusted to reflect the position of the layers relative to the reinforcement. The third relationship, shown in Figure 2.30(c), has piece-wise linear diagrams with a discontinuity at the initial cracking stress. This third relationship was proposed by Gilbert and Warner. The stress-strain relationship for tensile steel, based on the second technique, is shown in Figure 2.31. The cracked concrete is assumed not to carry any load but an additional stress is carried by the steel. The additional force acting on the steel represents the total internal force carried by the concrete between the cracks. Gilbert and Warner suggested using the second technique as it required considerably less computing time and yet produced good results when compared with the first technique.

The effect of tension stiffening is ignored in the present study because the main concern is to obtain the ultimate loads of frames under short term loading. Though tension stiffening is important around and below the working load regions, it usually has little effect on ultimate loads.

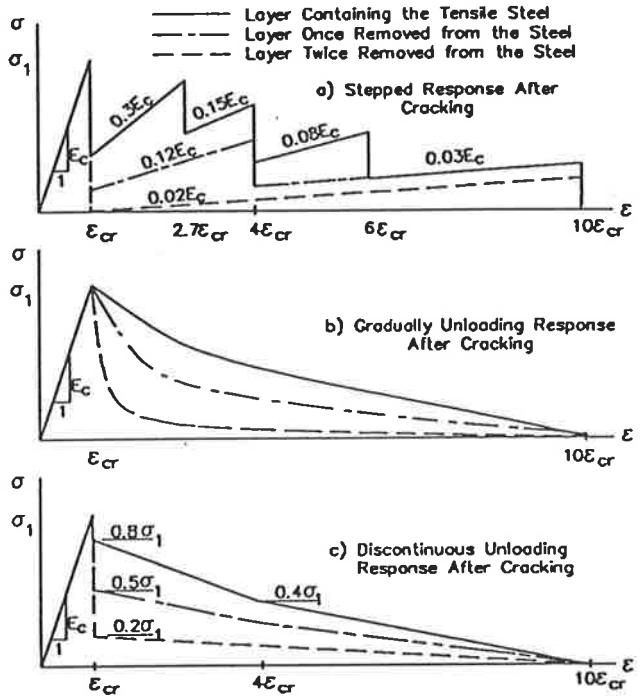

Figure 2.30: Stress-strain diagrams for concrete in tension (Gilbert and Warner, 1978b)

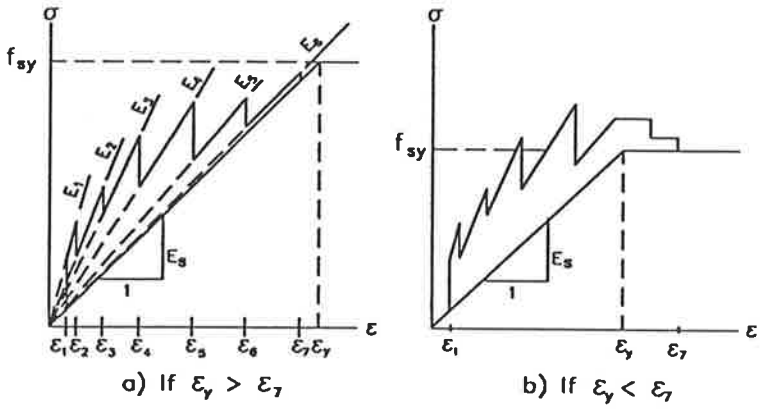

Material Modelling Law:

ε_1	ε_2	ε_3	ε_4	ε_5	ε_6	ε_7
ε_{cr}	$1.5\varepsilon_{cr}$	$3.0\varepsilon_{cr}$	$5.0\varepsilon_{cr}$	$8.0\varepsilon_{cr}$	$11.0\varepsilon_{cr}$	$14.0\varepsilon_{cr}$

E_1	E_2	E_3	E_4	E_5	E_6
$4.0E_s$	$2.7E_s$	$2.0E_s$	$1.6E_s$	$1.15E_s$	$1.05E_s$

Figure 2.31: Modified stress-strain relation for tension steel after cracking (Gilbert and Warner,1978b)

2.7 Summary and Conclusions

The literature review carried out in this chapter looked into different methods to obtain the moment-thrust-curvature relations for reinforced concrete sections. These included the use of direct integration, numerical integration in the form of Gauss quadrature, and the use of summation directly as an approximation to the integrals. From this review, it was decided to adopt the direct summation method in the present study.

Two techniques to obtain axial strain and curvature from known axial force and bending moment were described. The search technique is selected for use in the program SAFRAME.

Two methods for carrying out section analyses for use in structural analysis are described. One relies on the automatic generation of M-κ-N data points; the other uses pre-generated M-κ-N relations. The former is chosen as it requires less input data and thus is less prone to human error. It also allows the effect of thrust to be taken into consideration easily and accurately.

The section analysis routine of program SAFRAME is described. The use of N and κ as inputs and ϵ and M as the output variables improves the efficiency of the routine by reducing the number of search procedures from two to one.

A few factors affecting the M-κ-N relations are discussed and it was found that sectional thrust effect is important in numerical modelling of the behaviour of sections under the influence of a significant amount of thrust.

The tension stiffening effect and its numerical modelling are described. This effect is ignored in the present study as the major concern is to determine the ultimate load of concrete structures. Nevertheless, the techniques described for including the effect of tension-stiffening can be incorporated easily into the present section analysis routine for future studies.

Chapter 3

Methods of Analysis of Reinforced Concrete Structures

3.1 Introduction

In this chapter, several basic methods for the analysis of reinforced concrete structures are reviewed. Section 3.2.1 describes numerical models which take account of material non-linearities. In Section 3.2.2, numerical models which take into account of geometric non-linearities are described. Such elastic analyses which allow only for the effect of geometric non-linearities are useful for approximate analysis and are referred to in existing concrete design standards.

In Section 3.3, the tangent stiffness approach, the secant stiffness approach and the initial stiffness approach are considered as procedures for obtaining solutions for non-linear problems which result from material nonlinearity and/or geometric nonlinearity.

In Section 3.4, several numerical models for the analysis of reinforced concrete frames, including the effect of material non-linearity used by previous researchers, are described and discussed. In some of these analyses, geometrical non-linearity effect is included in the numerical models.

The use of the tangent stiffness, secant stiffness or initial stiffness approach by itself, generally, does not enable the softening behaviour of reinforced concrete frames to be obtained. They have to be used in conjunction with other techniques. Several strategies suitable for tracing the softening behaviour of frames are described and discussed in Section 3.5.

Previous analytical studies of the softening behaviour of reinforced concrete structures are described and discussed in Section 3.6. Several previous proposals for hinge length are also described in this section.

3.2 Nonlinearities

Concrete structures display increasingly non-linear behaviour as they progressively deform under load. There are two major causes of nonlinear behaviour under short-term loading. The first is material nonlinearity resulting from the non-linear stress-strain relationships of concrete and steel, and the nonlinear material unloading effects resulting from material strain reversal. The second is geometric nonlinearities resulting from the deflections along the members and the displacements of the nodes of the frame under loading. For long-term loading, time-dependent material effects such as creep and shrinkage of concrete also contribute to the non-linear behaviour, however, they are not included in the present study.

3.2.1 Material Nonlinearity

Earlier approaches to analyse reinforced concrete frames followed those used for steel structures. Material non-linear effects were considered by assuming that perfect plastic hinges formed at the critically stressed section once their moments reach the plastic moment required for the formation of a "plastic" hinge. These hinges were assumed to be localised at a point.

Bažant et al(1987b) pointed out that when the hinge size is reduced to zero, strain-softening material models give physically meaningless solutions as the energy dissipated tends to zero. This indicates that the approach mentioned above is not suitable for modelling the strain-softening behaviour of concrete structures.

Recognising the limitation of using a point hinge, Cranston(1965a) and Darvall(1983) used hinges with finite length. This allows the softening behaviour of regions to be included in the analysis.

Another shortcoming of using localised hinges is that the positions of potential hinges have to be pre-determined before the analysis as they are modelled to occur at the ends of the elements. The analysis gives errors in predicted peak loads if the positions of pre-assumed hinges do not correspond to the positions of actual hinges. Furthermore, the accurate prediction of the positions of potential hinges is difficult in cases where the frames have complicated load patterns.

The variation of secant stiffnesses along members in a structure is modelled by Aas-Jakobsen and Grenacher(1974) and Gunnin, Rad and Furlong(1977) by discretising entire members into small elements. This approach not only allows the non-linear behaviour at the most highly stressed element to be taken into consideration, but also includes the non-linear effect of all the elements along a member. The position of hinges can be at any of the numerous elements

making up the structure, thereby doing away with the need to pre-assume the positions of concrete hinges.

The advantage of this approach is that it is easy to develop a computer program to carry out the analysis as it requires only the modification of either a linear-elastic frame analysis (Gunnin et al,1977) or a second-order elastic (with geometric nonlinearity built-in) frame analysis (Aas-Jakobsen and Grenacher,1974). The disadvantage of this approach is that it requires a large amount of computer storage and involves the manipulation of large matrices which is inefficient with respect to both storage and program execution speed.

3.2.2 Geometric Nonlinearity

In order to allow for geometric nonlinearities, the equilibrium equations have to be formulated for the deformed frame. This results in nonlinear relationships between loads and displacements. Several procedures to obtain moments and deflections, taking into consideration the effect of geometric nonlinearity are outlined:

3.2.2.1 The P-Δ Method

An iterative method to estimate the second-order shears, moments and forces in an elastic structure, such as a tall building designed for normal deflection limitation, can be obtained by an iterative calculation which make use of fictitious "sway forces" induced by the P-Δ moments (Macgregor,1972). The computation of sway forces involves the use of a first-order elastic analysis to calculate the relative lateral displacements Δ_i in each storey. Additional storey shears due to the vertical loads (assumed to act at floor level) are then calculated as $(\sum P_i\Delta_i)/h_i$, where $\sum P_i$ is the sum of the axial forces in all the

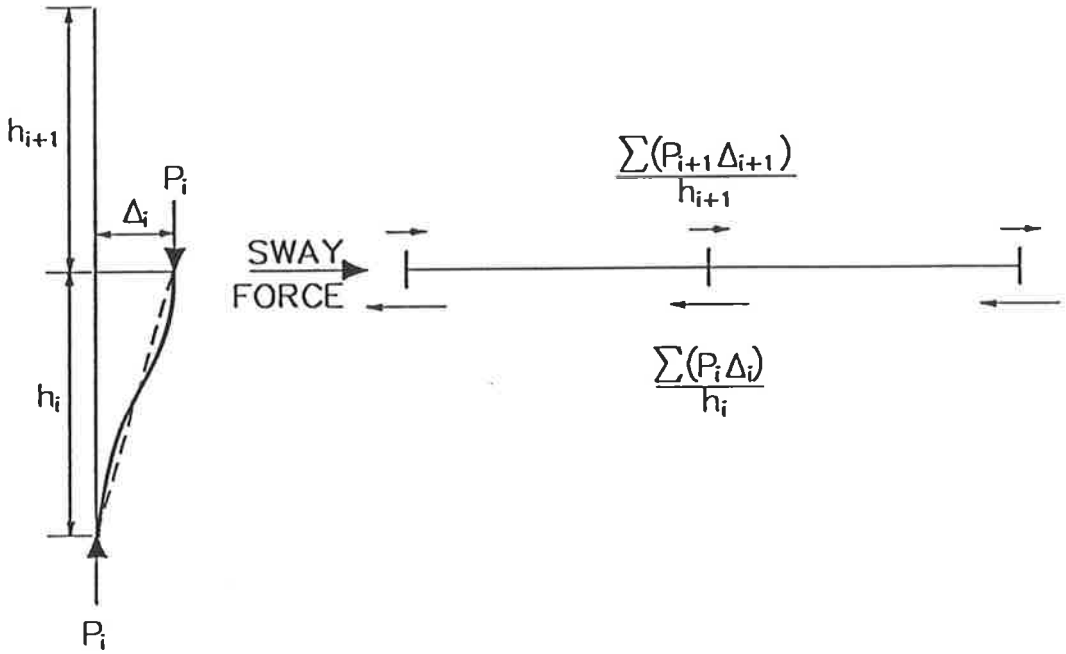

Figure 3.1: Calculation of storey shear (after MacGregor and Hage,1977)

columns of the i-th storey and h_i is the height of the storey. At any given floor level, the sway force is the algebraic sum of the storey shears from the column above and below the floor (see Figure 3.1). The sway forces are then added to the applied lateral loads for the computation of the total forces and moments in the structure in the next iterative cycle. One or two cycles are generally adequate to obtain a converged solution. This method has the advantage that it can be easily understood and requiring only a first order linear elastic method of analysis.

An alternative method proposed by Fey(1966) and Parme(1966) involves the direct determination of the second-order effect without the use of iteration. They have shown that the second-order deflection, Δ_{2i} in the i-th storey of an elastic structure can be evaluated approximately using the equation below:

$$\Delta_{2i} = \frac{\Delta_{1i}}{1 - \frac{\sum P_i \Delta_{1i}}{H_i h_i}} \tag{3.1}$$

where

H_i = shear in the storey due to the applied lateral loads; and

h_i = height of the i-th storey.

A second-order analysis using this method requires:

- A first-order analysis to determine Δ_{1i} in each storey.
- Calculation of the second-order deflection in each storey using Equation 3.1.
- Evaluation of the sway forces as in the case of the iterative method described earlier in this section.
- Carry out another first-order analysis for the frame subjected to the applied vertical and lateral loads, plus the sway forces calculated earlier. This gives the second-order moments and forces.

The methods described above take into consideration the geometric non-linearity effect resulting from the deflection of the joints of the frame but do not allow for the P-Δ effect within the length of the members.

3.2.2.2 Second-Order Finite Element Methods

Solution for second-order analysis, including the effect of geometric nonlinearity, can be obtained more accurately by means of the finite element method (Jennings,1968; Przemieniecki,1968; Gunnin et al,1977).

One commonly used approach is to use a geometric element stiffness matrix k_g to augment the normal element stiffness matrix $\mathbf{k}_e$. Derivation of this matrix is given in a number of publications (Przemieniecki,1968; Young,1973). The

matrix k_g is given below for the case of a prismatic member:

$$\mathrm{k}_g = \frac{N}{L}\begin{bmatrix} 0 & 0 & 0 & 0 & 0 & 0 \\ & \frac{6}{5} & \frac{L}{10} & 0 & -\frac{6}{5} & \frac{L}{10} \\ & & \frac{2L^2}{15} & 0 & -\frac{L}{10} & -\frac{L^2}{30} \\ & SYMME- & & 0 & 0 & 0 \\ & TRIC & & & \frac{6}{5} & -\frac{L}{10} \\ & & & & & \frac{2L^2}{15} \end{bmatrix} \tag{3.2}$$

where

N = axial force acting on the element; and

L = the length of the element.

The secant stiffness matrix of the member k is obtained from:

$$\mathrm{k} = \mathrm{k_e} + \mathrm{k_g} \tag{3.3}$$

This approach was used by Aas-Jakobsen and Grenacher (1974) to include the P-Δ effect along the members, and a solution procedure using this approach is described in greater detail in Section 3.4.1.

Another approach is to use an updated Lagrangian formulation which separates the effect of pure member deformations from the joint displacements. This is achieved by introducing a local, convective reference system attached to the members. Jennings(1968) has derived matrices based on this approach. With this approach it is possible to determine the behaviour of an elastic skeletal plane structure until it has deformed so much that the deformed shape bears little resemblance to its original configuration (Jenning,1968; Meek and Tan,1983).

Yet another approach is to ignore deformations within the length of the elements and assume that changes in geometry are reflected only by node point movements (Gunnin et al,1977; Saafan and Brotton,1962; Oran,1973; Oran

and Kassimali, 1976). The deformed shape of the structure, specified by the most recent position of the nodes, is used for the transformation of forces. An iterative technique is used to calculate the out-of-balance forces at the nodes at each iterative cycle and the forces are added to the load to be used for the next iterative forces until these out-of-balance forces are negligible. When this occurs, an equilibrium position has been obtained for the frame in its deformed configuration. Ignoring the P-Δ effect within the length of a member can always be made acceptable by including a sufficient number of nodes along the deformed member to trace its deflected shape. This has the effect of shortening the length of the element and thereby reducing the inaccuracy caused by not taking the P-Δ effect along the element into consideration.

3.3 Analysis for Frames with Non-linear Behaviour

The non-linear behaviour of a frame under load cannot be determined in a direct manner, and iterative techniques therefore have to be developed. Repeated cycles of linear analysis usually provide the basis for the solutions. One such iterative approach, commonly referred to as the Newton-Raphson or tangent stiffness approach is described in the text by Livesley (1975). This approach is illustrated in Figure 3.2a. For the first iterative cycle, the starting point is chosen to be at displacement zero. The structural stiffness at this point is K_o. Using this stiffness, the deformation of the frame Δ_1 is obtained from the relation:

$$\Delta_1 = \frac{\lambda_w}{K_o} \tag{3.4}$$

where λ_w is the total applied load.

For the displacement Δ_1, the corresponding load level λ_1 is determined, and hence the structural stiffness at this stage is updated to K_1. The out-of-balance

load is $(\lambda_w - \lambda_1)$. A second iterative cycle is then carried out to get a better estimate of the deformation using the relation:

$$\Delta_2 = \Delta_1 + \frac{\lambda_w - \lambda_1}{K_1} \tag{3.5}$$

Thus, for the i-th iteration:

$$\Delta_i = \Delta_1 + \Delta_2 + \ldots + \Delta_{i-1} + \frac{\lambda_w - \lambda_{i-1}}{K_{i-1}} \tag{3.6}$$

In the above equation, the calculation of K_{i-1} includes the effect of all non-linearities.

Iterations are carried out until either the out-of-balance load at the end of the iterative cycle, or the change in deformation between successive iterative cycles, is less than a pre-determined tolerance.

The process described above will not converge if the starting point is too far away from the solution (Livesley,1975). This can be overcome by dividing the load into numerous load steps. The solution of each load step is obtained in turn, starting from the first increment, until the final load is reached. The starting point of each load step is taken to be the converged solution point of the previous load step. This approach has the advantage that in addition to obtaining the final solution point, the entire loading path up to this point is also obtained.

Variations to the tangent stiffness approach have been used by other researchers. The commonly used variations are the secant stiffness approach and the initial stiffness approach. Both these approaches are similar to the tangent stiffness approach except that different stiffnesses are used. As the name suggests, the secant stiffness approach makes use of the secant structural stiffness throughout the analysis (Figure 3.2b). In the initial stiffness approach, the stiffness at the beginning of the first cycle is used throughout the analysis (Figure 3.2c).

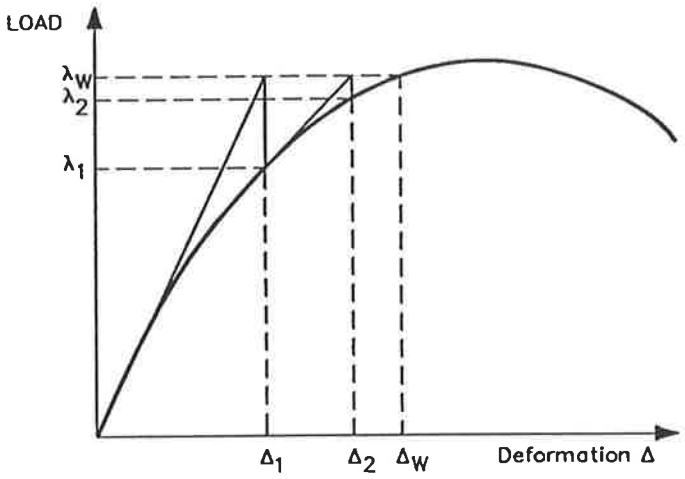

(a) Tangent Stiffness Approach

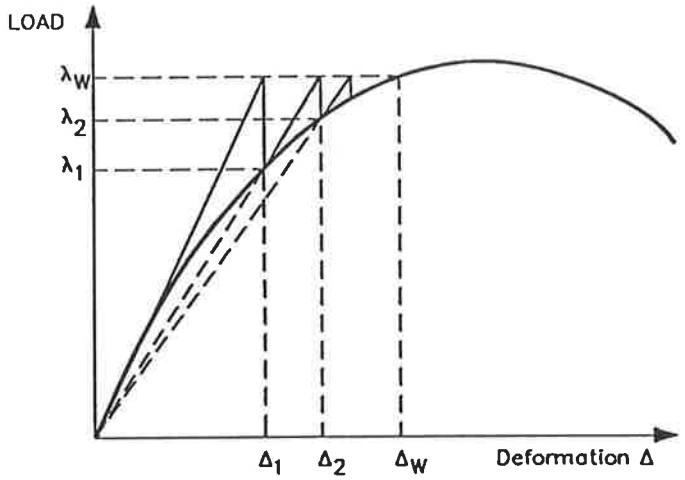

(b) Secant Stiffness Approach

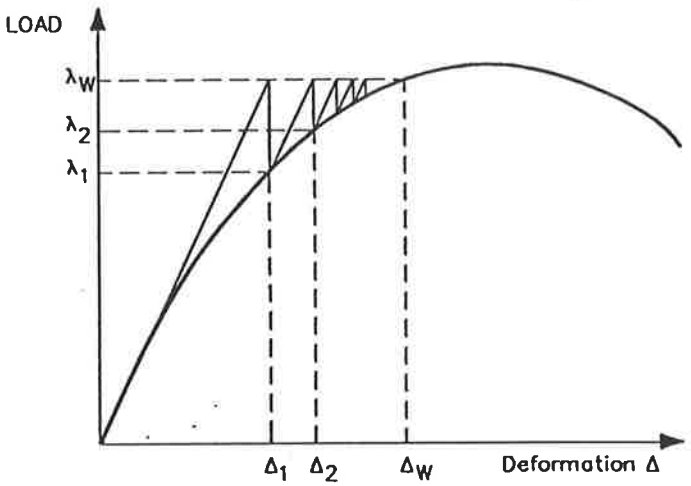

(c) Initial Stiffness Approach

Figure 3.2: Iterative solution techniques for non-linear problem

Of the three approaches described earlier, the tangent stiffness approach requires the least number of cycles to obtain the solution for a given load step. This can be seen in Figure 3.2.

Both the tangent stiffness approach and the secant stiffness approach require the updating of the structural stiffness matrix (to reflect the most recent state of the structure, including non-linear effects) at the beginning of each cycle. In contrast, the initial stiffness approach uses the initial stiffness throughout the analysis, thereby eliminating the considerable effort required to update the stiffness matrix. The initial stiffness approach requires more cycles to obtain a solution for a given load step as compared to the other two approaches. This approach is suitable for structures with stiffnesses that do not change change much with loading and is therefore not suitable for highly non-linear structures.

Though all three techniques described earlier are suitable for analysis up to the peak load, they generally fail to give a satisfactory solution beyond this point. This is due to: (1) the tangent stiffness of the frame being zero at the peak load;(2) the multiple stable solutions available for a single value of load; and (3) snapback instabilities in softening structures caused by some parts of the structures either unloading as a result of strain-softening or strain-reversal. Strategies for predicting post-limit response have been proposed by previous researchers and some of these are described in Section 3.5.

3.4 Non-linear Analysis of Concrete Frames

In modelling the behaviour of reinforced concrete frames it is common practice to use a large number of line elements. The stiffness of an element is normally assumed to be uniform within its length and is determined from the behaviour of a section at mid-length. Based on the moment-curvature thrust relations

of this section, the stiffness of each element in the structure, and hence of the entire structure, is determined. It is common in this approach to follow the non-linear behaviour of the frame by iteratively solving an equivalent elastic frame with the element properties being updated at each iteration by means of a non-linear section analysis carried out for a section in each element.

This approach was used by Aas-Jakobsen and Grenacher (1974) and Gunnin, Rad and Furlong (1977). This approach will be referred to in this thesis as the line element approach.

An alternative approach for modelling concrete frames is to use the properties of layered elements directly in the formation of the element stiffness matrix. In this approach, section analyses to obtain moment-curvature thrust relations are not required. The layers are used to model the behaviour of the steel reinforcement and concrete within the elements. This approach was used by Bažant et al(1987a); Blaauwendraad (1972); Kreonke, Gutzwiller and Lee (1973); Menegotto and Pinto (1974); Aldstedt and Bergan (1974);and Kang and Scordelis (1980) for the analysis of frames. A similar approach was also used for the analysis of slabs by Gilbert and Warner (1978b). In this approach, the entire frame is modelled by elements consisting of steel and concrete layers. The terms in the element stiffness matrix are formed directly from the stress-strain relationships of the materials of the layers making up the elements. This approach will be referred to as the layered element approach.

Numerical models based on the line element approach and those based on the layered approach are presented in Section 3.4.1 and 3.4.2, respectively.

3.4.1 Line Element Approach

Lazaro and Richards (1973) used a procedure which they referred to as the "successive linear approximation" approach (Lazaro and Richards,1973). This

approach is similar to that of Becker (1967, cited by Lazaro and Richards,1973) who modified a flexibility approach developed by Cranston(1965a) for simple frames.

The approach of Lazaro and Richards involves the modification of an existing stiffness approach for elastic frames to analyse reinforced concrete structures. The authors stated that this approach is superior to the plastic mechanism approach for the determination of collapse load as it eliminates the guesswork required to determine all possible failure modes in the latter approach.

According to Lazaro and Richards, the method developed can be divided into two main phases. The first phase involves the formulation of the stiffness coefficients and the fixed end forces, and the solution of the resulting simultaneous equations for the joint forces and displacements as in the case of a normal stiffness approach for an elastic structure. In the second phase the cross-section properties of the elements are modified as the analysis progresses. Geometric nonlinearities were not considered in the method. The method is illustrated by Lazaro and Richards using the flow diagram reproduced in Figure 3.3.

Aas-Jakobsen and Grenacher (1974) proposed a non-linear analysis of concrete frames which takes into account both material and geometric nonlinearities.

In this method, the concrete frame to be analysed is discretised into numerous line elements. Each of these elements is assumed to be uniform, having axial and flexural stiffnesses equal to those of the sections at mid-length of the elements. Loading is assumed to be applied only to the nodes.

A displacement control, secant stiffness approach was used. For each value of the specified displacement w (chosen to be the sway displacement at beam level by Aas-Jakobsen and Grenacher), the corresponding load factor λ is obtained interactively. First, stiffnesses are assumed for all the elements. The

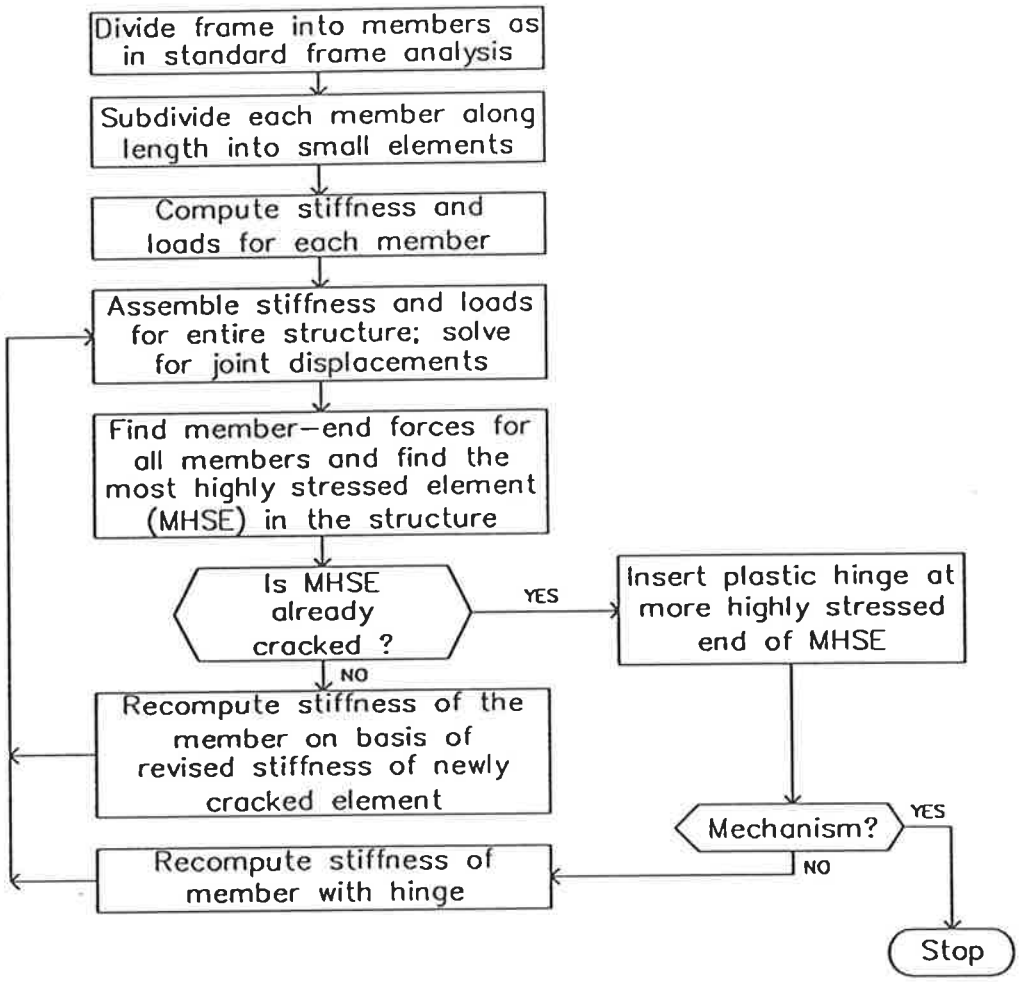

Figure 3.3: Successive Linear Approximation Method (Lazaro and Richards, 1973)

load factor is then increased in steps until the calculated and specified displacement coincide. Updated axial and flexural stiffnesses are then obtained from a cross sectional analysis taking into consideration the stress-strain relationship of both the concrete and reinforcing steel. The procedure is repeated until agreement is obtained between the assumed and calculated stiffnesses. The displacement control procedure enables the onset of instability of the frame to be determined.

Geometric nonlinearity within the elements, caused by the interaction of axial forces with deflections, is accounted for by the addition of a non-linear geometric stiffness matrix k_g to the normal first order elastic stiffness matrix k_e. These two matrices are given in Figure 3.4. Derivation of the k_g matrix can be found in a number of papers and texts (Przemieniecki, 1968; Young, 1973).

For the start of the analysis the axial forces in the elements are assumed to be zero and the stiffnesses of the elements are calculated from uncracked gross section properties. The element stiffness matrix in local co-ordinates is formed from the expression below:

$$k = k_e + k_g \tag{3.7}$$

Using standard procedures (Hall and Kabaila, 1977; Cheung and Yeo, 1979), the global stiffness matrix K of the structure is obtained. The equilibrium relation of the structure is:

$$Q = K \times D \tag{3.8}$$

where

Q = load vector in the structural system; and

D = deformation vector in the structural system.

Solving the equations above gives nodal deformations which in turn enables nodal forces to be obtained. From these, the updated axial and flexural stiff-

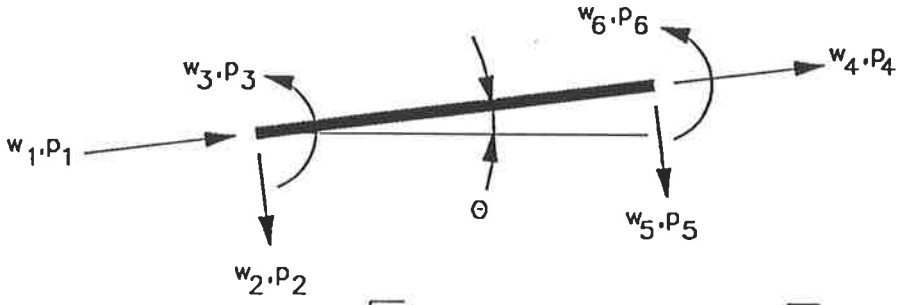

$$[k_e] = \begin{bmatrix} \frac{EA}{L} & 0 & 0 & -\frac{EA}{L} & 0 & 0 \\ & \frac{12EI}{L^3} & \frac{6EI}{L^2} & 0 & -\frac{12EI}{L^3} & \frac{6EI}{L^2} \\ & & \frac{4EI}{L} & 0 & -\frac{6EI}{L^2} & \frac{2EI}{L} \\ & & & \frac{EA}{L} & 0 & 0 \\ & \text{SYMMETRIC} & & & \frac{12EI}{L^3} & -\frac{6EI}{L^2} \\ & & & & & \frac{4EI}{L} \end{bmatrix}$$

(a) First–order stiffness matrix

$$[k_g] = N \begin{bmatrix} 0 & 0 & 0 & 0 & 0 & 0 \\ & \frac{6}{5L} & \frac{1}{10} & 0 & -\frac{6}{5L} & \frac{1}{10} \\ & & \frac{2L}{15} & 0 & -\frac{1}{10} & -\frac{L}{30} \\ & & & 0 & 0 & 0 \\ & & & & \frac{6}{5L} & -\frac{1}{10} \\ & \text{SYMMETRIC} & & & & \frac{2L}{15} \end{bmatrix}$$

(b) Second–order geometric stiffness matrix

$$[T] = \begin{bmatrix} c & s & 0 & 0 & 0 & 0 \\ -s & c & 0 & 0 & 0 & 0 \\ 0 & 0 & 1 & 0 & 0 & 0 \\ 0 & 0 & 0 & c & s & 0 \\ 0 & 0 & 0 & -s & c & 0 \\ 0 & 0 & 0 & 0 & 0 & 1 \end{bmatrix}$$

NOTE:
C = COS Θ
S = SIN Θ

(c) Transformation matrix

Figure 3.4: First order and second order element stiffness matrices

nesses are obtained from the moment-curvature relations. These updated values are then used in the analysis for the next cycle. Iterative cycles are carried out until the stiffnesses converge.

The analysis of Aas-Jakobsen and Grenacher is illustrated by the flowchart shown in Figure 3.5. This procedure is not suitable for obtaining post collapse behaviour of frames.

In the form proposed by Aas-Jakobsen and Grenacher, the method does not take into consideration the geometric non-linearity caused by the moving of the joints as the structure deformed. The modelling of the material nonlinearity effect by using numerous elements results in the need to store and manipulate large matrices. This results in inefficiency with respect to storage and program execution time.

Gunnin, Rad and Furlong (1977) proposed a line element approach which differs from that proposed by Aas-Jakobsen and Grenacher in that it not only includes the effect of the geometric nonlinearity caused by the lateral deformation of the members but it also includes the geometric nonlinearity caused by the displacements of the joints during loading. The movement of the joints is included in the analysis by updating the positions of the nodes (by modifying the transformation matrices of the elements). The out-of-balance nodal forces for the frame under loading are calculated and these are used to adjust the applied forces until the out-of-balance nodal forces become zero. When this occurs, an equilibrium position has been obtained for the deformed frame under the prescribed loading.

This, as in the case of the earlier method, requires large number of elements and suffers the same inefficiency.

Darvall and Mendis(1985) proposed a method to carry out analysis of softening frames. This method differs from those described earlier in that the

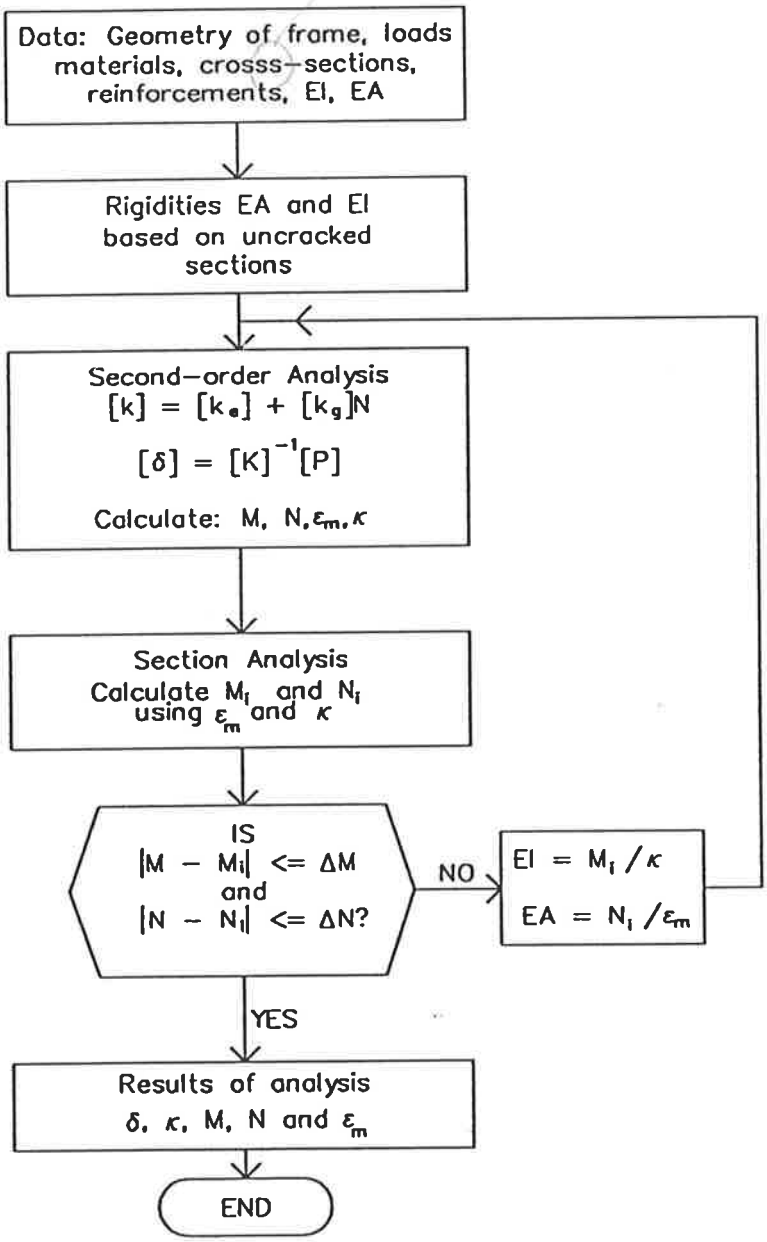

Figure 3.5: Flowchart illustrating approach of Aas-Jakobsen and Grenacher (1974)

structure stiffness matrix is formed from elements which can soften at the ends. This was an extension of an earlier approach proposed by Darvall (1983) to study softening effects in concrete structures to include the effect of geometric nonlinearities. The softening behaviour of a typical element is defined by the softening length l_p and the linearised moment curvature relationship of typical sections.

The linearised moment-curvature relationship is assumed to be made up of three portions, a linear elastic, a plastic and finally a linear softening branch. Parameters a and b control the degree of softening of the finite-length hinge at the left and right end of the beam respectively (see Figure 3.6). Beam tests carried out by Darvall and Mendis suggested that the linearised relationship is a reasonable model for the behaviour of reinforced concrete sections without thrust.

Mendis and Darvall(1987) derived stability functions for elements with softening hinges at the ends of the elements. Such an element is shown in Figure 3.6. The functions proposed reduce to the well known stability functions of Livesley and Chandler(1956) for a beam without any plasticity. The accuracy of this approach depends on the values of the hinge lengths used in the elements. To obtain good accuracy these values need to be comparable with the actual values in the real structures. The behaviour of concrete hinges depends on many factors, some of these being thrust, amount of reinforcement and shear force. Extensive test programs must therefore be carried out to determine suitable hinge length values for different types of elements. The positions of potential hinges are constrained to occur at the end of the elements. To obtain accurate modelling of the behaviour of frames, finite elements have to be placed correctly in the computer model so that the hinge positions of the computer model correspond to the actual hinge positions in the real structure. The position of hinges cannot always be determined with certainty, especially in building frames under a combination of imposed loading on the beams and wind load-

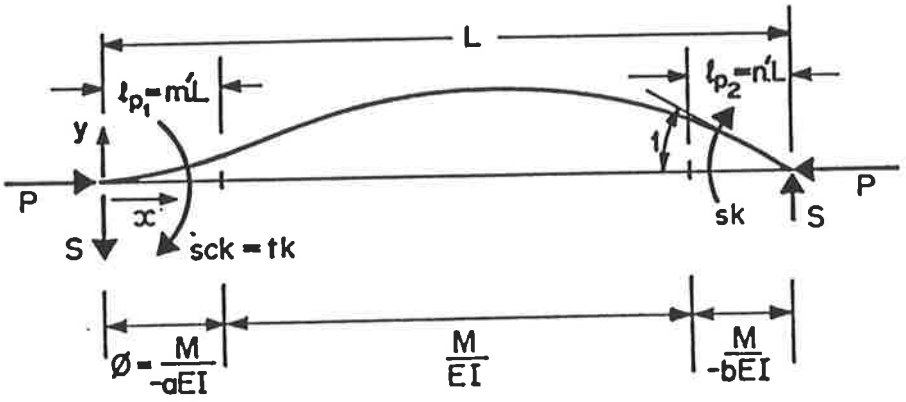

Figure 3.6: Beam with concrete hinges (Mendis and Darvall,1987)

ing at floor levels. In such cases some trial and error would presumably be required to locate the hinges.

The effect of sectional thrust on the moment-curvature relation which affects the behaviour of softening hinges cannot easily be incorporated into the analysis. This would require the pre-generation and pre-linearisation of the moment-curvature relations for key sections along the elements. An alternative approach which requires less input data is to automatically generate the moment and curvature values as and where required during the analysis.

3.4.2 Layered Element Approach

Blaauwendraad (1972) used a layered finite element technique to model reinforced concrete frames. The structure is divided into members and the

members are divided into layers of concrete and reinforcing steel. To take into consideration the varying position of the centroidal axis resulting from cracking and plasticfication, he assumed a parabolic variation of u along a fixed reference axis, where u is the axial deformation.

He included geometrical nonlinearities in his formulation: these include the effect of axial deformation along the members, and the effect of movements of the ends of the members as a result of loading. Hence, he included all the geometrical nonlinearities likely to be present in a structure.

Retaining the author's notations, the formulation relating the member end forces $\mathbf{k^e}$ and deformations $\mathbf{v^e}$ (Figure 3.7) is:

$$\mathbf{k^e} = \mathbf{S^e v^e} \tag{3.9}$$

$$\text{where} \quad \mathbf{k^e} = \begin{bmatrix} H_i & V_i & M_i & H_j & V_j & M_j \end{bmatrix}^T \tag{3.10}$$

$$\text{and} \quad \mathbf{v^e} = \begin{bmatrix} u_i & v_i & \phi_i & u_j & v_j & \phi_j \end{bmatrix}^T \tag{3.11}$$

The member stiffness matrix $\mathbf{S^e}$ in global co-ordinates given in Equation 3.9 is obtained from the expression below:

$$\mathbf{S^e} = \mathbf{C^T S^o_\epsilon C} + \Delta \mathbf{S^{nn}} \tag{3.12}$$

$$\text{where} \quad \mathbf{S^o_\epsilon} = \mathbf{S_{\epsilon\epsilon}} - \mathbf{S_{\epsilon u} S_{uu}^{-1} S_{u\epsilon}} \tag{3.13}$$

$$\mathbf{S_{\epsilon\epsilon}} = \begin{bmatrix} S_{22} & S_{23} & S_{24} \\ S_{23} & S_{33} & S_{34} \\ S_{24} & S_{34} & S_{44} \end{bmatrix} \tag{3.14}$$

$$\mathbf{S_{\epsilon u}} = \begin{bmatrix} S_{12} & S_{13} & S_{14} \end{bmatrix}^T \tag{3.15}$$

$$\mathbf{S_{u\epsilon}} = \begin{bmatrix} S_{12} & S_{13} & S_{14} \end{bmatrix} \tag{3.16}$$

$$\mathbf{S_{uu}} = [S_{11}] \tag{3.17}$$

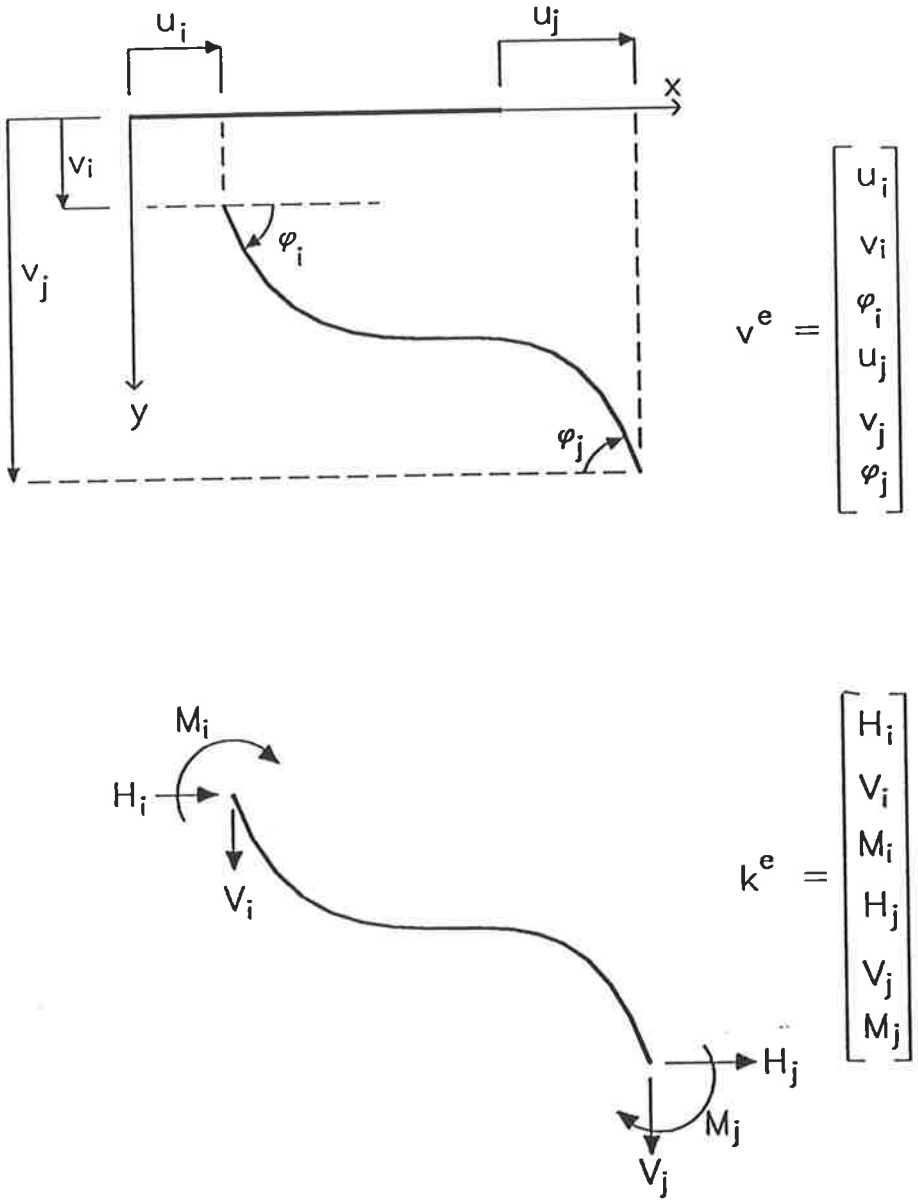

Figure 3.7: Displacements $\mathbf{v}^e$ and member end forces $\mathbf{k}^e$ in the e^{th} member (after Blaauwendraad, 1972)

$$\text{where} \quad S_{11} = \frac{1}{L}\int_0^1 (4-8\phi)^2\, D_{11}\, d\phi \tag{3.18}$$

$$S_{12} = \frac{1}{L}\int_0^1 (4-8\phi)\, D_{11}\, d\phi \tag{3.19}$$

$$S_{13} = \frac{1}{L}\int_0^1 (4-8\phi)(4-6\phi)\, D_{12}\, d\phi \tag{3.20}$$

$$S_{14} = \frac{1}{L}\int_0^1 (4-8\phi)(2-6\phi)\, D_{12}\, d\phi \tag{3.21}$$

$$S_{22} = \frac{1}{L}\int_0^1 D_{11} d\phi \tag{3.22}$$

$$S_{23} = \frac{1}{L}\int_0^1 (4-6\phi)\, D_{12}\, d\phi \tag{3.23}$$

$$S_{24} = \frac{1}{L}\int_0^1 (2-6\phi)\, D_{12}\, d\phi \tag{3.24}$$

$$S_{33} = \frac{1}{L}\int_0^1 (4-6\phi)^2\, D_{22}\, d\phi \tag{3.25}$$

$$S_{34} = \frac{1}{L}\int_0^1 (2-6\phi)(4-6\phi)\, D_{22}\, d\phi \tag{3.26}$$

$$S_{44} = \frac{1}{L}\int_0^1 (2-6\phi)^2\, D_{22}\, d\phi \tag{3.27}$$

$$\text{where} \quad D_{11} = EA \tag{3.28}$$

$$D_{21} = y_z EA \tag{3.29}$$

$$D_{12} = D_{21} \tag{3.30}$$

$$D_{22} = EI + y_z^2 EA \tag{3.31}$$

where

E = secant modulus of material;

A = cross-sectional area;

I = second moment of area of the layer under consideration;

ϕ = x/L where L is the length of the member and x is the horizontal distance measured from the centroid of the layer to the left end of the member; and

y_z = distance measured from the centroidal axis of the layer to the chosen reference axis.

The term $\Delta \mathbf{S}^{\mathbf{nn}}$ in Equation 3.12 takes into consideration the effect of geo-

metrical nonlinearities. The expression for this term is:

$$\Delta S^{nn} = C^T S_\epsilon^n C + \Delta S^n \tag{3.32}$$

$$\text{where} \quad \Delta S^n = \begin{bmatrix} 0 & 0 & 0 & 0 & 0 & 0 \\ 0 & \frac{N}{L} & 0 & 0 & -\frac{N}{L} & 0 \\ 0 & 0 & 0 & 0 & 0 & 0 \\ 0 & 0 & 0 & 0 & 0 & 0 \\ 0 & -\frac{N}{L} & 0 & 0 & \frac{N}{L} & 0 \\ 0 & 0 & 0 & 0 & 0 & 0 \end{bmatrix} \tag{3.33}$$

$$\text{and} \quad S_\epsilon^n = \begin{bmatrix} 0 & 0 & 0 \\ 0 & \frac{2NL}{15} & -\frac{NL}{30} \\ 0 & -\frac{NL}{30} & \frac{2NL}{15} \end{bmatrix} \tag{3.34}$$

The transformation matrix C in Equations 3.12 and 3.32 is given by the expression:

$$C = \begin{bmatrix} -1 & 0 & 0 & 1 & 0 & 0 \\ 0 & \frac{1}{L} & 1 & 0 & -\frac{1}{L} & 0 \\ 0 & \frac{1}{L} & 0 & 0 & -\frac{1}{L} & 0 \end{bmatrix} \tag{3.35}$$

The solution procedure is illustrated in Figure 3.8 by a flow diagram reproduced from Blauuwendraad's paper (Blauuwendraad, 1972). First a reference axis is chosen for each member. At the start of the analysis axial thrust N is assumed to be zero and the modulus of elasticity E is taken to be the value at the origin of the stress-strain diagram. Matrix S_ϵ^o is obtained using Expression 3.13. Matrix ΔS^{nn} is obtained using Expression 3.32. The total element stiffness matrix in global co-ordinates S^e is then obtained from Expression 3.12. The assembling of the global stiffness matrix S from the element stiffness matrices follows the normal procedure as that for a linear analysis. The global displacement matrix v is obtained by solving the following equation:

$$Sv = k \tag{3.36}$$

where k is the load matrix in the global co-ordinates.

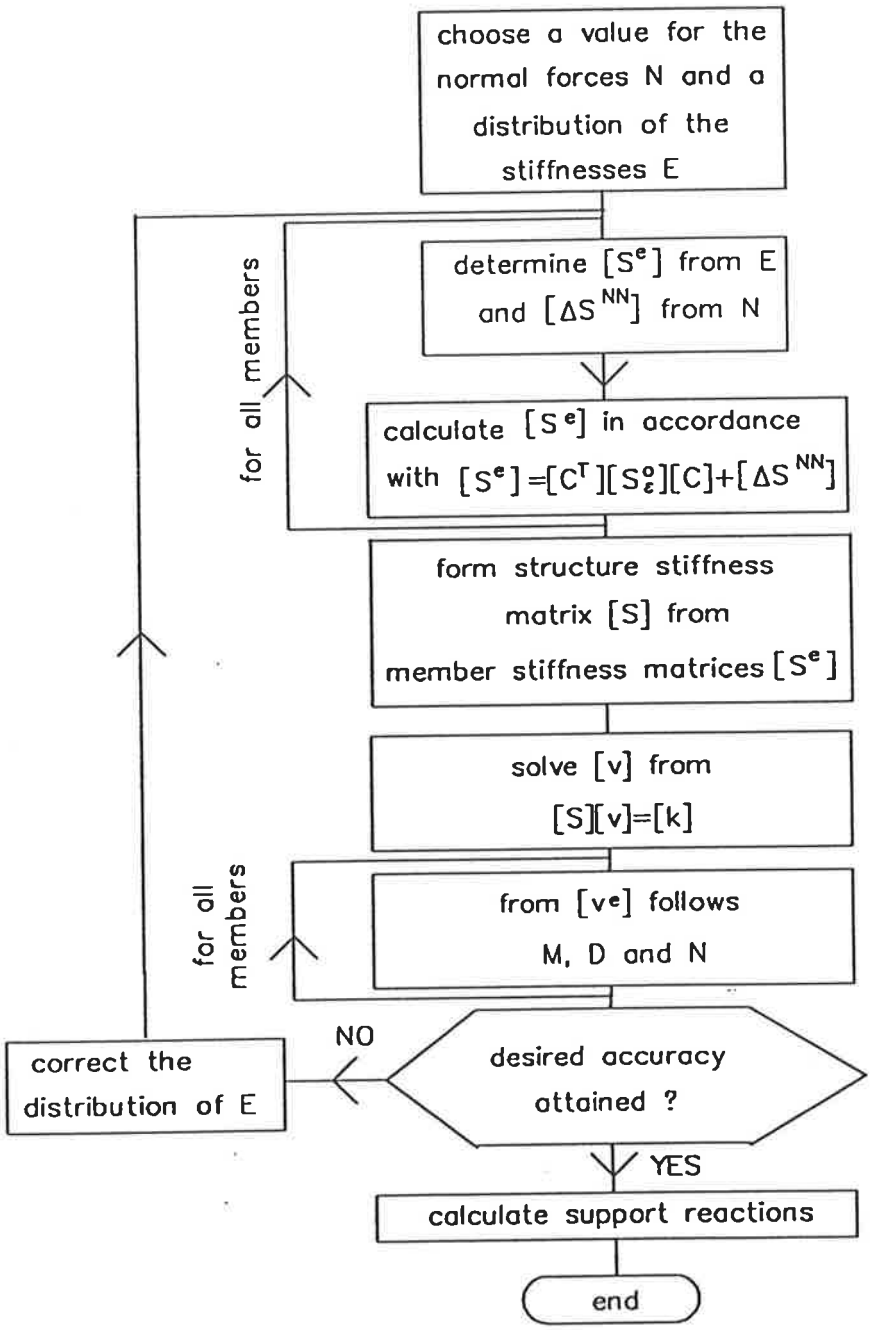

Figure 3.8: Flow diagram for non-linear analysis of frame using Blaauwendraad's approach(after Blaauwendraad, 1972)

Member displacements $\mathbf{v^e}$ and axial thrusts N are then obtained for all the members and an updated $\mathbf{S^e}$ is then used for the next cycle of calculations.

The updating of E for each layer is carried out by using information obtained from the displacement matrix $\mathbf{v^e}$. From this matrix, the axial extension at midspan of a typical member u_k and the rotations at the ends of the member θ_i and θ_j are obtained thus:

$$\theta_i = \phi_i - \frac{(v_j - v_i)}{L} \tag{3.37}$$

$$\theta_j = \phi_j - \frac{(v_j - v_i)}{L} \tag{3.38}$$

$$u_k = -\frac{S_{12}}{S_{11}}(u_j - u_i) - \frac{S_{13}}{S_{11}}\theta_i - \frac{S_{14}}{S_{11}}\theta_j \tag{3.39}$$

Based on known values of u_i, u_j, u_k, θ_i and θ_j, the strain at reference level ϵ_g and the curvature κ are calculated from the expressions :

$$\epsilon_g = \frac{v_j - v_i}{L} + \frac{4L - 8x}{L^2}u_k \tag{3.40}$$

$$\kappa = \frac{4L - 6x}{L^2}\theta_i + \frac{2L - 6x}{L^2}\theta_j \tag{3.41}$$

Once ϵ_g and κ are known, the strain distribution across the section is known. The modulus of elasticity for each layer can then be obtained from known stress-strain relationship of the material.

The derivations for all the formulae given above for this approach can be found in the paper by Blaauwendraad (1972).

Bažant, Pijaudier-Cabot and Pan(1987a) also used the layered finite element approach (Zienkiewicz,1977) for the analysis of some softening beams and symmetrically loaded frames. Geometrical non-linearities are not included in the analysis. Their analysis was based on a secant stiffness approach using deflection control. The entire structure is divided into a number of elements. The secant stiffness matrix generated includes the effect of variation of stiffness across the section and along the elements. Sections are divided into finite layers

and the section properties are obtained by summation of all the concrete and steel layers as an approximation to the integration required. He used a linear shape function for the axial deformation along the arbitrary chosen reference axis. Bažant et al used a deflection control procedure to follow the softening behaviour of reinforced concrete structures. The derivations of the matrices, reproduced from the paper by Bažant et al(1987a), are given in Appendix C.

Kulicki and Kostem (1974) earlier used an approach similar to that of Bažant et al(1987a). Instead of using one matrix, two matrices were used to form the element stiffness matrix in their studies on the behaviour of concrete beam columns. These matrices are $\mathbf{k}_e$ and the geometrical stiffness matrix $\mathbf{k}_g$. The element stiffness matrix $\mathbf{k}_e$ is of the same form as that used by Bažant et al except that they used a tangent stiffness formulation.

Kang and Scordelis (1980) used a tangent stiffness approach for the analysis of reinforced and prestressed concrete structures. In obtaining the tangent stiffness matrices of members, layer integration for the steel reinforcement and concrete is carried out at the centre of the elements. However, in the evaluation of the internal resisting forces, Gaussian quadrature integration is based on three points along the element.

The modelling of a structure using this approach is shown in Figure 3.9. The structure is divided into numerous elements with each having the usual six degrees of freedom at the ends. The standard shape functions along the elements are assumed to be linear for the axial displacements and cubic for the transverse displacements. Shear deformation was not included in the analysis. The local co-ordinate system of each element passes through the ends of the element, and is assumed to follow the element as it deforms. This approach where the local co-ordinate system changes with the deformed shape of the structure is commonly referred to as the updated Lagrangian approach.

The nonlinear geometric effect within the element is taken into consideration

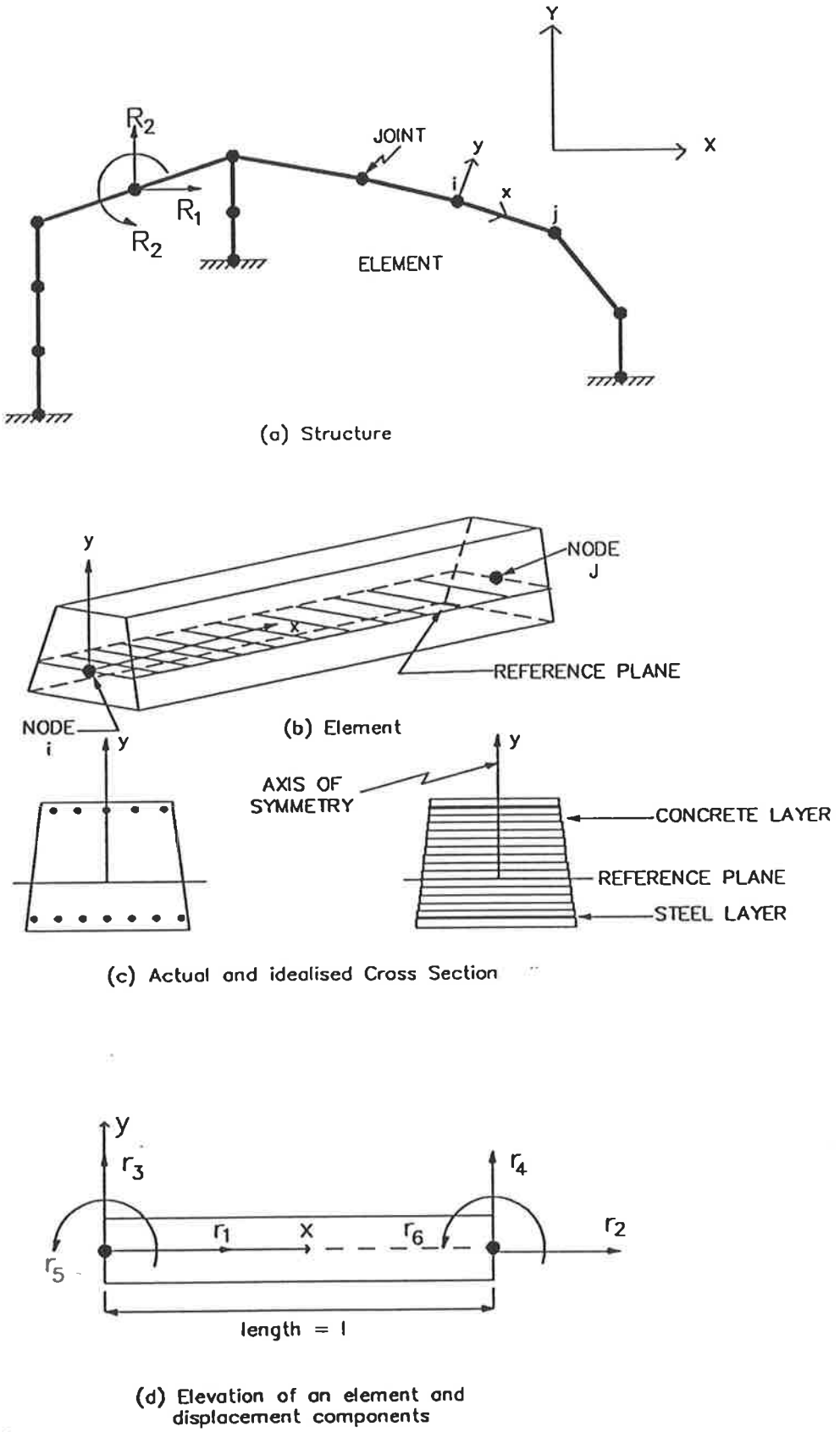

Figure 3.9: Modelling of structure using approach of Scordelis and Kang(1980)

by adopting a nonlinear geometric stiffness matrix $\mathbf{k}_g$. The nodal positions and the element transformation matrix between local and global co-ordinates are regularly updated.

The cross section at mid-element is assumed to be representative of the sections along the element when forming the element stiffness matrix. The section, symmetrical about the local y-axis, is divided into concrete and steel layers. Each of these layers is assumed to be under uniaxial strain.

Other basic assumptions made in the analysis are:(1) plane section remains plane after bending, and (2) bond slip does not occur between the interface of the reinforcing bars and the concrete.

Employing the unusual order used by the authors for labelling the degrees of movement, the incremental equilibrium equation relating incremental load $d\mathbf{q}$ to incremental nodal displacement $d\mathbf{r}$ in the local co-ordinate system is:

$$\mathbf{k}_t \, d\mathbf{r} = d\mathbf{q} \tag{3.42}$$

$$where \quad \mathbf{k}_t = \mathbf{k}_e + \mathbf{k}_g \tag{3.43}$$

$$and \quad \mathbf{r} = \begin{bmatrix} r_1 & r_2 & r_3 & r_4 & r_5 & r_6 \end{bmatrix}^T \tag{3.44}$$

$$and \quad \mathbf{q} = \begin{bmatrix} q_1 & q_2 & q_3 & q_4 & q_5 & q_6 \end{bmatrix}^T \tag{3.45}$$

The component stiffness matrices $\mathbf{k}_e$ and $\mathbf{k}_g$ are given below:

$$\mathbf{k}_e = \begin{bmatrix} \frac{EA}{L} & -\frac{EA}{L} & 0 & 0 & \frac{ES}{L} & -\frac{ES}{L} \\ & \frac{EA}{L} & 0 & 0 & -\frac{ES}{L} & -\frac{ES}{L} \\ & & 12\frac{EA}{L^3} & 12\frac{EA}{L^3} & 6\frac{EI}{L^2} & 6\frac{EI}{L^2} \\ & & & 12\frac{EA}{L^3} & -6\frac{EI}{L^2} & -6\frac{EI}{L^2} \\ & & SYMMETRIC & & 4\frac{EI}{L} & 2\frac{EI}{L} \\ & & & & & 4\frac{EI}{L} \end{bmatrix} \tag{3.46}$$

$$\mathrm{k}_g = \begin{bmatrix} 0 & 0 & 0 & 0 & 0 & 0 \\ & 0 & 0 & 0 & 0 & 0 \\ & & \frac{6N}{5L} & -\frac{6N}{5L} & \frac{N}{10} & \frac{N}{10} \\ & & & \frac{6N}{5L} & -\frac{N}{10} & -\frac{N}{10} \\ & & SYMMETRIC & & \frac{2NL}{15} & -\frac{NL}{30} \\ & & & & & \frac{2NL}{15} \end{bmatrix} \tag{3.47}$$

$$\text{where} \quad EA = \sum_{i=1}^{n_c} E_{ci}A_{ci} + \sum_{i=1}^{n_s} E_{si}A_{si} \tag{3.48}$$

$$\text{and} \quad ES = -\sum_{i=1}^{n_c} E_{ci}y_{ci}A_{ci} - \sum_{i=1}^{n_s} E_{si}y_{si}A_{si} \tag{3.49}$$

$$\text{and} \quad EI = \sum_{i=1}^{n_c} E_{ci}y_{ci}^2A_{ci} + \sum_{i=1}^{n_s} E_{si}y_{si}^2A_{si} \tag{3.50}$$

where n_c and n_s are the number of concrete and steel layers respectively, and the subscripts c and s refers to the concrete and steel respectively.

The structure or global tangent stiffness matrix $\mathbf{K}_t$ is assembled from the element tangent stiffness using standard procedures (Hall and Kabaila, 1977; Cheung and Yeo, 1979).

For a typical step where the load increment is $\Delta\mathbf{Q}$, iterative cycles are carried out to obtain convergence. Within each cycle, the tangential equilibrium Equation 3.51 for the structure is solved for global displacement increments, $\Delta\mathbf{R}$. These increments are then transformed to give local displacement increments, $d\mathbf{r}$ for each element.

$$\mathbf{K}_t\,\Delta\mathbf{R} = \Delta\mathbf{Q} \tag{3.51}$$

Strain increment $\Delta\epsilon$ at any point (defined by x-ordinate $p = x/L$ and y-ordinate y) within the element is obtained from the expression below:

$$\Delta\epsilon = \mathbf{B}\,dr + \frac{1}{2}\,dr^T\,\mathbf{C}^T\,\mathbf{C}\,dr \tag{3.52}$$

$$\text{where} \quad \mathbf{B} = \left[-\tfrac{1}{L} \quad \tfrac{1}{L} \quad \tfrac{6}{L^2}y(1-2p) \right.$$
$$\left. \tfrac{6}{L^2}y(-1+2p) \quad \tfrac{2}{L}y(2-3p) \quad \tfrac{2}{L}y(1-3p) \right] \tag{3.53}$$

$$\text{and} \quad \mathbf{C} = \left[0 \quad 0 \quad \tfrac{6}{L}(-p+p^2) \right.$$
$$\left. \tfrac{6}{L}(p-p^2) \quad 1-4p+3p^2 \quad -2p+3p^2 \right] \tag{3.54}$$

B is the strain-displacement matrix for large deformation; and C is the strain-displacement matrix for large deformation.

The strain increments are obtained for the layers of sections at three Gaussian quadrature points along the lengths of the elements. Based on these elemental strain increments, the total strains are obtained for the layers. From these total strains and predefined stress-strain relationships of materials, total stresses are then calculated. The internal end forces of each element in local co-ordinates are then computed by integrating the current total stresses of the layers. These end forces are then transformed into global co-ordinates using the updated transformation matrices, and they are assembled into a matrix consisting of the internal resisting joint forces $\mathbf{R}^i$.

From the resisting force $\mathbf{R}^i$ and the current total applied joint loads $\mathbf{Q}^j$, the out-of-balance loads $\mathbf{Q}^u$ are obtained, i.e.,

$$\mathbf{Q}^u = \mathbf{Q}^j - \mathbf{R}^i \tag{3.55}$$

These out-of-balance loads are applied as forces for the next iterative cycle, and the cycle is repeated until the out-of-balance loads are within acceptable tolerances. The updating of the nodal forces is represented by the expression:

$$\Delta\mathbf{Q} = \mathbf{Q}^u \tag{3.56}$$

The out-of-balance loads are then added to the load increment for the next load steps and the whole process of carrying out iterating cycles is continued until convergence.

As the cross section at mid-element is assumed to be representative of the sections along the element when forming the element stiffness matrix, numerous elements are required to give accurate modelling of the material non-linearity effect for the structure. This will result in inefficiency with respect to program execution time and storage.

The layered element approach does not require the use of separate section analysis to generate the moment-thrust-curvature relations. Instead of using flexural stiffnesses of the elements to form the global stiffness matrix as for the line element approach, the properties of the layers are used directly. The layered element approach is not suitable to be used for deformation control technique which uses curvature as the control criterion. This is because the stiffness of the structure is not formed directly from the stiffnesses of the elements but rather from the material and geometric properties of the layers.

3.5 Strategies for Traversing Limit Points

Limit points exist in a structure at peak strength (where $dP/d\Delta=0$) or at local ultimate deflection (where $dP/d\Delta=-\infty$). Typical limit points are illustrated in Figure 3.10 for a one degree of freedom structure.

In Figure 3.10, point A represents a limit point for a structure under load control, while points B and C represent limit points for a structure under displacement control. Behaviour that gives rise to both point B and point C is referred to as snapback instability, a behaviour shown numerically to exist by Bažant, Pijaudier-Cabot and Pan (1987b) for a softening beam with elastic

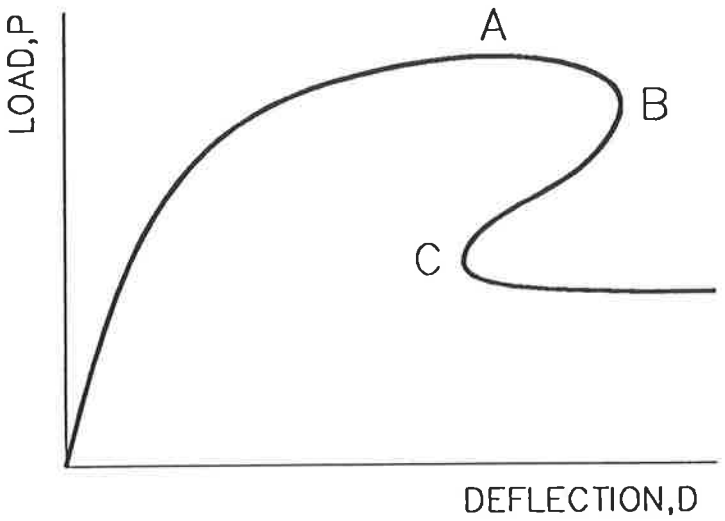

Figure 3.10: Limit points

end restraints. (This phenomenon of snapback instability had independently been observed to occur in portal frames in computations carried out during the course of the present study.)

For a structure with the behaviour shown in Figure 3.10, a load control procedure using monotically increasing load can only follow the behaviour up to approach point A, unless special techniques are devised as discussed below. If the displacement D is to be prescribed as the displacement control parameter, and this displacement is monotically increased, the limit point A can be traversed and the softening range AB can be traced. However, such a procedure would fail at a point approaching limit point B. For a one degree of freedom structure, the ability to trace the behaviour up to this point is normally sufficient to give an indication of the peak load. For structures with many degrees of freedom of movement, a wrong choice of the displacement control parameter can result in premature termination of the analysis before reaching the peak

load. Such termination will occur if the chosen control parameter is not monotically increasing, i.e., there is a reduction in the value of the control parameter as the global structural load continues to either increases or decreases. This would amount to forcing the control parameter to take on a value larger than its peak value which will result in non-convergency of the solution procedure. To ensure that such premature termination does not occur during the analysis, numerical strategies have been developed to traverse limit points. Some of these are reviewed below.

3.5.1 Strategy of Bergan

Bergan (1980a) introduced the concept of a current stiffness parameter S_p. The parameter S_p at a point on the load-deflection curve is the ratio of the current slope to the initial slope of the curve. Mathematically this parameter is defined by Bergan as (see Figure 3.11):

$$S_p = \frac{\left(\frac{dP}{dr}\right)_i}{\left(\frac{dP}{dr}\right)_o} = \left(\frac{\Delta P_i}{\Delta P_o}\right)^2 \frac{\Delta \mathbf{r_o}^T \mathbf{K_o} \Delta \mathbf{r_o}}{\Delta \mathbf{r_i}^T \mathbf{K_i} \Delta \mathbf{r_i}} \tag{3.57}$$

where the basic terms are shown in Figure 3.11.

The current stiffness parameter starts off with an initial value of one at the origin and progressively reduces until it reaches a value of zero at the singular point. This parameter is therefore useful to sense in advance the approach of a limit point. Equilibrium is disregarded by Bergan when the magnitude of the parameter is less than a threshold value to prevent non-convergence of the solution procedure. The solution procedure, based on load control, can therefore bypass the limit point and advance along the solution path. In the softening region, the current stiffness parameter S_p is negative and when this occurs the load increment is reversed. The negative load increment is then

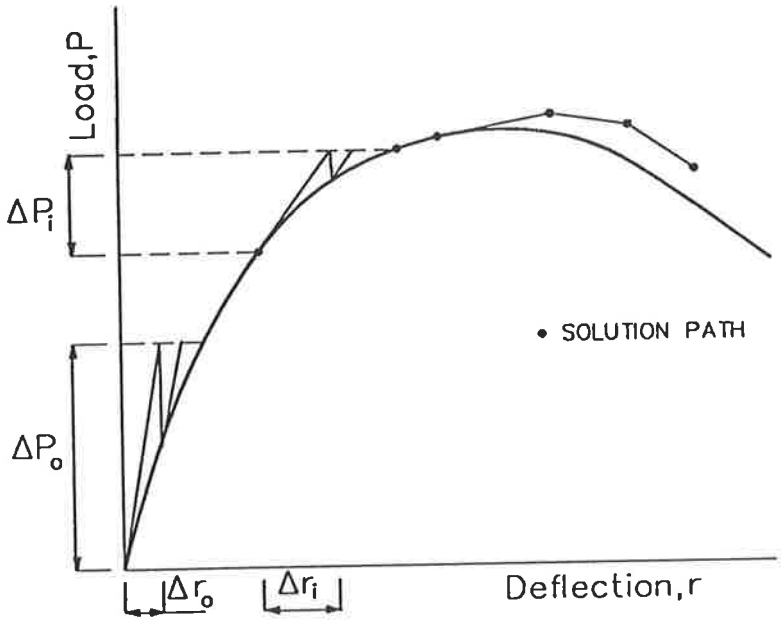

Figure 3.11: Figure illustrating the solution procedure of Bergan (1980a)

continued until the next limit point is reached.

The low stiffnesses of the structure around the limit points can produce uncontrolled displacements which may cause divergence. Small load increments are therefore necessary to prevent drifting away from the equilibrium path. Bergan pointed out that even with small load increments, the displacement can still be large. A simple method to prevent this, he suggested, is to calculate a norm of the displacement increment and scale down both load and displacement increments to be less than a specified maximum value.

3.5.2 Strategy of Crisfield

A popular method for traversing limit points is solve for displacements by incrementing the load parameter up to the limit point, and from then on

incrementing a characteristic displacement to obtain the corresponding load. This approach will work only if the control displacement component is monotically increasing. If the controlling displacement is poorly chosen and is found to snap back on incrementing the load, then this approach will not converge. Thus a proper choice of the controlling displacement is essential and for some structures this choice is not obvious.

A procedure, first proposed by Riks (1979) and Wempner (1971), can be used to overcome the problem described earlier. They proposed the use of a complete displacement vector as the constraint parameter instead of using a single component of the displacement vector. The proposed expression to constrain the load step $\Delta\lambda$ is:

$$\Delta\mathbf{u}^T\Delta\mathbf{u} + \Delta\lambda^2\Delta\mathbf{P}^T\Delta\mathbf{P} = \Delta l^2 \tag{3.58}$$

where

$\mathbf{P}$ = load vector;

$\mathbf{u}$ = displacement vector;

l = constrained vector; and

λ = load factor.

Originally this constraint equation was added to the incremental stiffness expression but unfortunately this resulted in the loss of bandedness and symmetry in the stiffness matrix.

Ramm (1981) modified the strategy of Riks and Wempner by using a two step technique, similar to the one first proposed by Batoz and Dhatt(1979). This modified technique allows both iteration in a "plane" normal to the tangent and iteration in a "sphere". The solution paths of Ramm are illustrated for a single degree of movement problem in Figure 3.12.

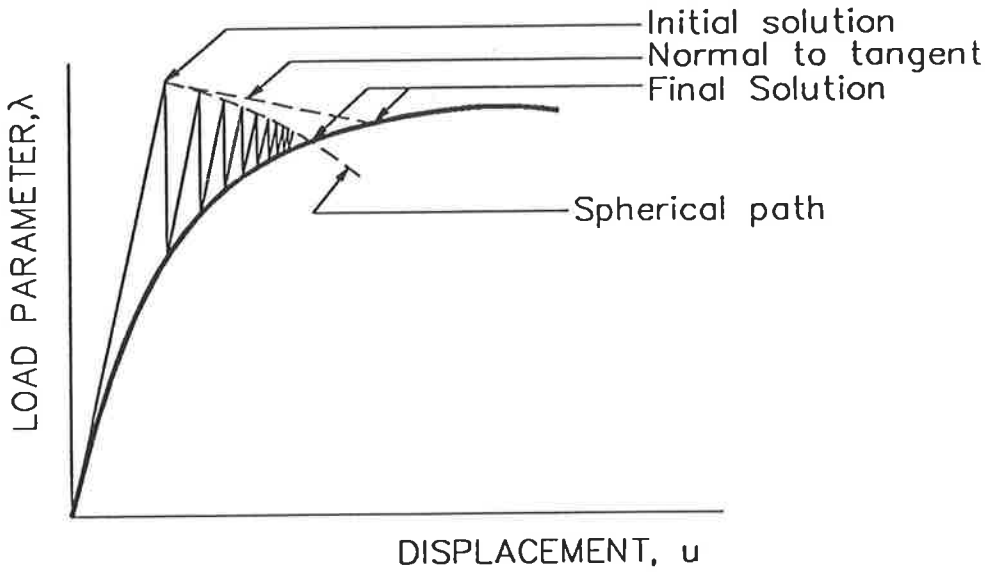

Figure 3.12: Figure illustrating the solution procedure of Ramm(1981)

Crisfield(1980) proposed the use of a spherical constraint surface which he claimed (Crisfield,1981) is less likely to fail than would a planar constraint surface. The constraint equation proposed by Crisfield is:

$$\Delta \mathbf{u}^T \Delta \mathbf{u} = (\Delta l)^2 \tag{3.59}$$

where

$\mathbf{u}$ = displacement vector; and

Δl = arc-length.

Crisfield(1986) proposed that an initial guess of the arc-length can be used and, thereafter, the arc-length adjusted according to the expression below:

$$\Delta l_j = \sqrt{\left(\frac{I_{j-1}}{I_d}\right)} \Delta l_{j-1} \tag{3.60}$$

where

Δl_j = arc-length to be used for the j-th increment;
Δl_{j-1} = arc-length required for the preceding increment; and
I_d = desired number of iterations.

Crisfield suggested that if convergence is not achieved within a specified maximum number of iterations, the arc-length may be reduced.

The constraint arc length strategy of Crisfield applied to a structure with one degree of freedom of movement is shown in Figure 3.13. Details of this strategy can be obtained from Crisfield's papers(Crisfield,1980;1983;1986).

The procedure, when applied to the materially nonlinear analysis of reinforced concrete beams and slabs has limited success (Crisfield,1983), particularly when significant strain-softening occurs in the constitutive laws. Crisfield (1983) successfully obtained solutions using standard displacement control after introducing line searches and simple accelerations into the analysis.

3.5.3 Strategy of Warner

Warner (1984) proposed a strategy suitable for the analysis of softening behaviour of structures. This strategy has been used to study the ductility of reinforced and prestressed concrete beams (Warner and Yeo, 1984a; 1984b;Ahmad and Warner, 1984) and partially prestressed bridge girder (Kgoboko, 1986; Kgoboko, Wyche and Warner, 1987).

A brief description of the strategy is given here. This strategy is described in greater details in Chapter 4 of this thesis. Warner modelled the entire structure using members, divided into small segments. The solution procedure involved carrying out, iteratively, a linear analysis on an equivalent elastic frame with segments having flexural stiffnesses reflecting the most recent updates of the

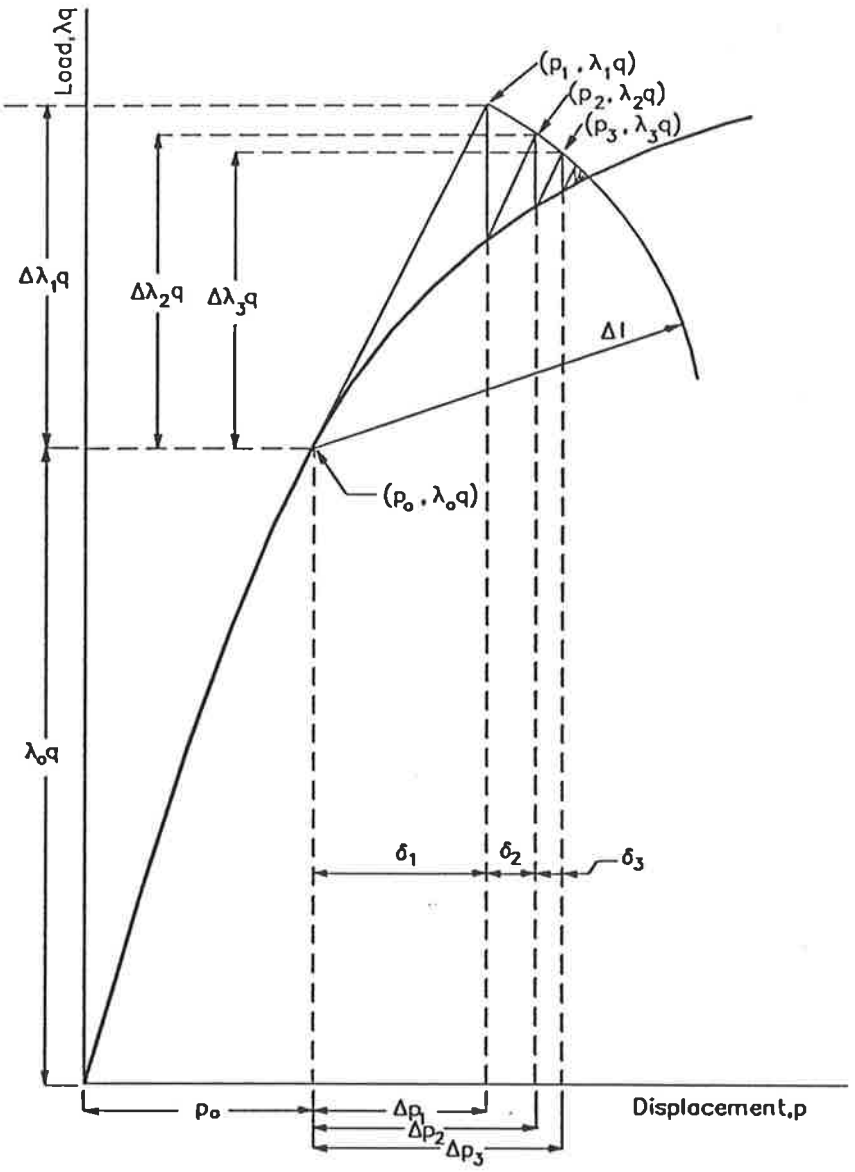

Figure 3.13: Arc-length Procedure (after Crisfield,1983)

segment properties. The analysis of the structure is carried out by selecting a "key" segment and imposing upon this segment increments of curvatures. The flexural stiffness is assumed to be uniform within each segment and is obtained from the properties and state of stress of the section at mid-segment. The linear elastic equivalent frame is solved to give forces and deformations. If the deflected shape does not give the targeted key curvature in a pre-selected key segment, then the secant stiffnesses of all the segments are updated and the linear frame is solved again. This calculation cycle is repeated until compatibility and equilibrium are achieved in the equivalent elastic frame. When this occurs, the solution for the actual frame is assumed to have been obtained. The behaviour of the frame is obtained by progressively increasing the curvature of the key segment by a small increment.

Warner and Yeo(1984) used this approach to study the collapse behaviour of indeterminate concrete beams with limited ductility. The nonlinear analysis was carried out by incorporating a standard linear elastic frame analysis. Segments are represented by individual elements and therefore require substantial computer storage capacity.

Ahmad and Warner (1984) used a similar approach to study the overload, collapse and post-collapse behaviour of continuous reinforced concrete beams with limited ductility. The analysis was based on a flexibility type approach which, according to Ahmad and Warner, is more efficient than the stiffness matrix approach when applied to the analysis of a continuous beam.

3.6 Softening Behaviour of Reinforced Concrete Structures

3.6.1 Hinge Length

Based on experimental investigations, Bažant(1984) found that strain softening is frequently distributed over finite-size regions of a heterogeneous material. These regions are normally referred to as *hinges*. At present, there is no satisfactory theoretical prediction for the length of these hinges. As hinge length l_p is an important parameter in softening analysis, several of the proposed formulae for determining it are described below.

The **I.C.E. committee (1962)** recommends the following formula for the equivalent plastic hinge length, l_p. The variable l_p is defined as the equivalent length over which plastic rotation occurred with constant curvature in that length.

$$l_p = k_1 k_2 k_3 \left(\frac{z}{d}\right)^{\frac{1}{4}} d \tag{3.61}$$

$$\begin{aligned} \text{where } k_1 &= 0.7 \text{ for mild steel} \\ &= 0.9 \text{ for cold-worked steel} \\ k_2 &= 1 + 0.5\left(\frac{P}{P_u}\right) \\ k_3 &= 0.9 - \frac{0.3}{23.5}(f'_c - 11.7) \end{aligned}$$

where

f'_c is assumed to be 0.85 × the cube strength of concrete (f'_c is in MPa);

z is the distance of critical section to the point

of contraflexure;

d is the effective depth of the member;

P is the axial force on member; and

P_u is the ultimate compressive strength of the member under axial load without bending moment.

Cohn and Petcu (1963) observed from tests carried out on two-span beams that the length to one side of the plastic zone at the internal support is between $0.3d$ and $0.9d$.

Baker and Amarakone (1964) proposed the following formula on the basis of experimental investigation of beams both with and without confinement by transverse steel.

$$l_p = 0.8k_1k_3\left(\frac{z}{d}\right)c \tag{3.62}$$

where c is the neutral axis depth at the ultimate moment and the other symbols have the same meaning as in Equation 3.61.

Sawyer (1964) proposed the following formula for the equivalent length of the plastic hinge:

$$l_p = 0.25d + 0.075z \tag{3.63}$$

The above equation is based on the assumptions that the maximum moment in the member is the ultimate moment, that $M_y/M_u = 0.85$, and that the zone of yielding is spread $d/4$ past the section in which bending moment is reduced to M_y.

Corley (1966) proposed the following formula for the equivalent length of the plastic hinge based on the results of tests on simply supported beams:

$$l_p = 0.5d + 0.2\sqrt{d}\left(\frac{z}{d}\right) \tag{3.64}$$

Mattock (1967), in discussing Corley's paper, suggested a simpler form of Equation 3.64 that fitted the trend of the data obtained in investigation at the

Portland Cement Association. This equation is:

$$l_p = 0.5d + 0.05z \tag{3.65}$$

Park et al (1982) found that the experimentally measured equivalent lengths of plastic hinge are comparatively insensitive to axial load level and had an average value of $0.42h$ where h is the overall section depth. Since the columns tested had overall depth of 550mm and effective depth, d, of 488mm, the average value of l_p/d is approximately 0.48.

Warner and Yeo (1984c) considered the flow of forces in a hinging region at an intermediate support, and concluded that in regions subjected to shear cracking, the region of steel yield spreads outward from the face of the support in steps of the stirrup spacing, s. Based on this observation, they suggested that a reasonable estimate of the final length of the hinging region to one side of the support was a multiple of s which is less than or equal to the effective depth, d of the beam.

Bažant et al (1987b) found that when the element size is refined to zero, strain-softening material models give physically meaningless solutions as the energy dissipated at failure tends to zero. Therefore, a certain minimum length of the strain-softening segment of the beam must be imposed. He suggested that this length may be approximately taken to be equal to the beam depth. This concurs with Bažant's earlier suggestion (Bažant,1976) that the element length must not be shorter than both three maximum aggregate sizes and the beam depth, H. The second condition is a consequence of the assumption of plane cross sections and in practice it always govern (Bažant et al, 1987b).

3.6.2 Previous Analytical Studies of Softening Behaviour

Softening behaviour has so far been observed experimentally in structures such as beams (Darvall and Mendis, 1984) and some portal frames (Cranston, 1965b) under the effect of point loads. To enable such behaviour to be studied in more complex structures, analytical studies to include the effect of strain softening have to be carried out. This section described several previous analytical studies on the softening behaviour of reinforced concrete structures.

Cranston(1965a) used a flexibility matrix approach to analyse a pin-ended portal frame subjected to symmetrical two-point loading on the beam span. The frame was tested by him and is described in another paper (1965b). He assumed two falling branch hinges: one at the mid-span of the beam and the other at the top portion of the column, just below its intersection with the beam. The discontinuity length was assumed to be be approximately equal to 4 per cent of the corresponding member length. The analysis carried out made use of experimentally derived moment-curvature curves. The results obtained show that the load falls only after the formation of the second hinge. The agreement between analytical and experimental results was good at all loading stages.

Ghosh and Cohn (1972) proposed a method of non-linear small-deformation analysis of reinforced concrete structures, considering the effect of the descending branches of the moment-curvature diagrams. The analysis of reinforced concrete structure of known configuration and geometry by this approach begins with the pre-generation of the moment-curvature relationships of various sections in the structure from a chosen stress-strain relationship and the known geometric properties of the section. The chosen material stress-strain relationship may be based on an idealised, proposed relation or based on experimental data defined at discrete points. Loads of some known intensity are imposed on the structure, and a moment-field in equilibrium with the load is assumed.

The associated curvature field is obtained from the pre-generated moment curvature relationships. Slopes and deflections along the member are calculated from the known curvature field and the boundary conditions are checked. A moment-field in equilibrium with the imposed loads and satisfying all boundary conditions is found by trial and error. After obtaining solution for a particular load intensity, the imposed load intensity is increased at desired intervals, and the solution process is repeated until the ultimate capacity is reached in at least one section along the member. Let the most critically stressed section be known as section A.

In carrying on the analysis beyond the above stage, section A is assigned a bending moment along the descending branch of its moment-curvature relationship. Ghosh and Cohn assumed that a section at an infinitesimal distance away is subjected to the same moment, but on the ascending branch of the same moment-curvature curve. A discontinuity therefore occurs at section A and its value can be calculated from the moment-curvature curve, as shown in Figure 3.14. Knowing this discontinuity curvature, and the gauge length on which the stress-strain relationship and moment-curvature relation of the section are based, the concentrated rotation at section A can be calculated. This concentrated rotation is considered as part of the compatibility conditions to be met in establishing, by trial and error, a load intensity for the structure with the prescribed moment at A. The above procedure is repeated with progressively decreasing values of descending branch moments assigned to the section A. For the two-span continuous beams analysed by Ghosh and Cohn, section A occurs at the support, and the analysis is terminated when the moment capacity is attained at the span sections. This method is based on the concept of concentrated rotations at critical sections, rather than on the concept of discontinuity length.

Ghosh(1977) used the above approach to analyse a number of symmetrically loaded two-span continuous beams with different amount of tension reinforce-

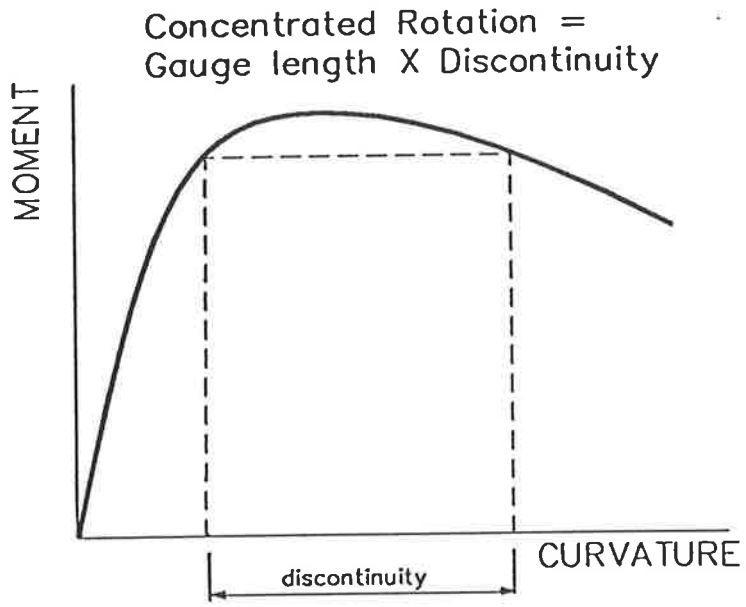

Figure 3.14: Discontinuity length(Ghosh and Cohn,1972)

ment and the strength of concrete. He reported that the non-linear load-deformation characteristics up to the point of collapse are in reasonable agreement with experimental results. From this study, he concluded that it is essential that the descending branches of the sectional moment-curvature relationships be considered in order to obtain accurate analytical predictions of the load-deformation characteristics of reinforced concrete structures.

The above approach proposed by Ghosh and Cohn is suitable for relatively simple structures. The accuracy of the method depends on the value of the gauge length used in the analysis.

Bažant(1976) and Darvall(1983) found that there exist a critical softening slope in the softening branch of the hinge. This results in the structure not being able to carry any extra loads.

Mendis(1986) included the effect of geometrical nonlinearity effect in the non-linear analysis of concrete frames. He concluded that by not including this effect, the order of hinge formation in the structure during loading may be affected. In his studies, he was concerned with structures with at least one hinge being formed at collapse.

Bažant et al(1987b) suggested the possibility of multiple snapbacks forming in load softening structure. They concluded from this study that:

- a statically indeterminate strain-softening structure of redundancy degree n can exhibit at most $n + 1$ points of snapback instability,
- a structure will exhibit all its snapbacks if it is sufficiently slender, or if the strain-softening slope is sufficiently steep,
- finite element analysis would encounter all these snapback instabilities if the finite elements were sufficiently small, and
- the strain-softening segment of a beam cannot be replaced, for the purpose of calculations, by a softening hinge, unless the beam is sufficiently slender.

3.7 Summary and Concluding Remarks

The commonly used load control techniques to analyse non-linear behaviour are the secant, tangent and initial stiffness techniques. These techniques, by themselves, are not suitable for following the load-softening behaviour of reinforced concrete frames. They must be used in conjunction with other techniques such as the those described above in Section 3.5. The technique proposed by Crisfield is difficult to program, especially when line searches and simple accelerations have to be incorporated into the approach in order to ob-

tain solutions for structures with strain-softening behaviour. Bergan's strategy has the disadvantage of bypassing the limit point. The region around the peak load, therefore, cannot be analysed and the peak load cannot be determined accurately. The technique proposed by Warner is chosen for the development of the computer program in the present study as a good compromise between simplicity of programming and efficiency.

Several numerical models for the analyses of concrete frames have been reviewed. The two common models reviewed are firstly one in which the frame is modelled by using numerous line elements and secondly the frame is modelled using numerous layered elements. In the latter approach the element stiffness matrix is formed directly from the behaviour of the layers comprising the elements. The numerical model used in the present study is based on the technique which uses line elements proposed by Warner.

The hinge length parameter has been reviewed and a hinge length value between 0.5 and 1.0 times the depth of the corresponding section, D, is to be adopted by the author.

Previous analyses to obtain the softening behaviour of reinforced concrete structures have been described. They have one or more of the the following limitations:

- limits to the analysis of simple structures;
- without the ability to follow the snapback instability behaviour of the structure;
- required guesses of the positions of concrete hinges to obtain accurate solution;
- concerns with softening behaviour with at least one hinge forming, thus ignore the possibility of softening before the formation of hinges; and

- requires the discretisation of structures into numerous elements resulting in large global stiffness matrices which causes the solution procedure to be inefficient.

The survey of the literatures carried out in this chapter suggests that there is a need to develop an efficient computer program to trace the behaviour of reinforced concrete frame over its full-range behaviour. It is important that the softening behaviour of frames be obtained to enable the peak load to be accurately determinated. To the knowledge of the author, snapback instability in concrete frames has not been observed in any computer analysis. To enable this phenomenon to be observed and studied, computer programs using efficient techniques to traverse limit points need to be developed.

To overcome the shortcomings in existing techniques, a computer program has been developed to trace the full-range behaviour of reinforced concrete frames. The computational technique used in this program is described in Chapter 4. The same program is also used, together with several other programs, to evaluate the accuracy of the present Australian Standard AS3600. These studies are described in Chapters 7 and 8.

Chapter 4

Segmental Method of Analysis

4.1 Introduction

The basic concept in the development of the segmental method of analysis is that reinforced concrete frames can be represented by elements, and the behaviour of these elements is influenced by the properties of short segments along them (Warner,1975), rather than individual cross sections.

Based on the above concept, studies have been carried out to define ductility limits for reinforced and partially prestressed concrete beams (Ahmad and Warner,1984; Warner and Yeo,1984a,1984b).

A similar approach was used to study the ductility limits of partially prestressed concrete girders (Kgoboko,1987; Kgoboko, Wyche and Warner,1988). In that study, the effect of thrusts on moment-curvature relations of the sections was not included. Use was made of linearised moment-curvature relations obtained from pre-generated relations using a separate section analysis

program. As this requires a large amount of input data compared with programs that use a built-in section analysis routine, greater care is required to ensure the accuracy of these data.

To enable more complicated structures to be analysed, a computer program based on the segmental approach has been developed (Wong, Yeo and Warner, 1987a, 1987b). The program, based upon a finite element formulation, has general applications in the analysis of plane skeletal frames with different configurations and under different types of loading. The computer program developed during the present study, program SAFRAME (abbreviation for Segmental Analysis of reinforced concrete FRAME) uses a built-in section analysis subroutine described in Chapter 2 to generate values of moment, thrust, and curvature for individual segments whenever required by the main routine in the program.

Computer program SAFRAME was written in Fortran77 to run initially on a VAX 750 operating under VMS. It was subsequently modified for a UNIX operating environment. As numerous cycles of calculations are carried out to obtain a solution, rounding-off errors may occur. To minimise the effect of rounding-off errors, values of real type are stored in a double precision (64 bits) internal representation.

Some of the material in this chapter has previously been published (Wong, Yeo and Warner,1987a, 1987b; Wong and Warner,1988).

4.2 Structural Analysis

The segmental method of analysis used here is similar in concept to one previously applied to the analysis of continuous reinforced and prestressed concrete beams (Warner,1984). However, to treat skeletal frame behaviour in an ad-

equate manner, it has been necessary to extend the analysis to allow for the following:

- axial deformations;
- geometric non-linearities in the frame;
- the effect of thrust on the moment-curvature relations for column segments; and
- inelastic (as well as non-linear) behaviour in segments subject to local unloading.

In order for the structure to be modelled accurately with respect to material nonlinearity, the length of the segments needs to be comparable with actual concrete hinges. An earlier study by Warner and Yeo (1984c) suggested that in regions of high shear, the length of hinges may be approximately equal to the effective depth. A study by Bazant et al(1987b) showed that the unloading path of softening structures is affected by the length of the segments used in the analysis and he recommended a length equal to the depth of the section.

Instead of the usual approach of using the behaviour of the segments to obtain the structural stiffness directly, a more efficient two-stage approach has been adopted. This involves grouping the segments together to form elements, and using the stiffnesses of the segments to determine element stiffnesses. As the behaviour of the elements is influenced by the behaviour of the component segments, this approach of modelling the structure reduces considerably the size of the structural stiffness matrix, but still maintains the same level of accuracy in modelling the material nonlinearities. Computer program SAFRAME contains a section analysis routine which automatically generates the moment-curvature-thrust relations during the analysis. This enables the program to be fully automated, thereby reducing the amount of input from users when

analysing concrete frames. Using moment-curvature-thrust relations generated within the program instead of using pre-generated moment-curvature relations also allows more accurate modelling of the effect of sectional axial thrust.

The frame to be analysed is divided into elements, and the elements into segments. The behaviour of the structure is analysed for a given loading pattern. The behaviour of each segment is defined by the moment-curvature-thrust relations obtained for the section at mid-segment. The analysis of the structure is carried out by selecting a "key" segment and imposing upon this segment increments of curvature. For each value of curvature, $K_{key}(1)$, ... $K_{key}(ISTEP)$, ... $K_{key}(NSTEP)$, the loads required to cause this curvature are computed, together with the displacements throughout the structure, by an iterative procedure based on a linear secant stiffness analysis. The final curvature $\kappa_{key}(NSTEP)$ represents an arbitrary state of post-ultimate softening of the key segment, and unloading of the structure as a whole.

At each computational step, the flexural secant stiffness and axial secant stiffness of each segment are progressively adjusted until all equilibrium and compatibility requirements are satisfied, taking account of the segmental moment-curvature-thrust relations.

For the start of a typical computational step $ISTEP$, in which the target curvature in the key segment is $\kappa_{key}(ISTEP)$, the trial flexural stiffness values, $EI_{trial}(n)$, for all the segments are set equal to the values at the end of the previous step, i.e. equal to the values already obtained to correspond to the key segment curvature of $\kappa_{key}(ISTEP-1)$. The trial axial stiffnesses of the elements $S(m)$, are also set equal to the values at the end of the previous step. For the first step in the analysis the secant stiffnesses are set equal to the EA and EI values of the gross cross-sections ignoring the presence of the steel reinforcement.

Computational cycles are then carried out until a solution is obtained for the frame under the prescribed load pattern and having a curvature of $\kappa_{key}(ISTEP)$ in the key segment. Steps in a typical computational cycle are described below:

1. Form the secant stiffness matrix for each element in turn, using in its build-up the most recent bending and axial stiffness trial value for each segment comprising the element. The derivation of the element stiffness matrix for a segmental element is given in Section 4.3. From these matrices and appropriate element transformation matrices, assemble the global stiffness matrix, $[K]$ using standard procedures (Hall and Kabaila, 1977; Cheung and Yeo, 1979).

2. Form the nodal load matrix, $\{Q_{unit}\}$, from a *unit applied load pattern.* Analysis is carried out to obtain scaling factors to this unit load pattern that will gives assigned values of curvatures in the key segment. This implies that the analysis is carried out for the structure under proportional loading. Contributions from unit load patterns within elements are taken into consideration by using equivalent nodal loads based on fixed end moments which are dependent on the flexural stiffnesses of all the segments within the elements. Expressions for fixed end moments for a segmented element are given in Section 4.4. The derivation of these expressions is similar to that for an elastic element with non-uniform section (Bull and Sved,1965).

3. Obtain the nodal deformations Δ_{unit} due to combined "unit" out-of-balance nodal forces from the previous cycle $\{Q_{out-of-bal}\}$ (appropriately taken to be zeros for the first cycle of the first step) and the unit load pattern $\{Q_{unit}\}$ by solving the equation:

$$\{Q_{unit}\} + \{Q_{out-of-bal}\} = [K]\{\Delta_{unit}\} \qquad (4.1)$$

4. From the nodal deformations of the frame, using standard procedures, obtain deformations and forces at the ends of all the elements. Based on these and the unit load patterns within the elements, determine the curvatures $\kappa_{unit}(n)$ of all the segments due to the unit load pattern:

$$\kappa_{unit}(n) = \frac{M_{unit}(n)}{EI_{trial}(n)} \tag{4.2}$$

5. If the curvature of the key segment, as given by this calculation using unit load is $\kappa_{unit}(key)$, whereas the required curvature for this segment is $\kappa_{key}(ISTEP)$ then the scaling factor is:

$$SF = \frac{\kappa_{key}(ISTEP)}{\kappa_{unit}(key)} \tag{4.3}$$

6. Obtain a trial set of segmental curvatures throughout the structure, $\kappa_{trial}(n)$, by multiplying $\kappa_{unit}(n)$ by the scaling factor SF.

$$\kappa_{trial}(n) = SF \times \kappa_{unit}(n) \tag{4.4}$$

Note that the trial curvature in the key segment $\kappa_{trial}(key)$ is always equal to the target curvature, $\kappa_{key}(ISTEP)$.

7. Store the previous stiffnesses prior to calculating the new stiffnesses(see Equation 4.6):

$$OLDEI(n) = EI_{trial}(n) \tag{4.5}$$

8. Use a section analysis routine in turn for each segment to determine the segmental moment $M_{trial}(n)$ to correspond to $\kappa_{trial}(n)$ and the thrust value for the element obtained earlier. Hence calculate the new secant bending stiffnesses from:

$$EI_{trial}(n) = \frac{M_{trial}(n)}{\kappa_{trial}(n)} \tag{4.6}$$

Obtain the total axial deformation of the element along its centroidal axis from the section analysis routine. This together with

the element thrust value $N(m)$ enables a trial axial stiffness $S(m)$ to be determined.

$$\delta(m) = \sum_{n=1}^{nseg} \epsilon(n) l(n) \tag{4.7}$$

$$S(m) = \frac{N(m)}{\delta(m)} \tag{4.8}$$

where $\delta(m)$= total axial deformation of element m along reference axis;

$\epsilon(n)$ = strain of segment n along reference axis; and

$l(n)$ = length of segment n.

9. Calculate the "total" out-of-balance nodal forces from the resisting forces at the nodes based on the latest deformed state of the structure in the full load system (not that in the unit load reference system) and the applied total loads. These forces are scaled down to unit load reference system to give the "unit" out-of-balance nodal forces $\{Q_{out-of-bal}\}$ using the latest scale factor, SF. This out-of-balance forces is used in item 3 to achieve joint equilibrium for the structure in its deformed configuration.

10. Convergence is considered to have been achieved when the change in flexural stiffness of each segment between two successive cycles and the out-of-balance nodal forces are less than acceptable tolerances. If convergence has not been achieved, the cycle is repeated.

When convergence is achieved, the state of the structural system corresponding to the key curvature $\kappa_{key}(ISTEP)$ is obtained by applying the scaling factor SF to the unit load analysis. The load producing this state is equal to the scaling factor, SF.

The gross section EI and EA values are used for the first step in the analysis (i.e. for $\kappa_{key}(1)$). For all subsequent steps in the analysis, the first trial stiffnesses are those obtained at the end of the previous step.

As can be seen from the steps described above, geometric non-linearity is allowed for by updating the nodal positions at the end of each iterative cycle, and applying the out-of-balance forces on top of the contribution from the applied loading as nodal loads of the next iterative cycle. At the end of the iterative cycles, when convergence is achieved, results (such as forces and deformations) are obtained for the structure in its deformed shape with equilibrium of forces been achieved at all nodes, and with the frame having the nominated curvature in the key segment for that particular step.

The computational procedure for a typical step is illustrated by the flowchart in Figure 4.1.

It has been found that in the unloading phase, convergence is improved if the updated flexural stiffness values are taken as the average of the previous and current values for any iterative cycle, instead of the current values. This also assists in damping out any oscillating effect occurring numerically during the analysis.

4.3 Derivation of Stiffness Matrix for a Segmented Element

In this section, the stiffness matrix of a segmented element is derived. A typical element of length L is divided into $nseg$ segments, each having a flexural stiffness value governed by the level of the curvature at mid-segment. The moments at the left and right ends of the element are M_o and M_{end} respectively; the shear forces are V_o and V_{end} respectively.

Let θ_i be the change in rotation within a typical segment i, assumed to occur at the mid-segment, and calculated from the bending moment at mid-segment,

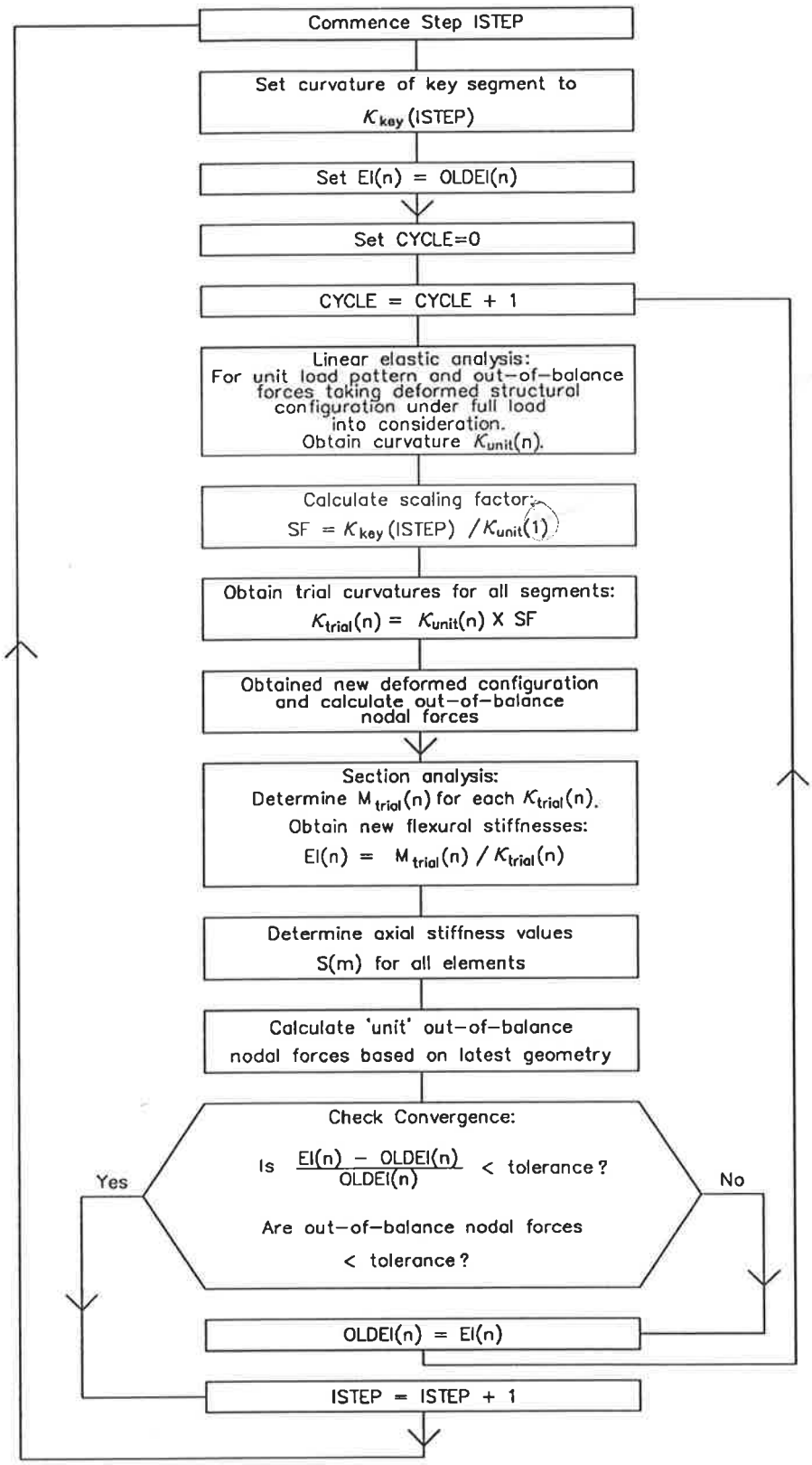

Figure 4.1: Calculation cycle for a typical step

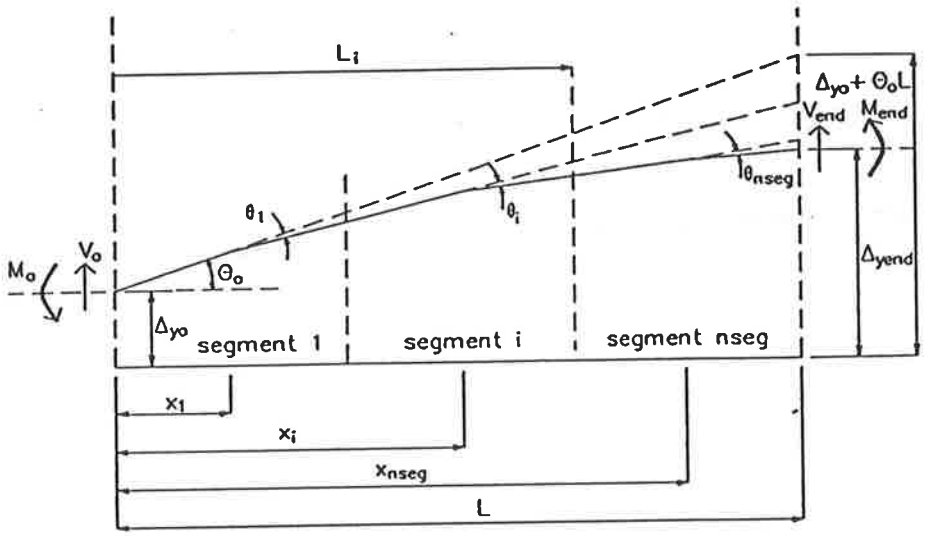

Figure 4.2: Typical Segmented Element

$M_o - V_o x_i$, and the flexural stiffness S_i using the equation:

$$\theta_i = \frac{M_o - V_o x_i}{S_i} \tag{4.9}$$

where

S_i = EI_i/l_i; and

l_i = length of segment i.

From Figure 4.2, the slopes and displacements at the end of a typical segment i are:

$$\Theta_i = \Theta_o - \theta_1 - \theta_2 - \cdots - \theta_i \tag{4.10}$$

$$\Delta_i = \Delta_{yo} + \Theta_o L_i - \theta_1(L_i - x_1) - \theta_2(L_i - x_2) - \cdots - \theta_i(L_i - x_i) \tag{4.11}$$

where L_i is the distance from the left end of the element to the end of segment i as shown in Figure 4.2 and $\tan\theta_j$ is assumed to be θ_j in Equation 4.11 above.

Hence, the deformations at the end of the element are:

$$\Theta_{end} = \Theta_o - \theta_1 - \theta_2 - \cdots - \theta_i - \cdots - \theta_n \tag{4.12}$$

$$\Delta_{yend} = \Delta_{yo} + \Theta_o L - \theta_1(L-x_1) - \theta_2(L-x_2) - \cdots - \theta_i(L-x_i) - \cdots - \theta_n(L-x_n) \tag{4.13}$$

Substituting Equation 4.9 into Equations 4.12 and 4.13 yields:

$$\Theta_{end} = \Theta_o - M_o \sum_{i=1}^{nseg} \frac{1}{S_i} + V_o \sum_{i=1}^{nseg} \frac{x_i}{S_i} \tag{4.14}$$

$$\frac{\Delta_{yend} - \Delta_{yo}}{L} = \Theta_o - M_o \sum_{i=1}^{nseg} \frac{1}{S_i} + \frac{M_o}{L} \sum_{i=1}^{nseg} \frac{x_i}{S_i} + V_o \sum_{i=1}^{nseg} \frac{x_i}{S_i} - \frac{V_o}{L} \sum_{i=1}^{nseg} \frac{x_i^2}{S_i} \tag{4.15}$$

Let $C_1 = \sum_{i=1}^{nseg} \frac{1}{S_i}$, $C_2 = \sum_{i=1}^{nseg} \frac{x_i}{S_i}$ *and* $C_3 = \sum_{i=1}^{nseg} \frac{x_i^2}{S_i}$.

Equations 4.14 and 4.15 become:

$$\Theta_{end} - \Theta_o = -M_o C_1 + V_o C_2 \tag{4.16}$$

$$\frac{\Delta_{yend} - \Delta_{yo}}{L} - \Theta_o = -M_o C_1 + \frac{M_o}{L} C_2 + V_o C_2 - \frac{V_o}{L} C_3 \tag{4.17}$$

Solving Equations 4.16 and 4.17 gives:

$$M_o = \frac{1}{C_1 C_3 - C_2^2} \left[C_2 \Delta_{yo} + C_3 \Theta_o - C_2 \Delta_{yend} + (C_2 L - C_3)\, \Theta_{end} \right] \tag{4.18}$$

$$V_o = \frac{1}{C_1 C_3 - C_2^2} \left[C_1 \Delta_{yo} + C_2 \Theta_o - C_1 \Delta_{yend} + (C_1 L - C_2)\, \Theta_{end} \right] \tag{4.19}$$

M_{end} and V_{end} are obtained from the equilibrium relationships given below:

$$V_o + V_{end} = 0 \tag{4.20}$$

$$M_o + M_{end} - V_o L = 0 \tag{4.21}$$

Equations 4.18, 4.19, 4.20 and 4.21 combined with the axial stiffness $S(m)$ described in the main text give the element stiffness matrix shown below:

$$\begin{Bmatrix} P_o \\ V_o \\ M_o \\ P_{end} \\ V_{end} \\ M_{end} \end{Bmatrix} = [K] \times \begin{Bmatrix} \Delta_{xo} \\ \Delta_{yo} \\ \Theta_o \\ \Delta_{xend} \\ \Delta_{yend} \\ \Theta_{end} \end{Bmatrix} \tag{4.22}$$

where $[K]$ is the segmental element stiffness matrix shown below:

$$\begin{bmatrix} S(m) & 0 & 0 & -S(m) & 0 & 0 \\ & S_{22} & S_{23} & 0 & -S_{22} & LS_{22} - S_{23} \\ & & S_{33} & 0 & -S_{23} & LS_{23} - S_{33} \\ & & & S(m) & 0 & 0 \\ & & SYMME- & & S_{22} & S_{23} - LS_{22} \\ & & TRIC & & & L^2S_{22} - 2LS_{23} + S_{33} \end{bmatrix} \tag{4.23}$$

where $S_{22} = C_1/(C_1C_3 - C_2^2)$, $S_{33} = C_3/(C_1C_3 - C_2^2)$, $S_{23} = C_2/(C_1C_3 - C_2^2)$

4.4 Derivation of Fixed End Moments for a Segmented Element

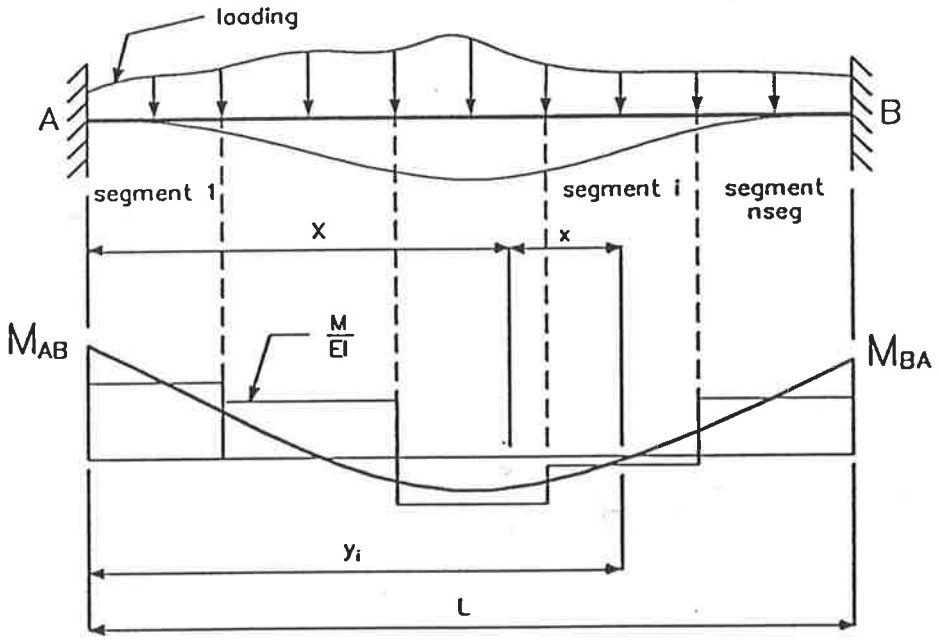

Figure 4.3: Fixed end moments for segmented element

As mentioned in Section 4.2, the fixed end moments of a segmented element have to be calculated to include the effect of transverse loading along the element. The derivation of the fixed end moments for a segmented element is presented in this section.

For the element shown in Figure 4.3, using the moment area method and noting that the tangent to the element at B passes through A and vice versa yields:

$$\left[\text{Moment of } \frac{M}{EI} \text{ diagram about A}\right]_A^B = 0 \tag{4.24}$$

$$\left[\text{Moment of } \frac{M}{EI} \text{ diagram about B}\right]_A^B = 0 \tag{4.25}$$

The bending moment at any mid-segment point G distant x_i from N is found by the summation of two bending moments; firstly, the bending moment, M_{ppi}, as if the element carrying the external loads was simply supported and secondly, the bending moment caused by the end moments M_{AB} and M_{BA}, as expressed by the equation below:

$$M_{xi} = M_{AB} - \frac{(X + x_i)}{L}[M_{AB} + M_{BA}] \tag{4.26}$$

The total moment at G is therefore:

$$M_{xi} = M_{ppi} + M_{AB} - \frac{(X + x_i)}{L}[M_{AB} + M_{BA}] \tag{4.27}$$

where M_{ppi} is the simply-supported bending moment which is a function of x_i and the applied loading.

For a segmented element, the moment area Equations 4.24 and 4.25 thus become:

$$\sum_{i=1}^{nseg} \left\{ \left[M_{ppi} + M_{AB} - \left(\frac{X + x_i}{L} \right) (M_{AB} + M_{BA}) \right] \frac{X + x_i}{EI_i} \right\} = 0 \tag{4.28}$$

$$\sum_{i=1}^{nseg} \left\{ \left[M_{ppi} + M_{AB} - \left(\frac{X + x_i}{L} \right) (M_{AB} + M_{BA}) \right] \frac{L - X - x_i}{EI_i} \right\} = 0 \tag{4.29}$$

The origin N is then chosen to be the centroid of the $1/EI$ diagram such that:

$$X = \frac{\sum_{i=1}^{nseg} (y_i/EI_i)}{\sum_{i=1}^{nseg} (1/EI_i)} \tag{4.30}$$

Since N is the centroid of the $1/EI$ diagram

$$\sum_{i=1}^{nseg} \frac{x_i}{EI_i} = 0 \tag{4.31}$$

Let $P = \sum_{i=1}^{nseg} \frac{1}{EI_i}$, $R = \sum_{i=1}^{nseg} \frac{x_i^2}{EI_i}$, $S = \sum_{i=1}^{nseg} \frac{M_{ppi}}{EI_i}$, $T = \sum_{i=1}^{nseg} \frac{M_{ppi}x_i}{EI_i}$

Equations 4.28 and 4.29 become:

$$XS + T + \frac{M_{AB}}{L}\left[X\left(L - X\right)P - R\right] - \frac{M_{BA}}{L}\left[X^2P + R\right] = 0 \tag{4.32}$$

$$\left[L - X\right]S - T + \frac{M_{AB}}{L}\left[\left(L - X\right)^2 P + R\right] - \frac{M_{BA}}{L}\left[X\left(L - X\right)P - R\right] = 0 \tag{4.33}$$

Solving Equations 4.32 and 4.33 simultaneously yields:

$$M_{AB} = \left[\frac{XT}{R} - \frac{S}{P}\right] \tag{4.34}$$

$$M_{BA} = \left[\frac{\left(L - X\right)T}{R} + \frac{S}{P}\right] \tag{4.35}$$

4.5 Convergence Criteria

Convergence criteria need to be decided for non-linear structural problems that are solved by iteration. According to Bergan and Clough(1972), these criteria can usually be classified into the following groups :(1) force criteria, (2) displacement criteria and (3) stress criteria. One of the main problems with

iterative techniques is deciding on whether the present iteration is sufficiently close to the true solution.

The force criteria described earlier in Section 4.2 are based on the unbalanced or residual forces. These forces are the differences between the actual loads acting on the structure and forces calculated from the internal resisting stresses. It is essentially an equilibrium check on the structure, normally in its deformed configuration. Use of such a criterion causes difficulty in deciding the acceptable tolerances as quantities under consideration may be of completely different order or even of different dimensions. For instance it is difficult to decide on the acceptable out-of-balance nodal forces and out-of-balance nodal moments for nodes that carry no loads but are free to move. Choosing over conservative values will result in inefficiency of the solution procedure with iterations will continuing even though the solution is close to the actual solution.

To overcome the problem associated with using force criteria, Bergan and Clough (1972) proposed the use of displacement criteria. They introduced a nondimensional vector based on displacements, which they referred to as the ϵ vector defined below:

$$\epsilon^{(j)} = \left[\frac{\Delta_{r_1}}{r_{1,ref}} , \frac{\Delta_{r_2}}{r_{2,ref}}, \cdots \frac{\Delta_{r_i}}{r_{i,ref}}, \cdots \frac{\Delta_{r_n}}{r_{n,ref}} \right]^T_{(j)} \tag{4.36}$$

where

n is the total number of unknown components;

Δ_{r_i} is the change in displacement component i during iteration cycle j; and

$r_{i,ref}$ are the reference displacement quantities.

The reference displacement quantities are generally not equal to the corresponding total components because, if r_i is close to zero, the ratio Δ_{r_i}/r_i could

be large even after convergence has occurred. Instead, every Δ_{r_i} is scaled by the largest displacement component of the corresponding "type". Bergan and Clough suggested that a mean value could be used instead of a maximum value.

Three alternative norms were suggested by Bergan and Clough for measuring the size of the ϵ vector. These are:

1) modified absolute norm

$$\epsilon = \frac{1}{n}\sum_{i=1}^{n}\left|\frac{\Delta_{r_i}}{r_{i,ref}}\right| \tag{4.37}$$

2) modified euclidean norm

$$\epsilon = \left[\frac{1}{n}\sum_{i=1}^{n}\left|\frac{\Delta_{r_i}}{r_{i,ref}}\right|^2\right]^{1/2} \tag{4.38}$$

3) maximum norm

$$\epsilon = max\left|\frac{\Delta_{r_i}}{r_{i,ref}}\right| \tag{4.39}$$

The convergence criterion for the above norms is:

$$\epsilon < \gamma \tag{4.40}$$

where the value of γ is usually of the order of 1×10^{-2} to 1×10^{-6}, depending on the required accuracy.

Figure 4.4 obtained by Bergan and Clough indicates that the various norms follow each other in a parallel manner during iteration so it is of no great significance which norm is chosen. As using deformation convergence criteria has the advantages described earlier in this section over using force criteria, the former was incorporated into program SAFRAME. The maximum norm

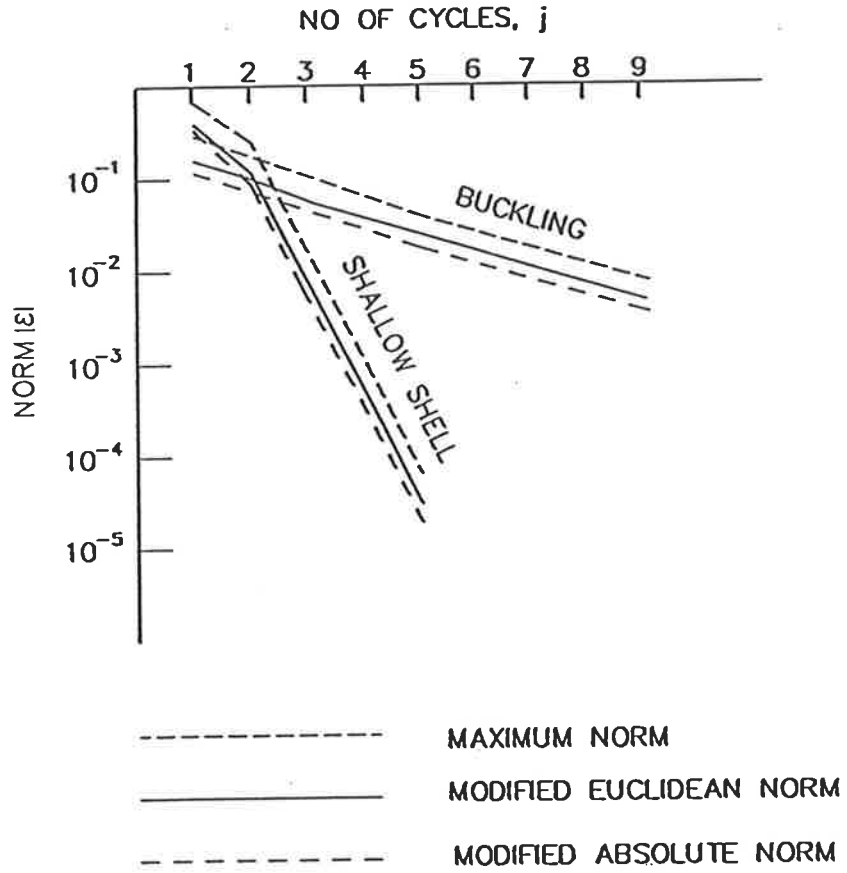

Figure 4.4: Comparison of different convergence criteria (after Bergan and Clough,1972)

is used as it gives an absolute bound for all displacement components instead of an average bound obtained using the other two norms.

4.6 Efficiency of the Segmental Approach

The efficiency of the solution procedure is related to the size of the global stiffness matrix of the structure as the solution procedure involves solving a set of simultaneous equations of size equal to that of this matrix. As most

non-linear analyses involve forming and solving a set of simultaneous equations repetitively, the size of the global stiffness matrix has great influence on the efficiency of the solution procedure..

The efficiency of the segmental approach is illustrated using a three-storey two-bay frame (see Figure 4.5). If all segments are treated as elements, the labelling is shown in Figure 4.6(a). The labelling of the nodes using the segmental approach, assuming that three internal nodes are required for accurate modelling of the P-Δ effect within the columns, is shown in Figure 4.6(b). Assuming that the banded nature of the global stiffness matrix is not exploited, the first approach results in a global stiffness of size 522 $\times$ 522 whereas the latter approach results in a global stiffness of size 108 $\times$ 108. In certain structures where the P-Δ effect for the columns is not significant, one element per member can be used. For the frame shown in Figure 4.5, this reduces the size of the global stiffness matrix to 27 $\times$ 27.

4.7 Summary

The development of the program SAFRAME has been described. Convergence criteria based on forces and deformations have been discussed and the latter are adopted for use in SAFRAME as a more efficient means of determining the convergence.

The efficiency in using a segmental approach was described using a three-storey two-bay frame. For the frame with the P-Δ effect of the columns ignored, the size of the global stiffness matrix is reduced from the usual 522 $\times$ 522 to 27 $\times$ 27.

Derivations of the elemental stiffness matrix have been presented in this chapter. To enable transverse loading along the elements to be included in the

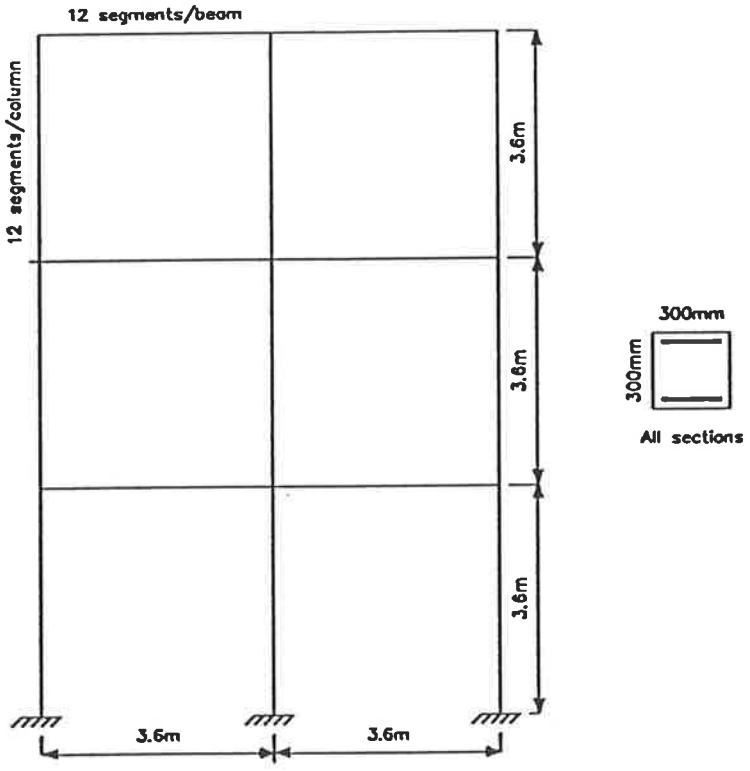

Figure 4.5: Configuration of 3-storey 2-bay frame

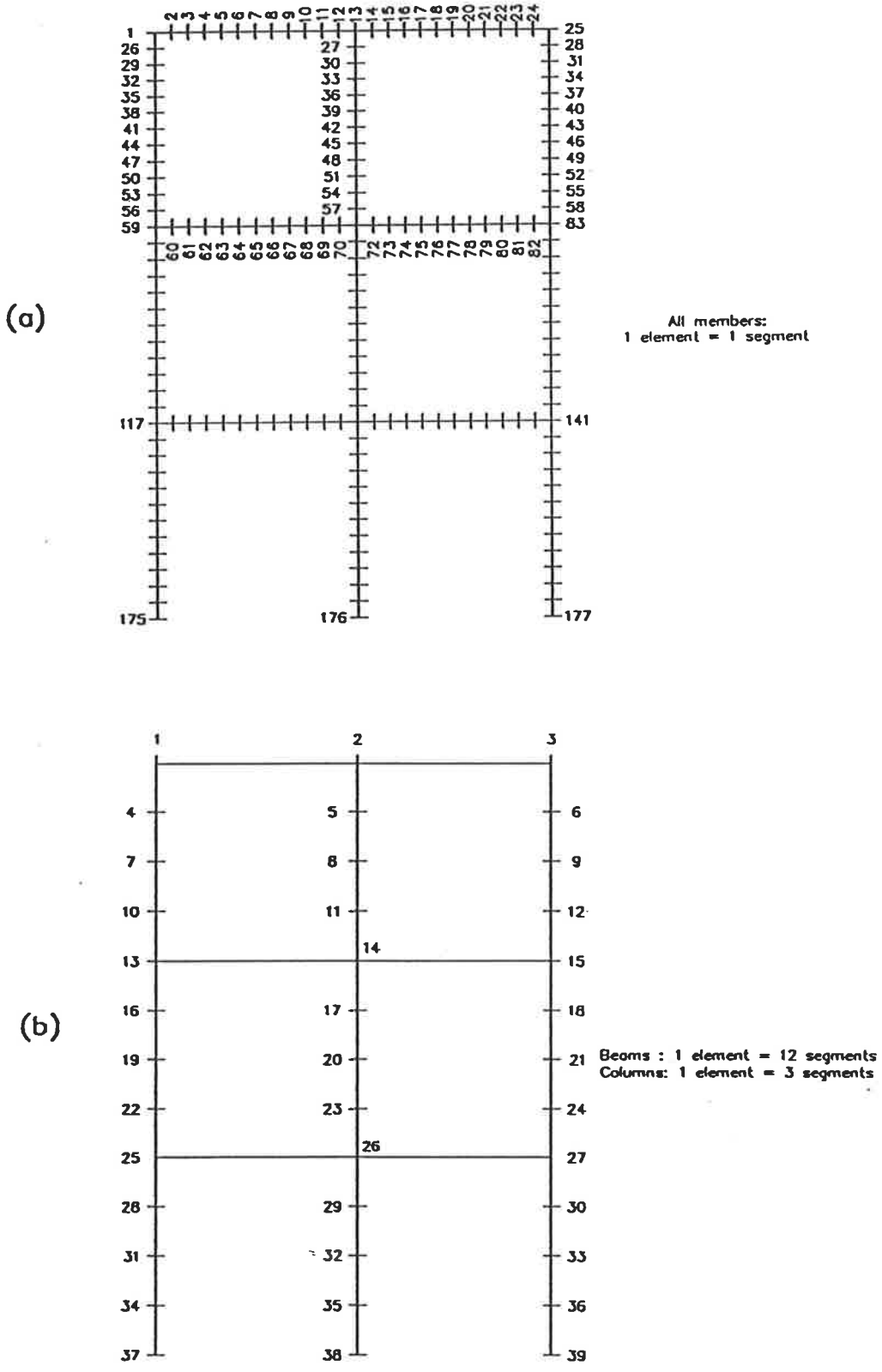

Figure 4.6: Efficiency of the segmental approach

analysis, expressions for fixed end moments for segmented elements have also been derived.

Chapter 5

Program Testing

5.1 Introduction

Before program SAFRAME can be used to study the collapse behaviour of reinforced concrete frames, the accuracy of the program in predicting the behaviour of actual reinforced concrete frames needs to be demonstrated. This was carried out by comparing results obtained from laboratory tests with those obtained using SAFRAME. Test structures chosen for analyses include columns and frames reported previously in literatures.

When analytical solutions are compared with experimental data, one must keep in mind that although the experimental results do give us a fair idea of the behaviour of the structures, the accuracy of the results obtained depends on a number of factors. These include the loading system, the accuracy of setting up the tests, the accuracy of the instruments used to obtain the data, and the consistency of concrete behaviour. In cases where the test structures

are simple, comparison between results obtained from the present analysis with those obtained using other sound analytical methods also give some indication of the accuracy of the present procedure.

Some of the results published in this chapter have previously been published (Wong, Yeo and Warner, 1987a; 1987b; 1988c; Wong and Warner, 1988).

5.2 Column Test

Hinged columns subjected to eccentric axial loading were tested by Ramu et al(1969). Column 24 was loaded in a short time test to failure. The structure is shown in Figure 5.1. Value of f_{sy} is 452 MPa. Value f_{cm} is assumed to be 25.2 MPa (0.80 f_{cube}) and value f_{cmax} is assumed to be 0.85 f_{cm}. Value of E_c is assumed to be 5000 $\sqrt{f_{cm}}$. Value ϵ_{cmax} is assumed to be 0.002 . Value γ_1 calculated from f_{cmax}, E_c and ϵ_{cmax} is 2.34 and γ_2 is assumed to be 3.0.

Using one element will not model the geometric nonlinearity effect within the member as the column failed by buckling. Figure 5.2 gives the results predicted by the program with two elements and a node at mid length and having a total of 32 segments. In the same figure, another plot is shown for 64 segments. The results obtained indicate that increasing the number of segments has little effect on the results obtained for the structure.

In Figure 5.3 theoretical results are shown for the same structure modelled using various numbers of elements. The total number of segments was maintained at 64. There was a significant change in the result when the number of elements was increased from two to four; however, a further increase from four to eight did not affect the results much. Thus, four elements were considered sufficient to model the behaviour of this column. Comparison between analytical and experimental results in Figure 5.3 shows that the predicted failure load

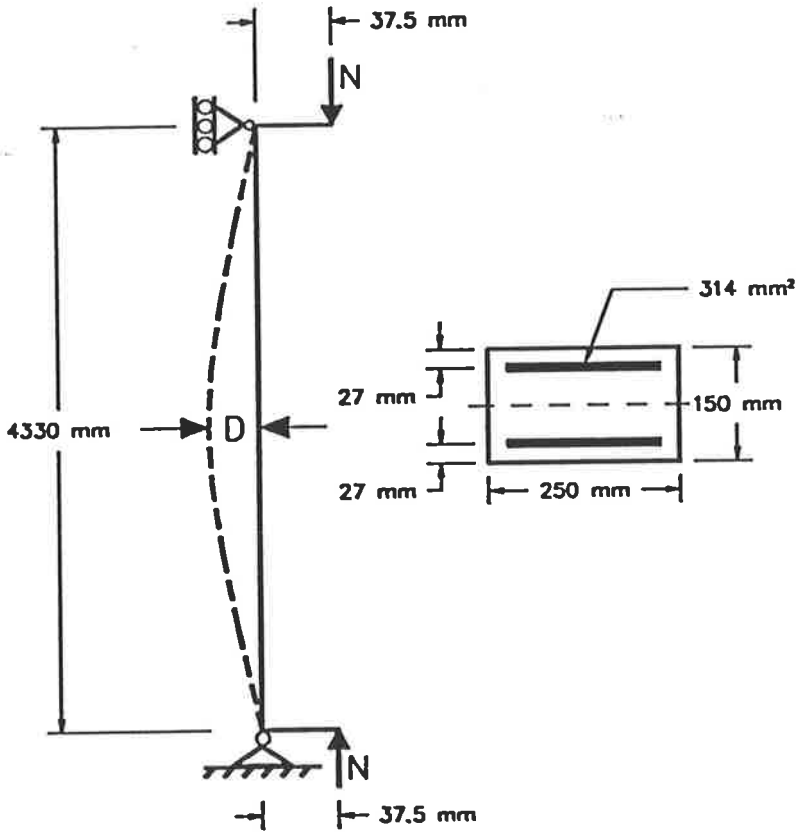

Figure 5.1: Hinged column tested by Ramu et al(1969)

is lower than the experimental value. This may be caused by the inaccuracy in the factor used to convert the strength of standard cubes to that of standard cylinders.

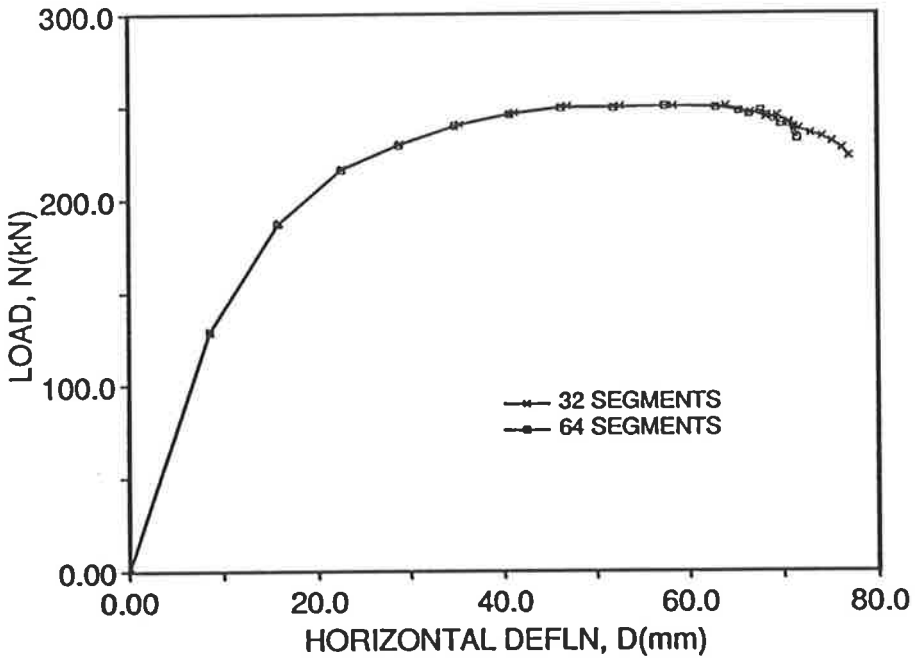

Figure 5.2: Load versus horizontal deflection plot for hinged column with 2 elements

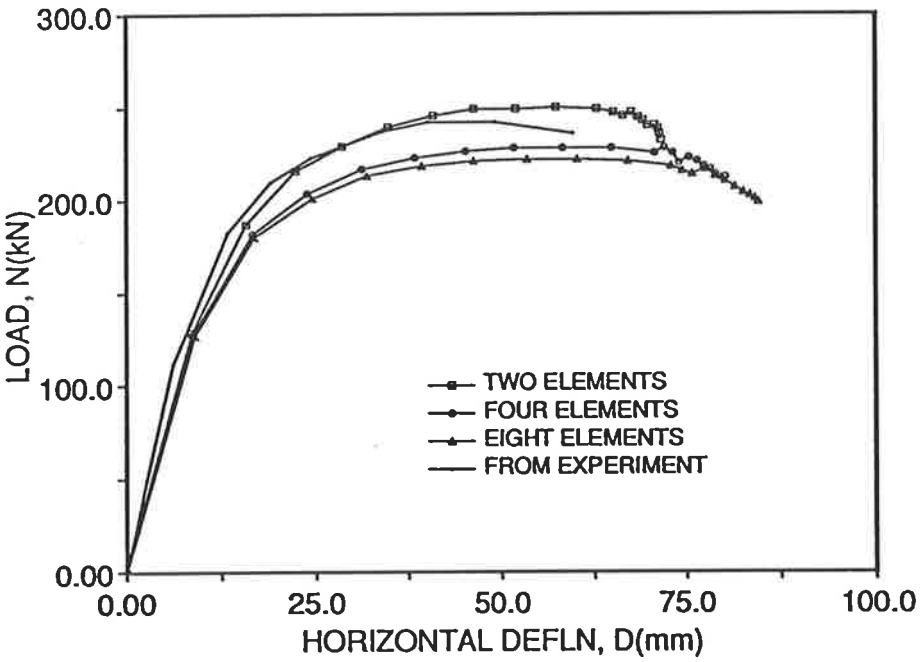

Figure 5.3: Load versus horizontal deflection plot for hinged column with various numbers of elements

5.3 Frame Tests

5.3.1 Sway Frame

Program SAFRAME was used to analyse an unbraced slender reinforced concrete frames L3, which had been tested by Ferguson and Breen (1966). The same frame had previously been analysed by other analytical techniques (Gunnin, Rad and Furlong, 1977, Epsion,1986). Reasonable agreement between experimental and theoretical load versus sway deflection relations had been obtained by Gunnin et al and Epsion.

The structural frame L3 is shown in Figure 5.4. Two cases were chosen for analysis. In case A, the frame was modelled using one element per member, each in turn was modelled by using ten segments. In case B, the number of elements used per member was maintained at one, but the number of segments was increased to twenty. Results obtained from these analyses are shown in Figure 5.5. The value f_{cmax} for concrete is assumed to be 0.85 f_{cm}. Value of E_c is assumed to be $5000\sqrt{f_{cm}}$. Value of ϵ_{cmax} is assumed to be 0.002. The average value for E_{steel} is 2.02×10^5 MPa. Value of f_{sy} for reinforcement bars in the beams and columns is 403 MPa. Value of γ_1 calculated from E_c, ϵ_{cmax} and f_{cmax} is 2.50 and γ_2 is assumed to be 3.00.

The results shown in Figure 5.5 show that increasing the number of segments from ten to twenty has little effect on the simulated behaviour of the structure. In the same figure, the experimental results are plotted. The plots indicate excellent agreement between analytical and experimental results.

To study the effect of the number of nodes on the accuracy of the theoretical results, the number of elements used to represent a member was increased. Keeping the total number of segments per member constant at twenty, an extra node was inserted into each member by using two elements per member.

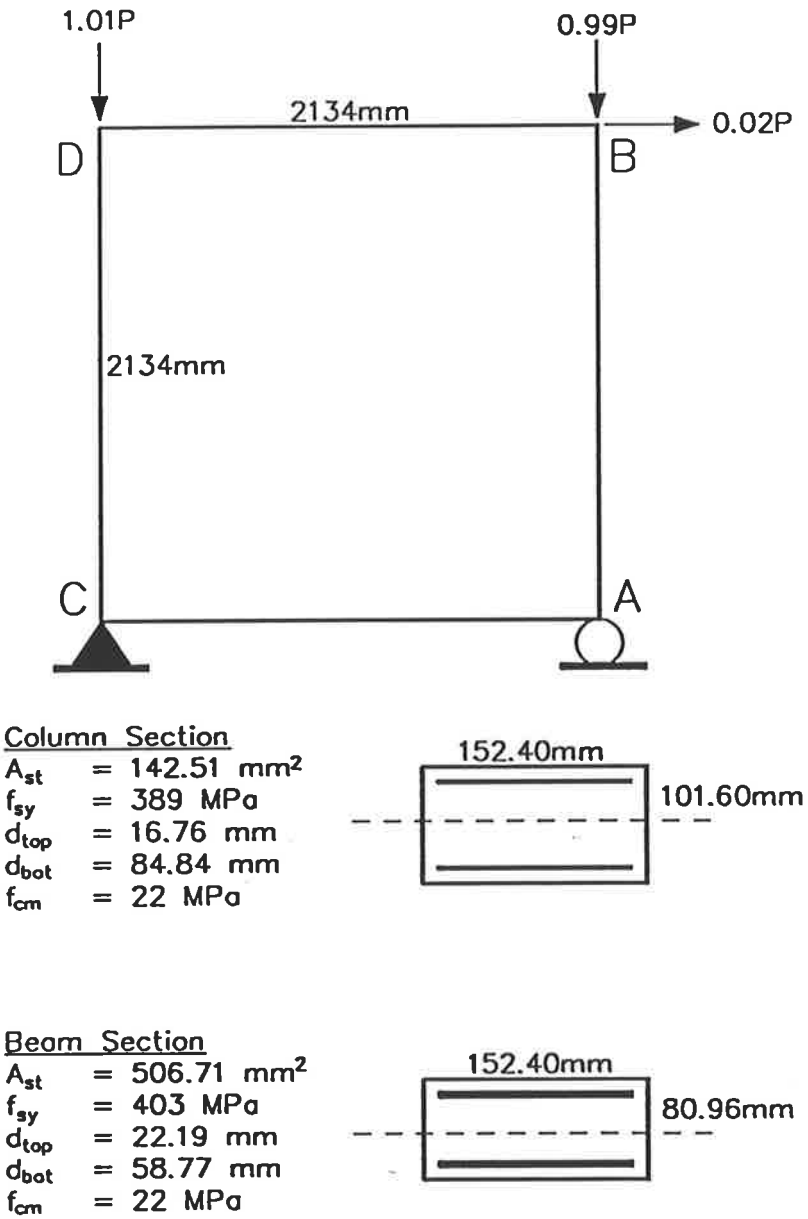

Figure 5.4: Sway frame L3 tested by Breen and Ferguson (1969)

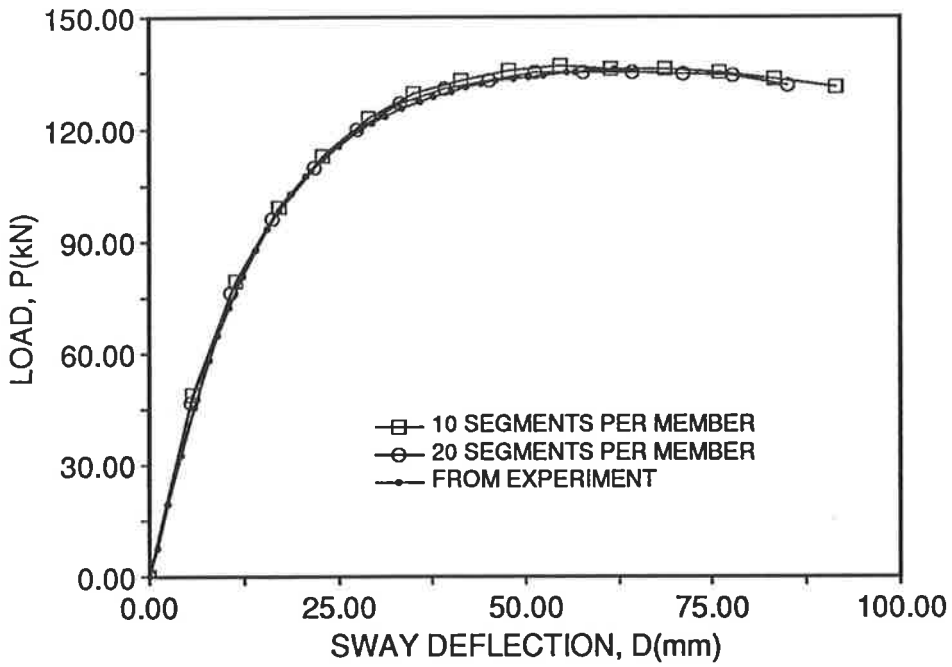

Figure 5.5: Load versus sway-deflection plot for sway frame L3 with 1 element per member

Another analysis was carried out by increasing the number of elements per member to four, resulting in three nodes within the member. Results from these analyses are shown in Figure 5.6. The results show that for this frame, where the columns deformed with double curvatures, one element per member is sufficient to give reasonably accurate results.

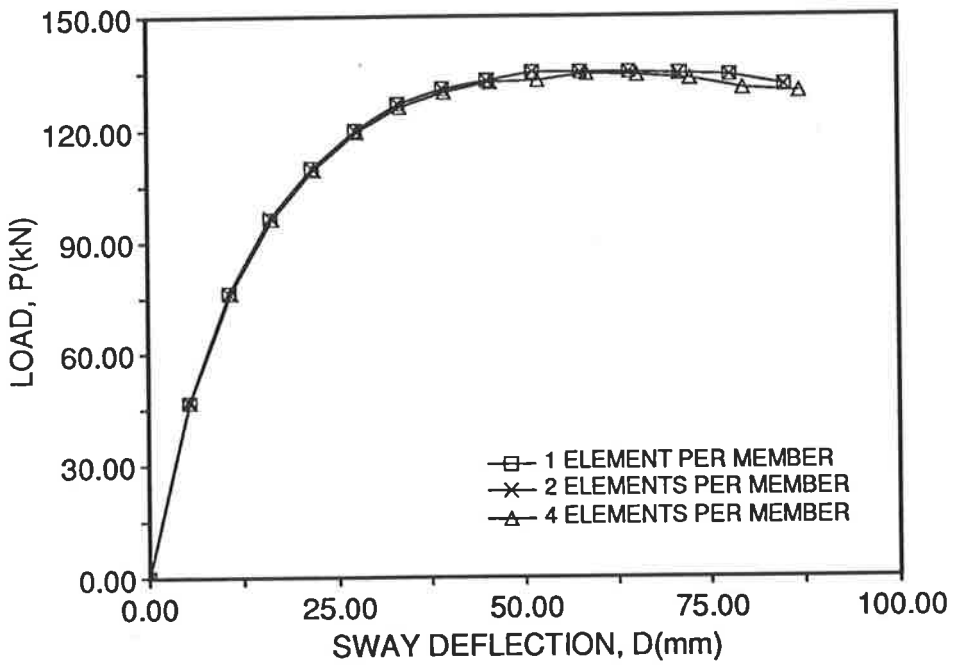

Figure 5.6: Load versus sway-deflection plot for sway frame L3 with various numbers of elements

The ability to obtain accurate prediction of the load versus sway deflection for this frame implies good agreement between the present analysis and analytical procedures developed by Gunnin et al and Epsion because, as pointed out earlier, they too get good prediction of the load versus sway deflection behaviour for this frame.

The load versus bending moment plots for the stations immediately adjacent to the joints were obtained theoretically using the present analysis assuming 10 segments per element and 1 element per member. These are shown by a continuous line in Figure 5.7. On the assumption that the correct column loads and lateral loads have been applied and that the frame behaviour is symmetrical, the column moments were computed by Ferguson and Breen as the sum of the nominal end moment and the product $Py/2$, where P is the column load and y is the measured lateral deflection of the upper joint of the column relative to the lower joint. The moments calculated from this assumption are shown in Figure 5.7 as a dashed line.

Moments were also obtained through curvature measurements by Ferguson and Breen using a series of 165 mm gage length rotation meters immediately adjacent to the four joints. Test results are shown as data points in Figure 5.7 for three of the joints (the rotation meter for corner A was faulty during the test). As bending moment could not be obtained directly, they were obtained from the curvature measurements indirectly by using a section analysis program based on the assumption that the stress strain relation of the concrete follows Hognested's model. Hence, the accuracy of the bending moments obtained depends on the accuracy of the moment-curvature calculations.

The bending moments obtained using deflection measurements give values close to the joints, whereas those obtained using rotation meters give average values over a gage length of 165 mm. This is reflected in the plot as the values obtained using the latter approach are smaller. Since the results obtained

theoretically by the present approach are adjacent to the joints, these were compared with those obtained experimentally from deflection measurements. The agreement is considered to be very good(Figure 5.7).

Investigation of the moment curvature relations of all the segments obtained from SAFRAME shows that no hinge was formed at collapse. The moment curvature relations of the critical segments are obtained using SAFRAME; those along the columns adjacent to joints A, B, C and D are shown in Figures 5.8 through 5.11. Thus, the collapse was caused by instability, whereby as a result of both material and geometrical non-linearity effects, the frame swayed to such an extent that deflection continued to increase without any increase in load. Eventually a stage was reached in the calculations when an equilibrium condition could not be found.

5.3.2 Frames with Columns in Single Curvature

Furlong and Ferguson (1966) tested seven rectangular frames loaded so that the columns were bent in single curvatures. Test frames F2 and F4 were selected for study here. These frames were also analysed by Gunnin, Rad and Furlong (1977) using numerical technique developed by them. Column loads P and beam loads αP were increased proportionally until the frame collapsed.

Half of the symmetric frame F2 is shown in Figure 5.12. Only one half of the frame was used in the present analysis, with supports A and B not allowed to rotate. The assumed properties of the concrete are: f_{cm} is 29.7 MPa; $E_c = 5000\sqrt{f_{cm}}$; $f_{cmax} = 0.85 \times f_{cm}$; γ_1, calculated from E_c, ϵ_{cmax} and f_{cmax}, is 2.16; and $\gamma_2 = 3.00$. For steel reinforcement: f_{sy} is 380 MPa; and $E_s = 2.0 \times 10^5$ MPa.

The load deflection plots obtained from the present analysis using 2 elements per column and 4 elements per column are shown in Figure 5.13. 20 segments

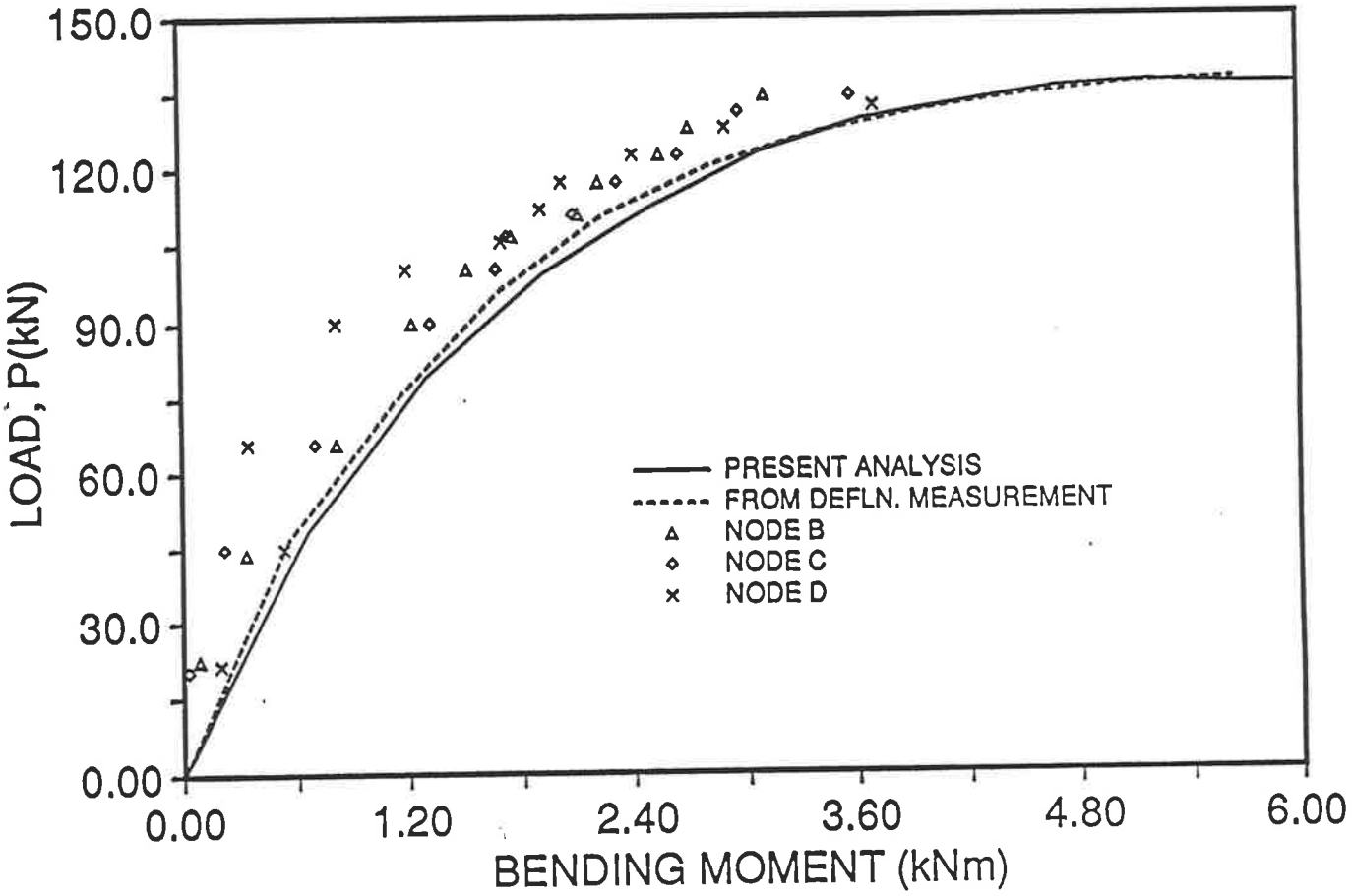

Figure 5.7: Load versus bending moment for sway frame L3

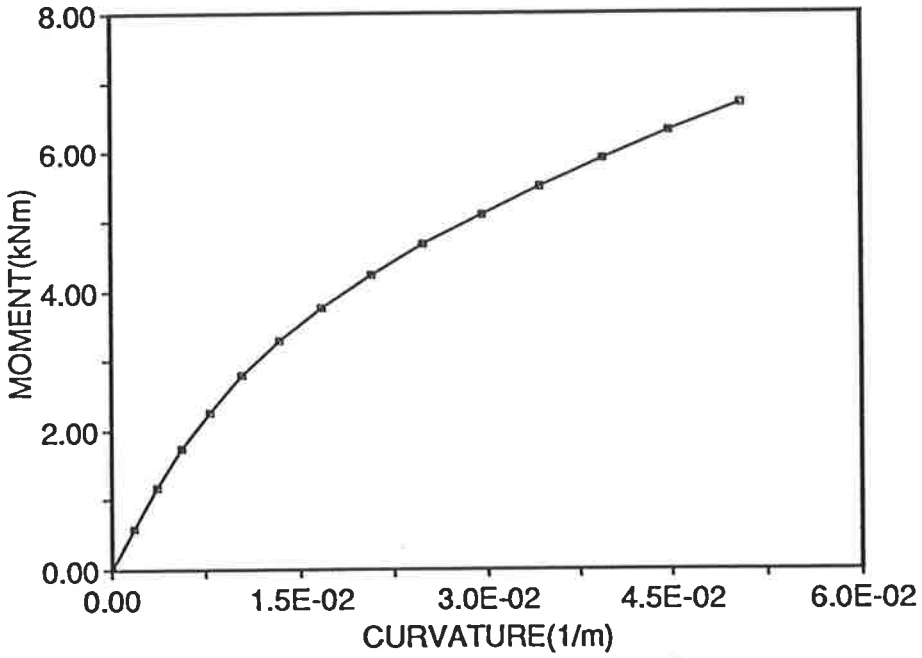

Figure 5.8: Moment curvature relation for segment adjacent to joint D

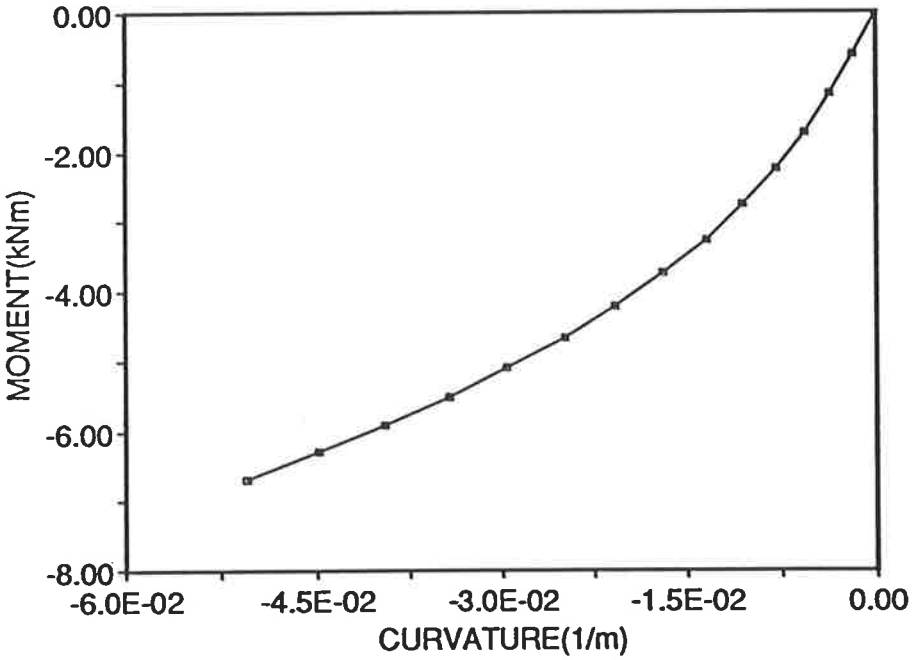

Figure 5.9: Moment curvature relation for segment adjacent to joint C

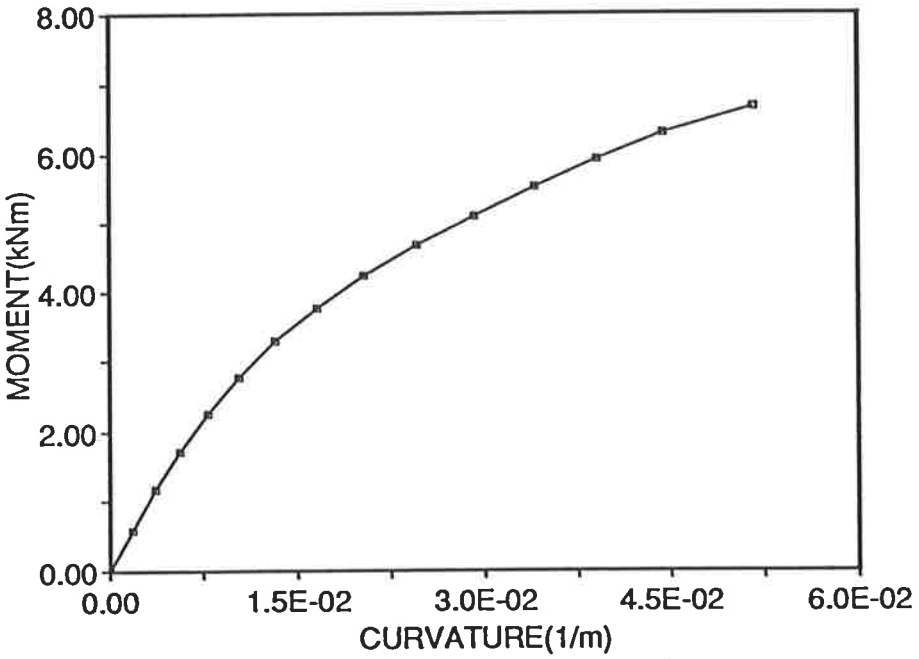

Figure 5.10: Moment curvature relation for segment adjacent to joint B

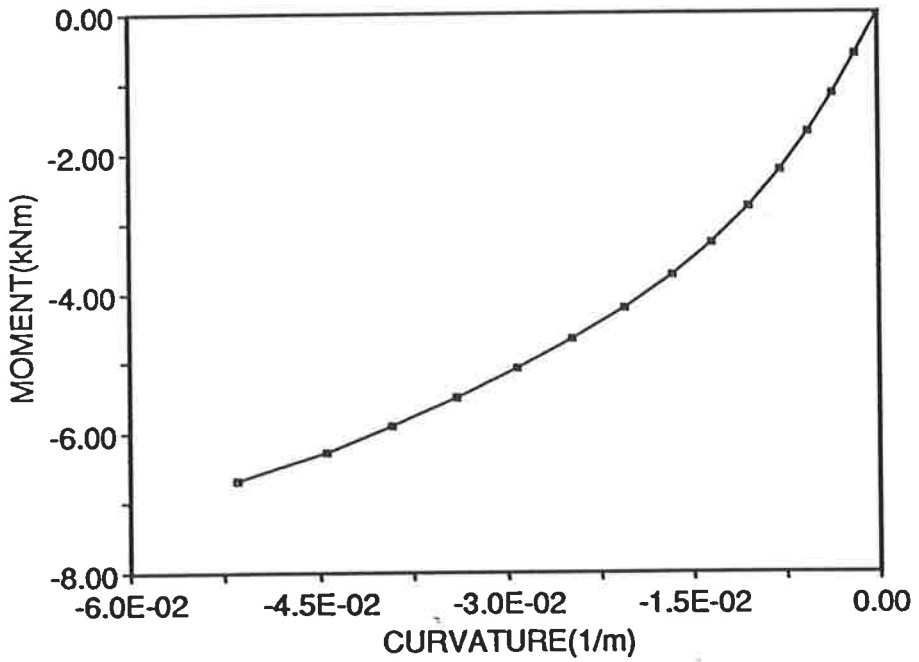

Figure 5.11: Moment curvature relation for segment adjacent to joint A

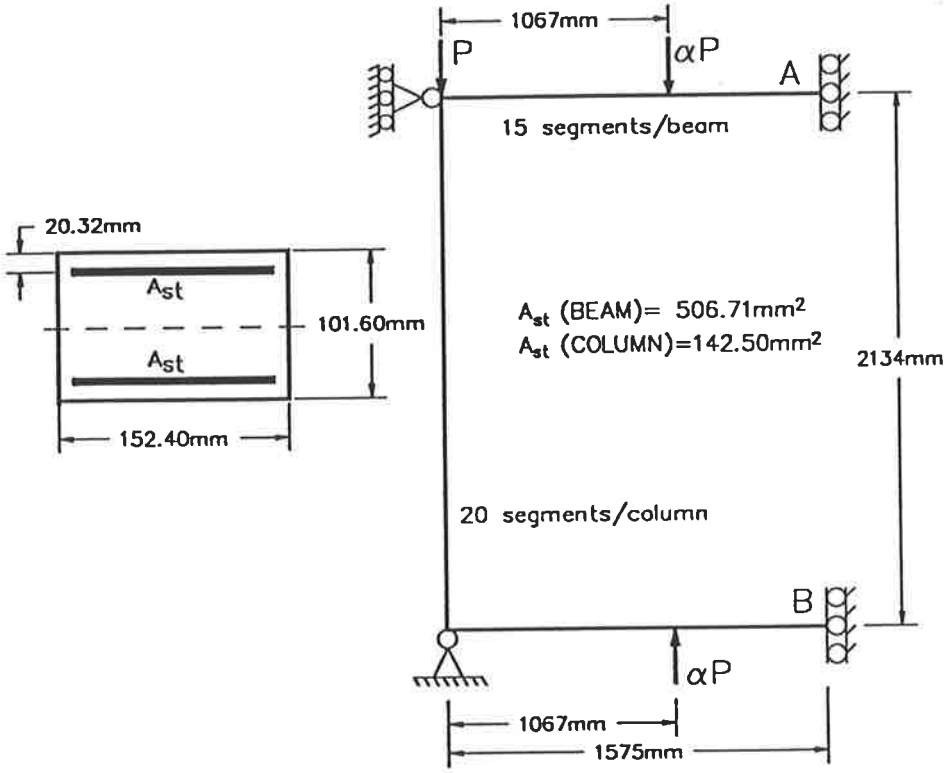

Figure 5.12: Test frame F2 tested by Furlong and Ferguson (1966)

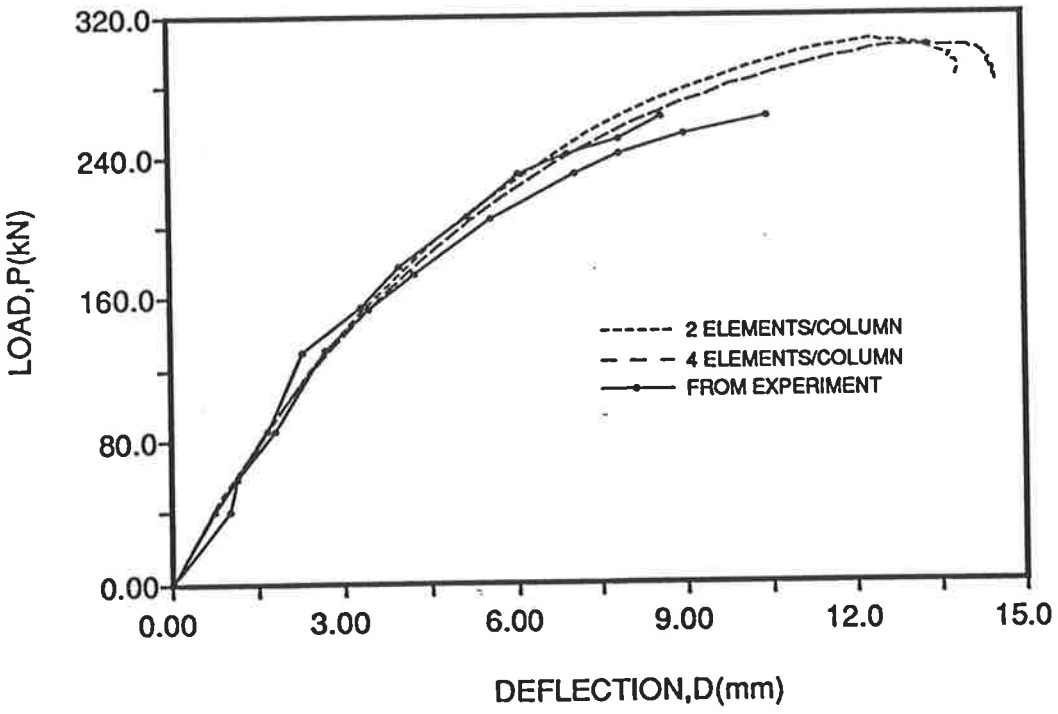

Figure 5.13: Load versus mid-column horizontal deflection for frame F2

were used for the entire column. In the same figure, experimental results obtained and reported by Furlong and Ferguson are also plotted. Although the frame is symmetric, two experimental curves are shown: one for the left column and the other for the right column. There is a large variation in the behaviour of the two columns. This non-symmetric behaviour in a supposedly symmetric frame is likely to be caused by difficulties involved in setting up such frames for testing; it is not only difficult to built perfectly symmetric frame, but also difficult to apply perfectly symmetric load. The horizontal deflections at mid-height of the columns are plotted along the x-axis. In light of the different test results obtained for the two columns, the present analysis gives a reasonably good estimate of the behaviour of this frame, over the range of the experimental results. With 4 elements per column an ultimate load of 302 kN is predicted as compared with 274 kN obtained from the experiment. Rad, Gunnin and Furlong obtained a failure load of 287 kN using their analytical analysis, which agrees well with the present estimate.

The axial load versus the magnitude of the bending moment plot obtained analytically by the present approach and that obtained experimentally by Furlong and Ferguson are shown in Figure 5.14. The moments obtained theoretically show the same trend in behaviour as those obtained from experiment. The behaviour can be divided into three stages. In the first stage, both the end moments and the mid-column moments increase. A second stage is reached where the end moments decrease, distributing some of their moments to the mid-column. Finally a stage is reached whereby both the end moments and the mid-column moments decrease with increasing curvature in a pre-selected key segment; a collapse condition having been reached. There is reasonable agreement between experimental and theoretical results for the end moments but agreement between the results for the mid-column is not good.

Results are also obtained for frame F4, a frame similar to frame F2 but having stiffer beams. The frame is shown in Figure 5.15. For this frame, the assumed

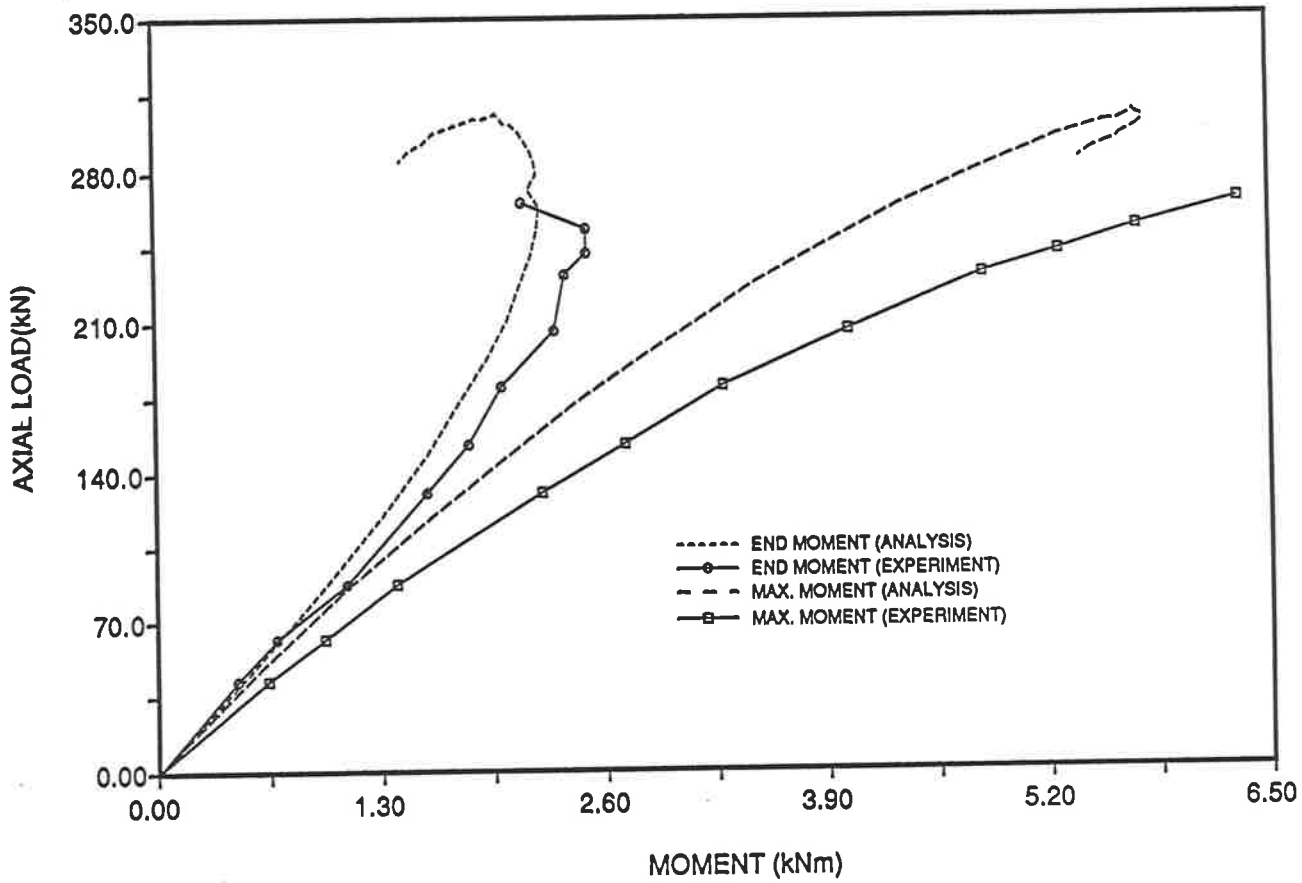

Figure 5.14: Load versus bending moment for test frame F2

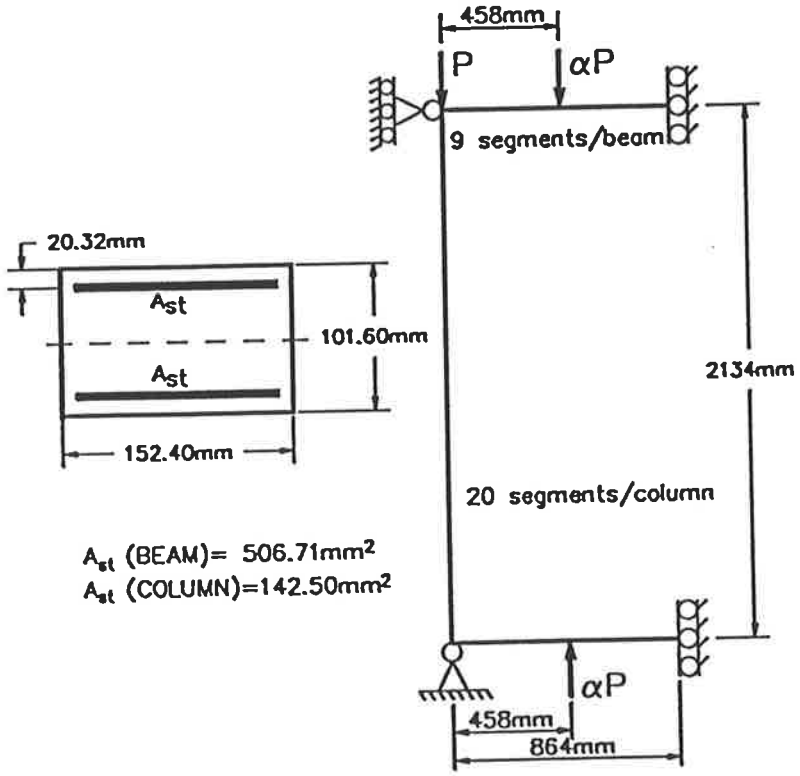

Figure 5.15: Test frame F4 tested by Furlong and Ferguson (1966)

properties of the concrete are: $f_{cm} = 22.3$ MPa; $E_c = 5000\sqrt{f_{cm}}$; $f_{cmax} = 0.85 \times f_{cm}$; γ_1 calculated from E_c, ϵ_{cmax} and f_{cmax} is 2.49; and $\gamma_2 = 3.00$. For the steel reinforcement: f_{sy} is 370 MPa; and $E_s = 2.0 \times 10^5$ MPa.

A plot of load versus horizontal deflection obtained from the present analysis using 2 elements per column is shown in Figure 5.16. Twenty segments were used for the entire column. In the same figure, the experimental results obtained and reported by Furlong and Ferguson are also shown. Although the results predicted by the present analysis is not particularly good, the large variation in the load versus deflection behaviour between the two supposedly similar columns suggests that it may be difficult to get a good fit. The present analysis gives an ultimate load of 207 kN as compared with 234 kN obtained from the experiment. Rad, Gunnin and Furlong obtained a failure load of 200 kN using their analytical technique, which agrees well with the present estimate.

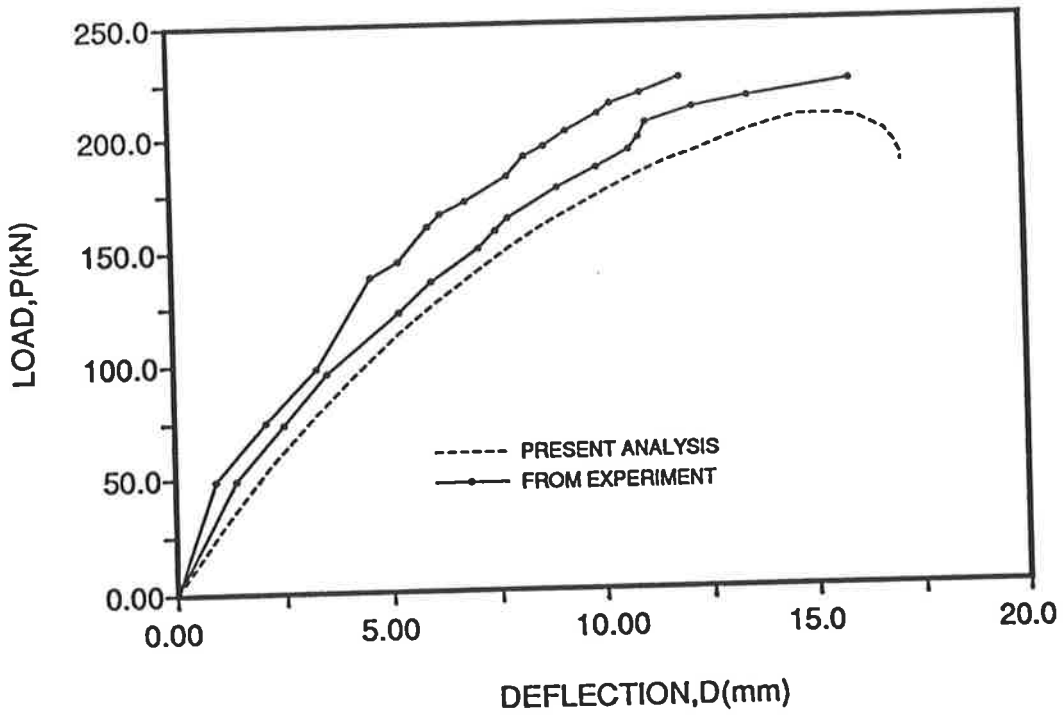

Figure 5.16: Load versus mid-column horizontal deflection for frame F4

The axial load versus the magnitude of the bending moment plots obtained analytically by the present approach and that obtained experimentally by Furlong and Ferguson are shown in Figure 5.17. This frame displays similar behaviour to that of frame F2. There is reasonable agreement between experimental and theoretical results for the moments at the ends and at mid-column.

5.4 Conclusions

Comparisons between results obtained from the present analysis with test results and results obtained by other analytical methods indicate that the present approach can give reasonably good predictions of the behaviour of reinforced concrete frames. Comparisons with test results obtained by other analytical methods suggest the the results obtained using the present approach are as good as any other "rigorous" method of analysis. Obviously, the program can be further developed to give better agreement with test results. An extensive study of all available frame and beam test data is required if the computational model is to be improved. Further possible improvements are proposed in Chapter 9.

For the present analytical approach, using segment size of length approximately equal to its depth is sufficient to produce accurate modelling of concrete frames. The number of elements required to model the behaviour of columns depends on whether the column failed in a sway mode or a buckling mode. It was found that 4 elements are usually sufficient to model accurately the behaviour of single column failing in a buckling mode. For frames failing in a sway mode, fewer elements are required. In the case of the sway frame (with columns in double curvature) analysed, it was found that one element per column was sufficient to model the behaviour.

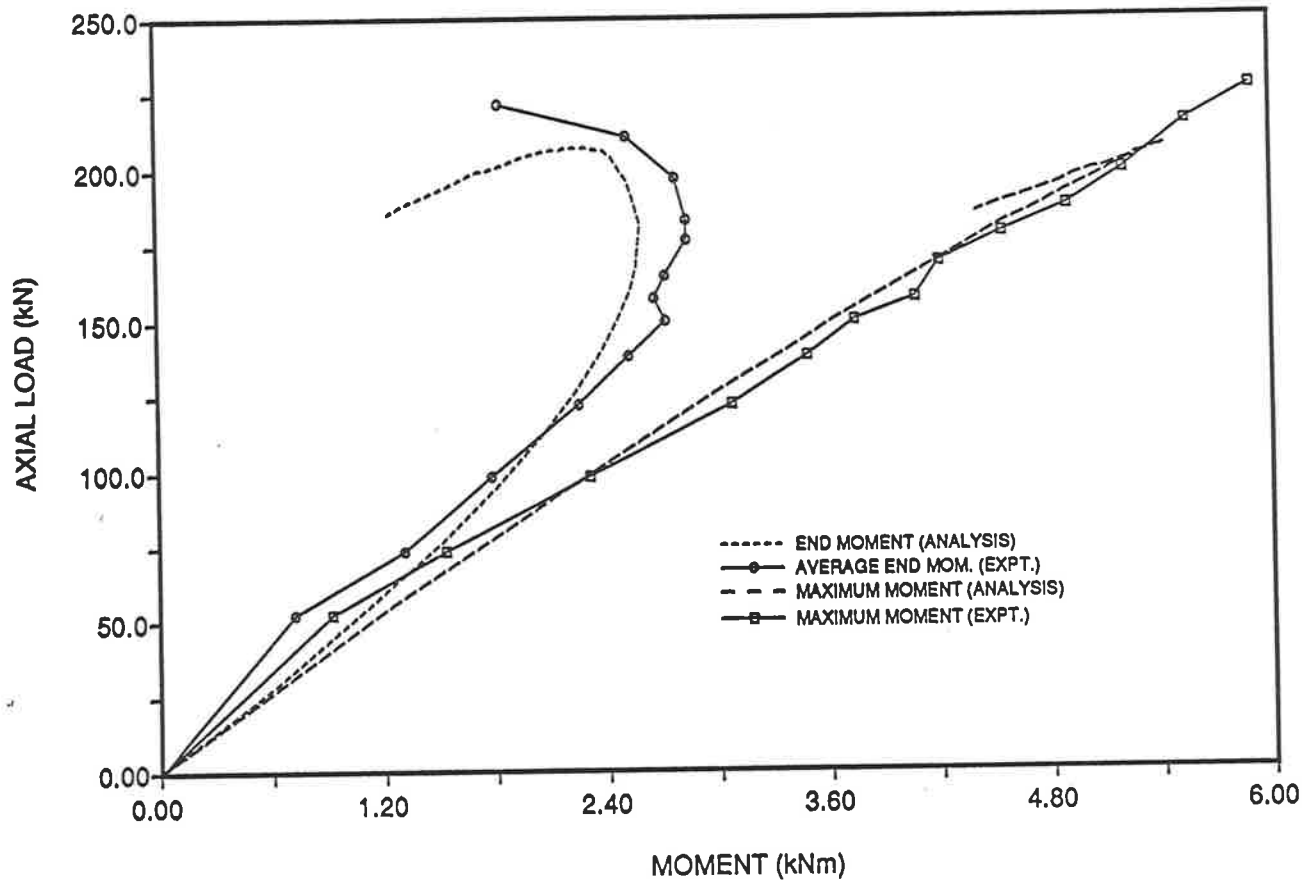

Figure 5.17: Load versus bending moment for test frame F4

Chapter 6

Study of the Non-linear Behaviour of Reinforced Concrete Frames using program SAFRAME

6.1 Introduction

In this chapter, the non-linear behaviour of reinforced concrete frames is studied up to peak load and into the post-peak range. This study was undertaken as a prelude to the investigations described in Chapters 7 and 8, the purpose of the study being to provide information on the conditions which exist when peak load occurs in a frame, on post-collapse peak load behaviour, and on the effect of several parameters (notably beam stiffness and the degree of geometrical nonlinearity modelling) on collapse and post-collapse behaviour.

Some of the frames, depending on geometry and load pattern, exhibit substantial softening and even snapback, a phenomenon described earlier in Chapter 3. In Section 6.2, the softening behaviour of a test frame, previously analysed in Chapter 5 is discussed. The frame softens before the formation of any concrete hinges. A concrete hinge is defined in this and subsequent chapters as a segment having moment-curvature relation (with the effect of thrust included) that has either a relatively flat plateau or a softening path, and which displays monotonic increase in curvature for the loading conditions being studied. Hinges which follow a softening path will be referred to as softening hinges. The behaviour observed in this test frame can also be reproduced in a simple cantilevered column. Another frame, similar to the test frame, but with more stocky columns, and with a larger applied horizontal load, can be used to illustrate the behaviour of frames which collapse immediately upon the formation of a plastic hinge mechanism.

Four sets of frames with different loading patterns are also analysed using SAFRAME to investigate the range of behaviour which may be expected to occur in concrete frames and the effect of the variations in the process of numerical modelling of the geometrical non-linearities. For each set, three numerical models are used. These include one without any geometrical nonlinerity effect (model I); one with P-Δ effect of the joints only (model II); and one with full treatment of geometrical nonlinearities (model III). For each set, frames with three-metre high columns and nine-metre high columns are analysed.

In Section 6.4, investigations are carried out on the effect of neglecting the thrust effect on frame behaviour. This is useful as some numerical models use a pre-determined moment-curvature relation for each segment which is assumed not to be affected by the change in thrust acting on the segment as loading progresses. The inaccuracy in neglecting thrust effect in the numerical model is investigated by analysing a frame with and without thrust effect being included into the analysis.

As the Australian code does not take into account the amount of beam reinforcement in the determination of the strength of frames with slender columns, Section 6.6 investigates the effect of beam reinforcement on the strength of frames. A portal frame is analysed with different amounts of reinforcement in the beam. Results obtained indicate the importance of beam behaviour on the strength of the frame.

Snapback instability, a phenomenon suggested to occur in strain softening structures, has been observed occasionally. Three frames displaying snapback behaviour are discussed in Section 6.4. The ability to trace snapback is important if the softening behaviour of frames is to be studied.

Finally, the non-linear behaviour of a few multi-storey frames is treated in Section 6.7. The behaviour, though more complex, can be related to the basic behaviour patterns displayed by the portal frames investigated in Section 6.3.

6.2 Softening Behaviour of Frames

In this section, the softening behaviour of reinforced concrete frames is studied using program SAFRAME. The causes of system softening are traced through the moment-curvature plots of the potential hinge forming segments in the frames. The effect of sectional thrust is included when obtaining the moment-curvature relations.

In Chapter 5, it was found that the frame $L3$ tested by Breen et al load softened before the formation of any concrete hinges, thus giving rise to instability failure. This happens as the result of combined geometrical and material non-linearities. The frame is shown together with the moment-curvature relations of the potential hinge-forming segments of the beams in Figure 6.1, and with those of the columns in Figure 6.2. These segments are next to the joints of

the frame. It can be observed that no hinges were formed at collapse.

This softening behaviour before the formation of concrete hinges is best illustrated using a simple structure such as a cantilevered column, with point loads at the free end, as shown in Figure 6.3. The load is plotted against horizontal deflection of the top of the column in Figure 6.4. The moment-curvature curve for the segment at the base is shown in Figure 6.5. In Figure 6.6, the load is plotted against curvature in the same segment.

As the analytic approach uses a deformation control procedure with a "key" segment, of which curvature is used as the controlling parameter, the structure under the effect of the specified load pattern is progressively solved for increasing curvature in the key segment. An increase in curvature in the key segment at the base of the column (and, presumably, in other adjacents segments) results in a horizontal movement of the tip of the column. The increase in moment of the base segment can result either from an overall increase in load magnitude or from the increase in the horizontal movement Δ and hence the moment $P\Delta$. If the column is sufficiently long, it is thus possible for the load to decrease even though M and κ both increase. This effect causes the column to display load-softening behaviour before the formation of any concrete hinges. This can be observed clearly in Figures 6.5 and 6.6.

Another analysis was carried out on a frame with the same beam and column cross section as the frame $L3$ tested by Breen, but with equal vertical loads applied above the columns and with the sway force increased to ten per cent of total vertical load. The height of the frame was reduced to half that of frame $L3$ (see Figure 6.7). The load versus sway deflection at the top of the left column is shown in Figure 6.8. The collapse of the frame occurs after the formation of four hinges, i.e., the formation of a complete plastic collapse mechanism. The term "plastic collapse mechanism" is used throughout this thesis to describe the formation of sufficient hinges for elastic-plastic collapse to occur. The

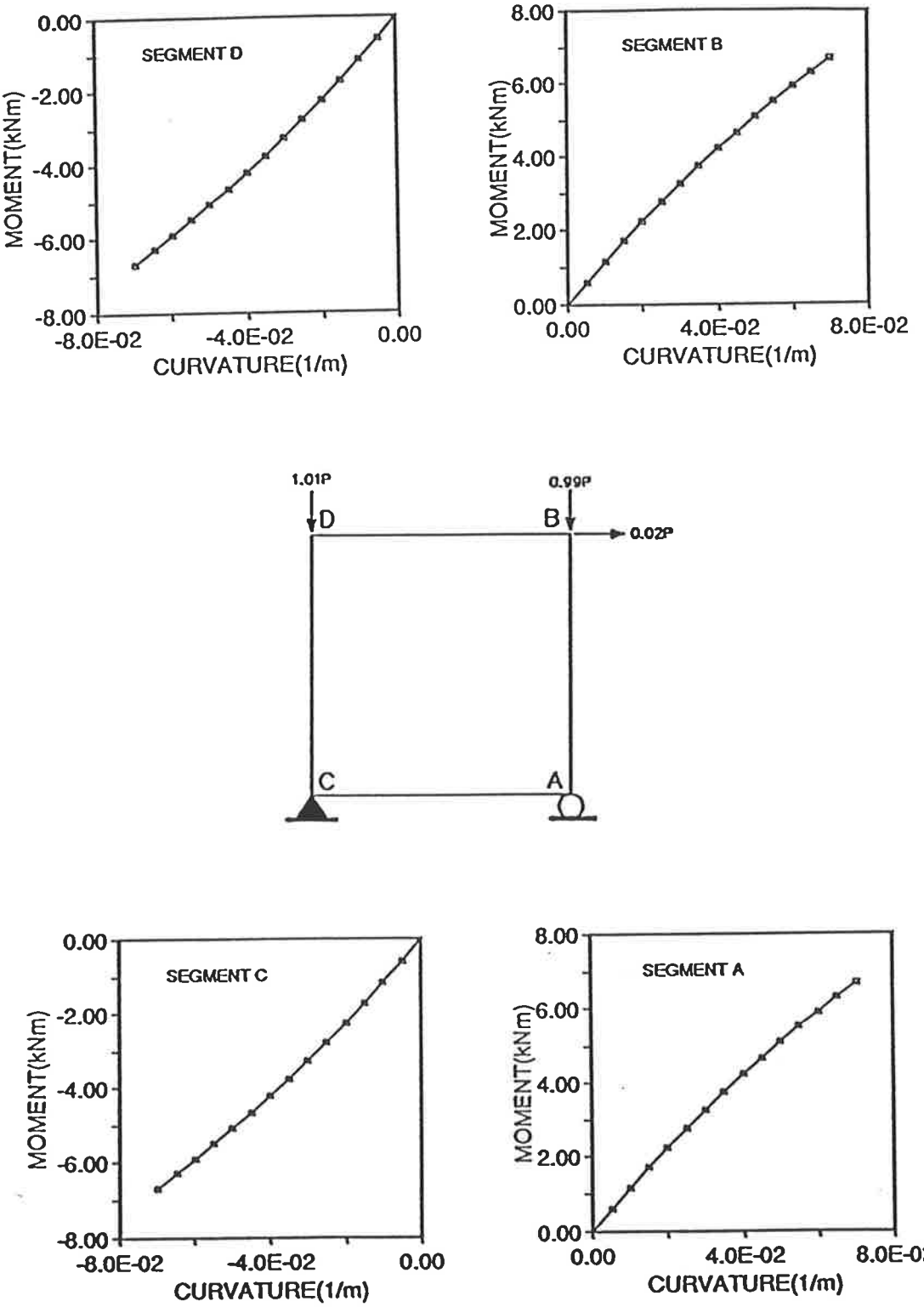

Figure 6.1: Moment-curvature relations of potential hinge-forming beam segments

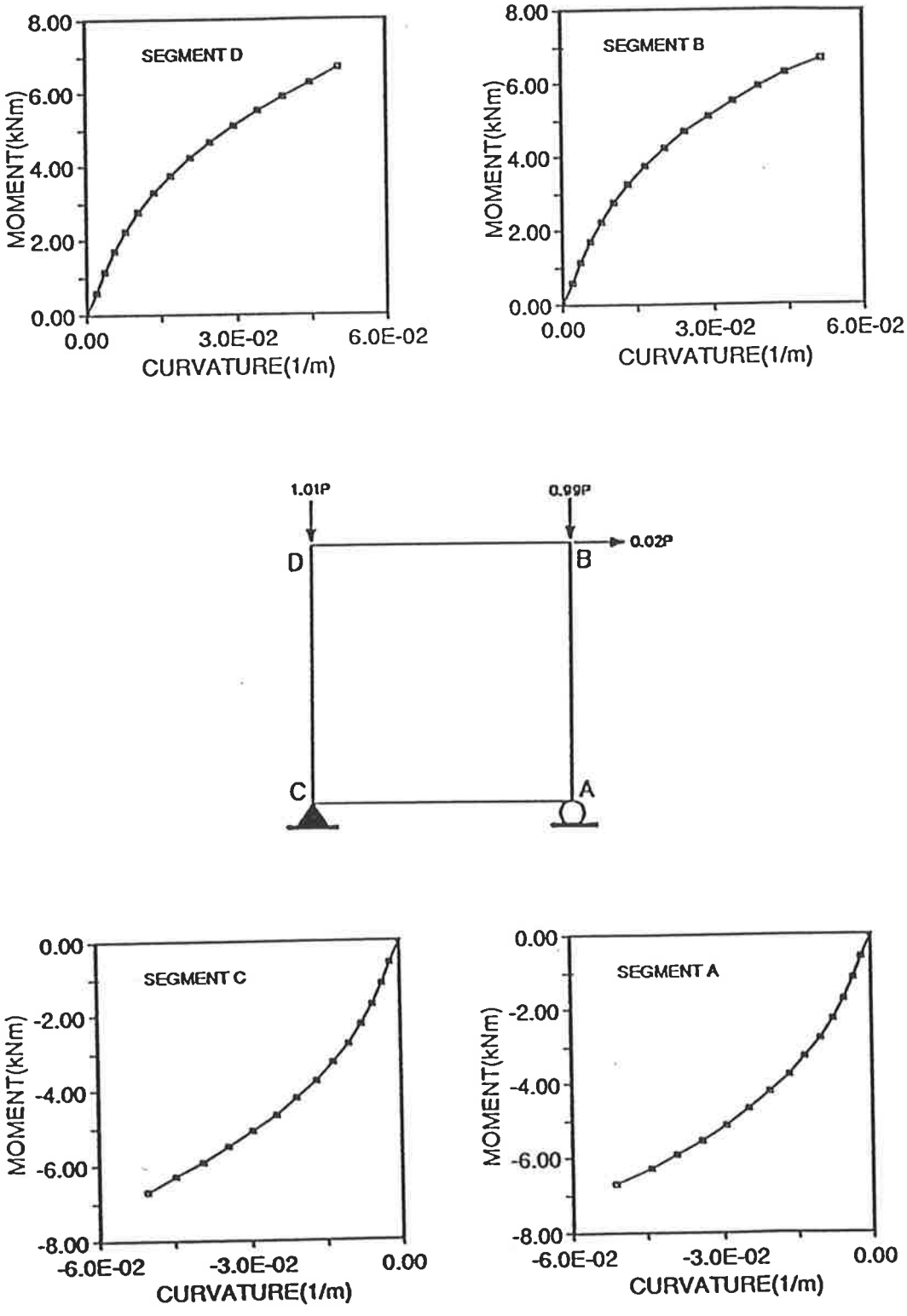

Figure 6.2: Moment-curvature relations of potential hinge-forming column segments

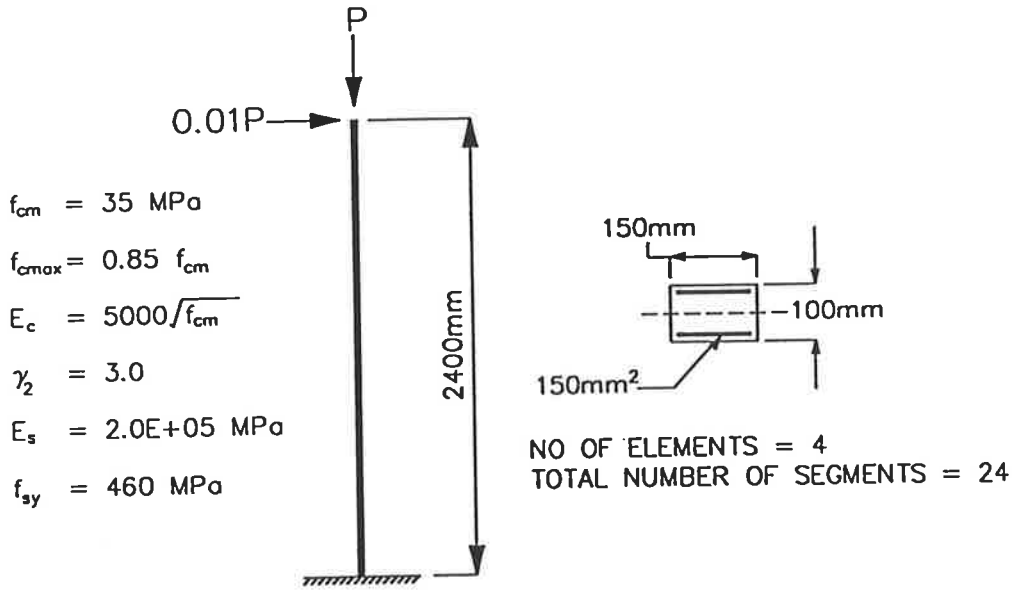

Figure 6.3: Free standing cantilever

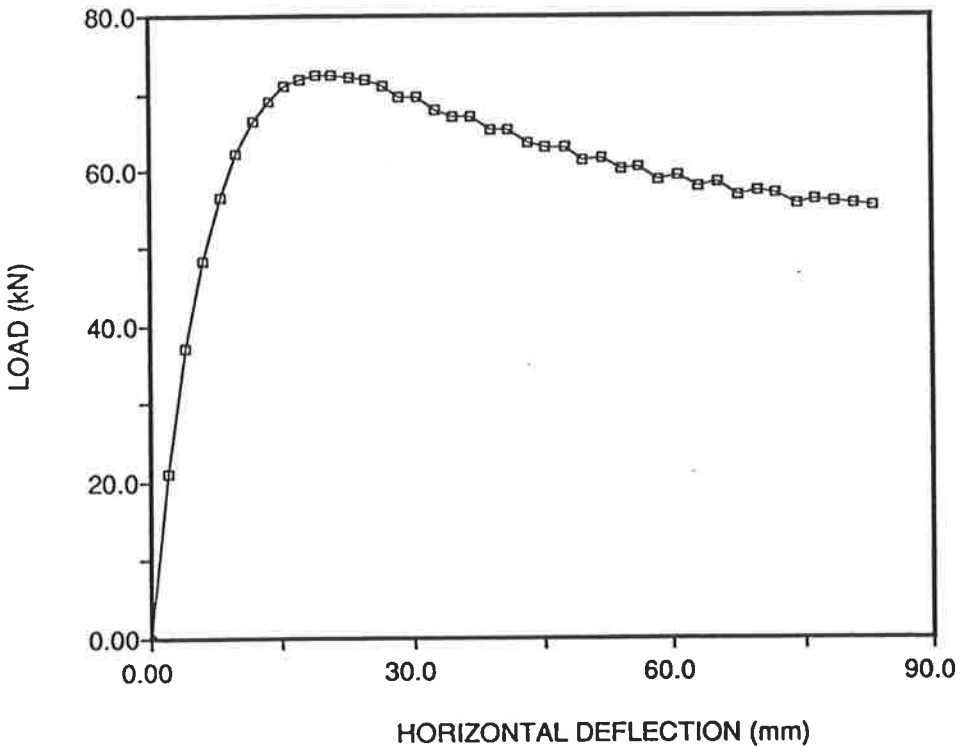

Figure 6.4: Behaviour of cantilevered column

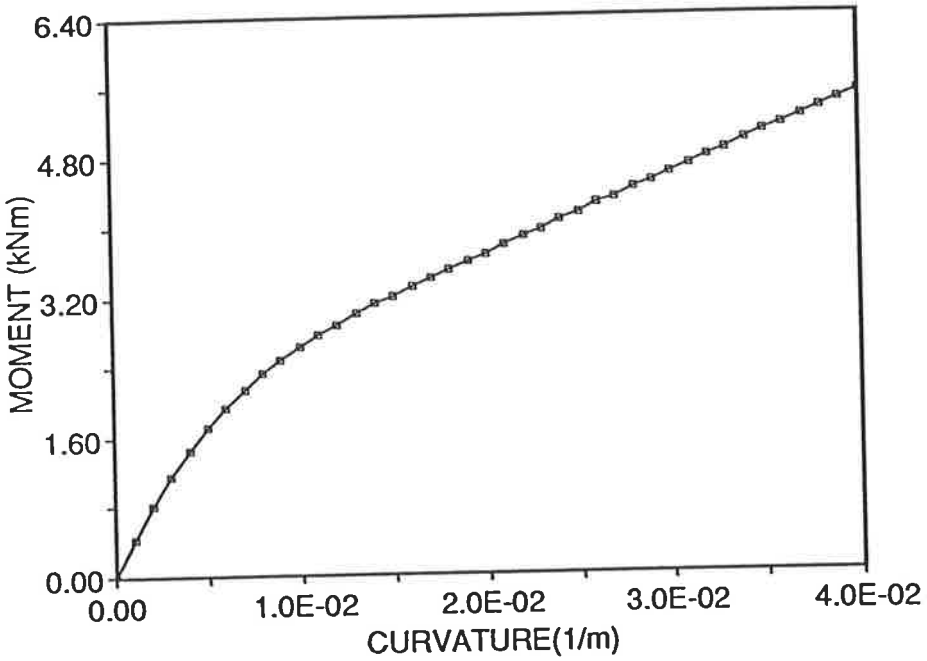

Figure 6.5: Moment-curvature plot for segment at base of column

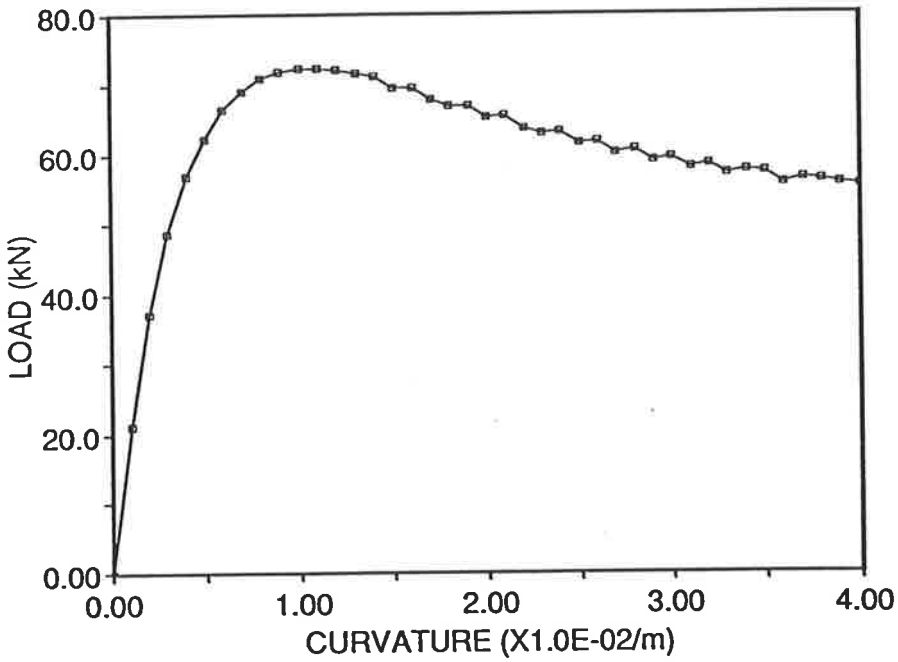

Figure 6.6: Load-curvature plot

moment-curvature relations of potential hinge-forming segments are shown in Figure 6.9 and Figure 6.10. These figures show that all the hinges are at the ends of columns as the beams have relatively higher amount of reinforcement.

The results of these two sway frames show that the the collapse of concrete frames can occur at any stage of hinge formation. Indeed, it is not necessary for any hinge to form at all, especially in very slender frames which display substantial geometrical nonlinearities. This observation throws some doubt on the use of elastic, perfectly plastic analysis both for the prediction of peak load and as the basis for design.

6.3 Non-linearities in Frame Behaviour

In order to study the effects of various assumptions regarding non-linear behaviour, a series of computer simulations were carried out using SAFRAME for a number of portal frames with various load pattern. Twenty-two frames were analysed using the three levels of accuracy of treating nonlinear effects. These levels are:

- Model I: material nonlinearity effect only.
- Model II: material nonlinearity effect and geometric nonlinearity effect caused by the deflections of the joints of the frames.
- Model III: material nonlinearity effect and full geometric nonlinearity effects: that caused by the movement of the joints and that caused by the deflection of the member away from the centerline joining the ends of the member.

Four sets of loadings were considered. These are referred to as SET1, SET2, SET3 and SET4. For each set, two frames are considered: one with a height of

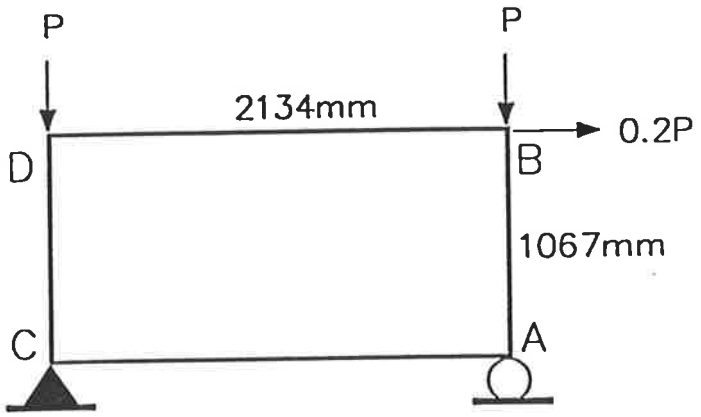

Figure 6.7: Details of sway frame

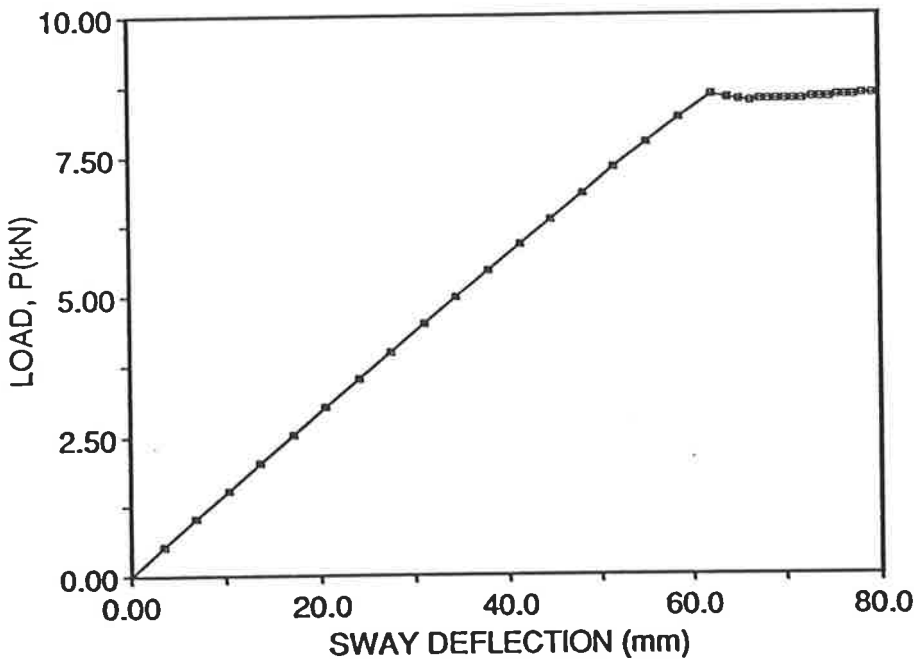

Figure 6.8: Behaviour of sway frame

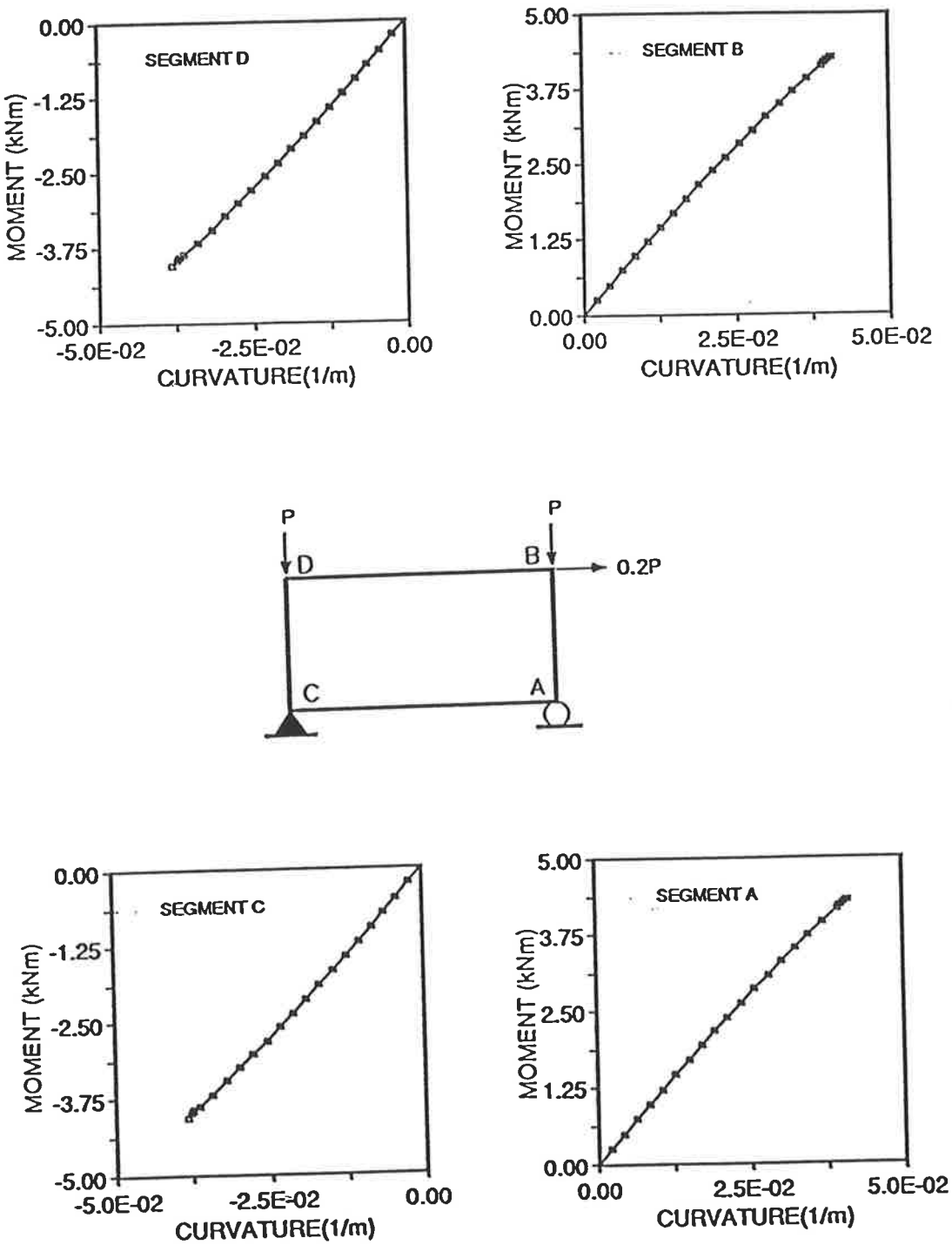

Figure 6.9: Moment-curvature relations of potential hinge-forming beam segments

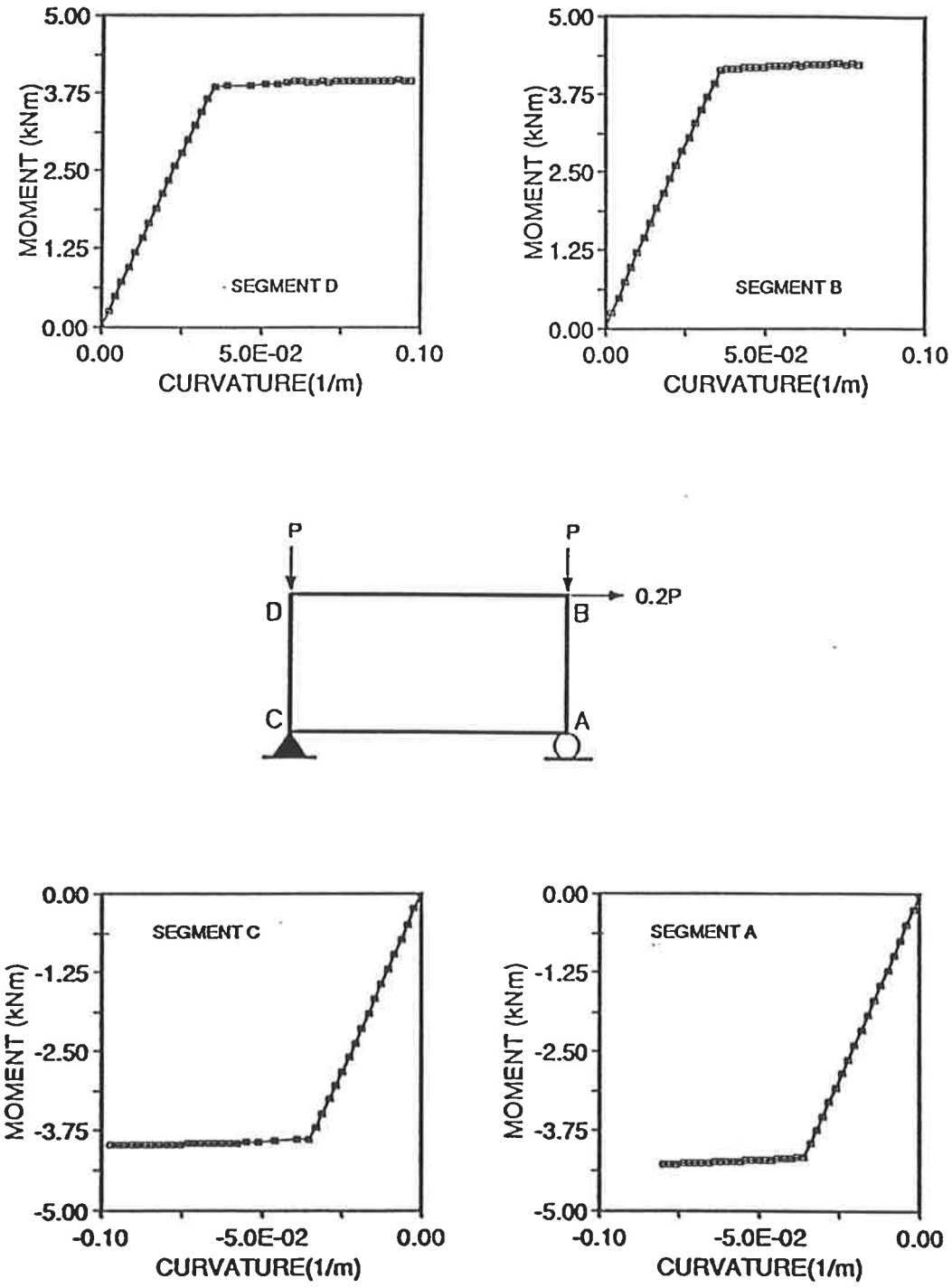

Figure 6.10: Moment-curvature relations of potential hinge-forming column segments

3 metres and the other 9 metres. Details of load patterns and frame geometry and properties are shown in Figure 6.11 and Figure 6.12.

For model I, the treatment of geometric effects in SAFRAME was bypassed.

Type II model includes the treatment of the geometric effects caused by the lateral movements of loaded joints. This assumes that only the joints reflect the deflected shape of the members.

The type III model was achieved by using four elements (and therefore inserting three additional internal nodes) per column. This, as shown earlier in Chapter 5, allows the deflected shape of a column (be it in single or double curvature bending) to be taken into consideration. No internal nodes were inserted along the beams.

For SET4, the frame is braced, and therefore model II is not applicable as it will give the same results as model I as the joints of the compression members are not allowed to move horizontally.

FRAME1S and FRAME1T are subjected to loading only at the joints to ensure that local beam collapse does not occur, as such collapse affects the overall behaviour of the frame.

The short frame, FRAME1S, is quite stiff laterally. This results in smaller sway at beam level and therefore reduces the amount of geometric nonlinearity caused by the deflection of the loaded joints. This in turn results in smaller bending moments in the potential hinge-forming segments next to the supports, thus, allowing these segments to carry larger axial thrust, and thereby increasing the load-carrying capacity of the frame.

The load versus sway deflection plot of this frame, shown in Figure 6.13, indicates steeply softening and local ultimate deflection for model I. D in this plot is the horizontal deflection at the top end of the left column. The moment

SET	NAME	CONFIGURATION	MODELS
FRAME1	FRAME1S	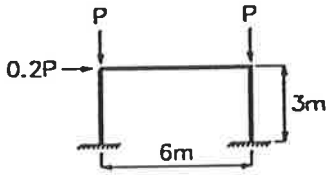	I,II,III
	FRAME1T	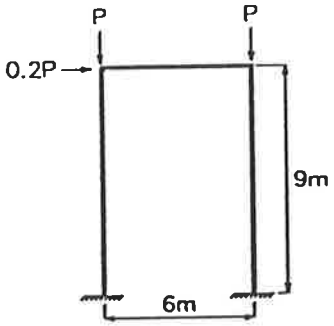	I,II,III
FRAME2	FRAME2S	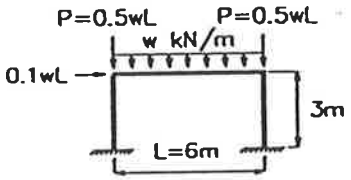	I,II,III
	FRAME2T	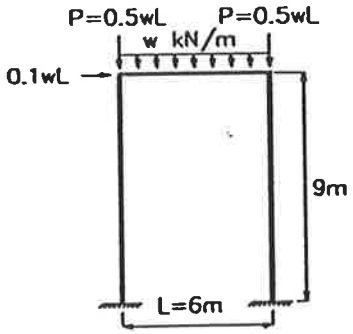	I,II,III

Figure 6.11: Portal frames SET1 and SET2

SET	NAME	CONFIGURATION	MODELS
FRAME3	FRAME3S	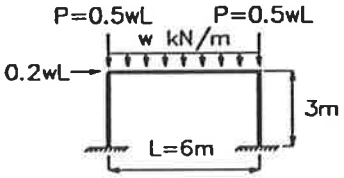	I,II,III
	FRAME3T	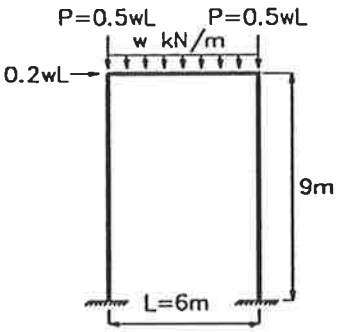	I,II,III
FRAME4	FRAME4S	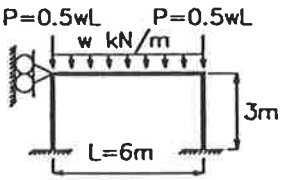	I,III
	FRAME4T	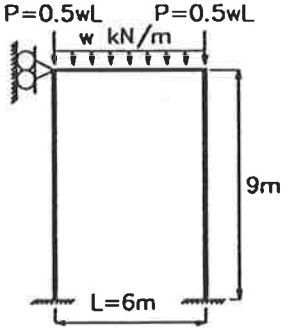	I,III

Figure 6.12: Portal frames SET3 and SET4

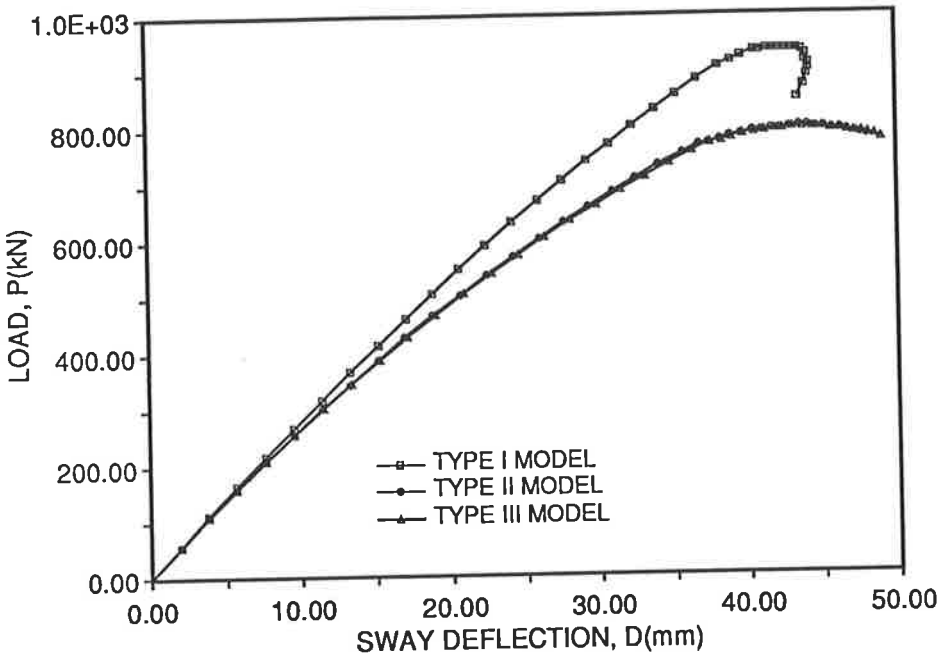

Figure 6.13: FRAME1S: sway deflection

curvature relation of the key segment, selected to be the segment at the base of the right column, has a relatively steep softening path (see Figure 6.14). The softening of the frame occurs at the same curvature step as the commencement of softening in this segment; this agrees with previous findings by other researchers (Bažant, 1976; Darvall and Mendis, 1985) that softening of a structure can be caused by a softening hinge. In the works of Darvall and Mendis, the softening slope in the linearised moment-curvature relation is predetermined and is fed as input data into the analysis. In reality, the softening is dependent on the stress history of the segment, and in particular also on the axial thrust acting. Model I analysis of FRAME1S takes this into account, but the effect of the degree of softening of a hinge on the post-ultimate behaviour of a frame cannot be investigated directly. However, the effect of changing thrust is obviously important and is usually ignored in the analysis based on predetermined moment curvature relations.

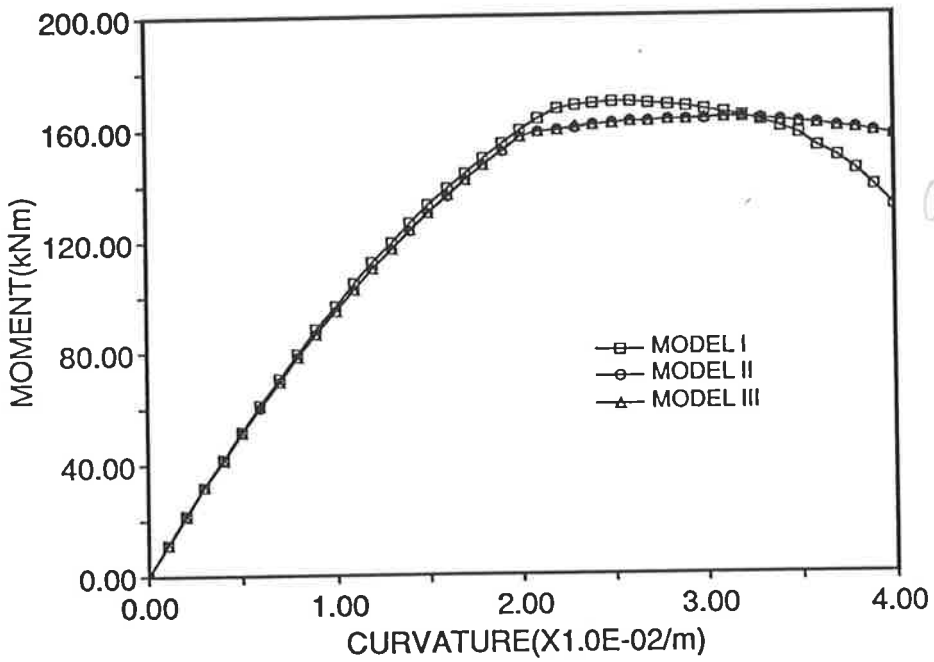

Figure 6.14: FRAME1S: moment-curvature plot for key segment

Though eventually four hinges formed in the frame (two at the ends of the beam and two at the bases of the columns), only two of these hinges were present at peak load. These were next to the supports of the frame. This agrees with previous observations by Darvall and Mendis(1985) that softening in one or several hinges can cause the load to soften.

When geometrical nonlinearities are included (in models II and III), the frame displays a more gradual softening slope (see Figure 6.13). The moment curvature relations of the key segment (also taken to be at the base of the right column) in these models have almost flat peaks (see Figure 6.14).

The importance of including geometrical non-linearity effects when modelling this frame can be observed from the load versus sway deflection plots; the peak load obtained using model I is about 940 kN and that for models II

and III is about 800 kN (see Figure 6.13). The peak load is overestimated by approximately 17.5 per cent when geometric nonlinearity effects are ignored in the numerical modelling. On the other hand, comparison of models II and III shows that deflections of the node points are clearly far more important than the additional deflections within the length of each column.

FRAME1T, which has nine-metre high columns, does not display steep softening (see Figure 6.15). The tallness of the frame results in large bending moment acting on the base segments caused by the applied horizontal load at beam level. The large moment and relatively small thrust acting at the base results in moment-curvature relations of the base segments with relatively flat softening paths. This causes the load versus sway deflection plots to have relatively flat plateaus (i.e. no steep softening)

The peak load of model I occurs after the formation of four concrete hinges (at positions required for the formation of a sway plastic collapse mechanism). When geometric nonlinearities are included (models II and III), fewer hinges are formed at peak load: two hinges for model II and three for model III, though eventually a complete set of four hinges is formed. This indicates that geometrical nonlinearity (frame instability) affects the collapse behaviour of this frame.

The importance of including the geometrical non-linearity effect when modelling this frame can be observed from the load versus sway deflection plots; the peak load obtained for model I is about 250 kN and that for model II and III is about 175 kN. Not including the effect of geometrical nonlinearity results in the peak load of this frame being over-estimated by approximately 43%.

Frame FRAME2S (see Figure 6.11) is subjected to point loads above the columns, a uniformly distributed load along the beam and a horizontal load at beam level with magnitude of five percent the total vertical load acting on the frame.

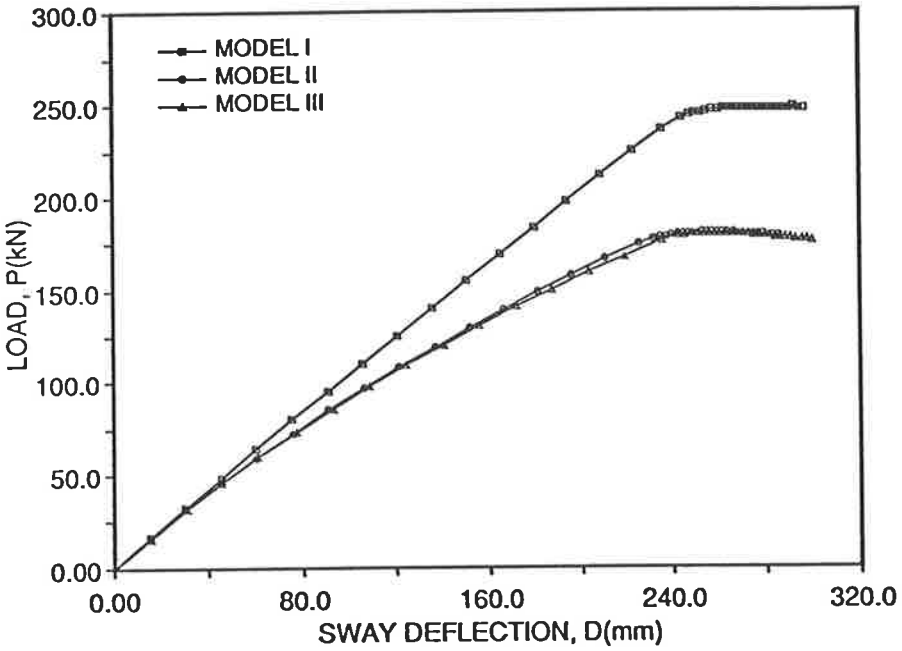

Figure 6.15: FRAME1T: sway deflection

The load versus mid-span vertical deflection plots show that the estimated peak loads are almost the same for models I, II and III (see Figure 6.16). This suggests the geometrical nonlinearity effect has little influence on the behaviour of this frame. The moment-curvature relations of potential hinge-forming segments obtained from the analysis indicate that three hinges have formed in the beam at peak load, one at each end of the beam and another at mid-span. No hinges form in the column.

The plots for load versus sway deflection for the same frame (see Figure 6.17) show that a "recovery" of sway deflection occurs in all three models during the later part of the analysis as increasing curvature is applied to the key segment during the analysis. This chosen segment is located in the beam, adjacent to the right end of the member. Such "recovery" of characteristic deflection

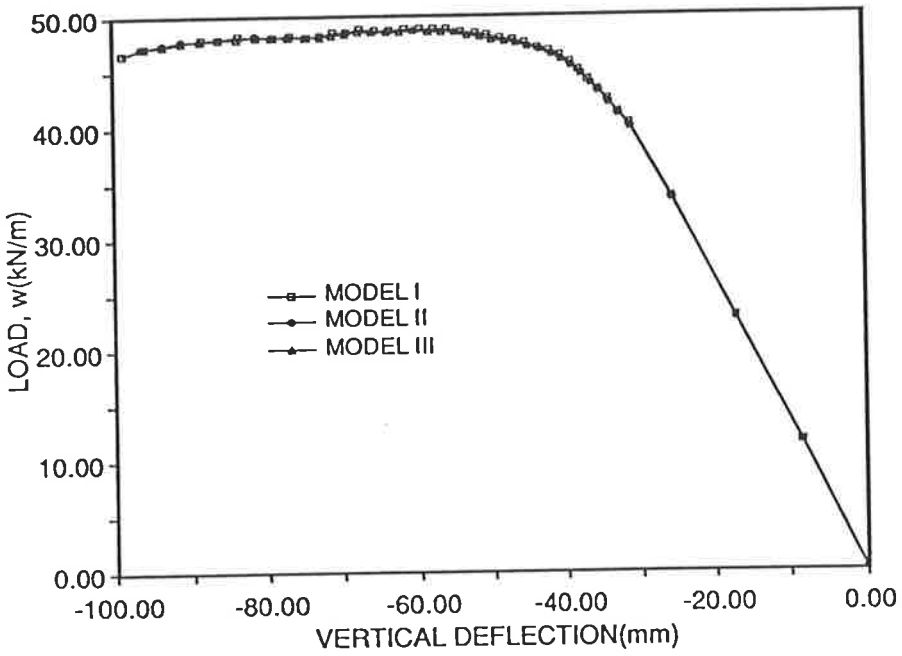

Figure 6.16: FRAME2S: vertical deflection

has been observed in structures exhibiting snapback behaviour (Bažant et al, 1987b). Snapbacks have been described earlier in Section 3.5. However, the analysis of frame FRAME2S has not been carried far enough to indicate the presence (or absence) of snapbacks.

In the case of the tall frame FRAME2T (see Figure 6.11), the load versus mid-span vertical deflection plots indicate significant difference in the peak load for model I compared with those of models II and III (see Figure 6.18). However, there is little difference between the peak loads of models II and III. This suggests that including the P-Δ effects caused by the lateral deflections of the joints is important, but including the the P-Δ effects within the length of the columns does not affect the results significantly. In all three models, two hinges are formed, one at the right end segment of the beam and the other at approximately mid-span.

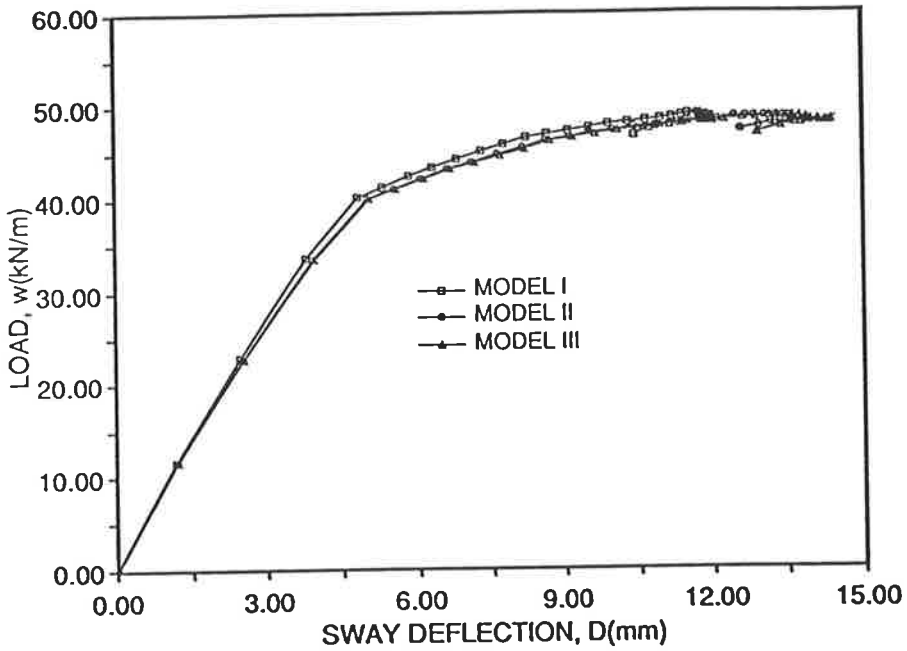

Figure 6.17: FRAME2S: sway deflection

The load versus sway deflection plots (Figure 6.19) indicate that model I is stiffer laterally when compared with models II and III. This observation suggests that reducing the degree of modelling with respect to geometric nonlinearities produces results which overestimate the sway stiffness of the frame.

FRAME3S is subjected to a uniformly distributed load along the beam, vertical point loads above the columns and a horizontal load at beam level (see Figure 6.12) with magnitude of ten percent the total vertical load acting on the frame. The load versus mid-span vertical deflection plot shown in Figure 6.20 indicates that type II and type III models give almost the same behaviour. The load versus sway deflection is given in Figure 6.21. The softening of the frame occurs at the eleventh curvature step, when only two hinges are formed along the beam, i.e., at a stage whereby the number of hinges is not sufficient to form

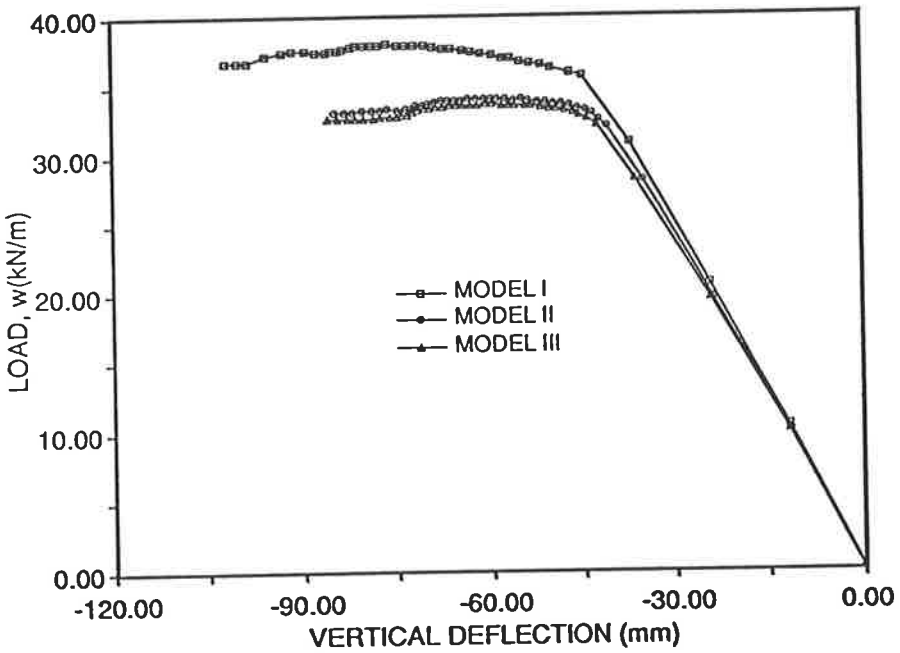

Figure 6.18: FRAME2T: vertical deflection

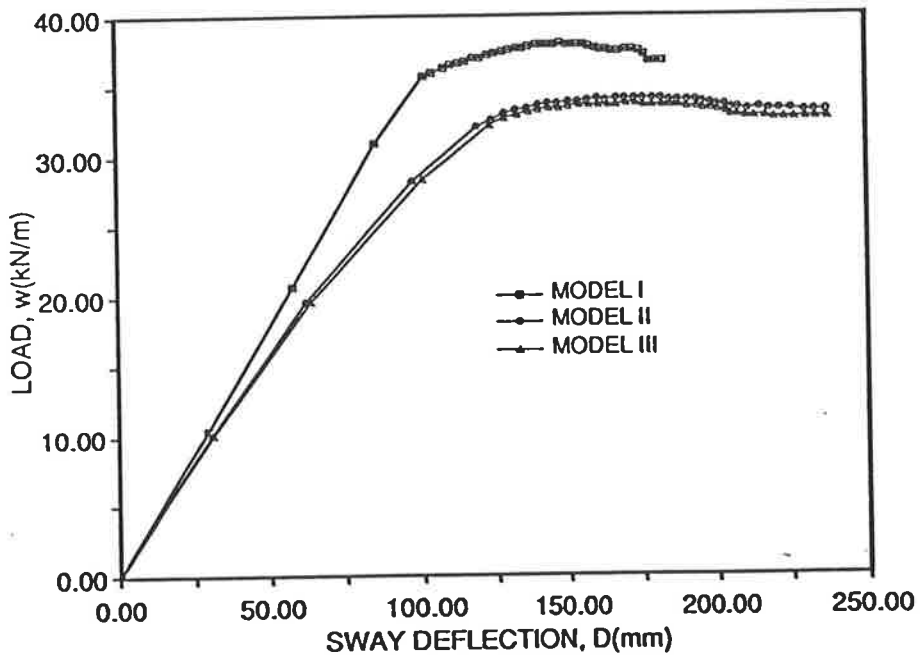

Figure 6.19: FRAME2T: sway deflection

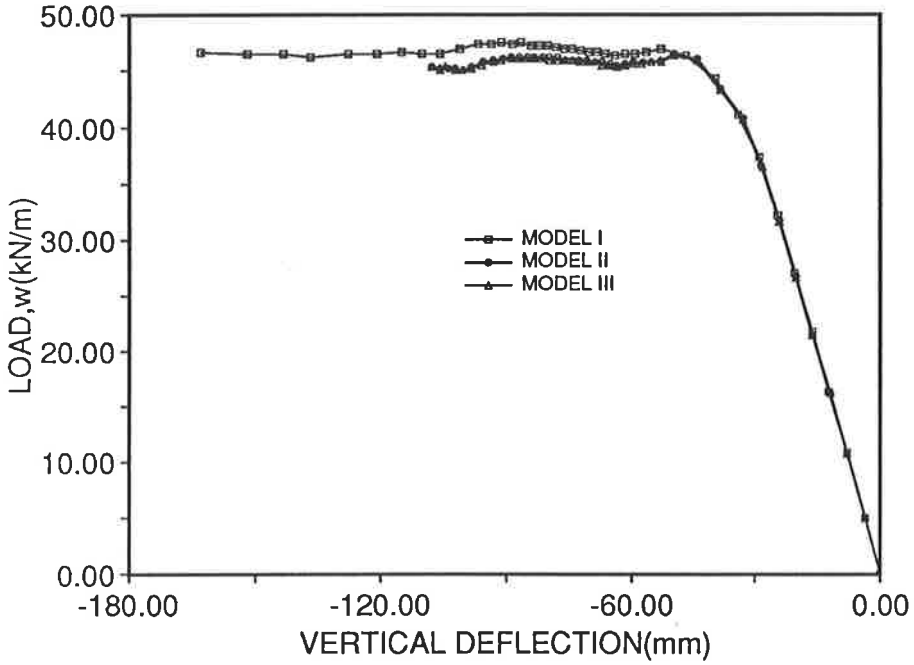

Figure 6.20: FRAME3S: vertical deflection

a beam plastic collapse mechanism, even though eventually three hinges are formed. Observation of the moment curvature relation of the segment at the right end of the beam for model I indicates that the softening slope increases significantly at the eleventh curvature step (see Figure 6.22), a likely cause for the softening behaviour of the frame at that stage.

Model II and III both display the same behaviour as model I, i.e., system softening corresponds with the onset of relatively steep softening in the right segment of the beam.

The peak load is not affected much by including the geometrical nonlinearity effect for this frame and this indicates that the load-carrying capacity of the frame is constrained numerically by local beam failure. This results from the use of pattern load, where the load acting along the beam is related to the forces acting at the joints.

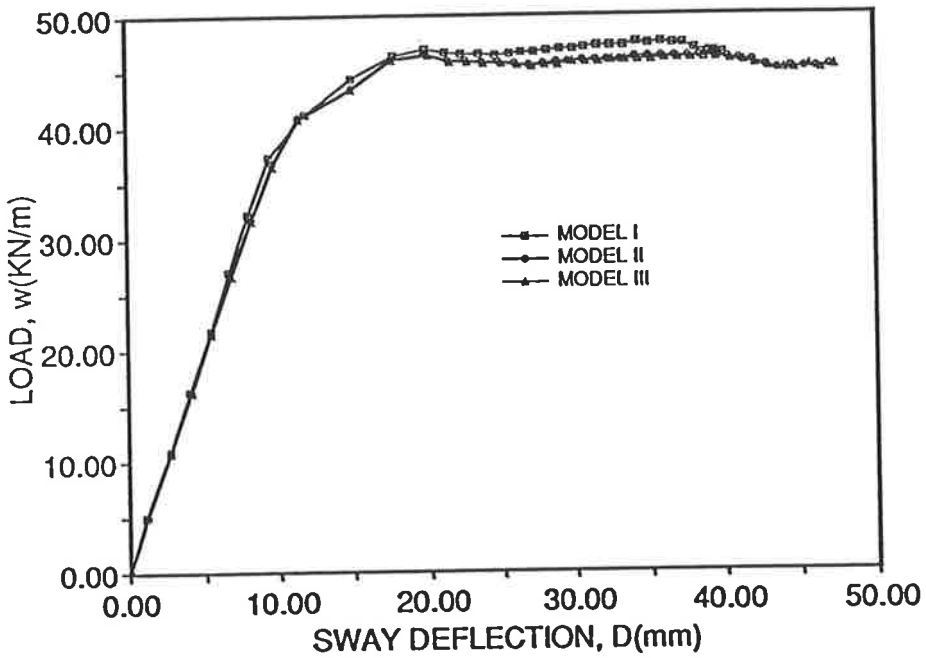

Figure 6.21: FRAME3S: sway deflection

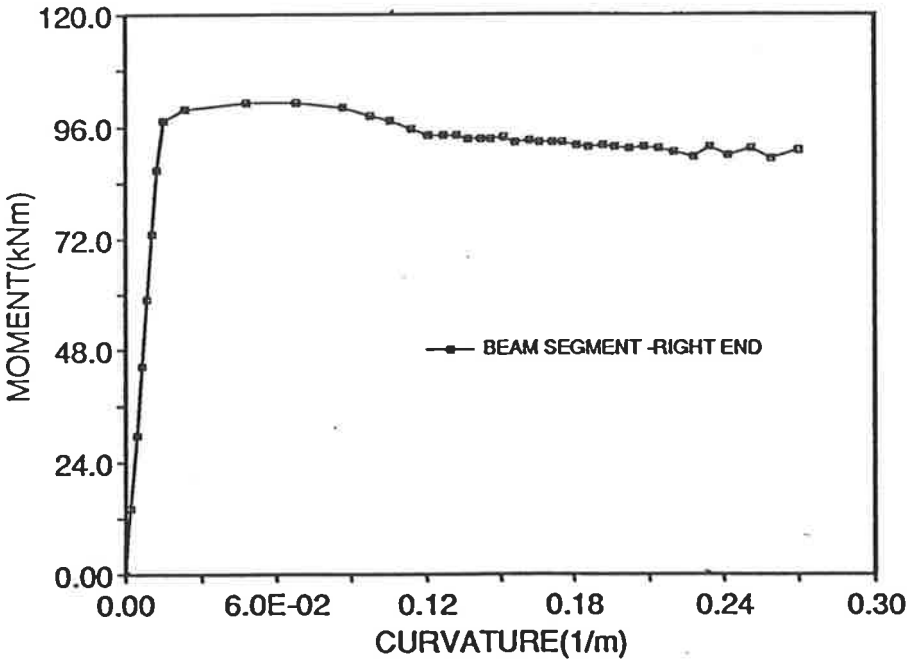

Figure 6.22: FRAME3S: moment-curvature plot for key segment

For model I of FRAME3T (see Figure 6.12), the peaks of the plots obtained are almost flat (see Figure 6.23 and Figure 6.24) Observation of the moment-curvature relations of the potential hinge-forming segments of the frame indicates that four hinges are formed when the frame reaches the peak load: two of these in the right column and two in the beam; one at about mid-span and the other at the right end of the beam. None of these hinges has steep unloading which explains the almost flat peaks observed.

Both models II and III display the same behaviour, with the load plateau (almost flat) occurring after the formation of three hinges in the frame. These hinges have flat peaks; two of them in the right column and the other in the segment next to the right end of the beam. As there are insufficient hinges at peak load to create a plastic collapse mechanism and the moment curvature relations of the hinges have relatively flat plateau (and therefore softening of hinges is not the cause), the peaks of these two frames are caused by frame instability occurring before the formation of a plastic collapse mechanism.

The peak load predicted by model I, of about 30 kN, is substantially different to the 25 kN (approximately) predicted by models II and III. Models II and III give almost the same peak load. This indicates that for tall sway frames, the geometrical nonlinearity effect of the loaded joints is important, but that including the effect of geometric nonlinearity within the member length has little influence on the behaviour of sway frames.

For FRAME4S (see Figure 6.12), model II is not relevant as the frame is braced laterally. Load versus mid-span deflection of the beam for model I is given in Figure 6.25 and the horizontal deflection at mid-column is given in Figure 6.26. Model III of this frame is analysed by using four elements, and hence three nodes, per column. This allows the geometrical non-linearity effect along the column to be modelled. Results are given in Figures 6.25 and 6.26. Peak load corresponds to the formation of a local beam collapse mechanism, i.e., three

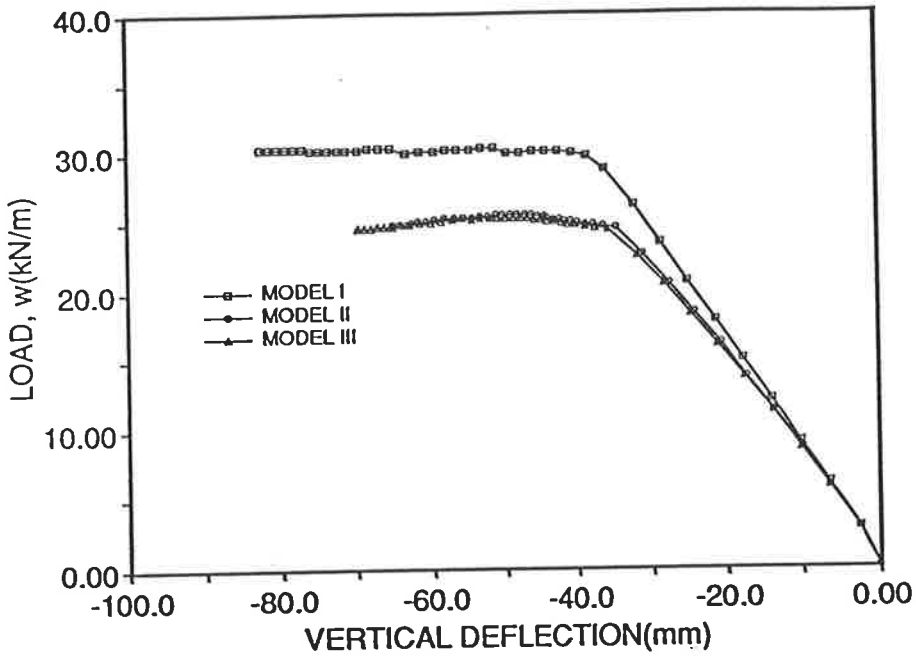

Figure 6.23: FRAME3T: vertical deflection

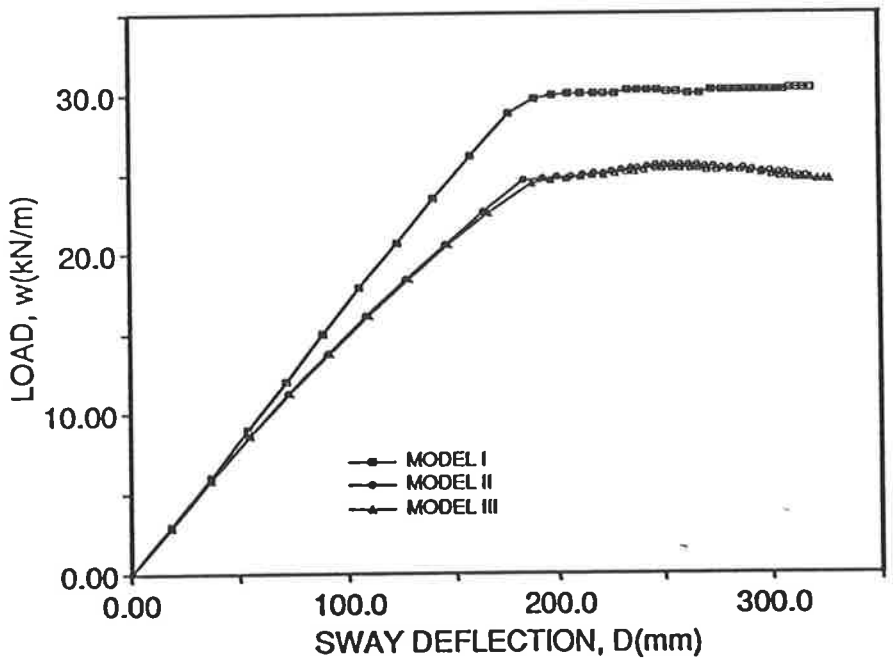

Figure 6.24: FRAME3T: sway deflection

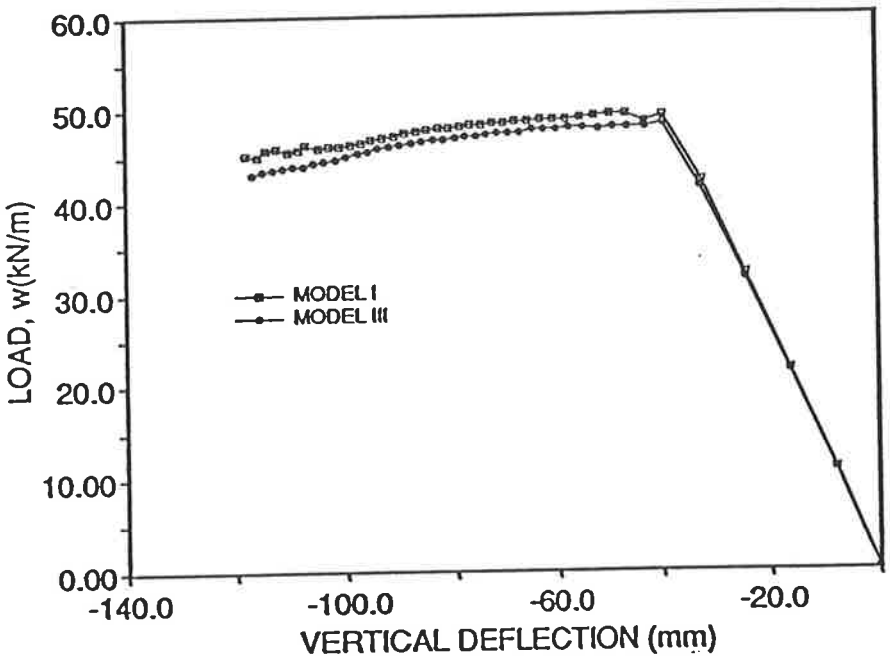

Figure 6.25: FRAME4S: vertical deflection of beam

hinges form in the beam, one at each end and one at midspan. The hinges form almost at the same instant, i.e., at the fifth curvature step, indicating that the local beam failure is the cause for the frame reaching its peak load.

Results obtained for a taller frame FRAME4T (see Figure 6.12) are given in Figure 6.27 and Figure 6.28. In this case, the columns are less stiff compared to those of FRAME4S. Peak load also occurs when a beam plastic collapse mechanism forms, but the hinges at the end of the beam and that at mid-span do not form at the same instant as in the case of FRAME4S. For model I, the hinge at midspan forms at the fifth curvature step whereas those next to the joints form at the twenty-fourth curvature step. Comparing the load versus vertical deflection plots of FRAME4S and FRAME4T shows that the the change in slope is quite sudden for FRAME4S whereas for FRAME4T, the change in slope is more gradual. This shows that even though local beam failure controls the peak load the frame can carry (if it is subjected to proportional loading), the nature of the load versus vertical deflection (at mid-span

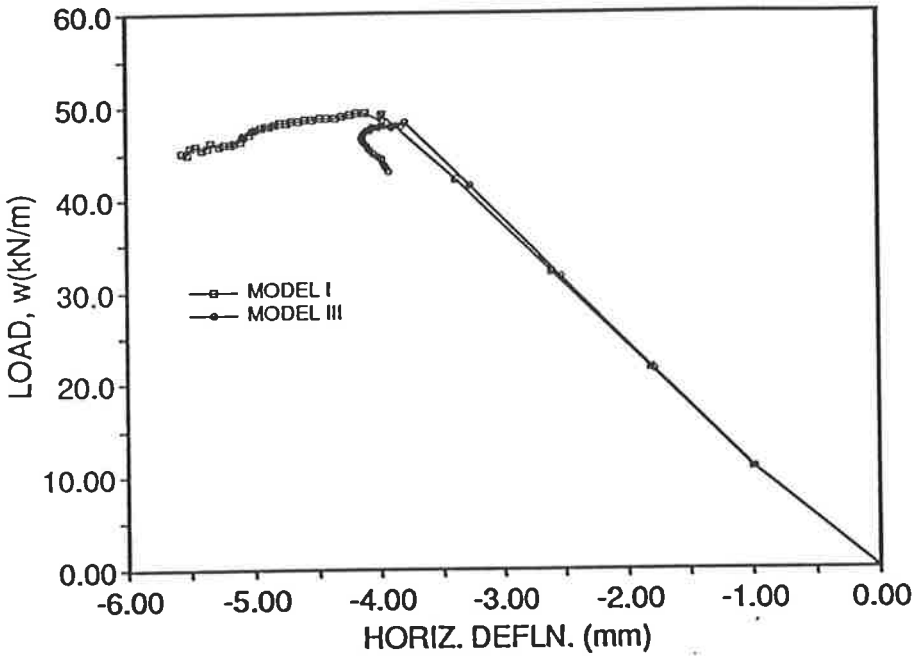

Figure 6.26: FRAME4S: horizontal deflection at mid-height of left column

of the beam) depends on the stiffness of the columns connected to the ends of the beam.

The effect of geometrical non-linearities is not pronounced in this frame. This is likely due to the local beam failure having the effect of limiting the amount of axial force in the columns.

The results obtained above indicate that softening in frames is caused either by the presence of a softening hinge or frame instability after the occurrence of one or more plastic hinges.

Comparisons of results obtained for the different models show the importance of including P-Δ effect caused by lateral movements of joints in numerical models. It was found that P-Δ effect within the member length has little

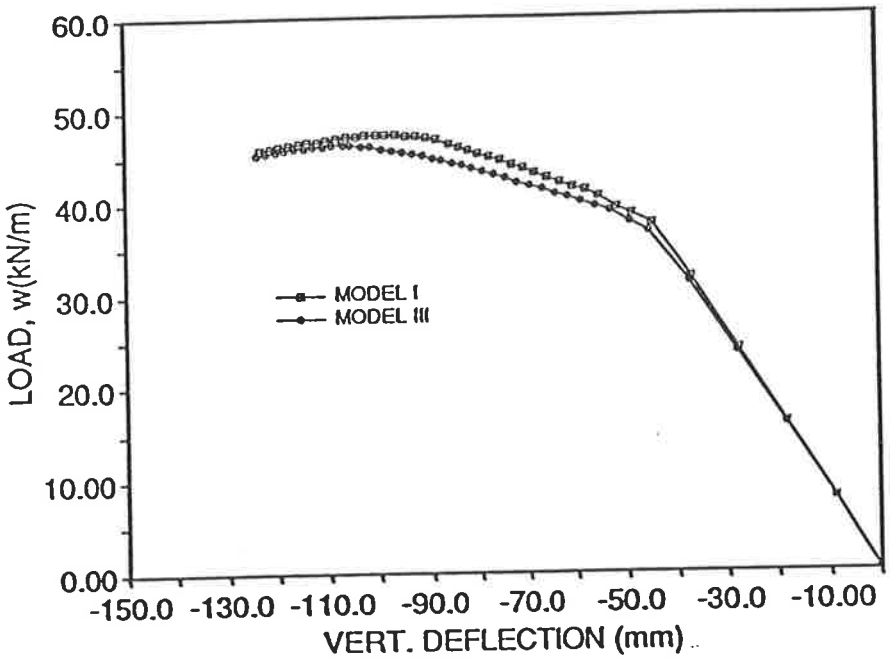

Figure 6.27: FRAME4T: vertical deflection of beam

influence on the behaviour of sway frames. The comparisons also indicate that ignoring geometric nonlinearity effect gives significant over-estimation of the peak loads of sway frames.

6.4 Effect of Sectional Thrust on the Behaviour of Reinforced Concrete Frames

In some proposed computational procedures, the effect of thrust on section behaviour is ignored when analysing reinforced concrete frames. The effect of ignoring thrust in concrete frame analysis is studied in this section.

A portal frame *A* under sway loading shown in Figure 6.29 is analysed both with and without the effect of thrust on the sectional behaviour. Results obtained for these two cases are plotted in Figure 6.30. It can be observed

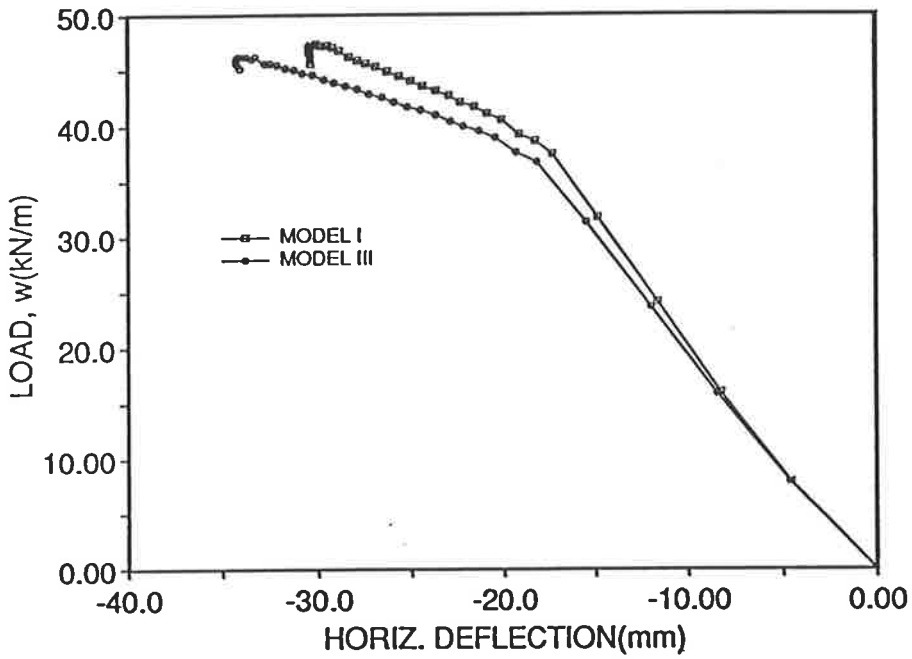

Figure 6.28: FRAME4T: horizontal deflection at mid-height of left column

that the frame is stiffened significantly when the effect of thrust on the section behaviour is taken into consideration in the analysis. The predicted collapse load changes from $P = 413$ kN for the frame without the effect of thrust to $P = 586$ kN for the frame with the effect of thrust.

The moment-curvature relations of all the potential hinge-forming segments are shown in Figure 6.31, obtained from the analysis of the frame with the effect of thrust and Figure 6.32, obtained from the analysis of the frame without the effect of thrust. The inclusion of thrust effect in the analysis has resulted in fewer hinges forming in the columns as compared with the case where thrust effect was excluded. The details of hinge formation from the two analyses are shown in Figure 6.33.

For the frame with the effect of thrust, four hinges are formed; two in the beam

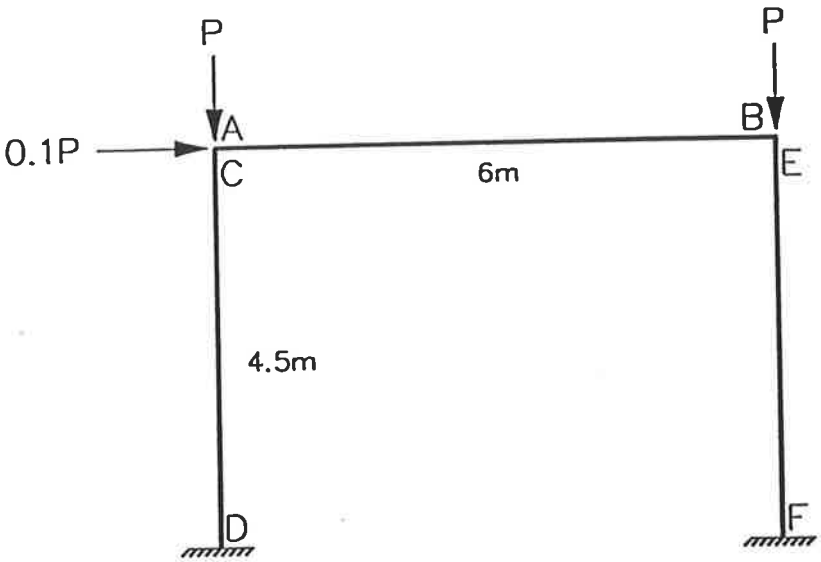

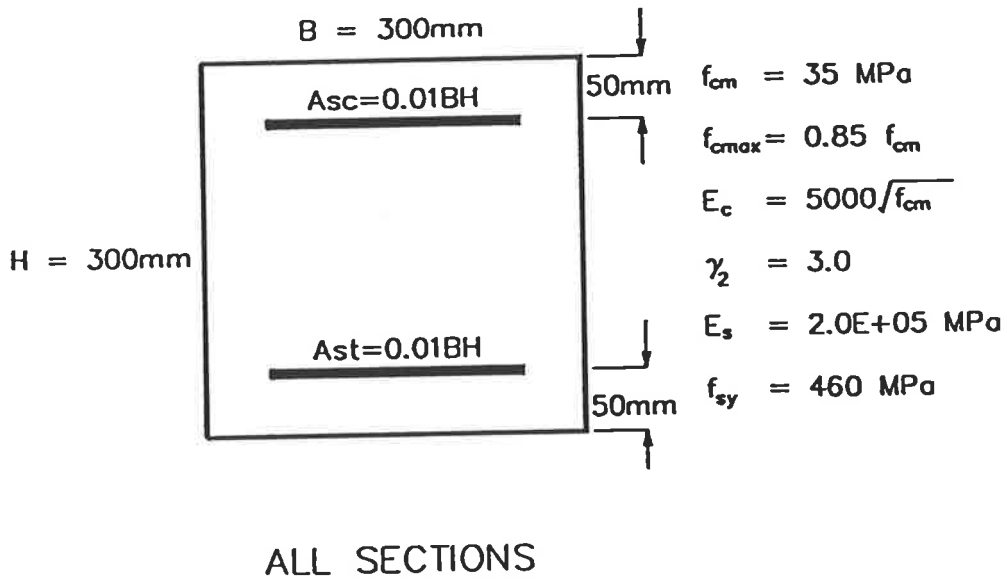

Figure 6.29: Portal frame *A*

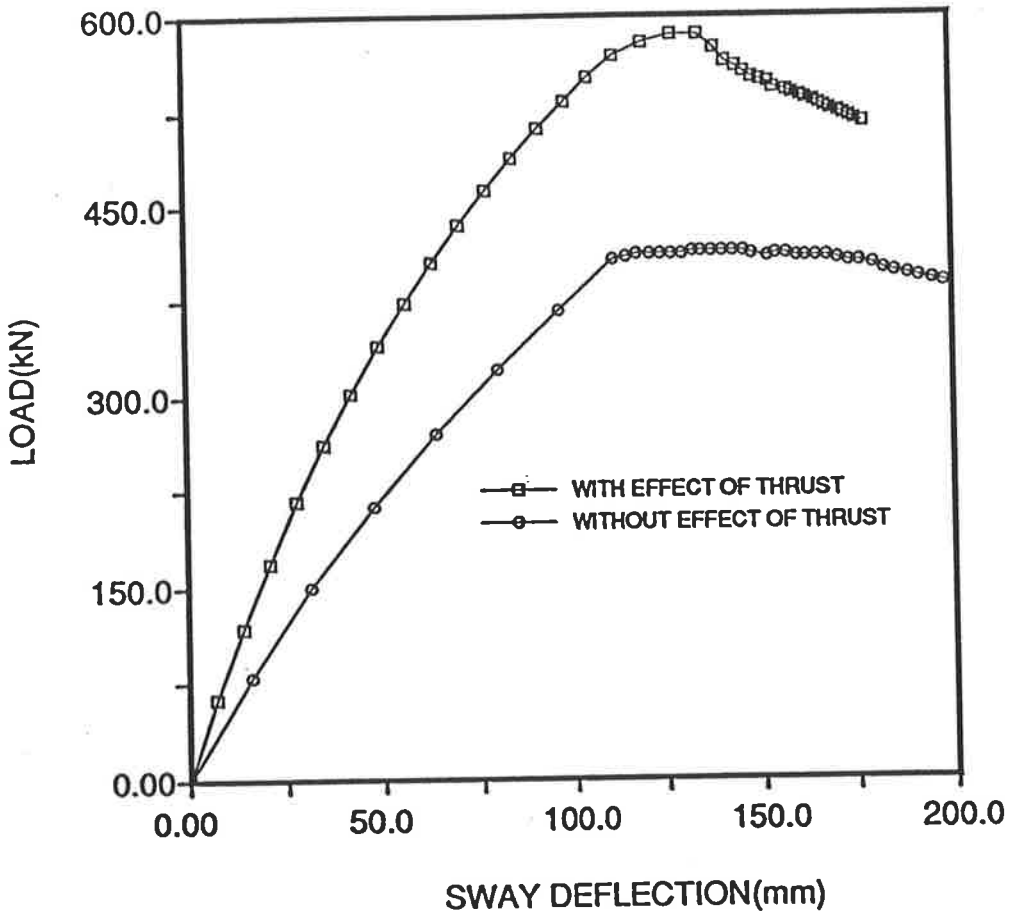

Figure 6.30: Load deflection behaviour of frame A

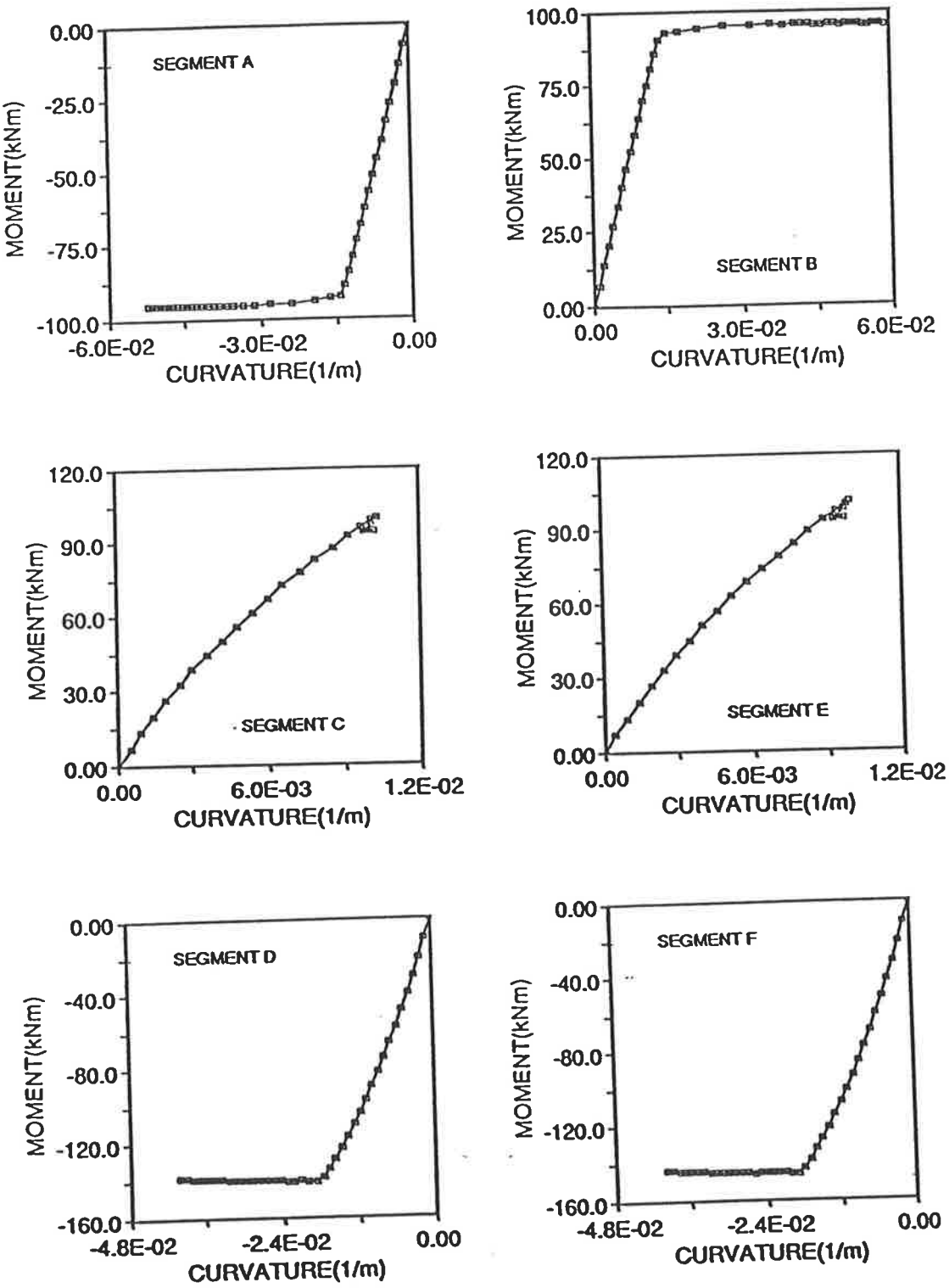

Figure 6.31: Moment-curvature relation of segments for frame A with thrust effect

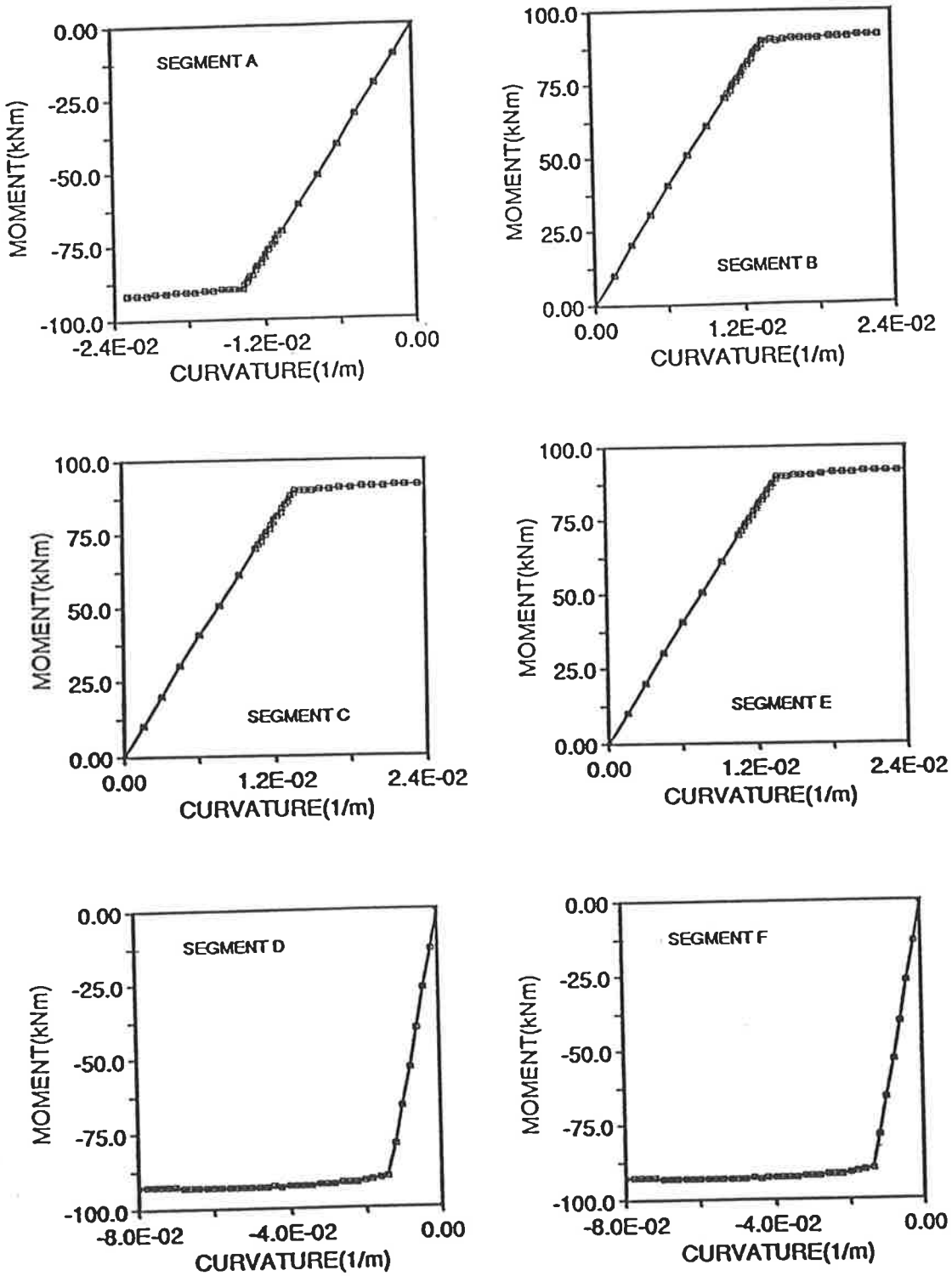

Figure 6.32: Moment-curvature relation of segments for frame A without thrust effect

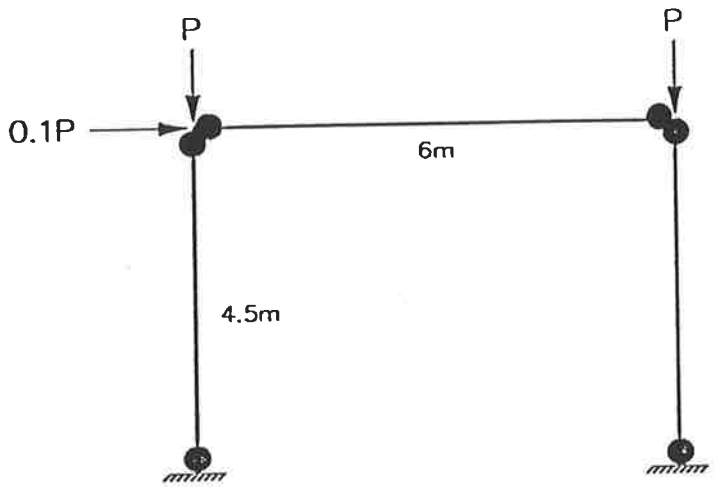

(a) WITHOUT THRUST EFFECT

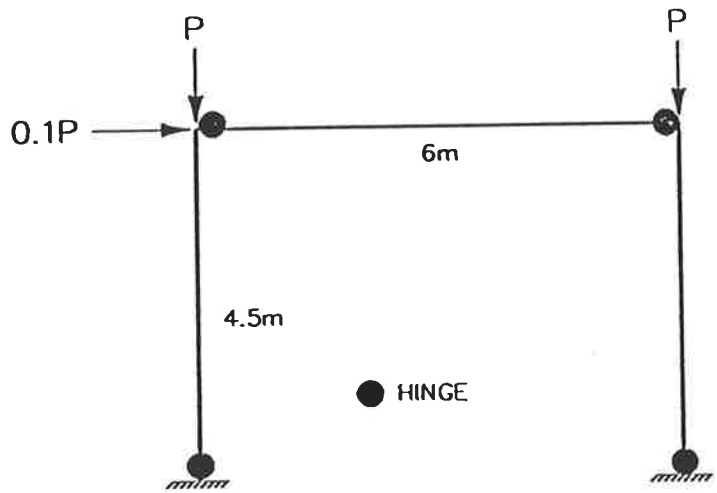

(b) WITH THRUST EFFECT

Figure 6.33: Hinge formations of frame A

and two in the columns. For the frame without the effect of thrust, six hinges were formed; two in the beam and four in the columns. The positions of the hinges indicates that the stiffening effect of axial thrust in the columns has prevented the formation of hinges at the top of the columns. Even the order of hinge formation is affected; in the case where the effect of thrust is included, hinges first formed at the ends of the beam whereas in the other case, hinges first formed at the lower ends of the columns (see Figure 6.31 and Figure 6.32).

The analyses show the importance of including the effect of thrust on moment-curvature relationships when analysing structures with substantial axial thrusts in the members. The collapse load, and the order and number of hinge formation can be affected by the exclusion of this effect from numerical models.

6.5 Effect of Beam Reinforcement on Frame Behaviour

In the Australian concrete standard AS3600, the reinforcement present in the beam is assumed not to have any effect on the strength of reinforced concrete columns forming part of a frame. In this section, a sway frame B subjected to joint loading shown in Figure 6.34 is analysed with different quantity of reinforcement in the beam.

Load versus sway-deflection plots for frame B with five different beam reinforcements of 0.5%, 1%, 2%, 3% and 4% of the gross cross-section area are shown in Figure 6.35. The reinforcement of the column section was maintained at 2% that of the gross sectional area. As can be seen from the plots, the strength increases significantly as the reinforcement in the beam was increased from 0.5% to 1%, and also from 1% to 2%. The strength increased slightly when the reinforcement was increased from 3% to 4%. For the first

three cases, four hinges were formed at collapse (peak load), two at the ends of the beams and two at the bases of the columns. For the last two cases, only two hinges were formed at the bases of the columns. This indicates that for the last two cases, the amount of reinforcement in the beam is sufficient to stiffen up the frame to enable the vertical loads to increase to a stage where stability failure of the frame occurred before the formation of a collapse mechanism.

The strength of the frame varies from P=335kN for the frame with beam having 0.5% reinforcement to P=685kN for the frame with beam having 4% reinforcement. This indicates the importance of beam reinforcement on frame behaviour, especially on the strength and stiffness.

6.6 Snapback Instability

Snapback instability has been described in Chapter 4. Occasionally snapback behaviour was observed when the analysis was carried far enough into the load softening region. This section looks at a few frames which exhibit this type of behaviour. Snapback behaviour was observed for the frame C shown in Figure 6.36. Plots of load versus sway deflection and load versus beam midspan deflection are shown in Figure 6.37 and Figure 6.38 respectively. It can be seen that snapback instability occurs for the sway deflection but not for the beam deflection in this case.

Another frame (Frame D) shown in Figure 6.39 also displays snapback instability behaviour, but this occurs for the midspan vertical deflection of the beam instead of the sway deflection as in the previous case. The load versus sway deflection, and the load versus beam midspan deflection plots for frame D are shown in Figure 6.40 and Figure 6.41 respectively.

In frame E, shown in Figure 6.42, two snapbacks occur, one in the curve of

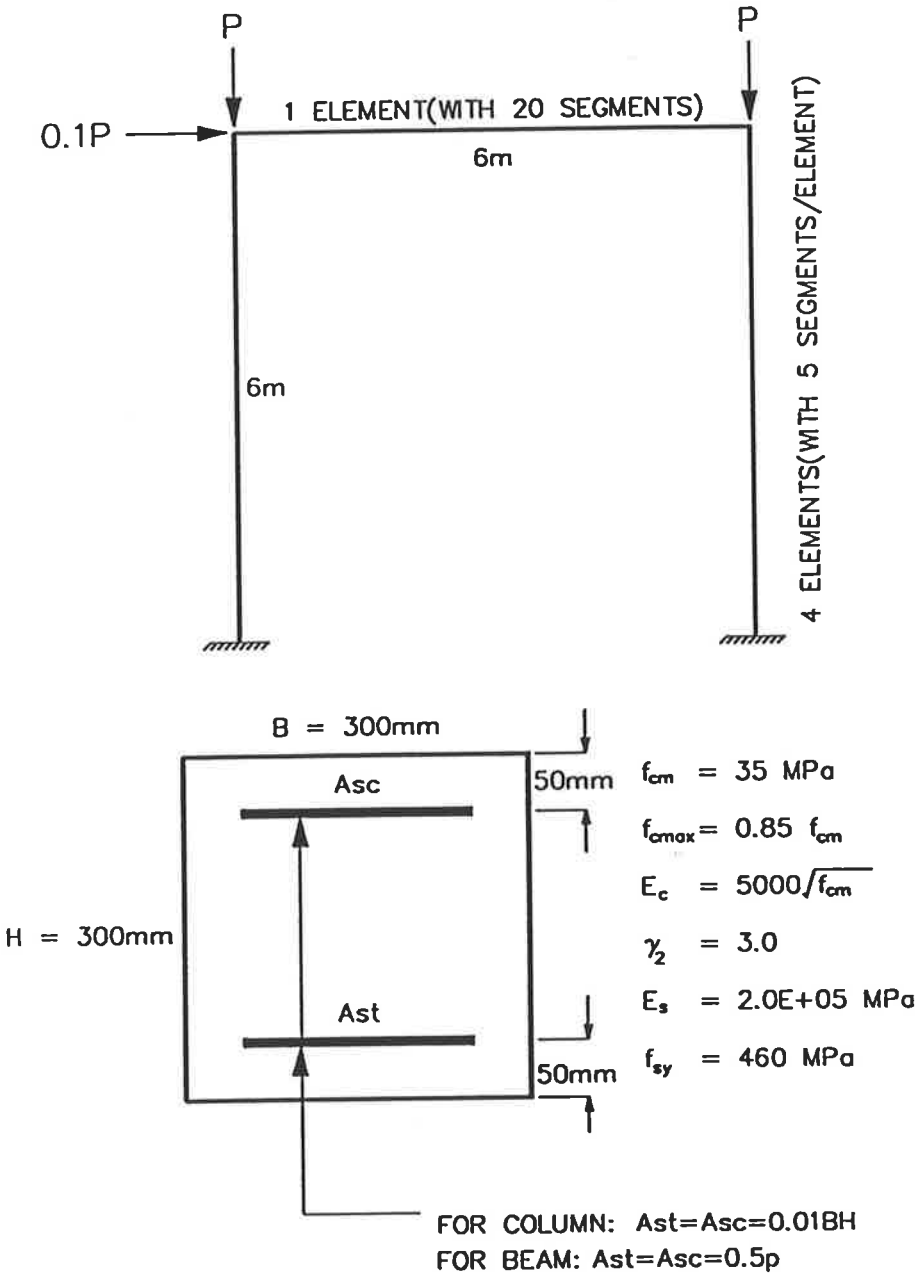

Figure 6.34: Frame B

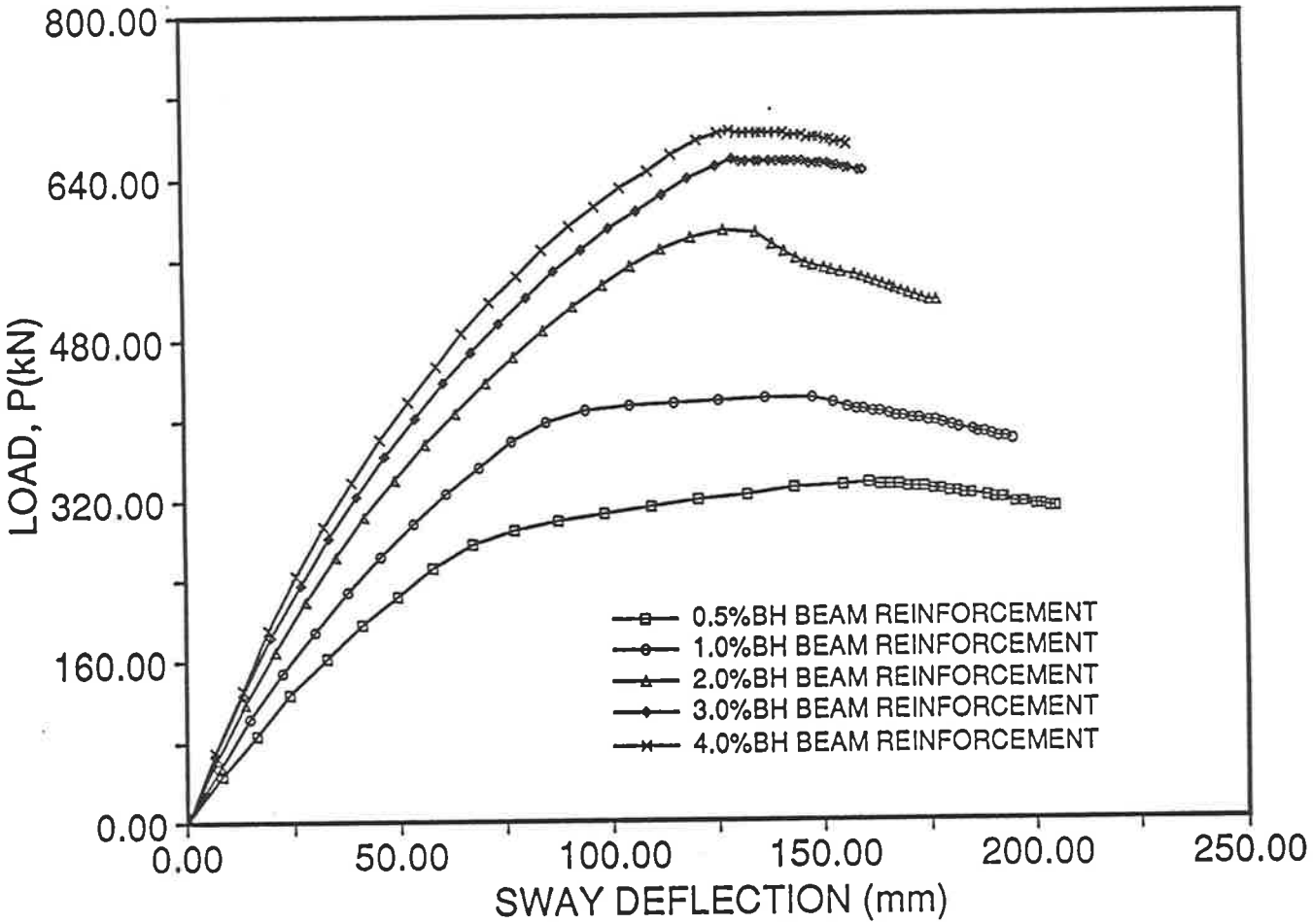

Figure 6.35: Effect of beam reinforcement on frame behaviour

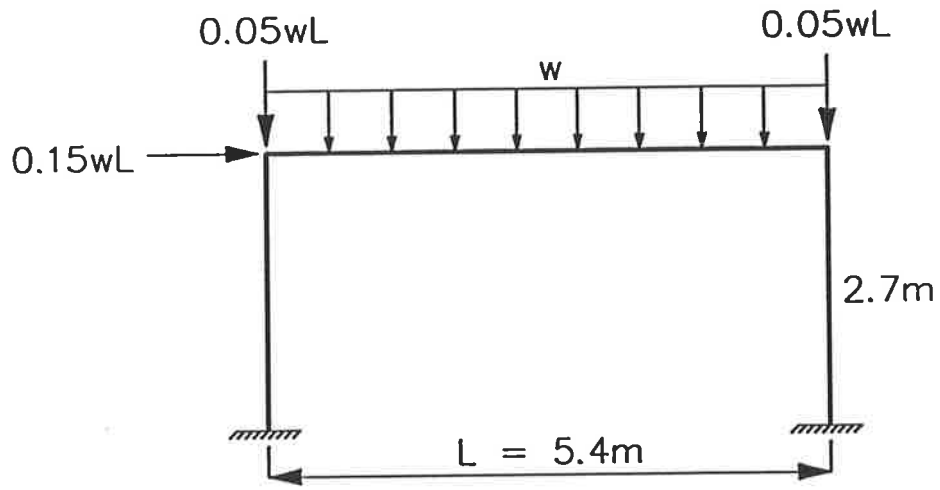

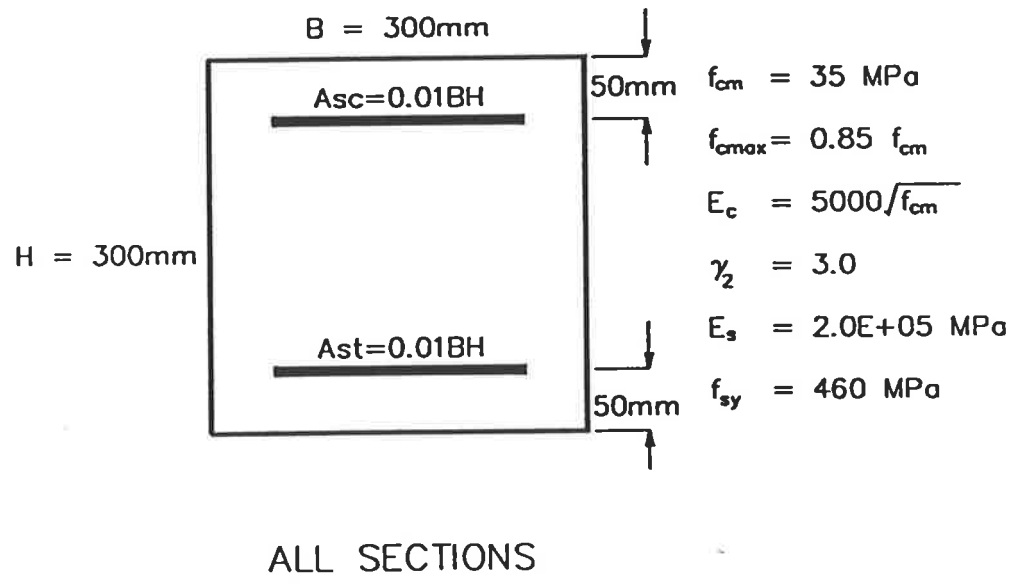

Figure 6.36: Frame C

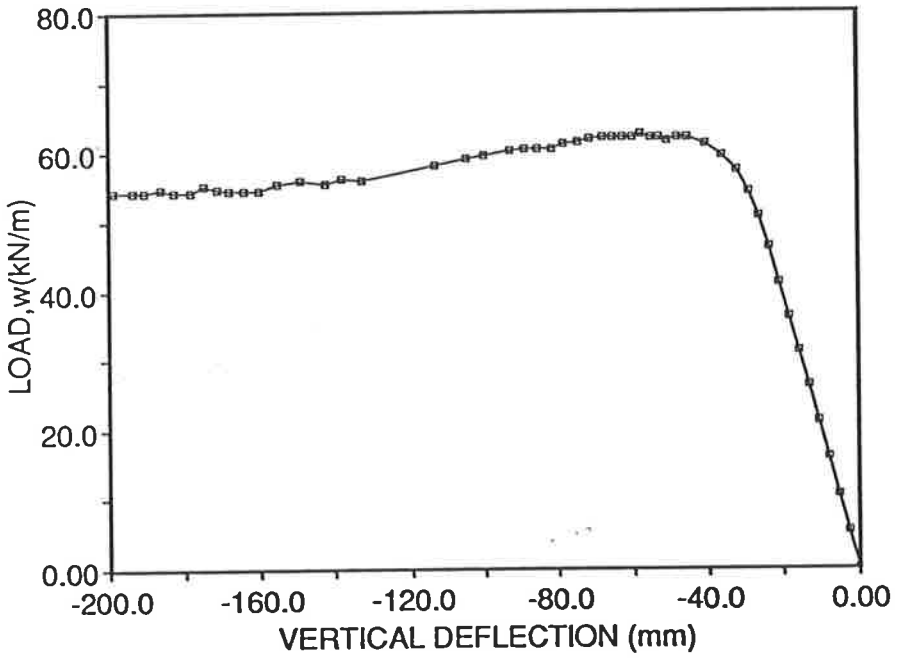

Figure 6.37: Load versus beam midspan deflection plot for frame C

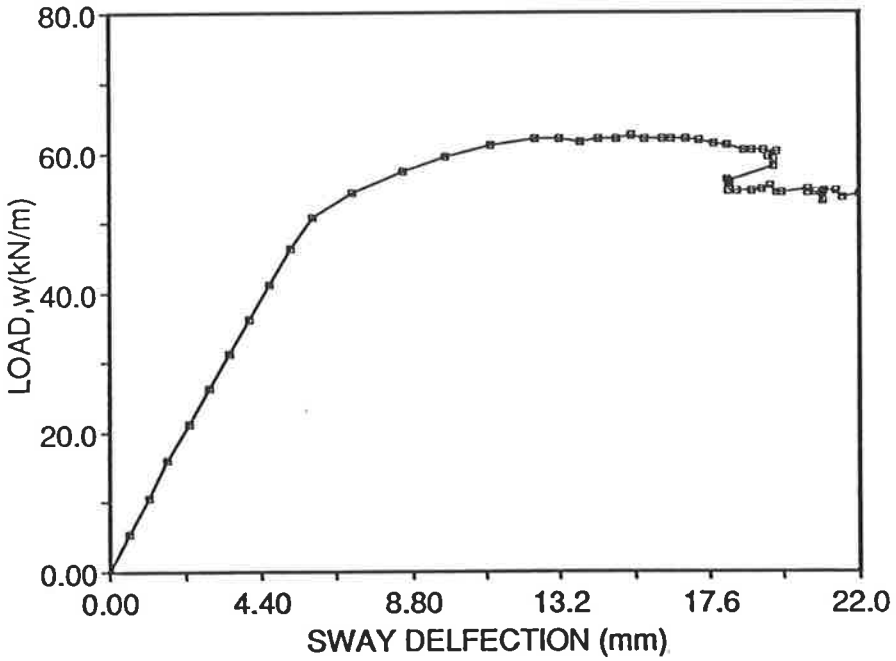

Figure 6.38: Load versus sway deflection plot for frame C

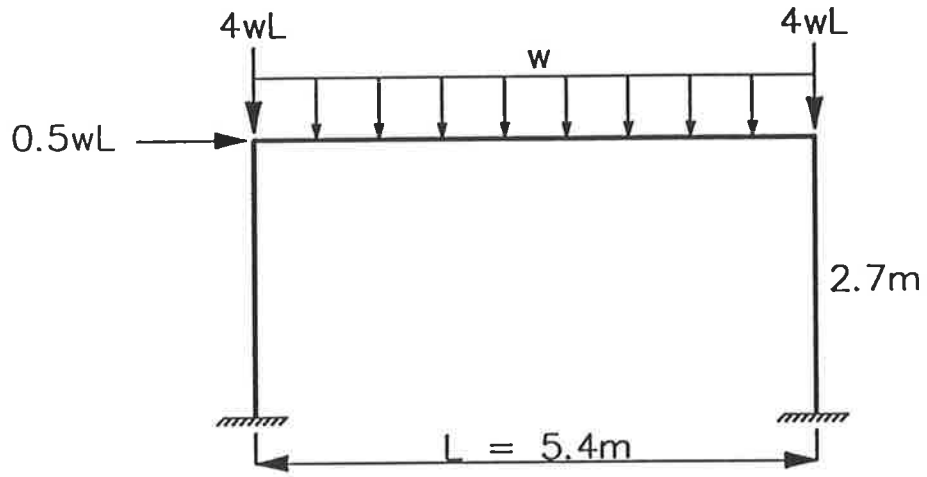

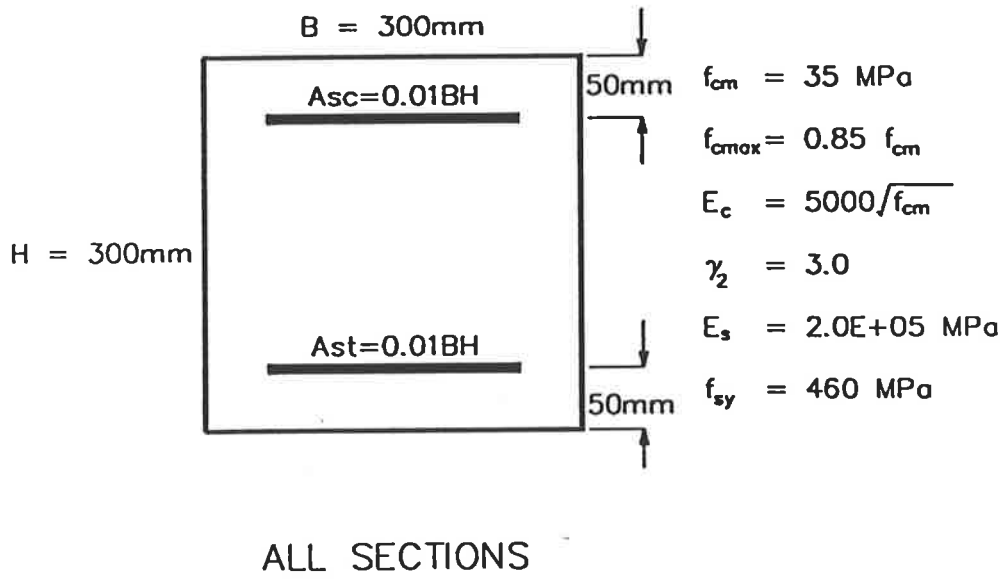

Figure 6.39: Frame *D*

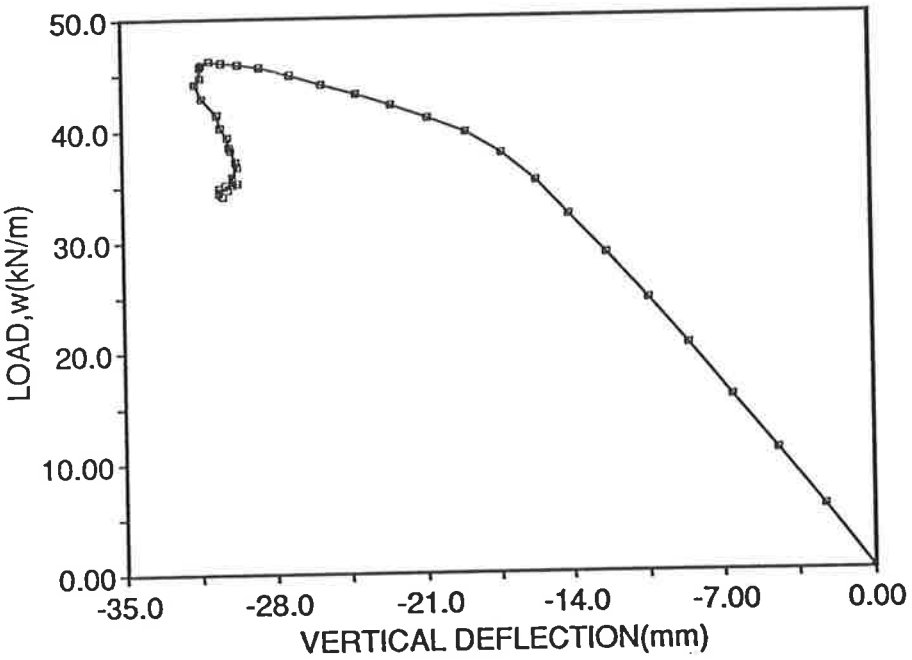

Figure 6.40: Load versus beam midspan deflection plot for frame D

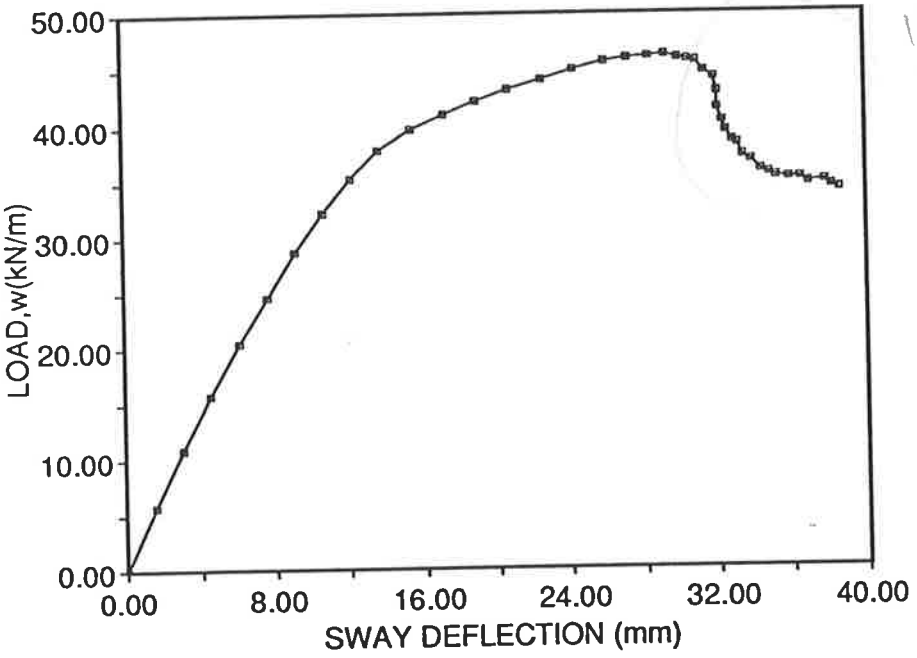

Figure 6.41: Load versus sway deflection plot for frame D

vertical beam deflection (Figure 6.43) and the other in the sway deflection at the top of the left column (Figure 6.44).

6.7 Multi-storey Frames

Two three-storey two-bay reinforced concrete frames are analysed using program SAFRAME. Material properties are as those used for the portal frame analyses described earlier in this chapter.

The load versus sway deflection plot for frame A (Figure 6.45) is shown in Figure 6.46. Each solution point indicates one curvature step in the control of a key segment use in the numerical analysis. Load deflection behaviour is linear until the formation of the first set of hinges next to the right ends of the left beams 6 and 11 of the frame (the number assigned to the beams is given in Figure 6.45). One curvature step later, hinges form next to the right ends of beams 1, 7 and 12. The slope remains almost constant until three curvature step later, when more hinges are formed. The order of the hinge formation is shown in Figure 6.46. After the eighth curvature step, the slope of the curve decreases to almost a plateau. The peak load occurs not long after at the tenth step. At peak load, the number of hinges formed is not sufficient to cause a frame plastic collapse mechanism. However, the frame sways sufficiently to cause a decrease in load.

Moment curvatures plots for the hinges show that all have relatively flat curves. A typical plot for the column segment at position 15B in Figure 6.46 is given in Figure 6.47. This suggests that the softening is not caused by steep softening in one of the hinges, and therefore instability is the main cause of the collapse.

Unloading behaviour in segments has also been observed in some of the segments in the frames; a typical segment with unloading hinge is shown in Fig-

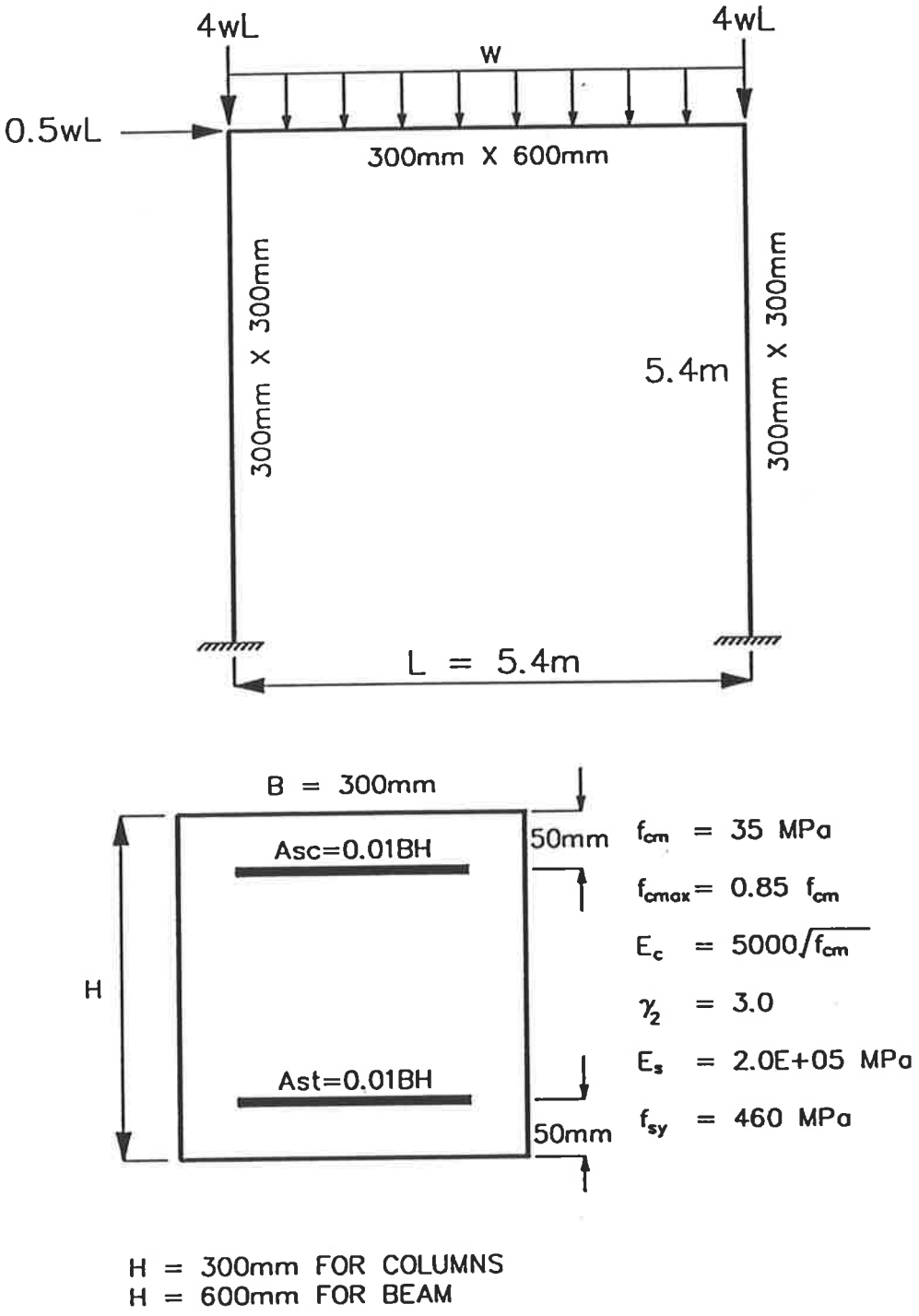

Figure 6.42: Frame E

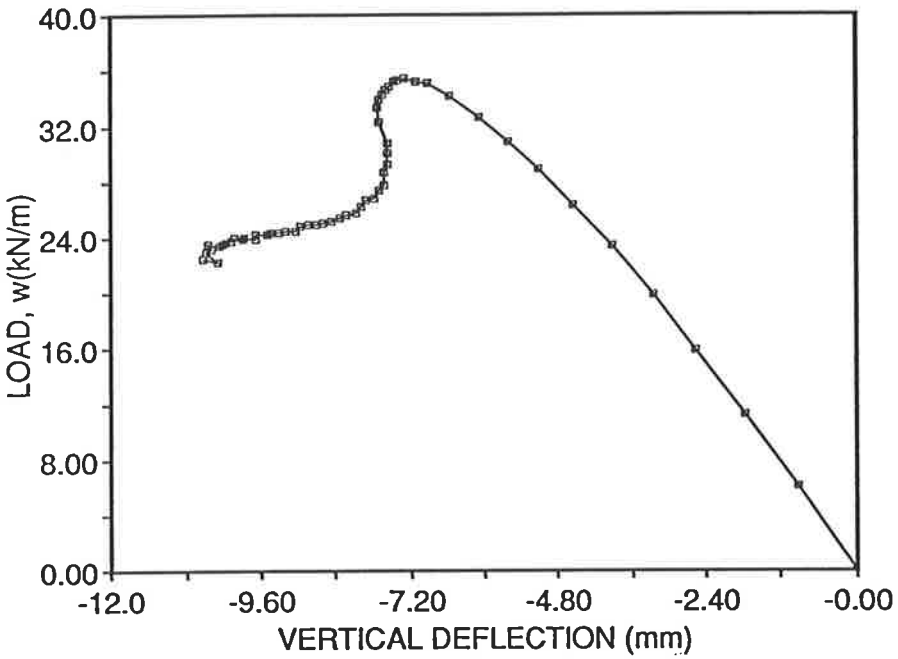

Figure 6.43: Load versus beam midspan deflection plot for frame E

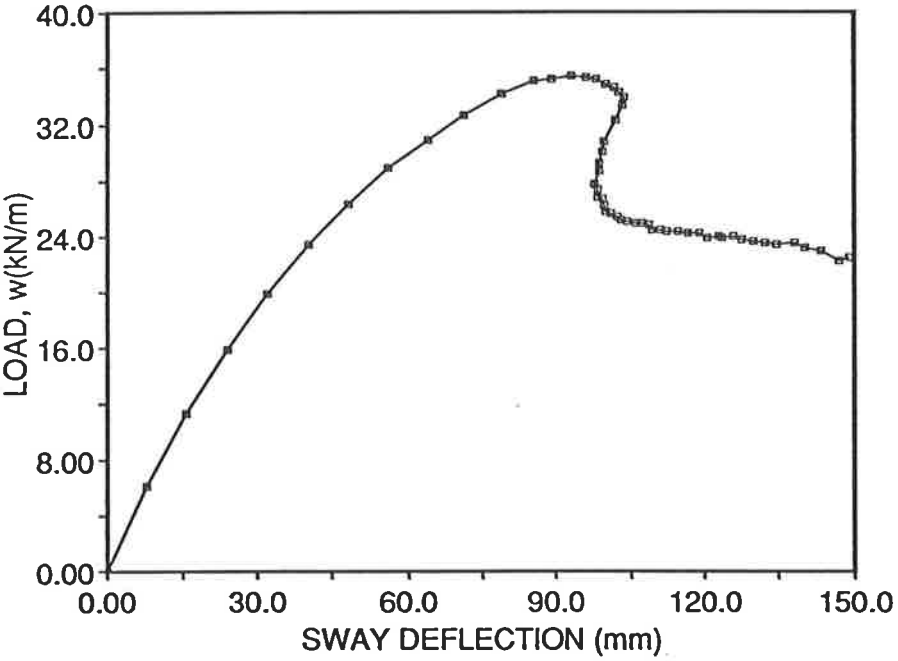

Figure 6.44: Load versus sway deflection plot for frame E

ure 6.48 for the segment close to the midspan of beam 11.

The load versus sway deflection plot for multi-storey frame B (Figure 6.49) is shown in Figure 6.50. This frame is the same as frame A, but is subjected to larger horizontal applied loads. As in the case of frame A, load-deflection behaviour is linear up to the formation of the first hinge. A distinct load-softening path can be observed from the plot. At peak load, the number of hinges formed are almost sufficient to form a frame plastic collapse mechanism. All the hinges formed have relatively flat plateaus, indicating that, as for the case of frame A, instability is the cause of softening. But in frame B, the softening is more severe, a reflection of the weak condition of the frame caused by the large number of hinges.

A simple calculation carried out on a beam similar to those of the frames, subjected to a uniformly distributed load, indicates that plastic collapse occurs when the load reaches 70 kN/m. The beam is assumed to be fixed at both ends. Though, the beams in the frames are subjected to additional moments and thrusts from the lateral forces acting on the frames, this simple analysis gives a rough estimation of beam collapse load. It is expected that the collapse loads of the frames do not exceed the actual beam collapse loads. The approximate value of beam collapse load of 70 kN/m compares well with the overall frame collapse load of 75 kN/m and 62 kN/m obtained for frames A and B respectively, even though no beam plastic mechanism forms at peak loads.

For both the above frames, the key segment is the one nearest to the base of the centre column. It was found that using this segment gives better numerical stability as compared with controlling a segment in the beam.

A total of 210 segments were used in each of the analyses to give segment lengths approximately equal to the depth of the respective members.

The failures of the two multi-storey frames analysed are due to instability,

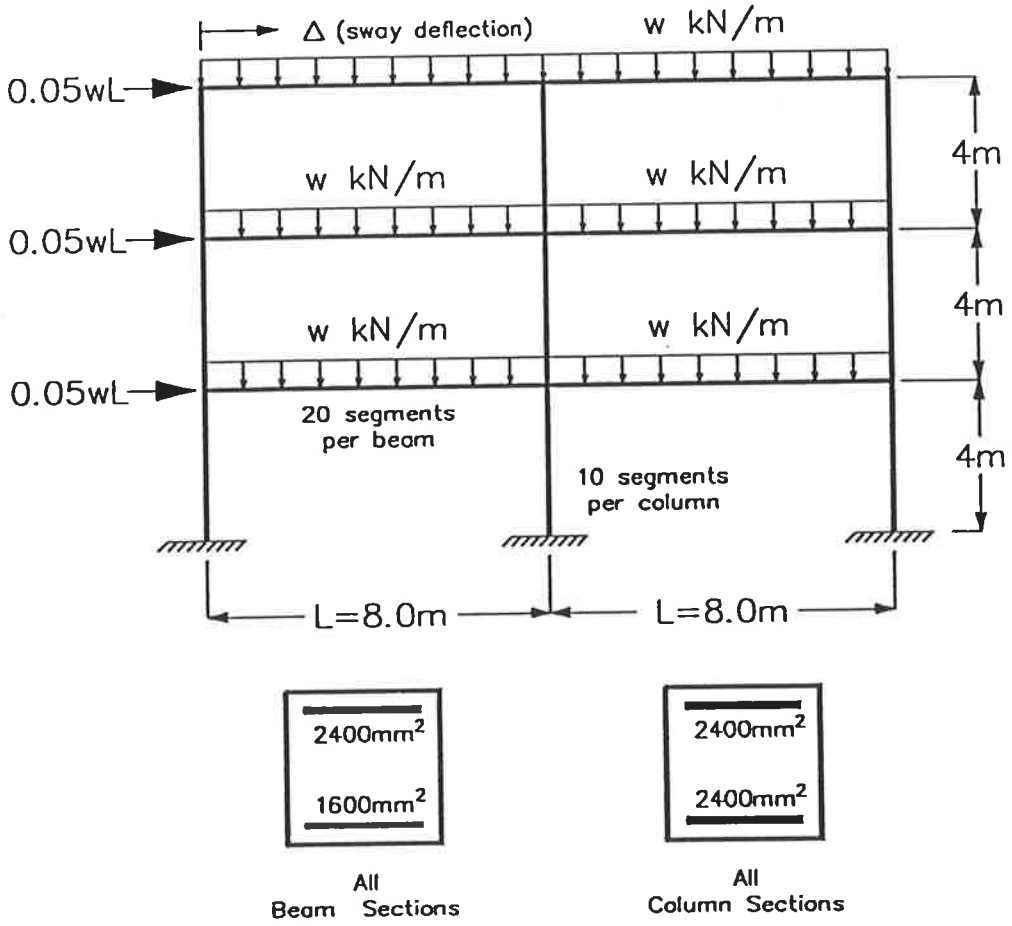

Figure 6.45: Multi-storey frame A

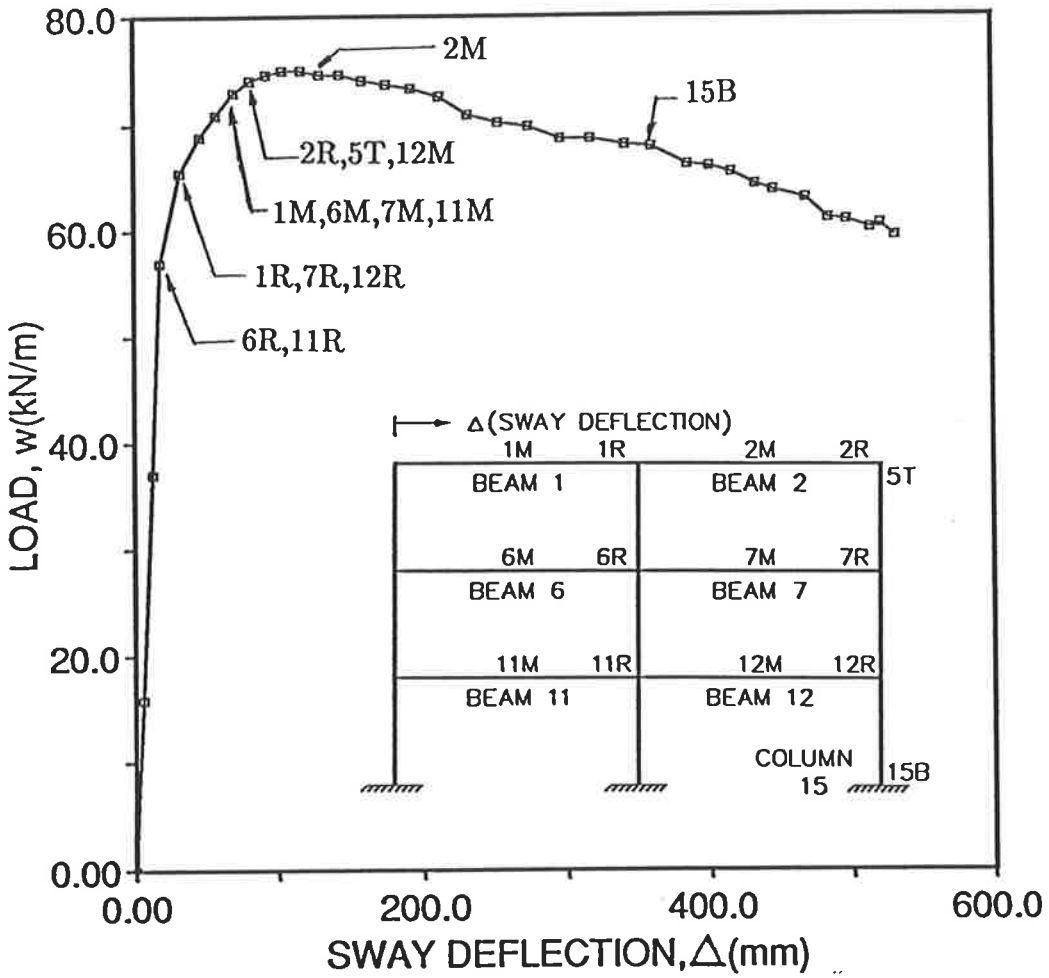

Figure 6.46: Sway deflection of frame *A*

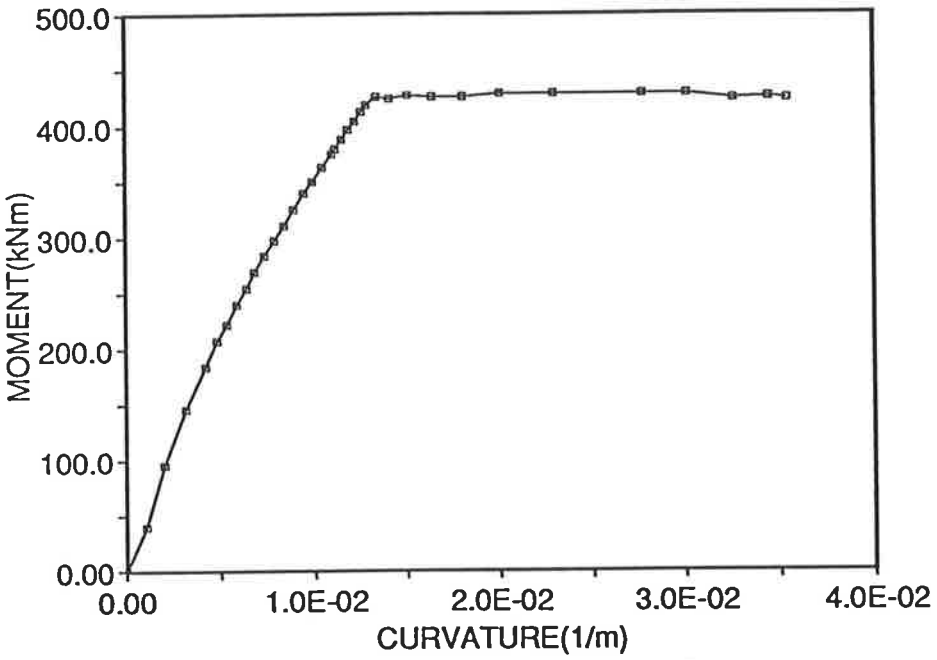

Figure 6.47: Moment-curvature plot for column segment

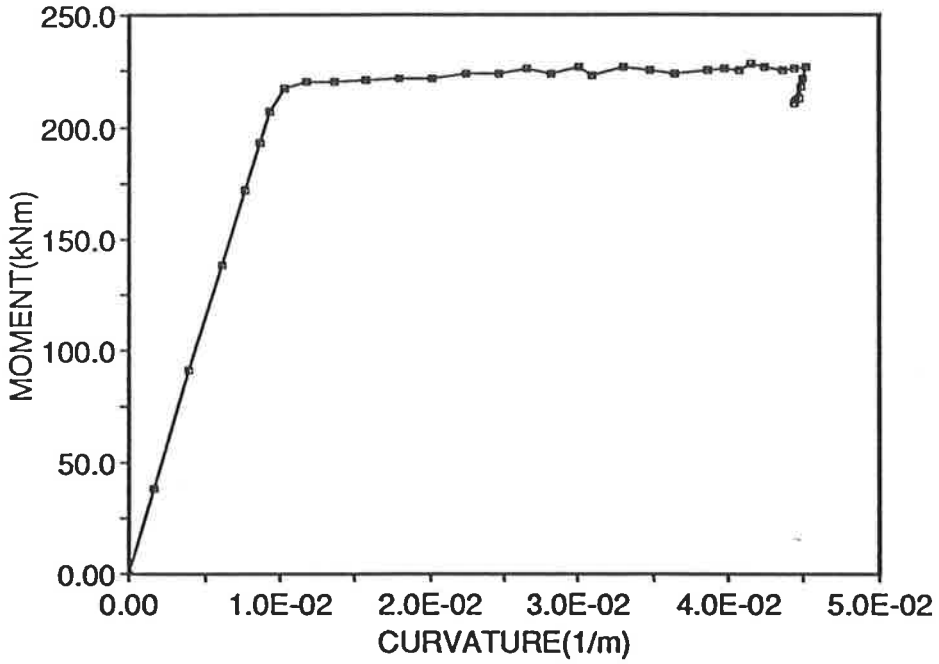

Figure 6.48: Moment-curvature plot for hinge with unloading

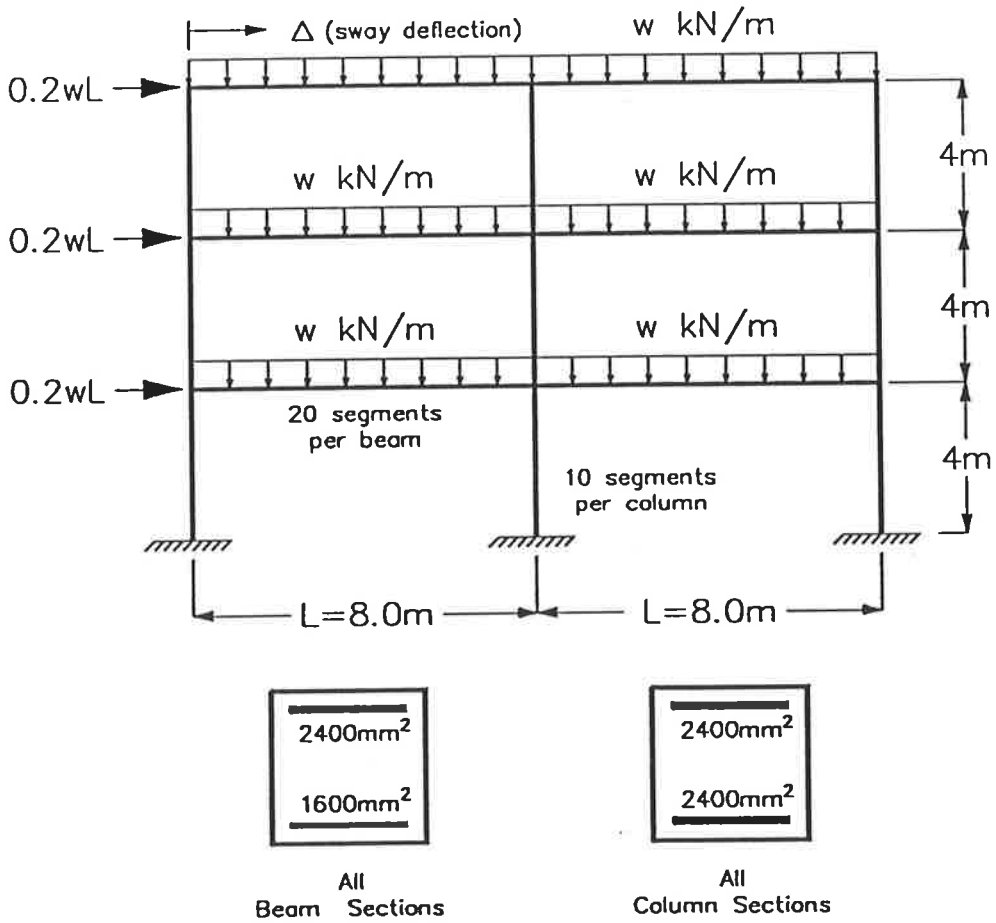

Figure 6.49: Multi-storey frame B

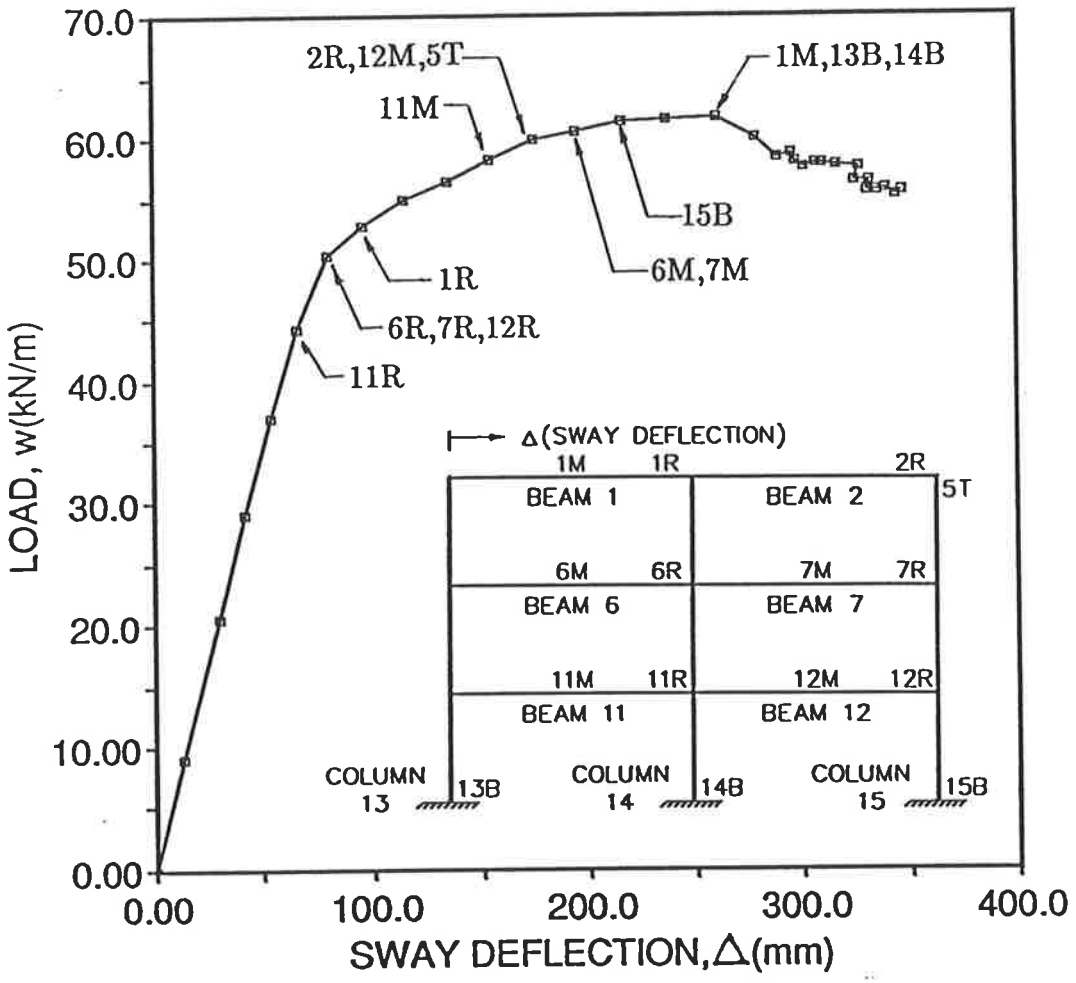

Figure 6.50: Sway deflection of frame B

whereby there is no plastic collapse mechanisms being formed at the peak load. This behaviour is very much like that obtained for most of the sway portal frames analysed in Section 6.3.

6.8 Conclusions

The load softening behaviour of reinforced concrete may occur even before the formation of any concrete hinges in the structure. This is mainly caused by the geometrical nonlinearity effect. The effect has been demonstrated using a simple cantilevered column.

The collapse behaviour of nonlinear reinforced concrete frames has been studied using portals. The following features have been observed:

- For a structure with mainly material nonlinearity effects (i.e., geometrical nonlinearities are not important), the peak load of the structure occurs after the formation of a plastic collapse mechanism provided the concrete hinges do not have steep softening slopes. In the case of a portal frame, this can either be a local beam mechanism or a sway mechanism. It is also possible for such a structure to reach peak load without the formation of a plastic collapse mechanism; the requirement is that at least one hinge has a softening slope.

- When carrying out non-linear analysis of a frame under proportional loading, local beam failure may limit the load a structure can carry. It has been observed in some of the frames analysed that the peak load is reached once a local beam failure occurs. Numerically, the entire frame seems is unable to carry extra load, but the actual situation could be that only the beam will collapse if the peak load is reached (especially if the frame has weak beams and strong columns). The assumption of

proportional loading is a convenience analytical device, but restricts the conclusions which can be drawn.

- Most of the portal frames analysed failed by frame instability, whereby the peak load is reached before the formation of a complete set of concrete hinges (to form a plastic collapse mechanism) or the formation of a critical softening hinge. Since this instability occurs for a non-linear structure with both material and geometric nonlinearities, it is highly complex and therefore difficult to model accurately using simplified approaches such as those used in design codes.

- The results of the analyses suggest that failure of the a frame in most practical cases is likely to occur either by a local plastic beam mechanism, or by a complex instability mode which occurs due to geometric non-linearities after one or several plastic and/or softening hinges have appeared.

- Geometrical nonlinearity due to movement of the ends of the columns during loading was found to be very important and therefore should be included in any numerical modelling of concrete frames. Results obtained suggest that geometric nonlinearity due to deflection along the column is less important for the modelling of behaviour of concrete sway frames.

- The results obtained for the braced portal frames indicate that the flexibility of neighbouring columns connected to the beam influence the collapse behaviour of the system. When the beam was connected to stiff columns, the fall off in load occurs suddenly without much warning whereas in the case where the beam was connected to less stiff columns, the load increments gradually decrease with increase in mid-span deflection before the load decreases. This gives ample warning of impending collapse in a real structure.

The effect of thrust on moment-curvature relation of reinforced concrete mem-

bers cannot be ignored in the analysis of reinforced concrete frames. Ignoring the effect of thrust has been shown to affect the strength and the stiffness of the structure. It also gives different results concerning the formation of the number of concrete hinges.

Effect of the quantity of beam reinforcement has been shown to affect the strength and stiffness of slender reinforced concrete frames. Simplified analysis such as that stipulated by AS3600, which does not take the reinforcement of the beam into consideration when calculating the stiffnesses of the columns, is not likely to give accurate estimate for the strength of the frames.

Snapback instability has been found to occur in reinforced concrete portal frames. It was observed from the frames analysed that at most one snapback occurs in each of the characteristic deflections of the frames. Snapbacks occurred either in the vertical deflection of the beam or in the sway deflection or in both the vertical and sway deflections.

Multiple snapbacks in one characteristic deflection, a phenomena postulated to occur by Bažant et al (1988b), was not observed in the frames analysed. However, multiple snapback is possible in a given frame, in the sense that individual snapback can occur with respect to different load-deflection curves (e.g., in the independent curves of load versus vertical deflection and load versus horizontal deflection). Indeed, multiple snapback of this type was obtained.

The ability of the approach to predict the softening behaviour of multi-storey frames is demonstrated using two practical size frames. The behaviour obtained indicates that these frames reaches their peak load before the formation of plastic collapse mechanisms, therefore suggesting stability failure caused by geometric nonlinearity effect in a frame with both material and geometric nonlinearity effects. This behaviour conforms to the behaviour of portals investigated earlier in this chapter.

Chapter 7

Investigation of the Accuracy of the Moment Magnifier Method for the Analysis/Design of Slender Columns

7.1 Introduction

The design of reinforced concrete columns in slender frames using a "rigorous" analysis taking into account the interactive effect of material and geometrical nonlinearities is seldom carried out because of the inherent complexities. Recognising this, the Australian Standard AS3600 allows slender columns to be designed to different tiers, or levels of sophistication. These are referred as the bottom-tier method (also known as the moment magnifier method), the middle-tier method, and the top-tier method.

Each of these methods requires a different type of analysis. The top-tier method, clearly, requires complex analytical tools in the form of computer programs that can perform non-linear analysis of frames including both the material and geometric non-linearities. The middle-tier method requires the use of a second-order elastic analysis program which takes only the geometric non-linearities into consideration. The bottom-tier method being the simplest of the three, is based on a first-order linear elastic analysis.

In this chapter, the moment magnifier method of AS3600 is described and studied. This highly idealised and simplified method of analysis is the most popular of the three mentioned above. To enable the study of the accuracy of strength predictions of slender frames using the moment magnifier method (as compared with using a more accurate method of analysis/design) to be carried out, a suite of computer programs have been developed to carry out the moment magnifier method of design/analysis. These programs are described in Appendix I.

Analysis and design calculations have been carried out for a wide range of portal frames using the simplified moment magnifier method. For comparison purposes, parallel analyses were made with the top-tier method in the form of program SAFRAME described in Chapter 4. Comparisons of the results obtained from these two methods provide the basis for evaluating the accuracy and adequacy of the bottom-tier method.

The purpose of the study in this chapter is to make comparisons between the simplified method and the more accurate method of design, i.e., the top-tier method, in order to evaluate the accuracy and adequacy of the former method.

Comparisons were first made of predicted ultimate loads, using the analytic procedures without safety coefficients. Comparisons were then made of the design procedures using design loads and all safety coefficients.

7.2 The Moment Magnifier Method

7.2.1 Background and Sources

Column design procedures in successive Australian codes and standards have generally followed developments in the ACI concrete code (with a time lag). For example, ACI 318-63 used a load reduction factor method for the design of slender columns. Comparable method was retained in the concrete code AS1480 until 1988, when AS1480 was replaced by the new Australian Standard, AS3600.

Recent attempts to rationalise the simplified design procedure resulted in both the American standard and the Australian standard using the moment magnifier method as the bottom-tier method. In contrast with the reduction factor method, the moment magnifier method magnifies the bending moment without increasing the axial force. This is more rational than the reduction factor method which requires the magnification of both the bending moment and the axial force.

The moment magnifier method used in AS3600 is similar to that used in ACI 318-83(1983). The sources of ACI 318-83 are therefore also those of AS3600. The moment magnifier method used in ACI 318-83 is based on that of AISC steel design specifications (American Institute of Steel Construction, 1963).

In the analysis of concrete structures to determine forces acting on members, assumption has to be made of the EI values (E is the modulus of elasticity and I is the second moment of area of cross-section) for beams and columns. ACI 318-83 and AS3600 both stipulate that any reasonable assumptions may be adopted for computing relative flexural stiffnesses of columns, provided consistency is maintained throughout the analysis.

The use of column buckling concepts in the moment magnifier method requires the determination of a buckling load, N_c; the calculation of N_c is based on the assumption that the column has a uniform EI value. Previous studies (described by Macgregor, Breen and Pfrang(1970)) resulted in ACI 318-83 adopting representative empirical values, for short-term behaviour, given by the Equation:

$$EI = \frac{E_c I_g}{2.5} \tag{7.1}$$

Studies by Menn(1974) and MacGregor et al(1975) suggested that the representative EI might be calculated conveniently at the "balanced" point on the strength interaction diagram. This point corresponds to the tensile steel just starting to yield when the moment capacity is reached.

For conditions of multiple layers of reinforcement and prestressing tendons, the "balanced" definition cannot be upheld and, therefore, a more general concept based on curvature of the section is applied. Based on this concept, the EI value is defined in AS3600 as:

$$EI = 200 d M_{ub} \tag{7.2}$$

where

d = effective depth of the section; and

M_{ub} =is the moment corresponding to a neutral axis depth of $k_u d = 0.6d$ and a strength reduction factor ϕ of 0.6.

7.2.2 The Method: Design

The Australian Standard AS3600 allows a slender column to be designed using the moment magnifier method provided the column slenderness lies within

prescribed limits. For a braced column, the lower limit for slenderness is specified by:

$$\frac{L_e}{r} > 25; \text{ or} \tag{7.3}$$

$$> 60\left(1+\frac{M_1^*}{M_2^*}\right)/\left(1-\frac{N^*}{0.6N_{uo}}\right) \tag{7.4}$$

whichever is the greater.

where

L_e = effective length of a column;

r = radius of gyration of a section;

M_1^*,M_2^* = The smaller and larger design bending moments respectively at the ends of a column;

N_{uo} = the ultimate strength in compression of an axially loaded cross-section, without eccentricity;

N^* = the design axial force.

For an unbraced column, the lower limit is specified by:

$$\frac{L_e}{r} > 22. \tag{7.5}$$

If the column slenderness is less than these specified limits, then it may be regarded as "short" and geometric slenderness effects can be ignored altogether.

An upper limit of the slenderness ratio of 120 is specified by the Australian standard for slender columns designed using the simplified methods. For frames with column slenderness greater than this value, a top-tier method is required.

The moment magnifier method, even though simplified, cannot be used to determine section sizes directly from given design loads. A trial and error approach has to be used whereby a trial section is chosen and then checked

for adequacy; if the column cannot carry the design loads according to the moment magnifier method of analysis, it must be adjusted accordingly.

To design/analyse slender columns in a given frame, the design load is first determined. This loading should reflect the proportional nature of the design loads, factored up from the service loads using the appropriate load factors of AS3600. Gross sectional EI and EA values are then used to carry out a linear elastic analysis of the frame to determine first-order forces.

To allow for geometric non-linearities, the bending moments determined from the first order analysis are magnified.

For a column in the frame, the linear analysis gives the end moments M_1^* and M_2^*, where M_1^* and M_2^* are the smaller and larger design bending moment respectively at the ends of a column. The axial force N^* is also obtained from the analysis. Next the end restraint coefficients γ_1 and γ_2 are calculated at each end of the column, as:

$$\gamma_1 \ , \ \gamma_2 = \frac{\sum \left(\frac{I}{L}\right)_C}{\sum \left(\frac{\beta I}{L}\right)_B} \tag{7.6}$$

where

I = second moment of area of the gross concrete section;

L = length of the member;

β = fixity factor for fixity condition at the far end of the beam;

$\sum \left(\frac{I}{L}\right)_C$ = sum of the stiffnesses in the plane of bending of all the columns meeting at, and rigidly connected to, the end of the column under consideration; and

$\sum \left(\frac{\beta I}{L}\right)_B$ = sum of the stiffnesses in the plane of bending of all the beams meeting at, and rigidly connected to,

the end of the column under consideration.

According to Clause 10.5.6 of AS3600, the end restraint coefficient γ may be taken as ten when the end restraint is provided by a footing with negligible restraint, and may be taken as one when the end of the column is restrained from rotating.

From these restraint factors, the effective length of the column is calculated as kL_u where the effective length factor k is determined from the Jackson-Mooreland charts provided in AS3600. Depending on whether the column is braced or unbraced, the appropriate chart is to be used.

For both braced and unbraced columns, the magnified moment obtained using the braced moment magnifier, δ_b, is obtained from the expression:

$$M^* = \delta_b \times M_2^* \tag{7.7}$$

where

$$\delta_b = \frac{k_m}{1 - \frac{N^*}{N_c}} \geq 1 \tag{7.8}$$

In the above equation, $k_m = 0.6 - 0.4M_1^*/M_2^*$ for a column without transverse loading between its ends and $N_c = (\pi^2/L_e^2)[200d(\phi\, M_{ub})/(1+\beta_d)]$. The value of k_m is limited to 0.4 to account for the unwinding, under high axial loads, of columns bending in double curvature where $0.5 < \frac{M_1^*}{M_2^*} \leq 1.0$. The design strength in bending $\phi\, M_{ub}$ corresponds to values of $k_u = 0.6$ and $\phi = 0.6$. β_d is a empirical factor equal to the ratio of the dead load to the total load; this factor is taken as zero when $L_e/r \leq 40$ and $N^* \leq M^*/2D$, i.e., when the eccentricity of load is large.

In the calculation of N_c above, a value of EI is implied. For a compression member, the stiffness EI varies with the magnitude of the moment and axial force acting. It also varies with the variation of the bending moment along the beam. In the Australian standard, the EI value at the "balanced point" on the

column interaction diagram is used. This contradicts the use of gross sectional EI in the frame analysis used to obtain forces described earlier. The use of this value of EI has no theoretical justification (Warner et al,1989) and is based on the studies by Macgregor, Oelhafen and Hage (1975); and Menn(1974) who suggested that a single representative value of EI might be calculated at the "balanced" point on the interaction diagram.

For a braced column the design moment is calculated from Equation 7.7.

For an unbraced column the design bending moment is taken to be the larger of two bending moments calculated: one obtained from Equation 7.7 and the other from Equation 7.9 below:

$$M^* = \delta_s \times M_2^* \tag{7.9}$$

where

$$\delta_s = \frac{1}{1 - \left(\frac{\sum N^*}{\sum N_c}\right)} \tag{7.10}$$

The summations in the above equation include all columns within the storey.

In lieu of Equation 7.9, the system moment magnifier can be obtained for the entire frame by using the critical buckling load of the frame using the equation below:

$$\delta_s = \frac{1}{\left(1 - \frac{1+\beta_d}{\phi_s \lambda_{uc}}\right)} \tag{7.11}$$

where

λ_{uc} = ratio of the elastic critical buckling load of the entire frame to the design load for the strength limit states; and

β_d = ratio of the dead load to the sum of the dead and live load, and ϕ_s is a correction factor taken as 0.6.

The value of δ_s obtained from the above expression is applied to all the columns in the frame.

The elastic buckling load used in Equation 7.11 above for a sway frame can be obtained approximately from the expression given below (Stevens, 1967; Rosenbluth, 1965; and MacGregor; 1972):

$$P_c = \frac{K_{1i} h_i}{\gamma} \tag{7.12}$$

where

h_i = height of the i-th storey; and

γ = a parameter which varies from 1.0 for frames with flexible beams to 1.22 for frames with rigid beams.

The lateral stiffness of the i-th storey, K_{1i} is calculated as $\frac{H_i}{\Delta_i}$ where H_i is the horizontal load above the i-th storey and Δ_i is the lateral sway within storey height h_i.

An upper limit on δ_s of 1.5 is proposed by AS3600. This is based on the study by MacGregor and Hage (1977) who found that above this value, instability failure occurs before the section with the maximum moment reaches its full strength.

The evaluation of the accuracy of the bottom-tier method using the system magnifier of Equation 7.11 is not covered in the present investigation, which is concerned only with the magnifiers of Equations 7.7 and 7.9. Attention is focussed on Equation 7.9 instead of Equation 7.11 as the former equation is normally used by designers in preference to the latter equation.

After obtaining the braced moment magnifier and the storey moment magnifier for the column with the most critically loaded section, the next step is to obtain the design strength interaction curve. Details of the steps involved to obtain

interaction curve for symmetrically reinforced concrete sections are given in Appendix D. For the purpose of design or determination of design strength, a strength reduction factor ϕ is applied to the calculated moment. This strength reduction factor, given in in Table 7.1, is dependent on the magnitude of N_u and k_u.

Table 7.1: Strength reduction factor ϕ for section under combined bending and axial compression

$N_u \geq N_{ub}$	0.6
$N_u < N_{ub}$ and $k_u \leq 0.4$ for the section strength in pure bending	$0.6 + 0.2\left(1 - \frac{N_u}{N_{ub}}\right)$
$N_u < N_{ub}$ and $k_u > 0.4$ for the section strength in pure bending	$0.6 + \left[\left(0.8\frac{M_{ud}}{M_u}\right) - 0.6\right]\left(1 - \frac{N_u}{N_{ub}}\right)$

The larger moment M_2^* of the column obtained from the linear analysis is multiplied by the larger of δ_b and δ_s, and together with the axial thrust value acting on the section, a point is located on the interaction diagram. If this point lies to the left of interaction curve, then the sizes and the amount of reinforcement chosen for the members of the frame are acceptable, else they have to be adjusted and the entire procedure repeated. Even if the point lies to the left of the interaction curve, adjustment may still be required to achieve an economical design.

7.2.3 The Method: Strength Determination

Sometimes it is necessary to determine the design strength of a frame given the load pattern and geometry. The design strength takes account of all the material reduction factors and other safety factors provided by the standard. The determination of design strength requires an approach different from the trial and error approach used in design.

For design strength calculations, Equation 7.7 can be written in a more appropriate form (Warner et al,1982). Substituting $M_2^* = N^* e_2$ (where e_2 is the eccentricity of axial force at the end with the larger moment M_2^*) into this equation and rearranging, gives:

$$N^* = \frac{1}{\left(\frac{k_m e_2}{M^*}\right) + \left(\frac{1}{N_c}\right)} \tag{7.13}$$

The Equation 7.13 defines the strength requirements of the critical section in a column and, therefore, is referred to as the loading line of the section. The N-M design strength interaction curve provides the second relation defining the permissible strength of the section. The point that satisfies the requirements of both curves gives the largest permissible N value to use in design.

The requirement that δ_b is greater than 1.0 (see Equation 7.8) results in a bounding straight loading line satisfying the following relationship:

$$N^* = \frac{M^*}{e_2} \tag{7.14}$$

The form of Equation 7.9 is not suitable for determining the design strength of a frame under the effect of the storey moment magnifier δ_s. Since the forces in the frame are obtained from a linear elastic analysis, it is possible to write the sum of all the axial forces in the columns within the same storey as the column under consideration, represented by the notation $\sum N^*$, as $\delta_n\ N^*$, where δ_n is a constant factor determined from the forces obtained from the linear elastic

analysis and N^* is the axial force in the column under consideration. Substituting this relation and $M_2^* = N^* e_2$ into Equation 7.9 and rearranging, as for the case of Equation 7.13, gives:

$$N^* = \frac{1}{\frac{e_2}{M^*} + \frac{\delta_n}{\sum N_c}} \tag{7.15}$$

This expression defines a loading line for the section with the larger load eccentricity e_2, under the influence of the moment magnifier δ_s.

For the analysis of a slender column, Equations 7.13 and 7.15 are used to plot two loading lines, the first representing the larger end moment M_2^* magnified by δ_b and the second representing M_2^* magnified by δ_s. The straight line defined by Equation 7.14 is the third loading line required. The intersection points between the loading lines and the design strength interaction diagram of the column section can be obtained either graphically or numerically. The design strength of this column is the intersection point with the lowest thrust value.

After locating the design strength of the column, the moment magnifier can be obtained from the expression below:

$$\delta = \frac{M^*}{e_2 N^*} \tag{7.16}$$

where

M^* = bending moment at the intersection point;

N^* = axial force at the intersection point; and

e_2 = the eccentricity of axial force at the end with the larger moment M_2^*

Once the value of the design strength N^* of the critical column is determined, the corresponding strength of the frame can be determined from the result obtained from the linear elastic analysis carried out earlier. In cases where the critically loaded column cannot be readily identified, analyses are carried

out for each column. The lowest value is chosen as the design strength of the frame.

The accuracy of the moment magnifier method has previously been checked by Smith and Bridge (1984) for isolated columns. They found that the method is accurate for slenderness ratios $L/r \leq 40$. This covers most practical cases of braced columns. For L/r above this limit, the method becomes increasingly conservative, particularly for column with small end moments. The study of Smith and Bridge was limited to isolated pinned-ended columns with end eccentricity loading. Unfortunately, no checks have been made of columns in frames, which is the major application in practice.

In fact gross simplifications and idealisations are introduced in order to apply the moment magnifier method to columns in frames. For example, there exists the inconsistency of assuming EI values based on the gross concrete sections for frame analysis and assuming the section having EI values corresponding to that of the balanced points when calculating N_c used to obtain the moment magnifiers.

In the calculation of the effective length, the effective length factor k is obtained for the frame assuming that the reinforcement in the beam has little or no effect on the strength. Previous analytical study by Pagay, Ferguson and Breen (1970) indicates substantial influence of the amount of beam reinforcement on the strength of concrete frames.

However, the major idealisation occurs in the use of the effective length concept to account for frame action. This comes from elastic buckling theory and is not logically related to real behaviour of concrete frames with lateral loads and beam loads.

A suite of computer programs has been developed to facilitate the design and ultimate strength calculations for slender frames. They are used to carry out

the analyses described for the frames below. The details of these programs are given in Appendix I.

7.3 Unbraced Portal Frames Analyses

7.3.1 Details of Frames Analysed

A total of 144 portal frames are analysed, with the configurations shown in Figure 7.1. The cross section of all beams and columns is 300 mm by 300 mm, with the concrete cover taken to be 50 mm.

The parameters varied in this study are:

- loading patterns: four types;
- amount of column reinforcement: two ratios— two per cent and four per cent of gross sectional area;
- total amount of beam reinforcement: six ratios— 0.5 per cent, 1 per cent, 2 per cent, 3 per cent, 4 per cent and 5 per cent gross sectional area; and
- column heights: three heights— 3m, 6m and 9m.

The portals have column slenderness ratios l_e/r (based on AS3600) of 48, 88 and 127, corresponding to the frame heights of 3 m, 6 m and 9 m respectively. These provide a good cover of the range allowed by AS3600 for the simplified method of design, i.e, from 36 to 120.

As previous studies by Pagay, Ferguson and Breen (1970) have shown that the quantity of beam reinforcement has a significant effect on overall frame behaviour, the six different reinforcement ratios given above were used. All

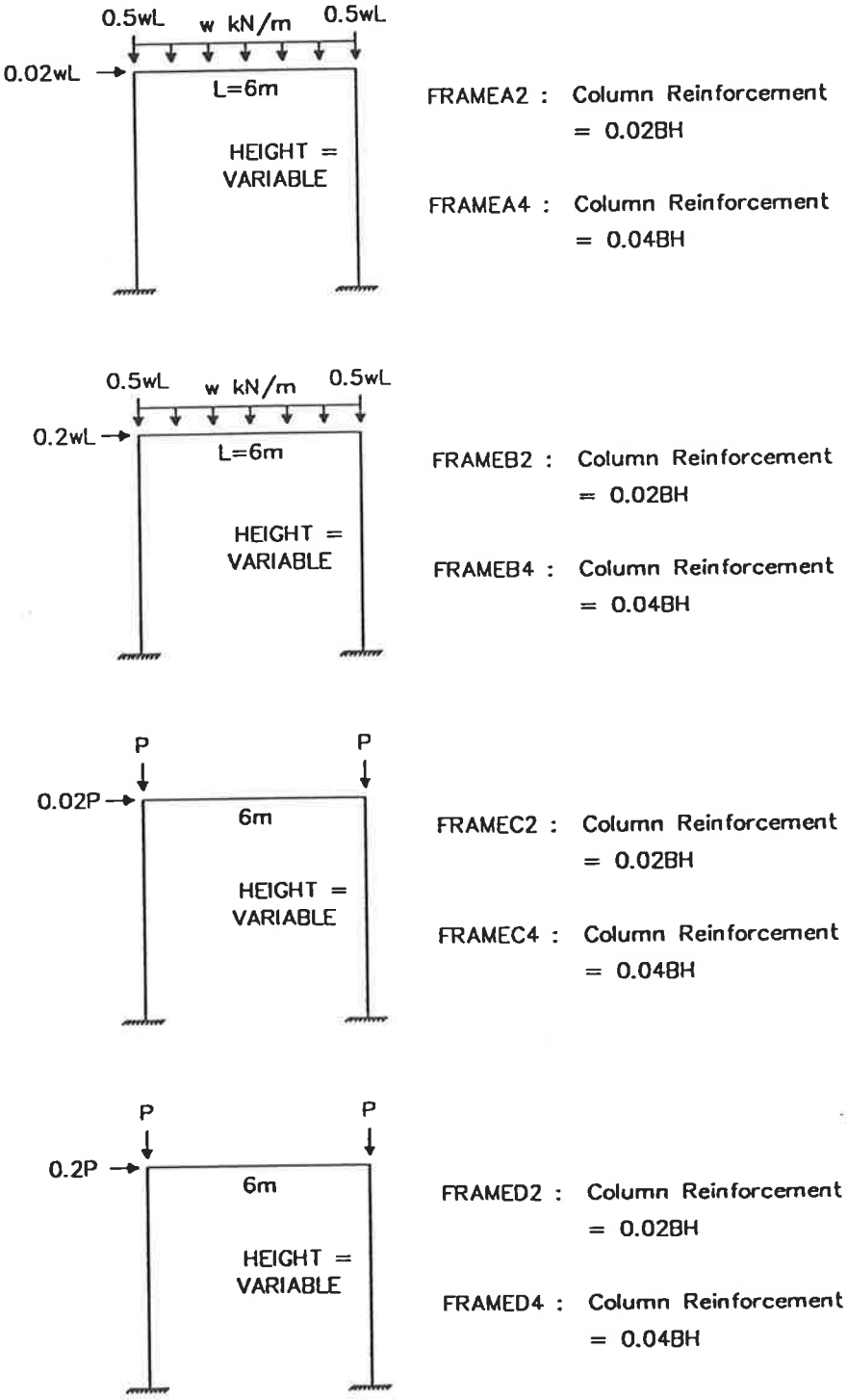

Figure 7.1: Configurations of portal frames analysed

beams are symmetrically reinforced with equal amounts of steels in the upper and lower regions over the full span length.

AS3600 stipulates the minimum and maximum amount of reinforcement allowed in beams and columns. For columns, the minimum reinforcement is $0.01A_g$ where A_g is the gross sectional area except that, when a column has a larger area than is required for strength, a reduced value may be used. The maximum amount of column reinforcement is $0.04A_g$ or less if proper placing and compaction of concrete is impeded. The "deemed to satisfy" minimum amount of tensile reinforcement for rectangular reinforced concrete beams specified in AS3600 is:

$$\frac{A_{st}}{bd} \geq \frac{1.4}{f_{sy}} \tag{7.17}$$

With the characteristic f_{sy} of 400 MPa, this gives a lower limit of 0.0035 (the effective depth d of the beams in the portals is 250 mm and the overall depth D is 300 mm). The lowest beam reinforcement value of $100A_s/BD$ (where A_s is the total amount of steel for symmetrically reinforced concrete section) of 0.5 per cent correspond to a value of 0.003, slightly less than the minimum requirement of Equation 7.17. No upper limit is given in AS3600 for symmetrically reinforced beam sections.

It is recognised that the upper limit of 5% chosen for steel content in the beams may not be feasible from the viewpoint of constructability; nevertheless, it was considered important to cover a full range of possibilities.

These portals are analysed by using 1 element per beam. Four elements are used for each of the columns to enable the insertion of sufficient nodes along each column to model the geometrical nonlinearity effect that occurs along the member.

7.3.2 Accuracy of Ultimate Strength Predictions

Material properties used in the analyses for the predictions of ultimate strength are average (not characteristic) values. They are as follows:

- concrete:
  - average compressive strength : $f_{cm} = 35$ MPa;
  - peak strength in members : $f_{cmax} = 0.85 f_{cm}$;
  - elastic modulus : $E_c = 5000\sqrt{f_{cm}}$ (E_c and f_{cm} in MPa)
- steel:
  - average yield stress : $f_{sy}(average) = 460$ MPa;
  - elastic modulus : $E_s = 200{,}000$ MPa.

To identify the frames within any series, the 3 m frame is referred to as Low, the 6 m frame is referred to as Medium and the 9 m frame is referred to as Tall. Thus, the 9 m frames of series FRAMEA2 are referred to as FRAMEA2T. An individual frame within this set which has 0.5 per cent beam reinforcement is referred to as FRAMEA2T_0.5.

A typical plot of ultimate strength versus quantity of reinforcement is illustrated using set FRAMEB2L (load configuration B, two per cent column reinforcement, and 3 m frame height) is given in Figure 7.2b. Results indicated by square symbols are obtained using program SAFRAME. The solid line represents ultimate load as limited by column failure, calculated by the moment magnifier method. This line is horizontal, indicating that the strength of the frame based on column failure is independent of the amount of reinforcement in the beam. The results indicated by circle symbols are ultimate loads of frames obtained based on the failure of the most critically stressed section in the beam. Axial thrust is taken into consideration when determining the

strength of critical beam sections from the corresponding strength interaction diagrams. The failure surface for the bottom-tier method is thus composed of an inclined line, with a positive slope with increasing reinforcement, changing over to a straight horizontal line at higher amount of reinforcement. For set FRAMEB2L, this crossover occurs at approximately 2.3 per cent beam reinforcement. This failure surface has a similar general shape as that obtained from the top-tier analyses, except that it flattens out at a lower percentage of beam reinforcement. This suggests that the failure surface predicted by the bottom-tier method using the coupled beam-failure column-failure representation is appropriate, at least qualitatively.

The ratios of collapse loads, obtained from the bottom-tier and the rigorous method, are plotted in Figure 7.2(a) against the amount of beam reinforcement. The results are in all cases conservative (i.e., less than 1.0), and probably overconservative for large percentages of beam reinforcement.

In Figure 7.3, the results of analyses for FRAMEB2T are presented. These have the same loading configuration and the same amount of column reinforcement as for FRAMEB2L, except that the frames are 9m high. Again, the bottom-tier results are conservative, but the bi-linear failure surface has a shape that agrees much better with that obtained from the rigorous analysis as compared with the results of FRAMEB2L. The top-tier results show a more pronounced flattening for steel percentages greater than 2.0 per cent.

The results obtained for the frames with two per cent column reinforcement (0.02BH), i.e., for series FRAMEA2, FRAMEB2, FRAMEC2, and FRAMED2, are summarised in Table 7.2 and those for the frames with four per cent column reinforcement (0.04BH), i.e., for series FRAMEA4, FRAMEB4, FRAMEC4 and FRAMED4, are summarised in Table 7.3. Histograms of the ratio of the ultimate load based on the bottom-tier method to that based on the top-tier method (obtained using program SAFRAME), $P_{bot}(ult.)/P_{top}(ult.)$ (or

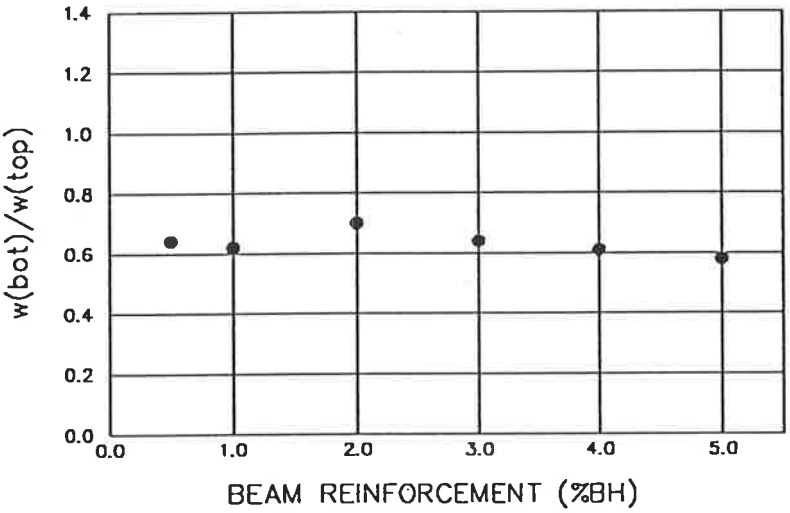

(a)

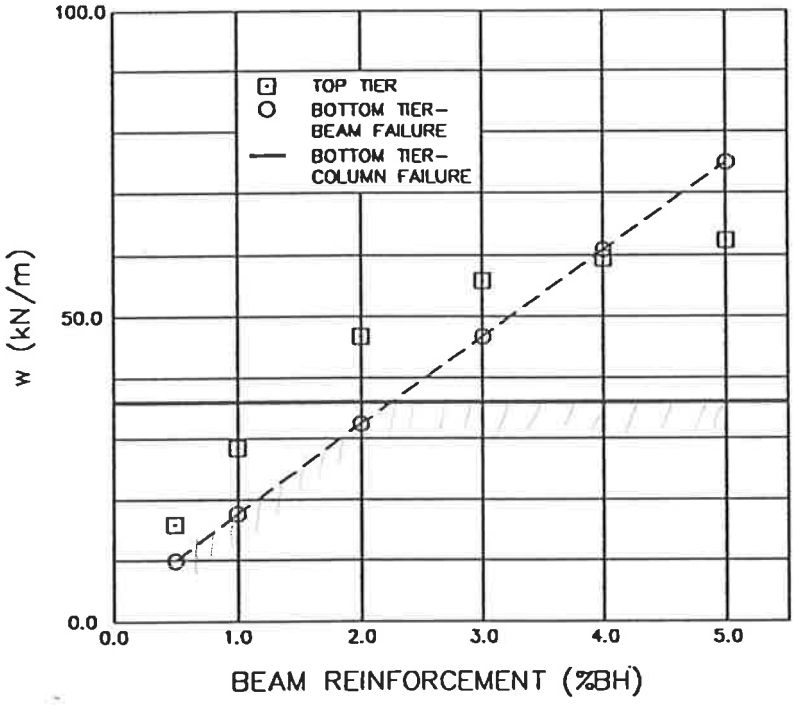

(b)

Figure 7.2: Results for set FRAMEB2L

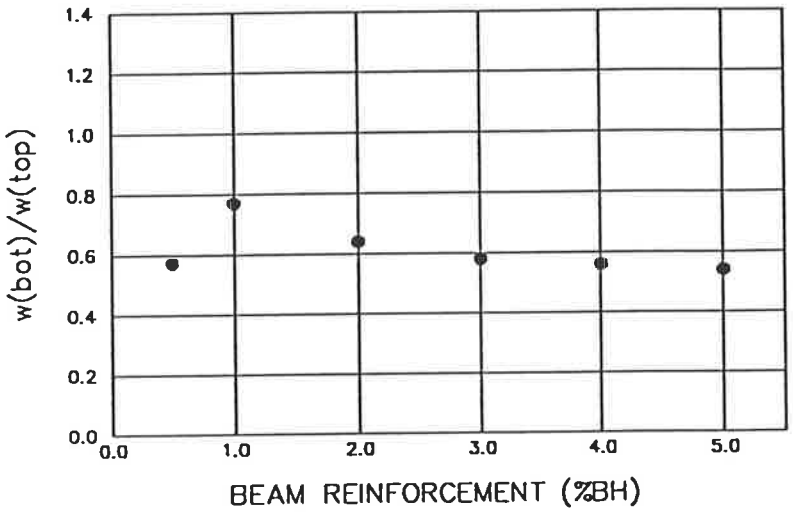

(a)

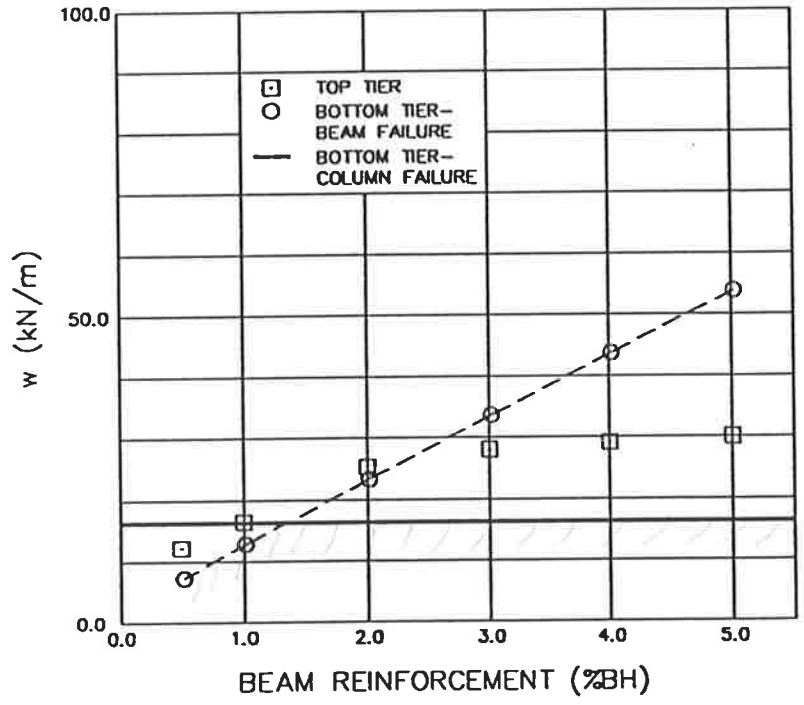

(b)

Figure 7.3: Results for set FRAMEB2T

$w_{bot}(ult.)/w_{top}(ult.)$), are given in Figure 7.4.

The histograms indicate that out of the 144 frames analysed, 60 frames are controlled by beam section failure and 84 frames are controlled by column failure. The comparison ratio $P_{bot}(ult.)/P_{top}(ult.)$ (or $w_{bot}(ult.)/w_{top}(ult.)$) lies between 0.35 and 1.34.

The largest unconservative strength ratio, of 1.34, occurs in frame FRAMEC4T_0.5, which has type C loading pattern, 9m columns with reinforcement of 4 per cent, and 0.5 per cent beam reinforcement. It has P_{top} of $550kN$. Comparing this ultimate load with that of FRAMEC2T_0.5 (with $P_{top} = 471kN$) indicates that increasing the amount of column reinforcement from 2 per cent to 4 per cent does not cause much increase in the ultimate load of the frame. Since there is no loading along the beam, plastic collapse mechanism cannot form in the beam. Simple plastic analyses, carried out on the frames, assuming sections failed by steel yielding, give sway plastic collapse loads of 1150 kN and 2070 kN for FRAMEC2T_0.5 and FRAMEC4T_0.5, respectively. Plastic hinges are assumed to occur next to the bases of the columns and the ends of the beam. Clearly, sway plastic mechanism has not formed at collapse. Therefore, the collapse is likely to be caused by instability.

Parallel analyses using the bottom-tier method, considering column failure, give an ultimate load of 526 kN for FRAMEC2T_0.5 and an ultimate load of 788 kN for FRAMEC4T_0.5. For both frames, the ultimate load predicted based on the bottom-tier method considering beam section failure is 735 kN. (Both the frames have an identical beam section failure load as the amount of column reinforcement is ignored in the first-order elastic analysis using gross section properties.) FRAMEC2T_0.5 therefore has an ultimate load of 526 kN (column failure) and FRAMEC4T_0.5 has an ultimate load of 735 kN (beam section failure). Thus the comparison ratio of the frame with 2 per cent column reinforcement is 1.12 and that for the frame with 4 per cent column reinforce-

ment is 1.34. Increasing the amount of column reinforcement twofold has resulted in an increase of the ultimate load of approximately 17 percent (according to the top-tier calculation) and a predicted increase of approximately 40 percent according to the bottom-tier method. This suggests that the use of the bottom-tier method may be over-optimistic when applied to frames which fail by loss of stability arising from lateral displacement of loaded joints.

Frames with unconservative strength ratios in excess of unity are all from the series FRAMEC2 and FRAMEC4. This suggests that care should be taken if the bottom-tier method is used to predict ultimate loads of frames with very slender columns that are are likely to have significant induced P-Δ moments caused by heavily loaded joints; these moment not being able to be determined from the linear elastic analysis. Such columns are likely to be found in lower floor columns which are subjected to large axial loads from the loads on the floors above.

There is no attempt made to locate the number and position of concrete plastic hinges in the frames using the results obtained from the top-tier analysis as it has been shown earlier in Chapter 6 that softening, and therefore the peak load, can occur at any stage of hinge formation, from no hinges to a complete set of concrete hinges required for the formation of a plastic collapse mechanism, and therefore this information is considered not useful for determining the onset of collapse.

7.3.3 Accuracy of Design Strength Predictions

In this section, a study is made of the adequacy of the safety provisions used when the moment magnifier method is applied to column design.

The frames analysed are the same as those described previously in Section 7.3.1. Instead of using mean values, characteristic values are used for the material

Table 7.2: Ratio $P_{bot}(ult.)/P_{top}(ult.)$(or $w_{bot}(ult.)/w_{top}(ult.)$) for the frames with column reinforcement of 2% BH

	frame	beam reinforcement (%BH)					
	height	0.5	1.0	2.0	3.0	4.0	5.0
FRAMEA2	3m	0.82(B)	0.82(B)	0.82(B)	0.73	0.63	0.58
	6m	0.83(B)	0.82(B)	0.83(B)	0.77	0.66	0.58
	9m	0.74(B)	0.75(B)	0.80(B)	0.69	0.61	0.52
FRAMEB2	3m	0.64(B)	0.62(B)	0.70	0.64	0.61	0.58
	6m	0.61(B)	0.68(B)	0.80	0.70	0.66	0.63
	9m	0.57(B)	0.77(B)	0.64	0.58	0.56	0.54
FRAMEC2	3m	1.03	0.98	0.93	0.91	0.90	0.89
	6m	1.10	0.87	0.71	0.64	0.61	0.59
	9m	1.12	0.86	0.68	0.62	0.59	0.57
FRAMED2	3m	0.53(B)	0.80(B)	0.87	0.80	0.76	0.71
	6m	0.61(B)	0.87(B)	0.90	0.82	0.80	0.78
	9m	0.68(B)	0.96(B)	0.91	0.86	0.84	0.84
(B) : bottom-tier beam failure							

Table 7.3: Ratio $P_{bot}(ult.)/P_{top}(ult.)$(or $w_{bot}(ult.)/w_{top}(ult.)$) for the frames with column reinforcement of 4% BH

	frame	beam reinforcement (%BH)					
	height	0.5	1.0	2.0	3.0	4.0	5.0
FRAMEA4	3m	0.72(B)	0.82(B)	0.82(B)	0.82(B)	0.83(B)	0.75
	6m	0.83(B)	0.84(B)	0.81(B)	0.83(B)	0.84(B)	0.79
	9m	0.74(B)	0.74(B)	0.77(B)	0.80(B)	0.80	0.70
FRAMEB4	3m	0.63(B)	0.63(B)	0.65(B)	0.67(B)	0.68(B)	0.71
	6m	0.59(B)	0.59(B)	0.68(B)	0.76(B)	0.78	0.73
	9m	0.50(B)	0.61(B)	0.75(B)	0.84(B)	0.80	0.76
FRAMEC4	3m	1.01(B)	1.05	1.00	0.98	0.95	0.94
	6m	1.04(B)	1.08	0.84	0.75	0.71	0.68
	9m	1.34(B)	1.09	0.85	0.77	0.72	0.70
FRAMED4	3m	0.35(B)	0.55(B)	0.85(B)	0.92	0.89	0.87
	6m	0.38(B)	0.62(B)	0.91(B)	0.94	0.86	0.83
	9m	0.45(B)	0.71(B)	0.98(B)	0.94	0.87	0.85
(B) : bottom-tier beam failure							

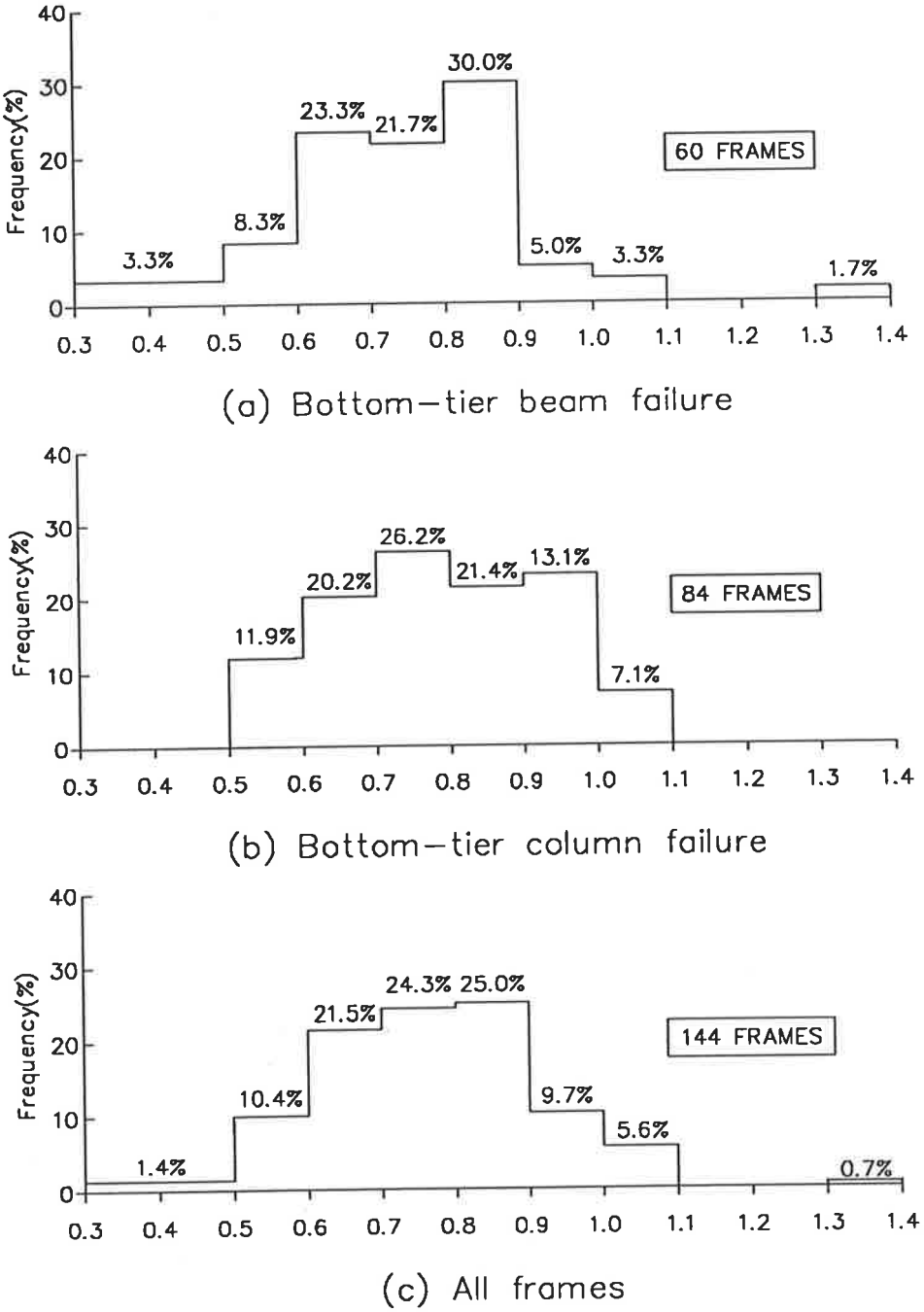

Figure 7.4: Histograms for bottom-tier (ultimate strength)

properties. The characteristic strength for concrete, f'_c, is assumed to be 30 MPa and the yield strength of reinforcement f_{sy} is assumed to be 400 MPa.

The strength reduction factor ϕ is included in the analysis to obtain the design strength of frames using the middle-tier and bottom-tier methods. For the top-tier method, AS3600 specifies that the strength of a frame is to be determined based on the critical section reaching its strength. Results obtained for the cantilevered column analysed in Chapter 6 indicate that the peak load of a structure can be caused by instability before sections in the structure reaching peak strengths. The results suggest that using the AS3600 top-tier method to determine strength may result in unconservative, and even dangerous, design as it is possible for the frame to be close to the peak load, even though the critical section has not reached its ultimate strength, owing to instability.

In order to enable realistic comparisons to be made between the simplified methods and the top-tier method, a global strength reduction factor is applied to the load determined using the top-tier method. Unlike the strength reduction factor used in the moment magnifier method, this factor is applied to the load instead of the section strength. This is more appropriate as the collapse load does not normally occur when the ultimate strength of a single cross-section is reached. As the global strength reduction factor can only be determined from a full reliability study, it is assumed to be equal to the strength reduction factor ϕ of the critical section governing the design strength of the simplified bottom-tier method. If such an approach is used in practice to carry out a design, it would be unrealistic to carry out a parallel analysis using the moment magnifier method to determine the global strength reduction factor. The more conservative value of 0.6 corresponding to column failure at N_{ub} should probably be used in such a case.

In making comparisons, load factors are assumed to be the same for both the rigorous method and the bottom-tier method, and therefore cancel out when

calculating the comparison ratios.

The results obtained for the sets of frames with columns having reinforcement of 2% BH (i.e., for FRAMEA2, FRAMEB2, FRAMEC2, and FRAMED2) are summarised in Table 7.4 and Table 7.5. and those for the sets of frames with columns having reinforcement of 4% BH, i.e., for FRAMEA4, FRAMEB4, FRAMEC4 and FRAMED4 are summarised in Table 7.6 and Table 7.7. Histograms of the ratio $P_{bot}(des.)/P_{top}(des.)$ (or $w_{bot}(des.)/w_{top}(des.)$) are given in Figure 7.5.

The histograms indicate that out of the 144 frames analysed, 55 frames have design strength controlled by beam section failure and 89 frames have design strength controlled by column failure. All the columns have their strength controlled by loading curves for the storey effect, i.e., by curves represented by Equation 7.9. The constraint of AS3600 that δ_s is to be less than or equal to 1.5 is ignored in this first set of plots. Thus the results from all 144 frames are included in producing Figure 7.5(c). The comparison ratio $P_{bot}(des.)/P_{top}(des.)$ (or $w_{bot}(des.)/w_{top}(des.)$) varies from 0.35 to 1.32 with 85.5 per cent between 0.5 to 0.9. Frames with a ratio greater than 1.0 are, as in the study of ultimate strength, mainly found within the series FRAMEC2 and FRAMEC4.

The use of a top-tier strength global reduction factor equal to the strength reduction factor of the critical section gives conservative bottom-tier results for a vast majority of the frames. The results obtained indicate that 7.0 per cent of the frames have comparison ratios greater than 1.1, which may be of concern, especially when this ratio may be as large as 1.32.

However, when the constraint specified by AS3600 that δ_s is to be less than or equal to 1.5 is included, the comparison ratios of the frames satisfying this requirement are between 0.3 to 1.0, with 93.4 per cent between 0.5 to 0.9 (see Figure 7.6(c)). Out of the 38 frames eliminated by the afore-mentioned requirement, 27 frames have a comparison ratio of less than unity. This indicates that

approximately 71 per cent of the frames eliminated by the application of this requirement are actually giving conservative estimates of design load, indicating the unsatisfactory consequence of using this requirement.

In general, the safety ratios for the design predictions have reduced in value, i.e., have become more conservative as compared with those obtained for the ultimate load condition. Approximately 21 per cent of the results show a safety ratio of less than 0.6. It should be emphasized that this represents safety over and above the safety purposely introduced in the form of ϕ factors, etc., and the use of characteristic strengths. These results may well be considered as over-conservative.

7.4 Braced Portal Frames

7.4.1 Details of Frames Analysed

A total of 36 braced portal frames were analysed. The configurations of these frames are shown in Figure 7.7. The parameters varied in these frames are:

- amount of column reinforcement: two ratios– two per cent and four per cent of gross sectional area;
- amount of beam reinforcement: six ratios– 0.5 per cent, 1 per cent, 2 per cent, 3 per cent, 4 per cent and 5 per cent gross sectional area; and
- column heights: three heights– 3 metres, 6 metres and 9 metres.

Table 7.4: Ratio $P_{bot}(des.)/P_{top}(des.)$ (or $w_{bot}(des.)/w_{top}(des.)$) for the frames with column reinforcement of 2% BH

	frame ht		beam reinforcement (%BH)					
			0.5	1.0	2.0	3.0	4.0	5.0
FRAMEA2	3m	ratio	0.81(B)	0.81(B)	0.82(B)	0.68	0.58	0.52
		ϕ	0.80	0.80	0.79	0.76	0.76	0.76
		δ_s	–	–	–	1.08	1.08	1.08
	6m	ratio	0.84(B)	0.81(B)	0.82(B)	0.70	0.60	0.52
		ϕ	0.80	0.80	0.80	0.76	0.76	0.76
		δ_s	–	–	–	1.28	1.28	1.28
	9m	ratio	0.75(B)	0.74(B)	0.76	0.61	0.53	0.46
		ϕ	0.80	0.80	0.77	0.77	0.77	0.77
		δ_s	–	–	1.64	1.64	1.64	1.64
FRAMEB2	3m	ratio	0.63(B)	0.61(B)	0.69(B)	0.59	0.56	0.53
		ϕ	0.80	0.80	0.79	0.77	0.77	0.77
		δ_s	–	–	–	1.06	1.06	1.06
	6m	ratio	0.59(B)	0.65(B)	0.76	0.64	0.59	0.56
		ϕ	0.80	0.80	0.78	0.78	0.78	0.78
		δ_s	–	–	1.17	1.17	1.17	1.17
	9m	ratio	0.56(B)	0.75(B)	0.73	0.65	0.63	0.62
		ϕ	0.80	0.80	0.78	0.78	0.78	0.78
		δ_s	–	–	1.29	1.29	1.29	1.29
(B): bottom-tier beam failure								

Table 7.5: Ratio $P_{bot}(des.)/P_{top}(des.)$(or $w_{bot}(des.)/w_{top}(des.)$) for the frames with column reinforcement of 2% BH - continue

	frame ht		beam reinforcement (%BH)					
			0.5	1.0	2.0	3.0	4.0	5.0
FRAMEC2	3m	ratio	1.23	1.18	1.13	1.11	1.09	1.08
		ϕ	0.60	0.60	0.60	0.60	0.60	0.60
		δ_s	2.72	2.72	2.72	2.72	2.72	2.72
	6m	ratio	0.95	0.77	0.61	0.56	0.54	0.53
		ϕ	0.68	0.68	0.68	0.68	0.68	0.68
		δ_s	4.65	4.65	4.65	4.65	4.65	4.65
	9m	ratio	0.91	0.71	0.54	0.48	0.47	0.46
		ϕ	0.74	0.74	0.74	0.74	0.74	0.74
		δ_s	5.59	5.59	5.59	5.59	5.59	5.59
FRAMED2	3m	ratio	0.52(B)	0.77(B)	0.75	0.69	0.65	0.64
		ϕ	0.80	0.79	0.72	0.72	0.72	0.72
		δ_s	–	–	1.19	1.19	1.19	1.19
	6m	ratio	0.60(B)	0.86(B)	0.80	0.73	0.71	0.70
		ϕ	0.80	0.80	0.77	0.77	0.77	0.77
		δ_s	–	–	1.30	1.30	1.30	1.30
	9m	ratio	0.66(B)	0.92(B)	0.82	0.77	0.76	0.75
		ϕ	0.80	0.80	0.78	0.78	0.78	0.78
		δ_s	–	–	1.40	1.40	1.40	1.40
(B): bottom-tier beam failure								

Table 7.6: Ratio $P_{bot}(des.)/P_{top}(des.)$(or $w_{bot}(des.)/w_{top}(des.)$) for the frames with column reinforcement of 4% BH

	frame ht		beam reinforcement (%BH)					
			0.5	1.0	2.0	3.0	4.0	5.0
FRAMEA4	3m	ratio	0.80(B)	0.83(B)	0.82(B)	0.81(B)	0.85	0.83
		ϕ	0.80	0.80	0.79	0.79	0.74	0.74
		δ_s	–	–	–	–	1.09	1.09
	6m	ratio	0.84(B)	0.81(B)	0.81(B)	0.81(B)	0.84	0.72
		ϕ	0.80	0.80	0.80	0.80	0.74	0.74
		δ_s	–	–	–	–	1.35	1.35
	9m	ratio	0.75(B)	0.74(B)	0.76(B)	0.78(B)	0.72	0.63
		ϕ	0.80	0.80	0.80	0.80	0.75	0.75
		δ_s	–	–	–	–	1.78	1.78
FRAMEB4	3m	ratio	0.62(B)	0.62(B)	0.62(B)	0.65(B)	0.71	0.68
		ϕ	0.80	0.80	0.79	0.79	0.75	0.75
		δ_s	–	–	–	–	1.07	1.07
	6m	ratio	0.58(B)	0.58(B)	0.66(B)	0.74(B)	0.72	0.67
		ϕ	0.80	0.80	0.80	0.79	0.76	0.76
		δ_s	–	–	–	–	1.21	1.21
	9m	ratio	0.51(B)	0.56(B)	0.73(B)	0.86	0.72	0.68
		ϕ	0.80	0.80	0.80	0.77	0.77	0.77
		δ_s	–	–	–	1.36	1.36	1.36
(B): bottom-tier beam failure								

The columns have slenderness ratio l_e/r values (based on AS3600) of 44, 79 and 114 corresponding to frame heights of 3 metres, 6 metres and 9 metres respectively.

The portals are modelled by using 1 element per beam and four elements per column. Four elements are used to enable the insertion of sufficient nodes along each column to model the geometrical nonlinearity within the length of the member.

For the analyses in this section, member sizes are all 300 mm × 300 mm. Material properties used are the same as for the unbraced frames described earlier in this chapter.

Comparison ratios $w_{bot}(ult.)/w_{top}(ult.)$ for the frames are summarised in Table 7.8. Of the 36 frames analysed, only 6 frames have column failures. The comparison ratio for the frames ranges from 0.63 to 0.99. This indicates that the moment magnifier method is conservative in predicting ultimate loads for the braced frames analysed.

Comparison ratios $w_{bot}(des.)/w_{top}(des.)$ for the frames are summarised in Table 7.9. Of the 36 frames analysed, only 7 frames have column failures. The comparison ratio for the frames ranges from 0.58 to 0.93. This indicates that the moment magnifier method is conservative in estimating design loads for the braced frames analysed.

7.5 Three-storey Two-bay Frames

A three-storey two-bay frame shown in Figure 7.8 is analysed. All members are assumed to be 300mm by 300mm. Material properties used for the frame are the same as those used for the portals analysed earlier in this chapter. All

Table 7.7: Ratio $P_{bot}(des.)/P_{top}(des.)$(or $w_{bot}(des.)/w_{top}(des.)$) for the frames with column reinforcement of 4% BH -continue

	frame ht		beam reinforcement (%BH)					
			0.5	1.0	2.0	3.0	4.0	5.0
FRAMEC4	3m	ratio	0.97(B)	1.32	1.28	1.21	1.21	1.20
		ϕ	0.80	0.60	0.60	0.60	0.60	0.60
		δ_s	–	2.42	2.42	2.42	2.42	2.42
	6m	ratio	0.99(B)	1.09	0.85	0.74	0.71	0.70
		ϕ	0.80	0.62	0.62	0.62	0.62	0.62
		δ_s	–	4.78	4.78	4.78	4.78	4.78
	9m	ratio	1.21	0.94	0.70	0.63	0.59	0.57
		ϕ	0.71	0.71	0.71	0.71	0.71	0.71
		δ_s	6.30	6.30	6.30	6.30	6.30	6.30
FRAMED4	3m	ratio	0.35(B)	0.53(B)	0.82(B)	0.87	0.84	0.82
		ϕ	0.80	0.79	0.79	0.68	0.68	0.68
		δ_s	–	–	–	1.21	1.21	1.21
	6m	ratio	0.38(B)	0.59(B)	0.88(B)	0.84	0.77	0.74
		ϕ	0.80	0.80	0.79	0.75	0.75	0.75
		δ_s	–	–	–	1.36	1.36	1.36
	9m	ratio	0.43(B)	0.68(B)	0.97(B)	0.84	0.78	0.75
		ϕ	0.80	0.80	0.79	0.77	0.77	0.77
		δ_s	–	–	–	1.50	1.50	1.50
(B): bottom-tier beam failure								

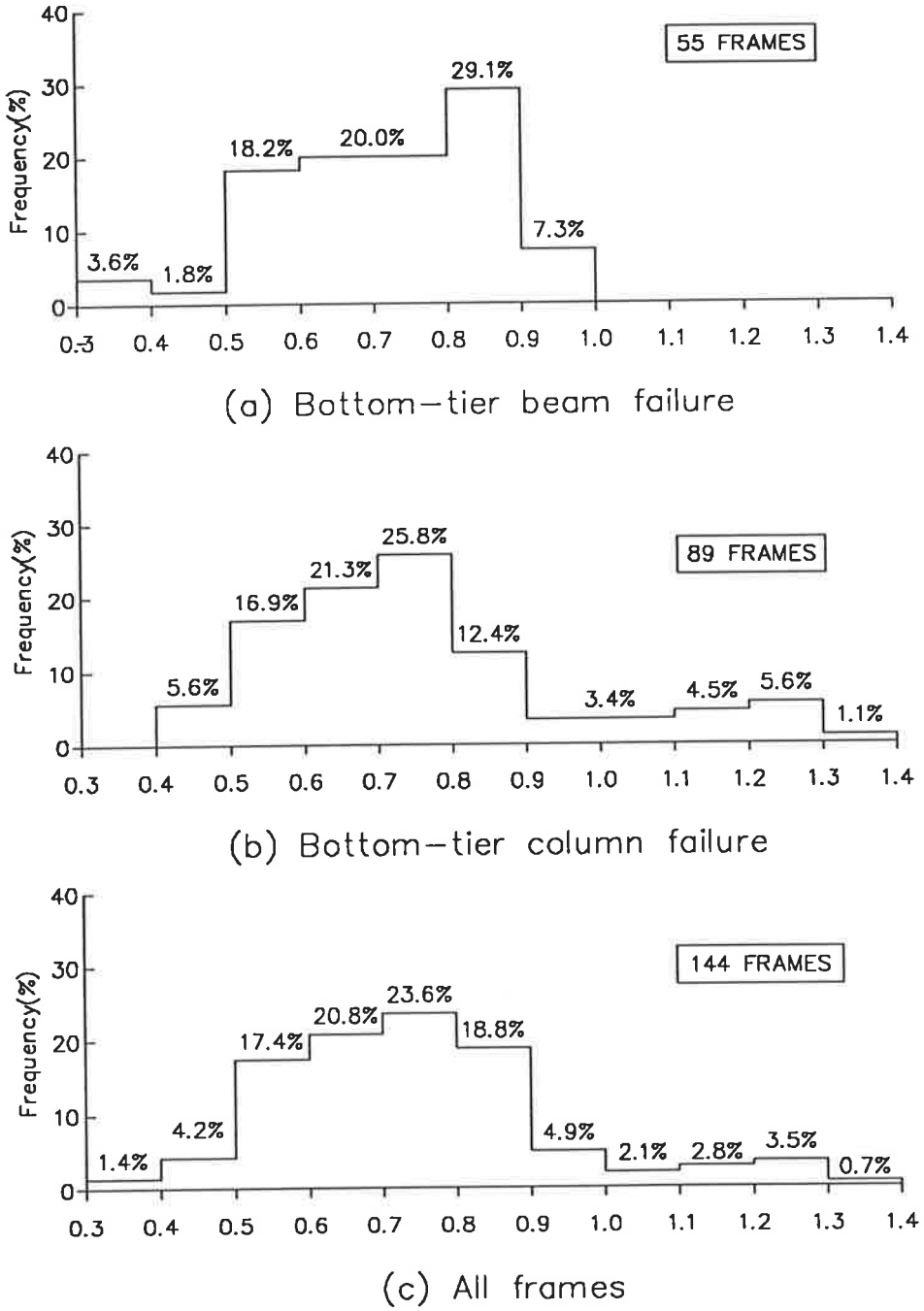

Figure 7.5: Histograms for bottom-tier (design strength)

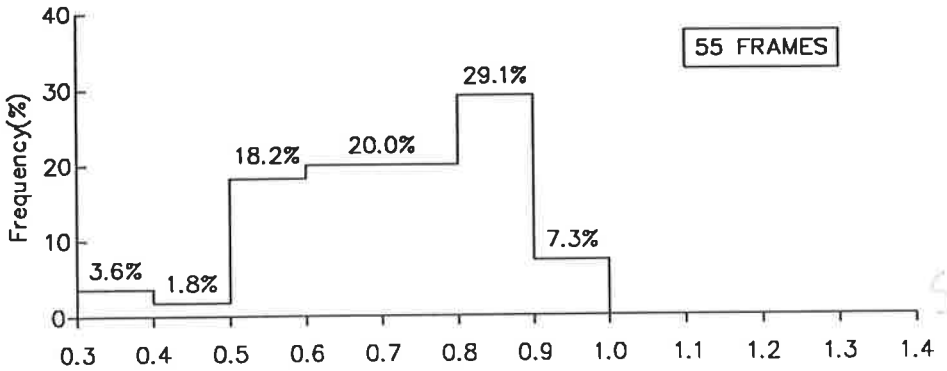

(a) Bottom−tier beam failure

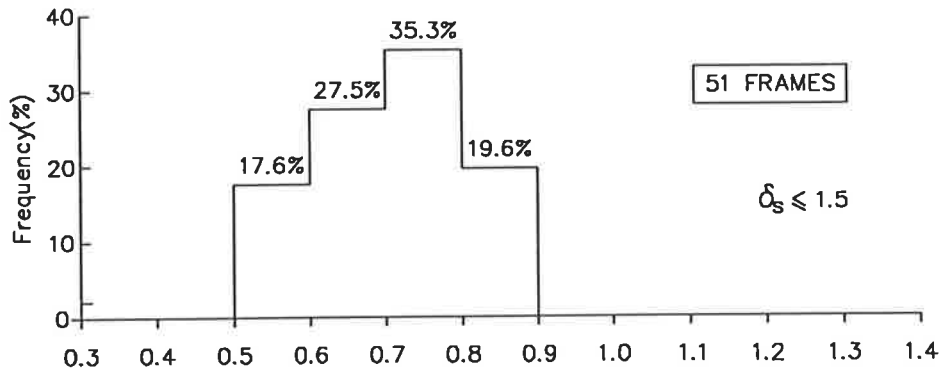

(b) Bottom−tier column failure

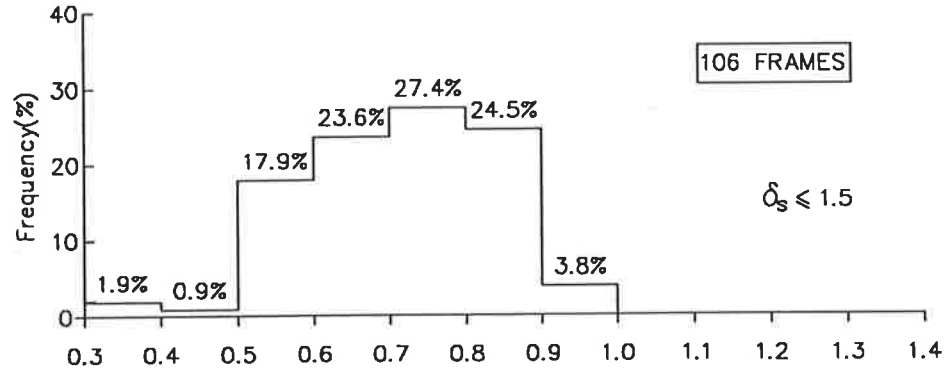

(c) All frames

Figure 7.6: Histograms for bottom-tier (design strength)($\delta_s \leq 1.5$)

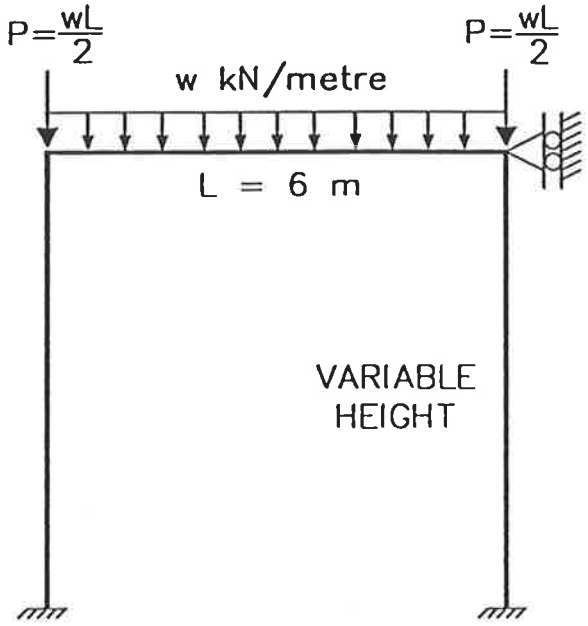

FRAMEE2: COLUMN REINFORCEMENT = 0.02BH

FRAMEE4: COLUMN REINFORCEMENT = 0.04BH

Figure 7.7: Configuration of braced portal frames Analysed

Table 7.8: Ratio $w_{bot}(ult.)/w_{top}(ult.)$ for braced frames

	frame	beam reinforcement (%BH)					
	height	0.5	1.0	2.0	3.0	4.0	5.0
FRAMEE2	3m	0.88(B)	0.96(B)	0.86(B)	0.83	0.72	0.63
	6m	0.91(B)	0.83(B)	0.81(B)	0.90(B)	0.92	0.80
	9m	0.75(B)	0.73(B)	0.73(B)	0.83(B)	0.92(B)	0.99(B)
FRAMEE4	3m	0.88(B)	0.86(B)	0.85(B)	0.84(B)	0.85(B)	0.88
	6m	0.85(B)	0.83(B)	0.81(B)	0.80(B)	0.81(B)	0.86(B)
	9m	0.75(B)	0.74(B)	0.72(B)	0.72(B)	0.73(B)	0.78(B)
(B) : bottom-tier beam failure							

Table 7.9: Ratio $w_{bot}(des.)/w_{top}(des.)$ for braced frames

	frame ht		beam reinforcement (%BH)					
			0.5	1.0	2.0	3.0	4.0	5.0
FRAMEE2	3m	ratio	0.85(B)	0.86(B)	0.85(B)	0.77	0.66	0.58
		ϕ	0.80	0.80	0.79	0.76	0.76	0.76
		δ_b	–	–	–	1.00	1.00	1.00
	6m	ratio	0.91(B)	0.81(B)	0.80(B)	0.89(B)	0.83	0.73
		ϕ	0.80	0.80	0.80	0.80	0.75	0.75
		δ_b	–	–	–	–	1.00	1.00
	9m	ratio	0.72(B)	0.72(B)	0.70(B)	0.78(B)	0.88(B)	0.93
		ϕ	0.80	0.80	0.80	0.80	0.80	0.74
		δ_b	–	–	–	–	–	1.00
FRAMEE4	3m	ratio	0.89(B)	0.85(B)	0.86(B)	0.83(B)	0.86(B)	0.84
		ϕ	0.80	0.80	0.79	0.79	0.79	0.73
		δ_b	–	–	–	–	–	–
	6m	ratio	0.84(B)	0.82(B)	0.80(B)	0.79(B)	0.79(B)	0.85(B)
		ϕ	0.80	0.80	0.80	0.80	0.79	0.79
		δ_b	–	–	–	–	–	–
	9m	ratio	0.72(B)	0.71(B)	0.71(B)	0.68(B)	0.70(B)	0.75(B)
		ϕ	0.80	0.80	0.80	0.80	0.80	0.80
		δ_b	–	–	–	–	–	–
(B): bottom-tier beam failure								

members have two per cent reinforcement, and are symmetrically reinforced with equal amounts of steel in the upper and lower regions. Slenderness ratio l/r calculated for the columns based on AS3600 ranges from 38 to 61.

In the top-tier method, the columns are each modelled using one element. This is acceptable, as the results obtained in Chapter 6 indicate that the P-Δ effect along columns does not affect significantly the ultimate load for unbraced frames subjected to sway-induced forces. 15 segments are used for each beam and 10 segments are used for each column, resulting in each segment having a length to depth ratio of unity.

Results obtained for the frame for ultimate strength determination are summarised in Table 7.10. The results indicate a beam section failure load of 47.9 kN/m. An estimate of the beam plastic collapse mechanism gives a failure load of about 65 kN/m (assuming the beam to be fixed at both ends, and the plastic capacity of sections calculated based only on the steel yielding). The ultimate load obtained SAFRAME is 84 kN/m.

The bottom-tier results suggest that beam section failure controls the ultimate load of the frame. The comparison ratio $w_{bot}(ult.)/w_{top}(ult.)$ for the frame based on the bottom-tier method is 0.57.

Table 7.10: Ratio $w_{bot}(ult.)/w_{top}(ult.)$ for multi-storey frame MULTI1

Method	Beam failure w(kN/m)	Coln failure w(kN/m)	Ultimate Load w(kN/m)	Comparison Ratio $w_{bot}(ult.)/w_{top}(ult.)$
Top-tier	–	–	84.1	–
Bottom-tier	47.9	88.0	47.9	0.57

Results obtained for the frame for design strength determination are sum-

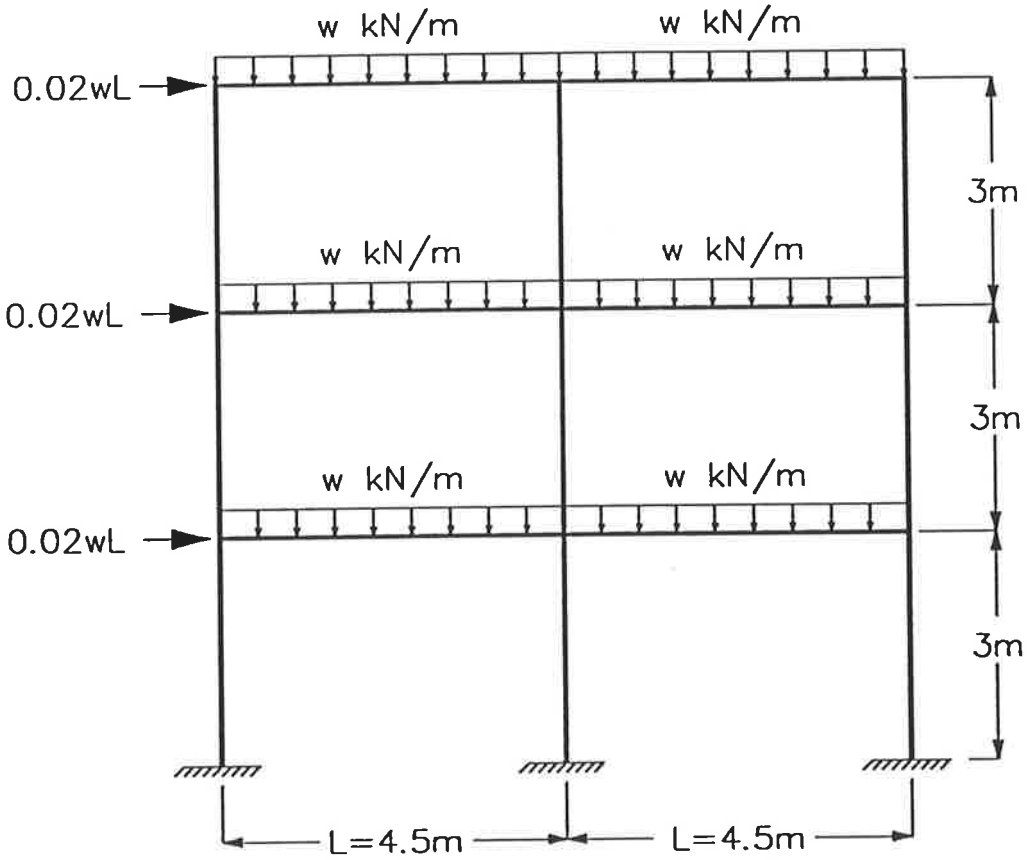

ALL COLUMNS: 300mm x 300mm with 0.02BH reinforcement

BEAMS: MULTI1– 300mm x 300mm with 0.02BH reinforcement

MULTI2– 300mm x 300mm with 0.04BH reinforcement

Figure 7.8: Configuration of multi-storey frame analysed

marised in Table 7.11. The bottom-tier results suggest that beam section failure controls the design load of the frame. The comparison ratio $w_{bot}(des.)/w_{top}(des.)$ for the frame based on the bottom-tier method is 0.57.

Table 7.11: Ratio $w_{bot}(des.)/w_{top}(des.)$ for multi-storey frame MULTI1

Method	Beam failure w(kN/m)	Coln failure w(kN/m)	Design Load w(kN/m)	Comparison Ratio $w_{bot}(des.)/w_{top}(des.)$
Top-tier	–	–	58.7 (for $\phi = 0.8$)	–
Bottom-tier	33.3 (ϕ=0.8)	63.3 (ϕ=0.77)	33.3 ($\phi = 0.8$)	0.57

Another multi-storey frame with the same frame geometry as that of frame MULTI1 is also analysed. This frame is the same as frame MULTI1, except that the amount of beam reinforcement is increased from two per cent to four per cent. Slenderness ratio l/r calculated for the columns based on AS3600, as for MULTI1, ranges from 38 to 61 because reinforcement in the beams is not considered in calculating the effective length, l. As the bottom-tier method uses gross concrete section properties of beams in the analysis/design of columns in a frame, the column failure load for the frame is the same as that obtained for frame MULTI1. The beam section failure load for the frame are larger than that of MULTI1, reflecting the doubling of the amount of beam reinforcement.

Results obtained for ultimate strength determination are summarised in Table 7.12. The beam section failure load is 98 kN/m. An estimate of the beam plastic collapse mechanism gives a failure load of about 131 kN/m (assuming the beam to be fixed at both ends, and the plastic capacity of sections calculated based only on the steel yielding). This estimate is close to the ultimate

load of approximately 146 kN/m obtained from the top-tier analysis. The bottom-tier result suggests that column failure now controls the ultimate load of the frame, instead of beam section failure in FRAME1. The comparison ratio $w_{bot}(ult.)/w_{top}(ult.)$ for the frame based on the bottom-tier method is 0.60.

Table 7.12: Ratio $w_{bot}(ult.)/w_{top}(ult.)$ for multi-storey frame MULTI2

Method	Beam failure w(kN/m)	Coln failure w(kN/m)	Ultimate Load w(kN/m)	Comparison Ratio $w_{bot}(ult.)/w_{top}(ult.)$
Top-tier	–	–	146.0	–
Bottom-tier	98.0	88.0	88.0	0.60

Results obtained for design strength determination are summarised in Table 7.13. The bottom-tier results suggest that beam section failure controls the design load of the frame. The load of the frame based on column failure is only slightly higher than that based on beam section failure. The comparison ratio $w_{bot}(des.)/w_{top}(des.)$ for the frame based on the bottom-tier method is 0.54.

Results obtained for the two multi-storey frames analysed indicate that for frames of practical proportions, the moment magnifier method gives very conservative estimates of both ultimate and design loads.

7.6 Summary and Conclusions

A suite of computer programs has been developed to carry out the determination of design and ultimate strengths based on the moment magnifier method.

Table 7.13: Ratio $w_{bot}(des.)/w_{top}(des.)$ for multi-storey frame MULTI2

Method	Beam failure w(kN/m)	Coln failure w(kN/m)	Design Load w(kN/m)	Comparison Ratio $w_{bot}(des.)/w_{top}(des.)$
Top-tier	–	–	102.0 (for $\phi = 0.8$)	–
Bottom-tier	62.8 (ϕ=0.8)	63.3 (ϕ=0.77)	62.8 $\phi = 0.8$	0.62

An equation has been derived that enables loading curves incorporating the storey magnifier δ_s to be obtained.

Analyses of 144 unbraced portal frames were carried out using the bottom-tier (moment magnifier) method, and results obtained were compared with results obtained from the top-tier method. 36 braced portal frames and two multi-storey frames of practical proportion were also analysed.

From the results obtained, the following conclusions can be drawn:

1. The failure surfaces of the strength versus the quantity of beam reinforcement plots obtained from the bottom-tier method have generally similar shapes as those obtained from the more accurate top-tier method. This indicates that the beam-failure column-failure combination model used to obtain the strength of frames for the bottom-tier method does give a fair, if oversimplified, representation of the behaviour of the frames analysed.
2. It has been found that the moment magnifier method when used to predict ultimate load could not model the complicated, interactive

behaviour between material and geometrical nonlinearities, resulting from the P-Δ introduced into the columns by the movement of loaded joints. This caused over-estimation of the ultimate strength for such frames.

3. The bottom-tier method, when used to estimate the ultimate load of frames, was found to be unconservative for frames likely to fail by loss of stability arising from movement of loaded joints. Thus, unconservative estimates of ultimate strength are likely to occur in vertical columns carrying large axial forces with relatively small first-order end moments. Such columns, as pointed out earlier in this chapter, are likely to be those in the lower floors of a multi-storey building.

4. The bottom-tier method was found to be conservative when the design standard requirement that δ_s be less than or equal to 1.5 is applied. Though this requirement succeeded in preventing the 11 frames with non conservative estimates of design loads to be designed using this method, it also prohibits 27 frames which give conservative estimates of design load. Of the 144 unbraced portal frames analysed, only 106 satisfy this requirement. According to the design standard, those frames that do not satisfy this requirement cannot be designed using the simplified moment magnifier method. This implies that either larger sections must be used, or the top-tier method must be applied.

5. Results obtained for the the limited number of braced frames analysed suggest that the moment magnifier method is conservative in estimating both the design and ultimate loads.

6. Results obtained for the two multi-storey frames suggest that the moment magnifier method is very conservative when applied to multi-storey frames of practical proportions. Comparison ratios of 0.57 and 0.62 have been obtained for design strength estimates for

frames MULTI1 and MULTI2 respectively. Corresponding ratios of 0.57 and 0.60 have been obtained for ultimate strength estimates.

Chapter 8

Investigation of the Accuracy of the Middle-Tier Method for the Analysis/Design of Slender Columns

---

8.1 Introduction

As described already in Chapter 7, the Australian Standard AS3600 allows the use of both a bottom-tier and a middle-tier method for the simplified design/analysis of slender frames.

In this chapter, the middle-tier method is described, and the accuracy of this method in the determination of ultimate and design loads of slender frames investigated.

8.2 Middle-Tier Method

The middle-tier method requires second order elastic analysis using computer programs which take into account the P-Δ effect caused by the movement of the joints in a loaded structure.

The material nonlinearity effects are taken into consideration to a certain extent by assuming the EI values of the beam and column sections to be 0.4 and 0.8 respectively of the gross sectional values. These values were first proposed by MacGregor and Hage (1977).

According to AS3600, the maximum moments in the columns are obtained using an analytical technique which allows for the relative movement of the joints of the frames. The moments thus obtained are then magnified by the braced moment magnifier δ_b, in order to allow for deformations within the length of the columns. For design, the column sections have to be able to carry the axial thrusts and moments calculated by second order analysis and magnified by δ_b, for the factored design loads.

Though not specifically stated in AS3600, it can be inferred that the second step of magnifying the moment obtained is not necessary if a complete second-order elastic analysis is carried out. A complete second-order elastic analysis is one which allows for joint displacements and deformations within the length of the members.

In this study of the accuracy of the second-tier method, a complete second-order elastic analysis is used. This analysis includes the P-Δ effect within the members as well as the P-Δ effect caused by the movement of the joints. The nonlinear equilibrium equations derived by Jennings(1968) were used to take account of the geometrical nonlinearity effects. The derivations of these equations are given in Appendix E.

To carry out a design strength determination using this method, the frame is subjected to a "unit" load pattern based on the configuration of the applied load. For increasing value of load (obtained by applying a load factor to the "unit" load pattern), loading curves are obtained for potential failure sections in columns. Note that these loading curves include all geometrical nonlinearity effects. The design strength of the column is obtained by locating the intersection point between the loading curve for the section and the design strength interaction curve of the section. From this strength value, the load factor of the frame is determined. The relationship between the thrust in the column and the applied load is non-linear and therefore a numerical procedure such as linear interpolation (acceptable when carried out between closely space solution points) is used to estimate the load factor corresponding to the intersection point. After obtaining the load factors associated with the intersections points of all the potential failure sections, the lowest value is selected to be the strength of the frame.

The procedure described above is for estimating the strength of a given frame. For design purposes, the full design load is applied to a frame with pre-selected trial sections. The conditions of thrust and moment at the potential failure sections are obtained using the complete second-order elastic analysis and are plotted as points on the design strength interaction diagram for the section. If all the points lie to the left of the design strength interaction curve then the trial sections chosen are safe. If not, the sizes or the amount of reinforcement of the trial sections are adjusted and another cycle of checking is required. Overconservative designs also require adjustment and further cycles of checking.

The middle-tier method has built-in assumptions which affect the accuracy of the prediction of ultimate load. In the middle-tier method, the assumptions of beam EI of 0.4, and the column EI of 0.8 of the gross concrete sections, obviously cannot represent all cases of loading on structures. The EI values

will depends much on the types of loading (e.g. whether it is uniformly distributed load or point load), the amount of thrust acting along the members, the amount of reinforcements, amongst others. This implied assumption that ultimate section strength governs frame failure load also ignores the possibility of system stability failure.

8.2.1 Method of Analysis

A suite of computer programs was developed to facilitate the design and ultimate strength calculations for slender frames based on the middle-tier method. They were used to analyse the frames described in the later part of this chapter. The details of these programs are given in Appendix J.

To obtain the strength of a frame by the middle-tier method, the frame is first analysed using program `NEWTONR`. The Stiffnesses of the beams and columns are assumed to be $0.4E_cI_g$ and $0.8E_cI_g$, where E_c is the mean modulus of elasticity of concrete and I_g is the moment of inertia of the gross concrete section. Program `NEWTONR` allows the user to nominate the ends of elements for which files with N, M, P values are created (P here represents the factor applied to the unit pattern load acting on the frame to give the total load). The ends of the elements used in the second-order analysis are positioned to coincide with potential failure sections. Program `NEWTONR` generates a few output files: The major output file, which has a name with suffix "out", consists of the complete output information of the frames including forces and deformations of all the elements. The others, which have file names with a suffix "nmc", consist of the N-M-P information of the potential failure sections. For a sway frame, these sections are usually at the ends of the columns.

Intersection points between the strength interaction curves of the sections and their respective loading curves are then obtained. The N value at the inter-

action point, $N_{intersect}$ for each of the loading curves is obtained and based on this, the corresponding load factor of the frame is calculated. As the analysis of the frame is non-linear, the relationship between the thrust N of a column and the load factor P of the frame is non-linear; therefore, P at the intersection point is determined from the results obtained from the second-order elastic analysis. To obtain P at the intersection, a non-linear curve should be fitted to the N-P solution points, and the P value corresponds to the $N_{intersect}$, $P_{intersect}$, is read off the curve. However, a good estimate of the $P_{intersect}$ can be obtained by using a curve with straight lines joining adjacent solution points, provided that the adjacent solution points are not too far apart. The load factors of the frame at the intersection points are automatically determined by program `INTERSECM`. The lowest value of P is chosen as the strength of the frame. The output results from program `INTERSECM` are stored in files with a suffix of "met".

8.3 Unbraced Portal Frames Analyses

8.3.1 Details of Frames Analysed

The portal frames analysed are the same as those used in Chapter 7. Material properties are also the same as those in Chapter 7.

8.3.2 Accuracy of Ultimate Strength Predictions

Typical results for sets FRAMEB2L and FRAMEA2L (i.e. for 3 m high frames with load configurations B and A respectively, with 2 per cent column reinforcement) are given in Figure 8.1 and Figure 8.2 respectively. In Figure 8.1, the inclined beam failure line intersects the horizontal column failure line at

a beam reinforcement ratio of approximately 2.5 per cent, which corresponds to a tensile steel proportion of 0.015. The rigorous analysis line shows signs of flattening at high beam reinforcement percentages, giving roughly a shape similar to that of the bilinear middle-tier failure line. The comparison ratios, shown in Figure 8.1(a), are consistently conservative, and have values of about 0.6.

The results in Figure 8.2(b) follow a rather different pattern, in that there is little flattening at high values of beam reinforcement. The failure line obtained from the rigorous analysis follows the beam failure line of the middle-tier method much more closely than the column failure line. The middle-tier method seems to under-estimate the frame failure load by a significant amount. The ultimate load drops to almost 0.5 times the rigorous method value at the top end of the beam reinforcement under consideration.

Results for set FRAMEC2T are shown in Figure 8.3. In this instance, the middle-tier method consistently over-estimates the ultimate load capacity. On the other hand, the over-estimation does not exceed 20 per cent of the top-tier values. The shape of the middle-tier failure line matches well with that of the rigorous analysis.

The results obtained for the sets of frames with column reinforcement of 2% BH, i.e., for FRAMEA2, FRAMEB2, FRAMEC2, and FRAMED2 are summarised in Table 8.1 and those for the sets of frames with column reinforcement of 4% BH, i.e., for FRAMEA4, FRAMEB4, FRAMEC4 and FRAMED4 are summarised in Table 8.2. Histograms of the ratio of $P_{mid}(ult.)/P_{top}(ult.)$ (or $w_{mid}(ult.)/w_{top}(ult.)$) are given in Figure 8.4. Comparisons between these plots with those obtained for the bottom-tier method shown in Figure 7.4 indicate that 11.8 % of the frames have comparison ratio greater than unity in the middle-tier method as compared with 6.3 % in the bottom-tier method. The bottom-tier method gives conservative estimates in more frames than the

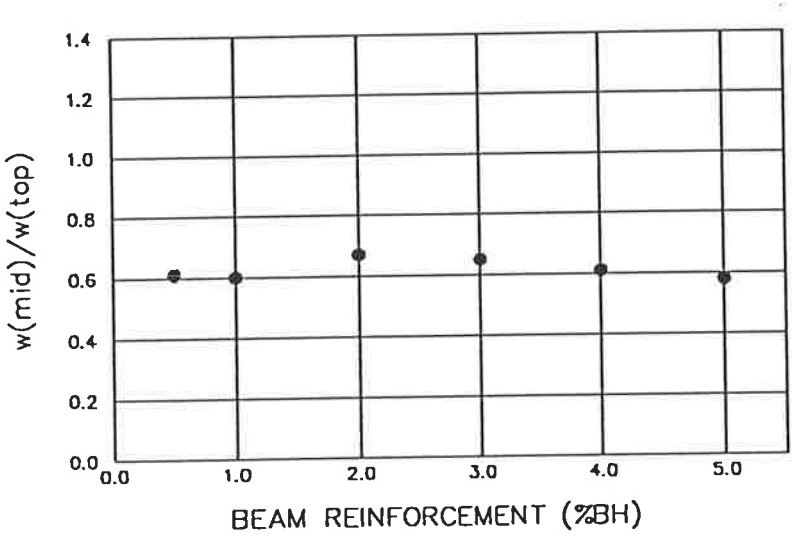

(a)

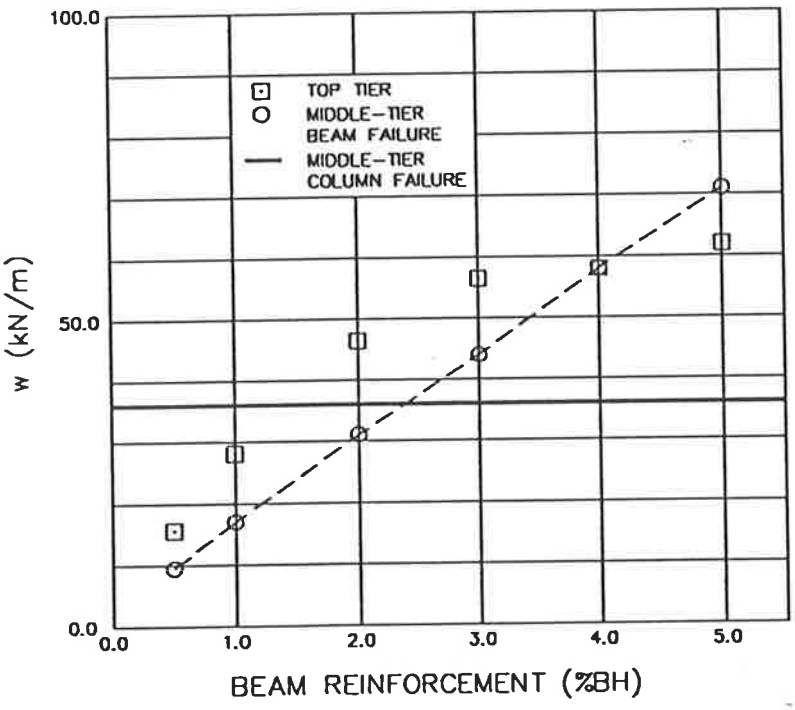

(b)

Figure 8.1: Results for set FRAMEB2L

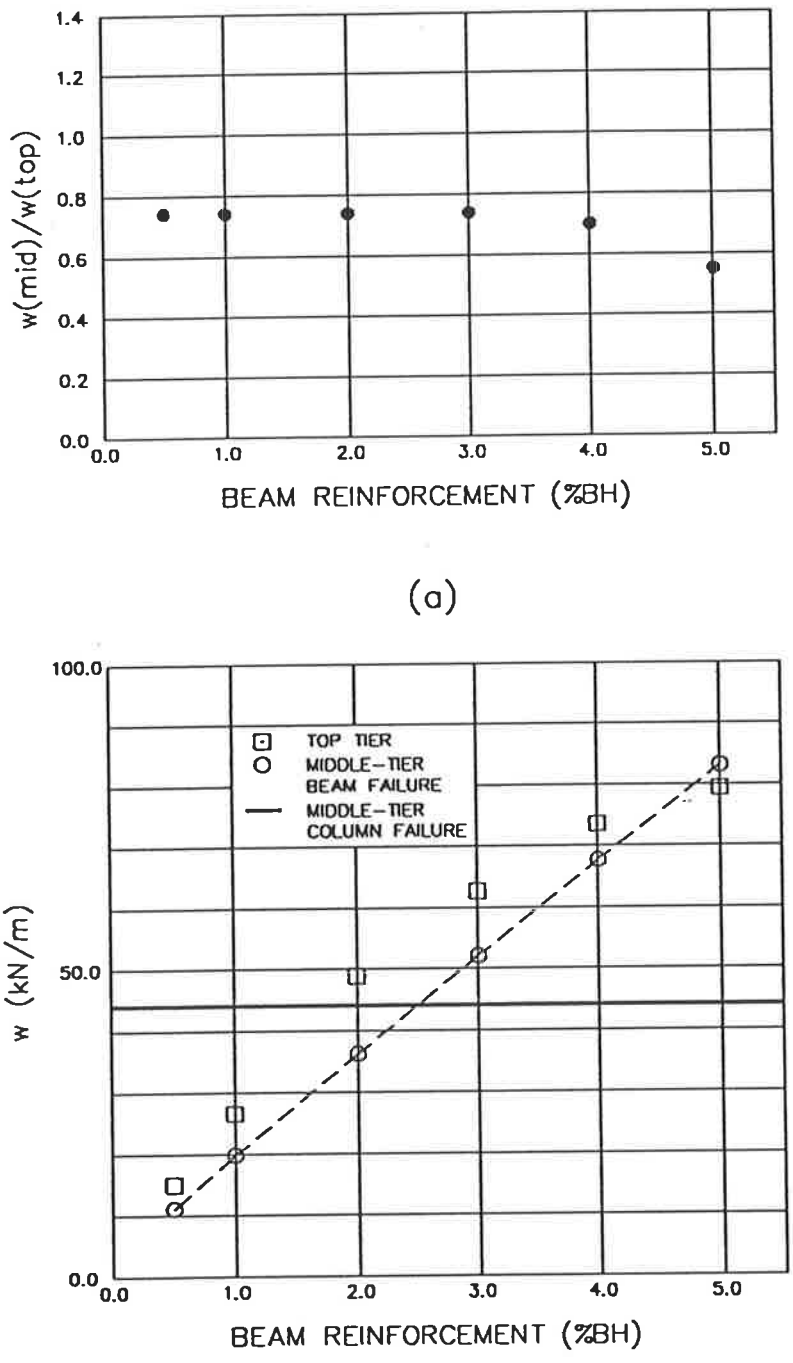

Figure 8.2: Results for set FRAMEA2L

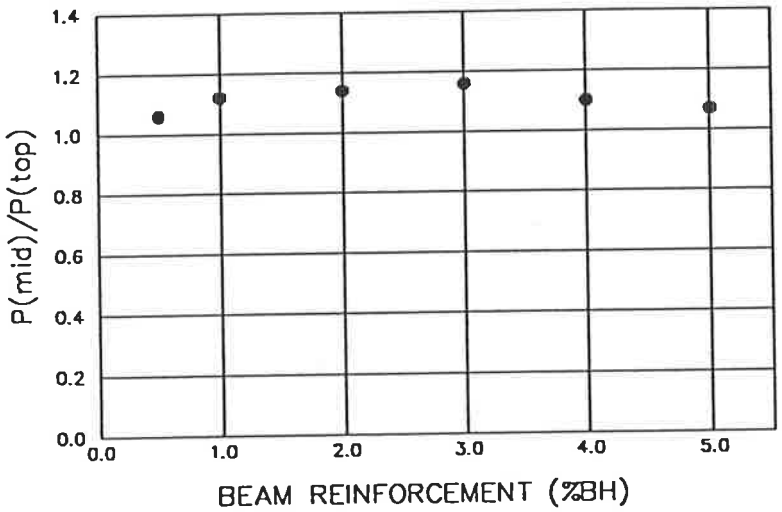

(a)

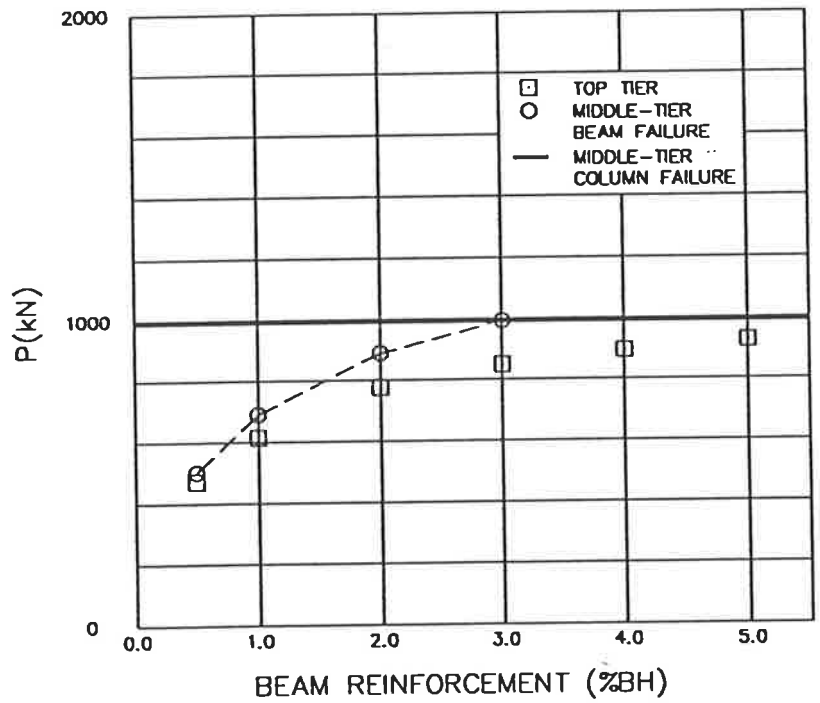

(b)

Figure 8.3: Results for set FRAMEC2T

middle-tier method.

The histograms indicate that out of the 144 frames analysed, 83 frames have ultimate strength controlled by beam section failure and 61 frames have ultimate strength controlled by column failure in the middle-tier method. The comparison ratio $P_{mid}(ult.)/P_{top}(ult.)$ (or $w_{mid}(ult.)/w_{top}(ult.)$) varies from 0.4 to 1.2 with approximately 79 per cent between 0.6 to 1.0. Frames with the ratio greater than 1.0 are, as in the case of the bottom-tier method, mainly found within the sets FRAMEC2 and FRAMEC4. This again indicates that the middle-tier method may be unconservative in frames with heavily loaded columns where the adjacent beams are lightly loaded and the frames resisting relatively small lateral loads at beam levels.

8.3.3 Accuracy of Design Strength Predictions

To obtain the design strength, the capacity reduction factor ϕ must be included in the analysis of frames based on the middle-tier method. As in the bottom-tier method, a global strength reduction factor equal to the ϕ value obtained for the critical section in the corresponding middle-tier analysis is applied to the load predicted by SAFRAME to give top-tier design load.

The results obtained for the sets of frames with columns having reinforcement of 2% BH, i.e., for FRAMEA2, FRAMEB2, FRAMEC2, and FRAMED2 are summarised in Table 8.3. and those for the sets of frames with columns having reinforcement of 4% BH, i.e., for FRAMEA4, FRAMEB4, FRAMEC4 and FRAMED4 are summarised in Table 8.4.

Histograms of the ratio of $P_{mid}(des.)/P_{top}(des.)$ (or $w_{mid}(des.)/w_{top}(des.)$) are given in Figure 8.5. Comparisons between these plots with those obtained for the bottom-tier method shown in Figure 7.5 indicate that 21.7% of the frames has comparison ratio greater than unity in the middle-tier method as

Table 8.1: Ratio $P_{mid}(ult.)/P_{top}(ult.)$(or $w_{mid}(ult.)/w_{top}(ult.)$) for the frames with column reinforcement of 2% BH

	column height	beam reinforcement (%BH)					
		0.5	1.0	2.0	3.0	4.0	5.0
FRAMEA2	3m	0.74(B)	0.74(B)	0.74(B)	0.70	0.60	0.55
	6m	0.82(B)	0.81(B)	0.82(B)	0.82	0.71	0.62
	9m	0.87(B)	0.87(B)	0.92(B)	0.92	0.78	0.70
FRAMEB2	3m	0.61(B)	0.60(B)	0.67(B)	0.65	0.61	0.58
	6m	0.57(B)	0.63(B)	0.74(B)	0.74	0.70	0.66
	9m	0.53(B)	0.71(B)	0.83(B)	0.85	0.82	0.79
FRAMEC2	3m	1.03(B)	1.08	1.04	1.01	1.00	0.99
	6m	0.91(B)	1.02(B)	1.10(B)	1.03	0.99	0.95
	9m	1.06(B)	1.12(B)	1.14(B)	1.16(B)	1.10	1.07
FRAMED2	3m	0.66(B)	0.94(B)	0.85	0.78	0.75	0.73
	6m	0.42(B)	0.65(B)	0.90(B)	0.97	0.89	0.85
	9m	0.70(B)	0.95(B)	1.01(B)	0.96	0.94	0.93
(B) : middle-tier beam failure							

Table 8.2: Ratio $P_{mid}(ult.)/P_{top}(ult.)$(or $w_{mid}(ult.)/w_{top}(ult.)$) for the frames with column reinforcement of 4% BH

	column height	beam reinforcement (%BH)					
		0.5	1.0	2.0	3.0	4.0	5.0
FRAMEA4	3m	0.65(B)	0.74(B)	0.74(B)	0.74(B)	0.74(B)	0.73
	6m	0.82(B)	0.83(B)	0.81(B)	0.82(B)	0.83(B)	0.88(B)
	9m	0.87(B)	0.84(B)	0.89(B)	0.90(B)	0.91(B)	0.98(B)
FRAMEB4	3m	0.60(B)	0.60(B)	0.62(B)	0.63(B)	0.64	0.62
	6m	0.55(B)	0.54(B)	0.63(B)	0.69(B)	0.73(B)	0.79
	9m	0.46(B)	0.56(B)	0.68(B)	0.73(B)	0.80(B)	0.85
FRAMEC4	3m	0.86(B)	1.09	1.04	1.02	0.95	0.99
	6m	0.80(B)	0.91(B)	0.94(B)	0.97(B)	0.91	0.87
	9m	0.91(B)	0.96(B)	0.95(B)	0.96(B)	0.99	0.95
FRAMED4	3m	0.43(B)	0.65(B)	1.00(B)	0.89	0.86	0.84
	6m	0.67(B)	0.92(B)	0.94	0.86	0.84	0.82
	9m	0.46(B)	0.71(B)	0.93(B)	0.99(B)	0.84	0.73
(B) : middle-tier beam failure							

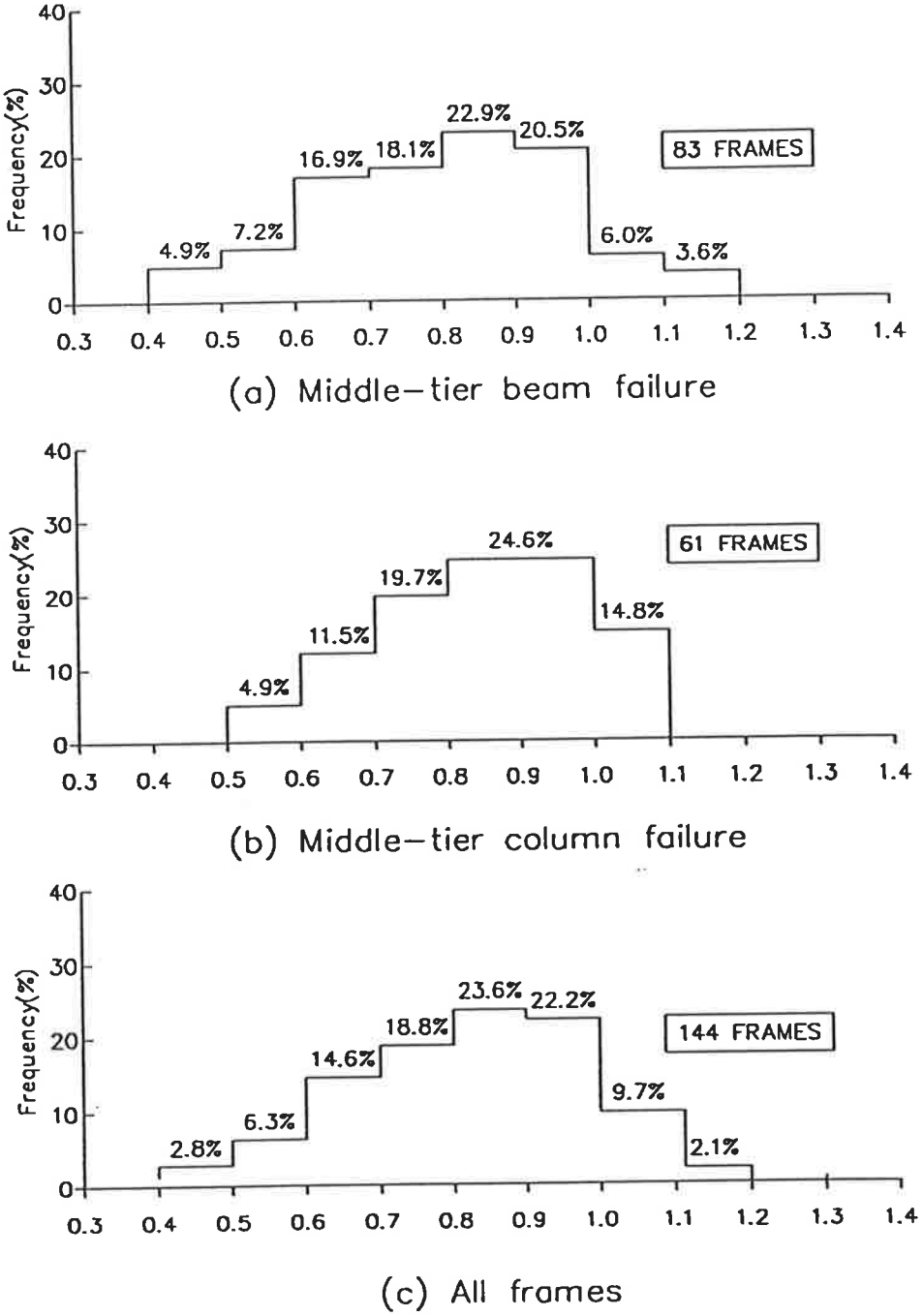

Figure 8.4: Histograms for middle-tier (ultimate strength)

compared with 9.1% in the bottom-tier method, the requirement of $\delta_s \leq 1.5$ of the latter method not being taken into consideration. This suggests that the bottom-tier method is a better design method than the middle-tier method.

Out of the 144 frames analysed, 75 frames have design strength controlled by beam section failure and 69 frames have design strength controlled by column section failure in the middle-tier method. The comparison ratio $P_{mid}(des.)/P_{top}(des.)$ (or $w_{mid}(des.)/w_{top}(des.)$) varies from 0.3 to 1.6 with 73 per cent between 0.5 to 1.0. Frames with the ratio greater than 1.0 are, as in the case of the bottom-tier method, mainly found within the sets FRAMEC2 and FRAMEC4. This also indicates that the use of the bottom-tier method to estimate design strength could be unconservative for frames with such loading pattern, i.e., with large vertical loads above the column with a relatively small horizontal load.

The use of a global strength reduction factor equal to the strength reduction factor of the critical section gives conservative results for a vast majority of the frames. The results obtained indicate that 21.7 per cent of the frames have comparison ratios greater than 1.0, which may be of concern, especially when this ratio may be as large as 1.60 (see Table 8.3).

In contrast to the bottom-tier method when used to determine design strength, whereby frames with loading pattern of types FRAMEC2 and FRAMEC4 are prevented from being designed using this method by the requirement of $\delta_s \leq 1.5$, there is no such requirement in the middle-tier method. This results in the possibility of unconservative designs when using the middle-tier method.

Table 8.3: Ratio $P_{mid}(des.)/P_{top}(des.)$ (or $w_{mid}(des.)/w_{top}(des.)$) for the frames with column reinforcement of 2% BH

	frame ht		beam reinforcement (%BH)					
			0.5	1.0	2.0	3.0	4.0	5.0
FRAMEA2	3m	ratio	0.73(B)	0.74(B)	0.74(B)	0.64	0.55	0.49
		ϕ	0.80	0.79	0.79	0.77	0.77	0.77
	6m	ratio	0.82(B)	0.80(B)	0.81(B)	0.73	0.66	0.58
		ϕ	0.80	0.80	0.80	0.76	0.76	0.76
	9m	ratio	0.87(B)	0.86(B)	0.87(B)	0.86	0.75	0.65
		ϕ	0.80	0.80	0.80	0.76	0.76	0.76
FRAMEB2	3m	ratio	0.60(B)	0.59(B)	0.66(B)	0.60	0.56	0.53
		ϕ	0.80	0.80	0.79	0.77	0.77	0.77
	6m	ratio	0.56(B)	0.63(B)	0.74(B)	0.70	0.64	0.62
		ϕ	0.80	0.80	0.80	0.77	0.77	0.77
	9m	ratio	0.52(B)	0.69(B)	0.81(B)	0.79	0.76	0.75
		ϕ	0.80	0.80	0.80	0.78	0.78	0.78
FRAMEC2	3m	ratio	1.09(B)	1.60	1.53	1.50	1.47	1.46
		ϕ	0.80	0.60	0.60	0.60	0.60	0.60
	6m	ratio	0.93(B)	1.11(B)	1.50	1.39	1.34	1.31
		ϕ	0.80	0.80	0.60	0.60	0.60	0.60
	9m	ratio	1.12(B)	1.25(B)	1.27(B)	1.47	1.45	1.40
		ϕ	0.80	0.80	0.80	0.64	0.64	0.64
FRAMED2	3m	ratio	0.62(B)	0.96	0.75	0.69	0.66	0.64
		ϕ	0.79	0.72	0.72	0.72	0.72	0.72
	6m	ratio	0.66(B)	0.92(B)	0.91	0.83	0.80	0.79
		ϕ	0.80	0.80	0.76	0.76	0.76	0.76
	9m	ratio	0.69(B)	0.95(B)	0.99	0.93	0.91	0.90
		ϕ	0.80	0.80	0.78	0.78	0.78	0.78
(B): middle-tier beam failure								

Table 8.4: Ratio $P_{mid}(des.)/P_{top}(des.)$ (or $w_{mid}(des.)/w_{top}(des.)$) for the frames with column reinforcement of 4% BH

	frame ht		beam reinforcement (%BH)					
			0.5	1.0	2.0	3.0	4.0	5.0
FRAMEA4	3m	ratio	0.72(B)	0.74(B)	0.74(B)	0.73(B)	0.73(B)	0.81
		ϕ	0.80	0.79	0.79	0.79	0.79	0.74
	6m	ratio	0.83(B)	0.80(B)	0.80(B)	0.81(B)	0.83(B)	0.84
		ϕ	0.80	0.80	0.80	0.79	0.79	0.73
	9m	ratio	0.87(B)	0.86(B)	0.87(B)	0.90(B)	0.91(B)	0.94
		ϕ	0.80	0.80	0.80	0.80	0.80	0.73
FRAMEB4	3m	ratio	0.59(B)	0.59(B)	0.59(B)	0.62(B)	0.66(B)	0.69
		ϕ	0.80	0.80	0.79	0.79	0.78	0.75
	6m	ratio	0.55(B)	0.54(B)	0.61(B)	0.68(B)	0.72(B)	0.75
		ϕ	0.80	0.80	0.80	0.79	0.79	0.75
	9m	ratio	0.48(B)	0.53(B)	0.68(B)	0.74(B)	0.81(B)	0.83
		ϕ	0.80	0.80	0.80	0.80	0.79	0.76
FRAMEC4	3m	ratio	0.91(B)	1.59	1.54	1.46	1.46	1.45
		ϕ	0.80	0.60	0.60	0.60	0.60	0.60
	6m	ratio	0.83(B)	0.97(B)	1.04(B)	1.33	1.28	1.25
		ϕ	0.80	0.80	0.80	0.60	0.60	0.60
	9m	ratio	0.95(B)	1.05(B)	0.95(B)	1.09(B)	1.38	1.34
		ϕ	0.80	0.80	0.80	0.80	0.62	0.62
FRAMED4	3m	ratio	0.39(B)	0.66(B)	0.95	0.87	0.84	0.82
		ϕ	0.79	0.79	0.68	0.68	0.68	0.68
	6m	ratio	0.34(B)	0.63(B)	0.90(B)	0.95	0.87	0.83
		ϕ	0.80	0.80	0.79	0.74	0.74	0.74
	9m	ratio	0.45(B)	0.70(B)	0.92(B)	1.03	0.94	0.92
		ϕ	0.80	0.80	0.80	0.76	0.76	0.76
(B): middle-tier beam failure								

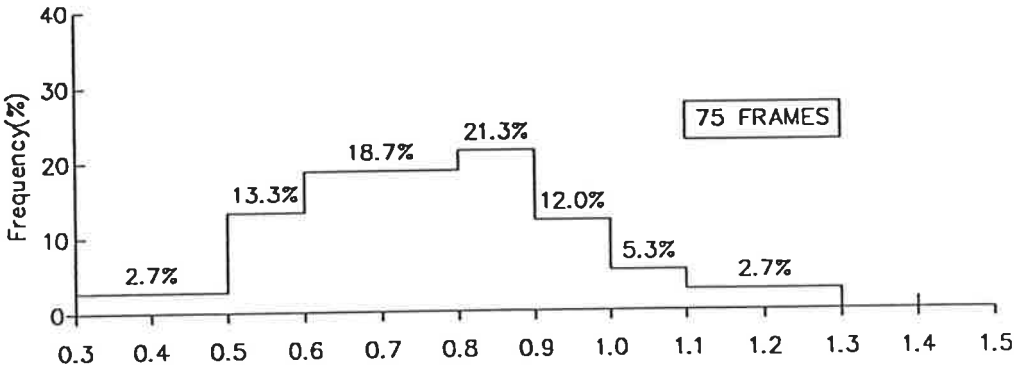

(a) Middle–tier beam failure

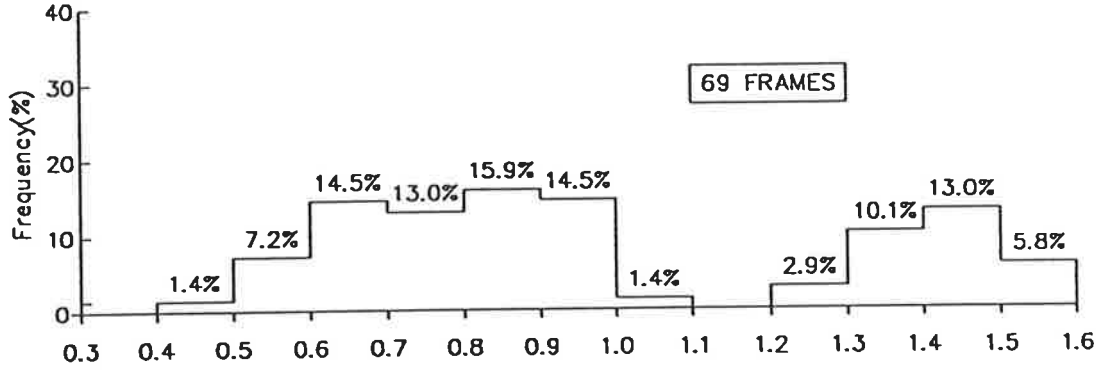

(b) Middle–tier column failure

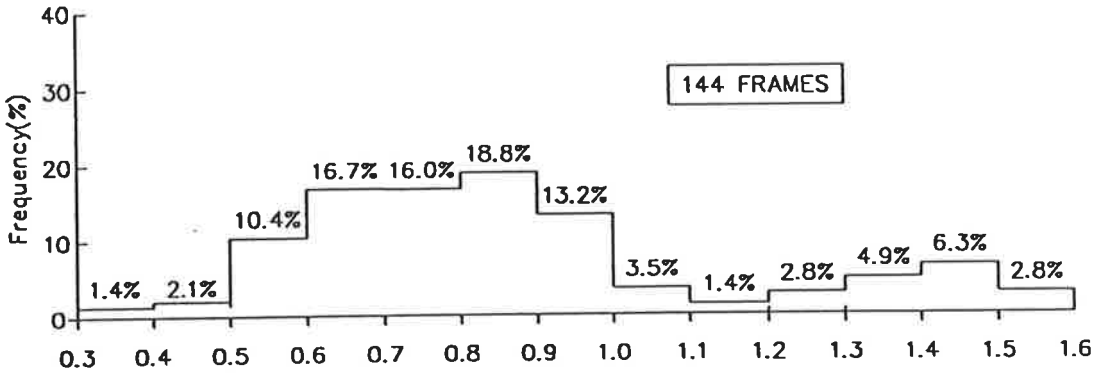

(c) All frames

Figure 8.5: Histograms for middle-tier (design strength)

8.4 Braced Portal Frames

8.4.1 Details of Frames Analysed

A total of 36 braced portal frames are analysed. These frames are the same as those analysed in Chapter 7.

Comparison ratios $w_{mid}(ult.)/w_{top}(ult.)$ for the frames are summarised in Table 8.5. Of the 36 frames analysed, only 8 frames have column failures. The comparison ratio for the frames ranges from 0.55 to 0.98. This indicates that the second-tier estimates for ultimate loads are conservative for the braced frames analysed.

Table 8.5: Ratio $w_{mid}(ult.)/w_{top}(ult.)$ for braced frames

	frame	beam reinforcement (%BH)					
	height	0.5	1.0	2.0	3.0	4.0	5.0
FRAMEE2	3m	0.79(B)	0.78(B)	0.78(B)	0.72	0.62	0.55
	6m	0.96(B)	0.87(B)	0.85(B)	0.85(B)	0.72	0.63
	9m	0.90(B)	0.88(B)	0.87(B)	0.98(B)	0.86	0.75
FRAMEE4	3m	0.79(B)	0.78(B)	0.76(B)	0.75(B)	0.76(B)	0.77
	6m	0.89(B)	0.87(B)	0.85(B)	0.84(B)	0.84(B)	0.90(B)
	9m	0.91(B)	0.88(B)	0.86(B)	0.86(B)	0.86(B)	0.91(B)
(B) : middle-tier beam failure							

Comparison ratios $w_{mid}(des.)/w_{top}(des.)$ for the frames are summarised in Table 8.6. Of the 36 frames analysed, only 11 frames have column failures. The comparison ratio for the frames ranges from 0.51 to 0.92. This indicates that the determination of design loads using the middle-tier method is conservative for the braced frames analysed.

Table 8.6: Ratio $w_{mid}(des.)/w_{top}(des.)$ for braced frames

	frame ht		beam reinforcement (%BH)					
			0.5	1.0	2.0	3.0	4.0	5.0
FRAMEE2	3m	ratio	0.76(B)	0.77(B)	0.77(B)	0.68	0.58	0.51
		ϕ	0.80	0.80	0.79	0.76	0.76	0.76
	6m	ratio	0.96(B)	0.86(B)	0.84(B)	0.79	0.67	0.58
		ϕ	0.80	0.80	0.80	0.76	0.76	0.76
	9m	ratio	0.88(B)	0.87(B)	0.84(B)	0.92	0.80	0.73
		ϕ	0.80	0.80	0.80	0.76	0.76	0.76
FRAMEE4	3m	ratio	0.80(B)	0.76(B)	0.77(B)	0.74(B)	0.76(B)	0.74
		ϕ	0.80	0.80	0.79	0.79	0.79	0.74
	6m	ratio	0.88(B)	0.86(B)	0.84(B)	0.83(B)	0.84(B)	0.86
		ϕ	0.80	0.80	0.80	0.80	0.79	0.73
	9m	ratio	0.88(B)	0.86(B)	0.85(B)	0.82(B)	0.84(B)	0.85(B)
		ϕ	0.80	0.80	0.80	0.79	0.79	0.74
(B): middle-tier beam failure								

8.5 Three-storey Two-bay Frames

Multi-storey frames MULTI1 and MULTI2 analysed using the moment-magnifier method in Chapter 7 are analysed using the middle-tier method. The geometry and material properties of the frames are assumed to the same as those given in Chapter 7.

Results obtained for the ultimate strength analysis of frame MULTI1 are summarised in Table 8.7. The middle-tier results suggest that beam section failure controls the ultimate load of the frame. The comparison ratio $w_{mid}(ult.)/w_{top}(ult.)$ based on the middle-tier method is 0.59.

Table 8.7: Ratio $w_{mid}(ult.)/w_{top}(ult.)$ for multi-storey frame MULTI1

Method	Beam failure w(kN/m)	Coln failure w(kN/m)	Ultimate Load w(kN/m)	Comparison Ratio $w_{mid}(ult.)/w_{top}(ult.)$
Top-tier	–	–	84.1	–
Middle-tier	49.8	79.7	49.8	0.59

Results obtained for the design strength analysis of frame MULTI1 are summarised in Table 8.8. The middle-tier results suggest that beam section failure controls the ultimate load of the frame. The comparison ratio $w_{mid}(des.)/w_{top}(des.)$ based on the middle-tier method is 0.47.

Table 8.8: Ratio $w_{mid}(des.)/w_{top}(des.)$ for multi-storey frame MULTI1

Method	Beam failure w(kN/m)	Coln failure w(kN/m)	Design Load w(kN/m)	Comparison Ratio $w_{mid}(des.)/w_{top}(des.)$
Top-tier	–	–	58.7 (for $\phi = 0.80$)	–
Middle-tier	27.7 (ϕ=0.80)	44.3 (ϕ=0.78)	27.7 ($\phi = 0.80$)	0.47

Results obtained for ultimate strength analysis of frame MULTI2 are summarised in Table 8.9. The middle-tier result suggests that column failure now controls the ultimate load of the frame, instead of beam section failure control in FRAME1. The middle-tier result still suggests that beam section failure controls the ultimate load of the frame. The comparison ratio $w_{mid}(ult.)/w_{top}(ult.)$

based on the middle-tier method is 0.51.

Table 8.9: Ratio $w_{mid}(ult.)/w_{top}(ult.)$ for multi-storey frame MULTI2

Method	Beam failure w(kN/m)	Coln failure w(kN/m)	Ultimate Load w(kN/m)	Comparison Ratio $w_{mid}(ult.)/w_{top}(ult.)$
Top-tier	–	–	146.0	–
Middle-tier	74.1	79.7	74.1	0.51

Results obtained for design strength analysis of frame MULTI2 are summarised in Table 8.10. The middle-tier result suggests that column failure controls the design load of the frame, instead of column failure in frame MULTI1. The comparison ratio $w_{mid}(des.)/w_{top}(des.)$ based on the middle-tier method is 0.44.

Table 8.10: Ratio $w_{mid}(des.)/w_{top}(des.)$ for multi-storey frame MULTI2

Method	Beam failure w(kN/m)	Coln failure w(kN/m)	Design Load w(kN/m)	Comparison Ratio $w_{mid}(des.)/w_{top}(des.)$
Top-tier	–	–	99.5 (for $\phi = 0.78$)	–
Bottom-tier	51.8 (ϕ=0.8)	44.3 (ϕ=0.78)	44.3 $\phi = 0.78$	0.44

For MULTI1, the comparison ratio obtained for ultimate load estimate is almost the same as that obtained from the bottom-tier method. The ratio obtained for design load estimate from the bottom-tier method is closer to unity than that obtained from the middle-tier approach. For MULTI2, the ratios for

both design and ultimate load estimates obtained from the bottom-tier method are closer to unity than those obtained from the middle-tier method. This indicates that, for the multi-storey frames, the bottom-tier method, generally, gives better estimation of strength.

8.6 Summary and Conclusions

Analyses of 144 unbraced portal frames were carried out using the middle-tier method, and results obtained were compared with results obtained from parallel top-tier (rigorous) method. 36 braced portal frames and two multi-storey frames of practical proportion were also analysed.

From the results obtained, the following conclusions can be drawn:

1. The failure surfaces of the strength versus the quantity of beam reinforcement plots obtained from the middle-tier method have generally similar shapes as those obtained from the more accurate top-tier method. This indicates that the beam-failure column-failure combination model used to obtain the strength of frames for the middle-tier method does give a fair representation of the behaviour of the frames analysed.
2. It has been found that the middle-tier method when used to predict ultimate load could not model the complicated, interactive behaviour between material and geometrical nonlinearities, resulting from the P-Δ introduced into the columns caused by the movement of loaded joints. This caused over-estimation of the ultimate strengths for such frames.
3. The middle-tier method also over-estimates the design load of the type of frames described in item 2. Unlike the bottom-tier method, whereby the use of the requirement that δ_s is to be less than or equal

to 1.5 prevents such frames from being unconservatively designed, no such requirement is imposed on the middle-tier method. This suggests that the middlle-tier method should be used with great care.

4. Comparisons of the bottom-tier and middle-tier methods indicate that the latter gives unconservative (i.e, comparison ratios greater than unity) estimates for more frames as compared with the other method. This suggests that the bottom-tier approach is a safer design method.

5. Results obtained from the limited number of braced frames analysed indicates that the middle-tier method is conservative in estimating both the design and ultimate loads.

6. Results obtained for the two multi-storey frames suggest that the middle-tier method is very conservative when applied to multi-storey frames of practical proportions. Comparison ratios of 0.47 and 0.44 have been obtained for design strength estimates for frames MULTI1 and MULTI2 respectively. Corresponding ratios of 0.59 and 0.51 have been obtained for ultimate strength estimates. The results obtained also indicates that, generally, the bottom-tier method gives better estimation of strength.

Chapter 9

Conclusions and Recommendations

9.1 Conclusions

This study of the non-linear behaviour of reinforced concrete slender frames has concentrated on two major areas, i.e., the non-linear behaviour of these frames and the accuracy of simplified code methods for predicting ultimate and design loads of such frames. The major contributions in these areas are listed below:

1. A computer program SAFRAME has been developed to study the non-linear behaviour of reinforced concrete frames. The program takes into consideration both the short-term material nonlinearities and the geometrical nonlinearities. It has the ability to predict the softening behaviour beyond the peak load with the use of a deformation-control tech-

nique whereby the curvature of a key segment is chosen as the controlling parameter during the analysis. The computational technique is efficient as the structure is modelled using segmented elements, thus reducing both the number of elements required to model the material nonlinearity effects and the size of the global stiffness matrix of the frame.

2. The accuracy of the computer program SAFRAME has been checked by comparing results obtained with experimental results obtained for some test structures. Comparison with results obtained using other analytical methods has also been carried out. Generally the accuracy of the results obtained from the present analysis is reasonable. Nevertheless, there is a need for further "tuning" of the program to provide better correlation with available test data. Indeed an extensive study of all available frame and beam test data is needed as a basis for program optimisation. One specific area where program improvement can be effected is in the treatment of tension stiffening. The inclusion of tension stiffening for all segments, particularly those at overload but not at the condition of hingeing, should improve the accuracy of SAFRAME.

3. Snapback instability behaviour has occasionally been observed in some of the portals analysed. Multiple snapback in the characteristic deflections of the portals has not been observed. Most of the portals have only one snapback. Occasionally portals with two snapbacks have been observed: one of these snapbacks occurs in the mid-span vertical deflection of the beam and the other occurs in the sway deflection of the frame at beam level.

4. The case of the double snapbacks mentioned in (3) above suggests the superiority of using the curvature of a key segment as the controlling parameter instead of using characteristic deflection. Using the latter would have resulted in non-convergence of the solution at one of the snapbacks, thus preventing the solution from being taken far enough to

indicate the presence of multiple snapback.

5. The study has shown that softening behaviour in reinforced concrete frames can be caused by geometric instability. A free standing column has been used to illustrate that this can occur even before the formation of a concrete "plastic" hinge or softening hinge.

6. The effect of ignoring the sectional thrust effect on the moment curvature relation of segments has been investigated. It was found that both the calculated sway stiffness and ultimate strength are reduced significantly if the effect of thrust is ignored. It was also observed that the number of concrete "hinges" at collapse is affected by ignoring the thrust effect.

7. A parametric study has been carried out in Chapter 6 on the effect of beam reinforcement on the behaviour of portals. When the amount of beam reinforcement is small, the beam provides little stiffening effect on the frame, thus resulting in the frame failing at low ultimate load. When the reinforcement is increased to an amount greater than about 4 %, there is little increase in the ultimate load of the frame. At this stage, the beam has exerted its maximum stiffening effect on the frame.

8. Computer programs have been developed to assist the predictions of the design and ultimate strengths of frames based on the simplified bottom-tier and middle-tier methods.

9. The bottom-tier or moment-magnifier method, when used to estimate ultimate load, generally gave conservative results for 144 unbraced portal frames. Nevertheless, the moment-magnifier method may be unconservative for frames with heavily loaded columns where the adjacent beams are lightly loaded and the frames resist relatively small lateral loads.

10. A requirement exists in the moment-magnifier method of AS3600 which prevent frames which are likely to fail by instability before section failure from being designed using this method. This requirement is effective in

eliminating those frames which give unconservative estimates, but also got rid of a large proportion of frames which give conservative estimates of design loads. This requirement does not therefore perform its function effectively.

11. The middle-tier method for estimation of design loads was found to give unconservative estimate for frames which are likely to fail by instability, caused by joint displacements. The bottom-tier method, is not applicable to these frames because of the requirement mentioned above in item 10. The absence of such a requirement in the middle-tier method can result in unconservative designs.

12. Comparisons of the bottom-tier and middle-tier methods indicate that the latter gives unconservative (i.e, accuracy ratios greater than unity) estimates for more frames than the former. This suggests that the bottom-tier approach is a safer design method.

13. Frames analysed by the top-tier method mainly failed by instability. The possibility of structures reaching peak loads before sections reaching their peak strength (an example is the cantilevered column analysed in Chapter 6) suggests that using the top-tier method may result in unconservative, and in extreme cases, unsafe design. An alternative and more logical approach of using a global strength reduction factor applied to the peak load determined from a rigorous is proposed.

9.2 Recommendations for Further Research

Further research into the following areas is recommended:

- Improvement to the present program by using more accurate models for materials. More laboratory tests have to be carried out to study the

softening behaviour of concrete.

- Inclusion of tension stiffening effect into SAFRAME should improve the accuracy of SAFRAME.
- Carry out probabilistic studies to determine an "under-performance" factor to be used in conjunction with the rigorous analysis to give design strength of frames analysed using the top-tier method.
- Inclusion of creep and shrinkage effects into the numerical model of SAFRAME to enable long-term behaviour of frames to be studied.

Appendix A

Analytical Moment-Curvature Relationship

For a section with stress and strain diagram shown in Figure A.1, the total compression force C is:

$$C = b\int_0^{kd} f dy \tag{A.1}$$

From the strain diagram:

$$\frac{y}{\epsilon} = \frac{kd}{\epsilon_u} \tag{A.2}$$

Therefore :

$$C = \frac{bkd}{\epsilon_u}\int_0^{\epsilon_u} f de \tag{A.3}$$

The stress-strain curve proposed by Smith and Young (1956) is:

$$f = f_c'\left(\frac{\epsilon}{\epsilon_o}\right)e^{\left(1-\frac{\epsilon}{\epsilon_o}\right)} \tag{A.4}$$

where f_c' is the compression strength of a 150mm × 300mm concrete cylinder and ϵ_o is the concrete strain corresponding to f_c'.

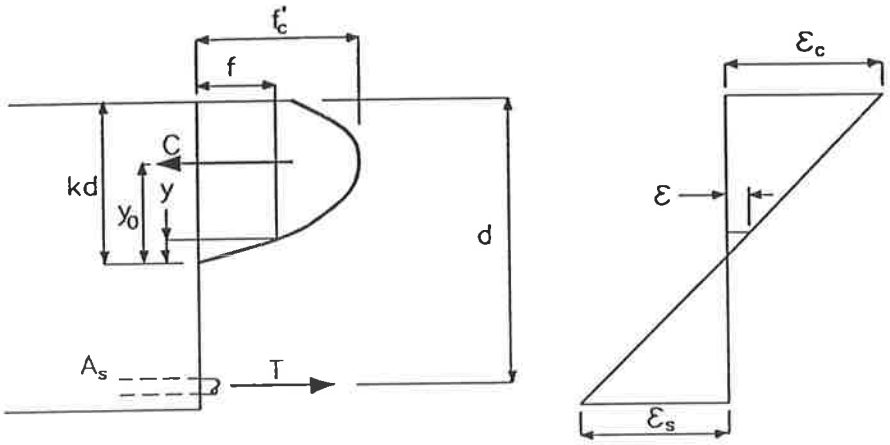

Figure A.1: Stress and strain diagram across section

Substituting f from Equation A.4 and integrating between limits:

$$C = b\ kd\ f'_c e \frac{\epsilon_o}{\epsilon} \left[e^{-\frac{\epsilon_u}{\epsilon_o}} \left(-\frac{\epsilon_u}{\epsilon_o} - 1 \right) + 1 \right] \tag{A.5}$$

where $f'_c e \frac{\epsilon_o}{\epsilon} \left[e^{-\frac{\epsilon_u}{\epsilon_o}} \left(-\frac{\epsilon_u}{\epsilon_o} - 1 \right) + 1 \right]$ is the average stress denoted by f_a.

Equation A.5 may be rewritten as follows:

$$C = b\ kd\ f_a \tag{A.6}$$

Before the ultimate moment can be determined, k_b has to be calculated to determine whether the beam is under-reinforced (failed by yielding before the concrete crushes) or over-reinforced (failed by crushing of concrete before the steel yields). The value of k_b is calculated as follows:

$$\frac{\epsilon_u}{\epsilon_{yp}} = \frac{k_b}{1 - k_b} \tag{A.7}$$

where ϵ_{yp} is the strain in the steel at yield point.

An under-reinforced section has k values less than k_b whereas a over-reinforced section has k values larger than k_b.

For an under-reinforced concrete beam, the steel has yielded and therefore:

$$T = A_s f_{yp} \tag{A.8}$$

where f_{yp} is the yield stress of the steel reinforcement.

For equilibrium:

$$bk_d f_a = A_s f_{yp} \tag{A.9}$$

Substituting $p = A_s/bd$ into Equation A.9:

$$k = \frac{p f_{yp}}{f_a} \tag{A.10}$$

For a over-reinforced concrete section, using similar triangles on the strain diagram:

$$\epsilon_s = \left(\frac{1-k}{k}\right)\epsilon_u \tag{A.11}$$

From equilibrium:

$$C = T = A_s E_s \epsilon_s = A_s E_s \left(\frac{1-k}{k}\right)\epsilon_u \tag{A.12}$$

Equation A.11 and A.12:

$$bk_d f_a = A_s E_s \left(\frac{1-k}{k}\right)\epsilon_u \tag{A.13}$$

Letting

$$p = \frac{A_s}{bd}, \tag{A.14}$$

and simplifying gives:

$$\frac{f_a}{f'_c}k^2 + p\frac{E_s\epsilon_u}{f'_c}k - p\frac{E_s\epsilon_u}{f'_c} = 0 \tag{A.15}$$

Writing $pE_s\epsilon_u/f'_c$ as β, Equation A.15 becomes:

$$\left(\frac{f_a}{f'_c}\right)k^2 + \beta k - \beta = 0 \tag{A.16}$$

Hence k is determined from Equation A.10 or A.16 depending on whether the section is under-reinforced or over-reinforced.

To calculate the ultimate moment, the position of the centroid of the stress block is determined as follows:

$$\frac{y_o}{k_d} = \frac{e^{\frac{\epsilon_u}{\epsilon_o}}\left[-1 - 2\frac{\epsilon_o}{\epsilon_u} - 2\left(\frac{\epsilon_o}{\epsilon_y}\right)^2\right] + 2\left(\frac{\epsilon_o}{\epsilon_y}\right)^2}{\frac{\epsilon_o}{\epsilon}\left[e^{-\frac{\epsilon_u}{\epsilon_o}}\left(-\frac{\epsilon_u}{\epsilon_o} - 1\right) + 1\right]} \tag{A.17}$$

Once y_o is calculated, the ultimate moment is obtained from:

$$M_u = T\left(d - kd + y_o\right) \tag{A.18}$$

Appendix B

Stress-Strain Relationships of Materials including Unloading

The numerical model used in program SAFRAME includes material unloading to allow for the possibility of strain reversal in the concrete and steel layers used to model the sectional behaviour. The shapes of the stress-strain curves of concrete and reinforcing steel are given in Chapter 2. In this appendix, flow diagrams are presented to illustrate the computational steps used to determine the stress-strain relationships of steel and concrete including the effect of strain reversal.

B.1 Steel Unloading

The flow diagram for the determination of steel stress from known strain in a typical steel layer within a computational step is given in Figure B.1.

For each steel layer, two variables are used to record the maximum historical

For each steel layer, two variables are used to record the maximum historical normalised stress and strain, represented by $\bar{f}_s^{max}$ and $\bar{\epsilon}_s^{max}$ respectively in the flow diagram. These values are kept constant at the start of a curvature step, are maintained throughout the entire step, and are then updated at the end of the step when a solution has been obtained for the curvature step. At the start of the analysis $\bar{f}_s^{max}$ and $\bar{\epsilon}_s^{max}$ are each assigned a value of zero.

As described above, the maximum historical normalised stress and strain are updated at the end of each curvature step after a solution has been obtained. This updating for a typical layer is illustrated by the flow diagram in Figure B.2.

B.2 Concrete Unloading

The flow diagram for the determination of normalised concrete stress from a given normalised strain value for a typical concrete layer is given in Figure B.3.

As in the case of the typical steel layer, for each concrete layer, two variables are used to record the maximum historical normalised stress and strain, represented by $\bar{f}_c^{max}$ and $\bar{\epsilon}_c^{max}$ respectively in the flow diagram. These values are kept constant at the start of a curvature step, are maintained throughout the entire step, and are then updated at the end of the step when a solution has been obtained for the curvature step. At the start of the analysis $\bar{f}_c^{max}$ and $\bar{\epsilon}_c^{max}$ are each assign a value of zero.

The maximum historical normalised stress and strain are updated at the end of each curvature step after the solution has been obtained. This updating for a typical layer is illustrated by the flow diagram in Figure B.4.

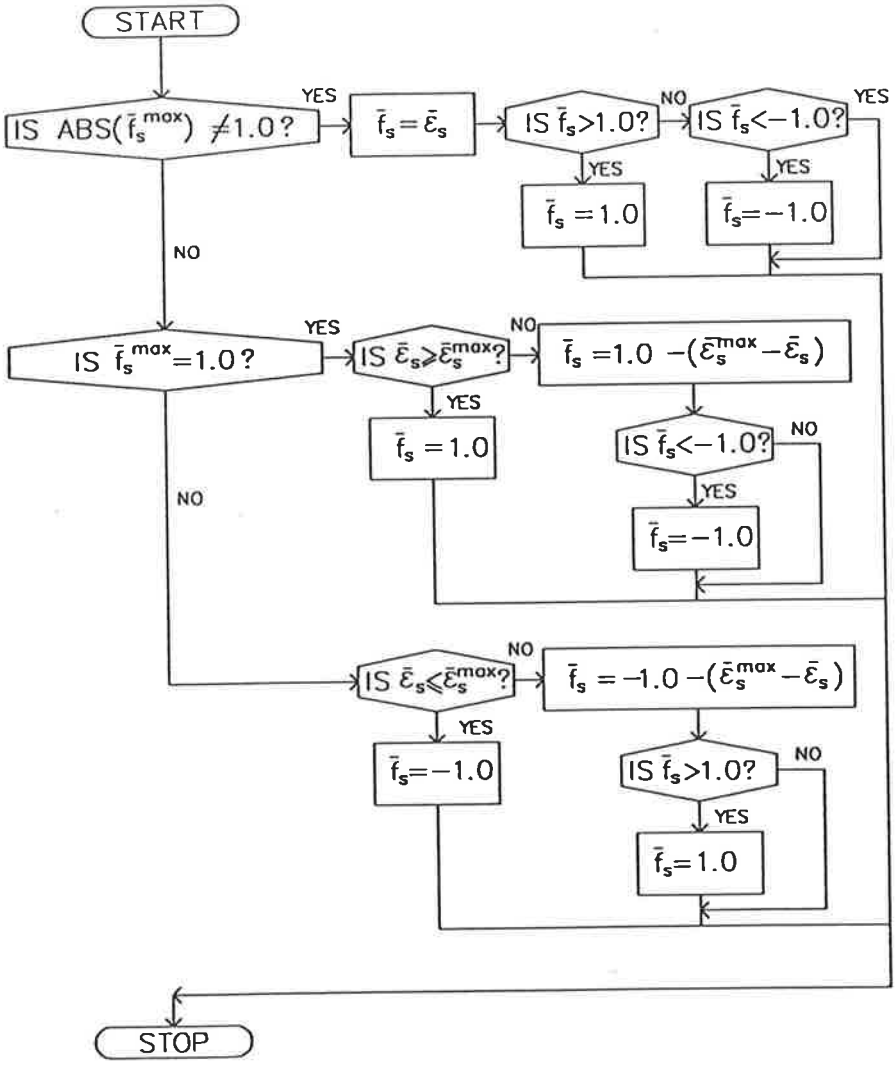

Figure B.1: Flow diagram for the calculation of stress in a typical steel layer within a curvature step

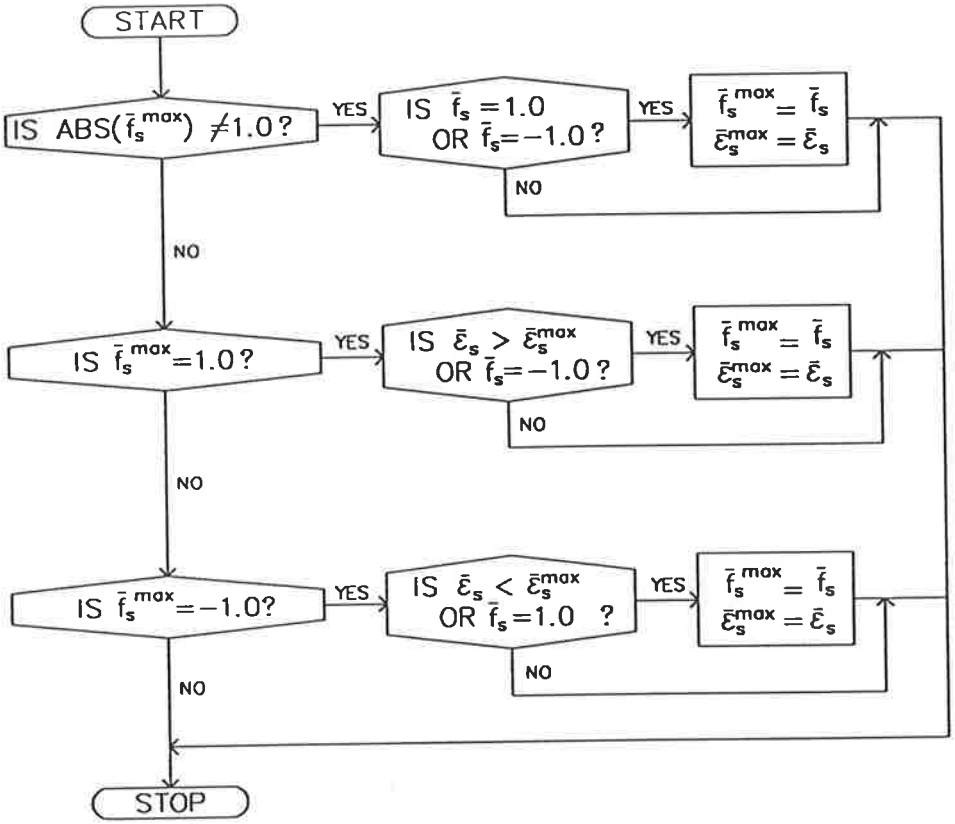

Figure B.2: Flow diagram for the updating of the maximum stress and strain in a typical steel layer at the end of a curvature step

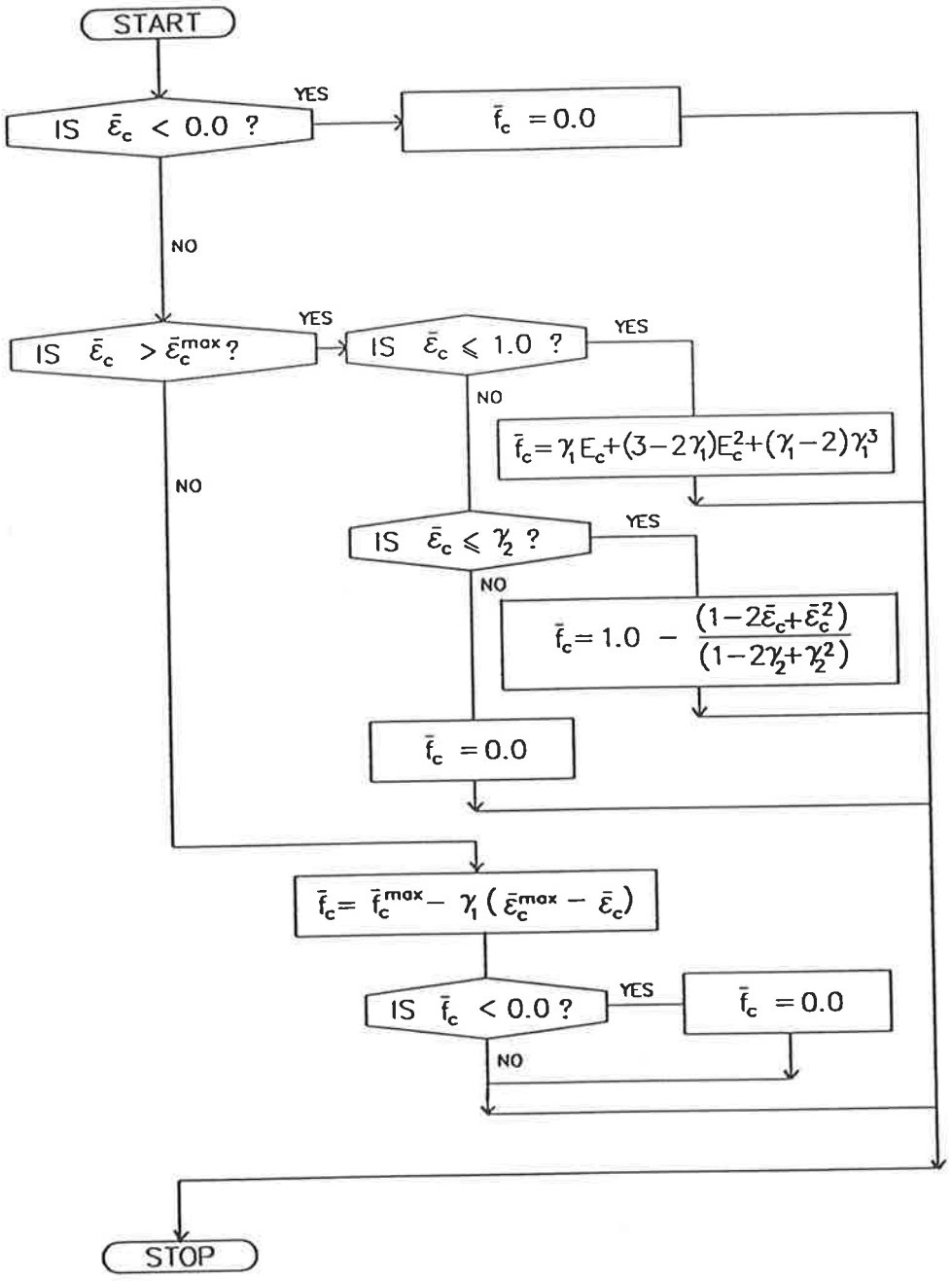

Figure B.3: Flow diagram for the calculation of stress in a typical concrete layer within a curvature step

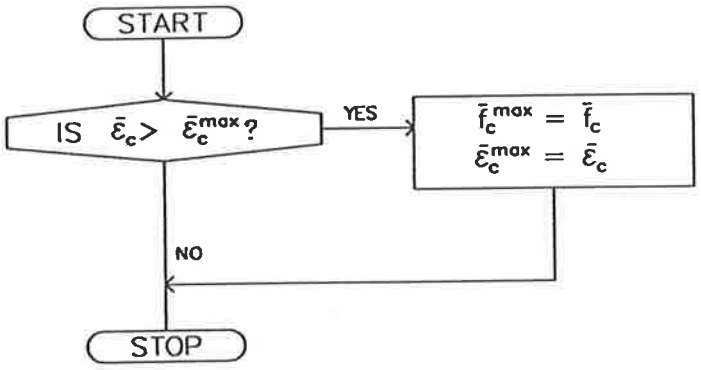

Figure B.4: Flow diagram for the updating of the maximum stress and strain in a typical concrete layer at the end of a curvature step

Appendix C

Layered Element Approach

The modelling of a typical element is shown in Figure C.1.

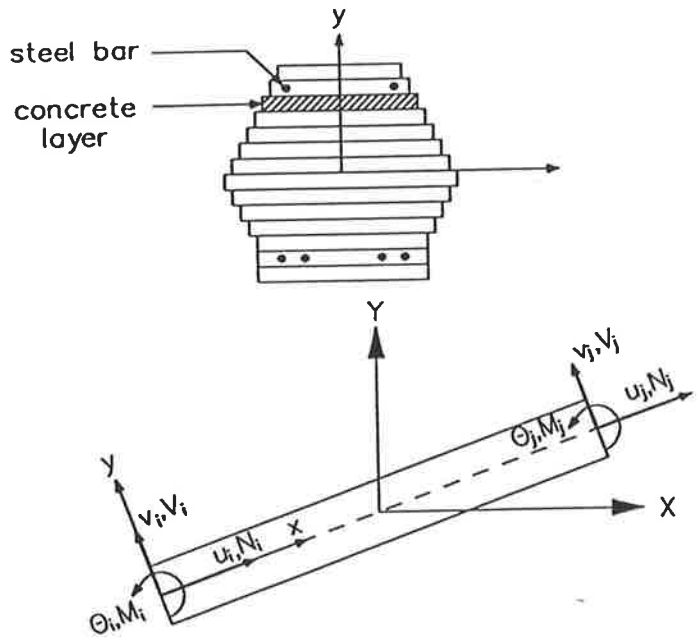

Figure C.1: Layered finite element

Each cross section is divided into N_l layers, some of which may represent the reinforcing bars. The column matrices of element displacements and forces are (see Figure C.1):

$$\mathbf{u} = \begin{Bmatrix} u_i \\ v_i \\ \theta_i \\ u_j \\ v_j \\ \theta_j \end{Bmatrix} \tag{C.1}$$

$$\mathbf{f} = \begin{Bmatrix} N_i \\ V_i \\ M_i \\ N_j \\ V_j \\ M_j \end{Bmatrix} \tag{C.2}$$

where

u is the axial displacement;

v is the transverse displacement;

θ is the rotation of cross section;

and subscripts i and j refer to the cross section i and j at the ends of the element.

The internal forces are referred to the centroidal axis x.

The strain at any point x, y (in cartesian coordinates x, y) is $\epsilon(x,y) = \partial u(x,y)/\partial x$, and the displacement in the axial direction is $u(x,y) = u(x,0) - y\partial v(x,0)/\partial x$. Finite elements with a cubic variation of v are used. For any point on the axis x:

$$u(x,0) = (1-\xi)u_i + \xi u_j \tag{C.3}$$

$$v(x,0) = (1-3\xi^2+2\xi^2)v_i + (3\xi^2-2\xi^3)v_j + \\ +L(\xi-2\xi^2+\xi^3)\theta_i + L(\xi^3-\xi^2)\theta_j \qquad \text{(C.4)}$$

where

ξ $= \frac{x}{L}$; and

L =element length.

Substituting these expressions into $\epsilon(x,y) = \partial u(x,y)/\partial x$ and $u(x,y) = u(x,0) - y\partial v(x,0)/\partial x$, we obtain the geometric relation $\epsilon(x,y) = \mathbf{Bu}$ where

$$\mathbf{B} = \frac{1}{L}\left[\begin{array}{cccccc} -1 & 6\eta(1-2\xi) & 2L\eta(2-3\xi) & 1 & 6\eta(2\xi-1) & 2L\eta(1-3\xi) \end{array}\right] \qquad \text{(C.5)}$$

where

η $= \frac{y}{L}$.

Then applying the virtual work principle to the beam element, we have $\delta\mathbf{u}^T\mathbf{f} = \int_V \delta\epsilon^T\ \sigma dV = \delta\mathbf{u}^T \int_V \mathbf{B}^T\sigma dV$, and since this must hold for an arbitrary variation $\delta\mathbf{u}$, we obtain $\mathbf{f} = \int_v \mathbf{B}^T\sigma dV = \int_V \mathbf{B}^T E_s\mathbf{B}\mathbf{u}dV = \mathbf{k_e u}$, where V = element volume, E_s is the secant modulus ($\sigma = E_s\epsilon$), and $\mathbf{k_e} = \int_V E_s\mathbf{B}^T\mathbf{B}dV$. $\mathbf{k_e}$ is a 6 × 6 element stiffness matrix. Along x, we may integrate analytically and the integral over the cross section area we approximate by a sum over all the layers m =1, ... , N_l. Matrix $\mathbf{k_e}$ must then be tranformed from element coordinates (x,y) to global coordinates; $\mathbf{K_e} = \mathbf{T}^T\mathbf{k_e}\mathbf{T}$ where $\mathbf{T}$ is a 6 × 6 transdormation matrix for coordinate rotation by angle α, which represents the angle between axes X and x. The $\mathbf{T}$ matrix is given below:

$$\mathbf{T} = \left[\begin{array}{cccccc} cos\theta & sin\theta & 0 & 0 & 0 & 0 \\ -sin\theta & cos\theta & 0 & 0 & 0 & 0 \\ 0 & 0 & 1 & 0 & 0 & 0 \\ 0 & 0 & 0 & cos\theta & sin\theta & 0 \\ 0 & 0 & 0 & -sin\theta & cos\theta & 0 \\ 0 & 0 & 0 & 0 & 0 & 1 \end{array}\right] \qquad \text{(C.6)}$$

In this manner, we obtain:

$$\mathbf{K_e} = \begin{bmatrix} k_1 & k_2 & k_4 & -k_1 & -k_2 & k_7 \\ & k_3 & k_5 & -k_2 & -k_3 & k_8 \\ & & k_6 & -k_4 & -k_5 & 0.5k_6 \\ & & & k_1 & k_2 & -k_7 \\ & SYMME- & & & k_3 & -k_8 \\ & TRIC & & & & k_6 \end{bmatrix} \tag{C.7}$$

where

$$\begin{aligned} k_1 &= QL_e^{-1}c^2 + 12SL_e^{-3}s^2 \\ k_2 &= (QL_e^{-1} - 12SL_e^{-3})\,cs \\ k_3 &= QL_e^{-1}s^2 + 12SL_e^{-3}c^2 \\ k_4 &= -RL_e^{-1}c - 6SL_e^{-2}s \\ k_5 &= -RL_e^{-1}s + 6SL_e^{-2}c \\ k_6 &= 4L_e^{-1}\mathrm{S} \\ k_7 &= RL_e^{-1}c - 6SL_e^{-2}s \\ k_8 &= RL_e^{-1}s + 6SL_e^{-2}c \end{aligned}$$

with

$$\begin{aligned} c &= cos\alpha; \\ s &= sin\alpha; \\ Q &= \textstyle\sum_m E_{s(m)} b_m h_m; \\ R &= \textstyle\sum_m E_{s(m)} b_m h_m y_m; \\ S &= \textstyle\sum_m E_{s(m)} b_m h_m y_m^2; \\ b_m &= \text{width of the } m\text{-th layer;} \\ h_m &= \text{thickness of the } m\text{-th layer;} \\ y_m &= \text{centroidal coordinate for the } m\text{-th layer.} \end{aligned}$$

Matrices $\mathbf{K_e}$ are finally assembled into the structural stiffness matrix K. After

the displacements are solved, the internal forces are calculated as:

$$N_i = -N_j = [(X_i - X_j)\,c + (Y_j - Y_i)\,s]\,QL_e^{-1} + (\theta_j - \theta_i)\,RL_e^{-1} \quad \text{(C.8)}$$

$$V_i = -V_j = [(X_j - X_i)\,s - (Y_j - Y_i)\,c]\,12SL_e^{-3} + (\theta_i + \theta_j)\,6SL_e^{-2} \quad \text{(C.9)}$$

$$M_i = [(X_j - X_i)\,c - (Y_j - Y_i)\,s]\,RL_e^{-1} + [(X_j - X_i)\,s - (Y_j - Y_i)\,c]\,6SL_e^{-2} + 2\,(2\theta_i + \theta_j)\,SL_e^{-1} \quad \text{(C.10)}$$

$$M_j = [(X_i + X_j)\,c - (Y_j - Y_i)\,s]\,RL_e^{-1} + [(X_j - X_i)\,s - (Y_j - Y_i)\,c]\,6SL_e^{-2} + 2\,(\theta_i + 2\theta_j)\,SL_e^{-1} \quad \text{(C.11)}$$

in which X_i, X_j, Y_i, Y_j are the displacement components in the global X and Y directions at the element nodes i and j.

Appendix D

Strength Interaction Diagrams

Strength interaction diagram of a given section gives combinations of N and M at failure. The key points of such diagrams represent the different conditions at failure. These are: (1) under axial load only (2) balanced condition and (3) pure bending. They are indicated in Figure D.1 as point D, B and A respectively.

The balanced failure condition occurs when the tensile steel yields simultaneously with the extreme concrete strain reaching ϵ_{cu} at the peak load N_{ub}. The corresponding effective depth parameter is k'_b and the corresponding eccentricity is e'_b. If e' is less then the balanced value e'_b, the tensile steel has not yielded at failure (normally referred to as primary compression failure). If e' is greater than e'_b, the tensile steel has yielded at failure (normally referred to as primary tension failure).

The key points described earlier are determined first. As the present work is concerned only with sections with significant amount of compressive re-

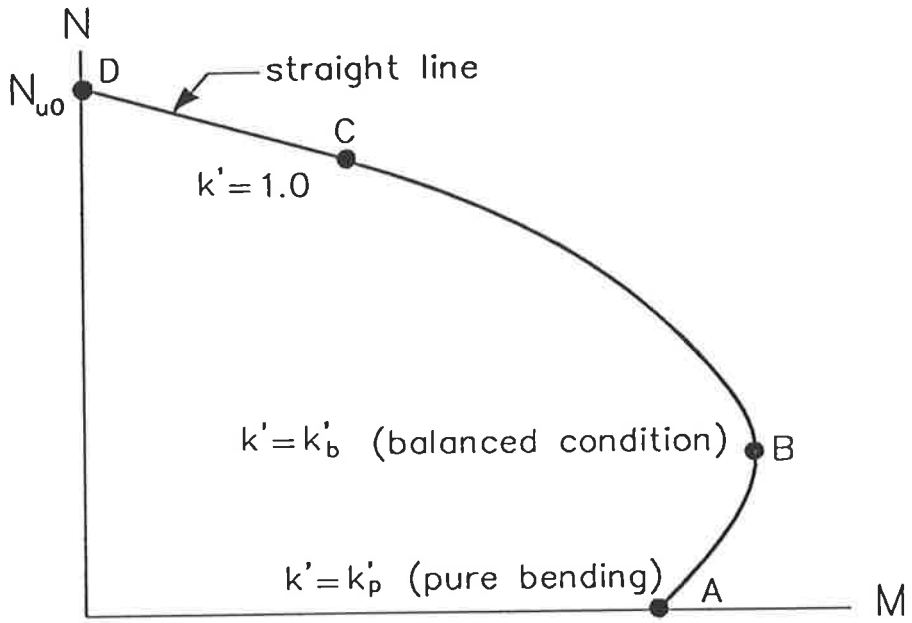

Figure D.1: Strength interaction diagram

inforcement, the program to develop strength interaction diagram will cater specifically for these sections. The calculation of the ultimate moment under pure bending for a double reinforced section is dependent on whether the compressive steel is at yield. For reinforced concrete section with large amount of compressive steel closed to the extreme fibre, it is unlikely that the compressive steel is at yield at ultimate moment. Therefore the program firstly assumes that the compressive steel is not yielded and a check is carried out later to check the validity of this assumption.

For a rectangular section under pure bending, based on the rectangular stress block concept, and assuming that the compressive steel has not yielded, the force in the compressive steel is:

$$C_s = E_s \epsilon_u \left(\frac{k'd - d_c}{k'd} \right) A_{sc} \tag{D.1}$$

The force in the concrete is:

$$C_c = 0.85\gamma F_c' b k' d \tag{D.2}$$

where γ is obtained as indicated below.

$$\gamma = 0.85 - 0.00725(F_c' - 28) \tag{D.3}$$

within the limits 0.65 and0.85

The equilibrium of forces across a section is:

$$C_s + C_c = T \tag{D.4}$$

Substituting Equation D.1 and Equation D.2 into Equation D.4 gives the quadratic equation below:

$$k'^2 + u_1 k' - u_2 = 0 \tag{D.5}$$

where

$$u_1 = \frac{\epsilon_u E_s A_{sc} - f_{sy} A_{st}}{0.85\ F_c'\ \gamma b d} \tag{D.6}$$

$$u_2 = \frac{\epsilon_u d_c E_s A_{sc}}{0.85\ F_c'\ \gamma b d^2} \tag{D.7}$$

Solving Equation D.5 gives k_p' value corresponding to the failure condition. Strain of the compressive steel corresponding to the k' value is check to ensure that the earlier assumption that the compressive steel has not yielded is acceptable. The strain in the compressive steel obtained from Equation D.8 is to be less than the strain at yield ϵ_{sy}.

$$\epsilon_{sc} = \epsilon_u \frac{k'd - d_c}{k'd} \tag{D.8}$$

After determining k_p', the compressive forces C_s and C_c are obtained from Equations D.1 and Equation D.2 respectively. M_u is then calculated using the equation below:

$$M_u = C_s(d - d_c) + C_c(d - 0.5\gamma k' d) \tag{D.9}$$

Next, the balanced condition indicated by point B in Figure D.1 is determined. First, the effective depth parameter at this condition is determined from the expression given below:

$$k'_b = \frac{\epsilon_u}{\epsilon_u + \epsilon_{sy}} \tag{D.10}$$

Multiplying both the numerator and denominator by the elastic modulus for steel, $E_s = 200000\ MPa$, and with $\epsilon_u = 0.003$, Equation D.10 becomes:

$$k'_b = \frac{600}{600 + f_{sy}} \tag{D.11}$$

The region of the curve between point B and point C can now be calculated from the steps given in the flow diagram shown in Figure D.2, now that we know the values of k' at B and C. This is carried out by obtaining N-M values for a discrete number of points at equal interval of k value between k'_p and k'_b. Similarly the region between point B and point D (point D represents a condition where k' of unity) is determined by varying k' from $k' = k'_b$ to $k' = 1.0$. For k' value greater than unity, strength calculation is complicated by a truncation of the compressive stress block, so that the rectangular stress block is not applicable. However, Warner et al (1982) suggested that this region can be approximated with good accuracy by using a straight line. This straight line joins the N-M point with $k' = 1.0$ to the point representing the failure condition under axial load only. The latter point is defined by the point $(0, N_{u0})$ where:

$$N_{u0} = 0.85F'_c bD + f_{sy}(A_{sc} + A_{st}) \tag{D.12}$$

Note that the correction to take into account of the concrete area replaced by the compressive steel area A_{sc} is not made when determining the interaction curve. This correction, as pointed out by Warner et al(1982), is of negligible importance unless the proportion of steel is very high.

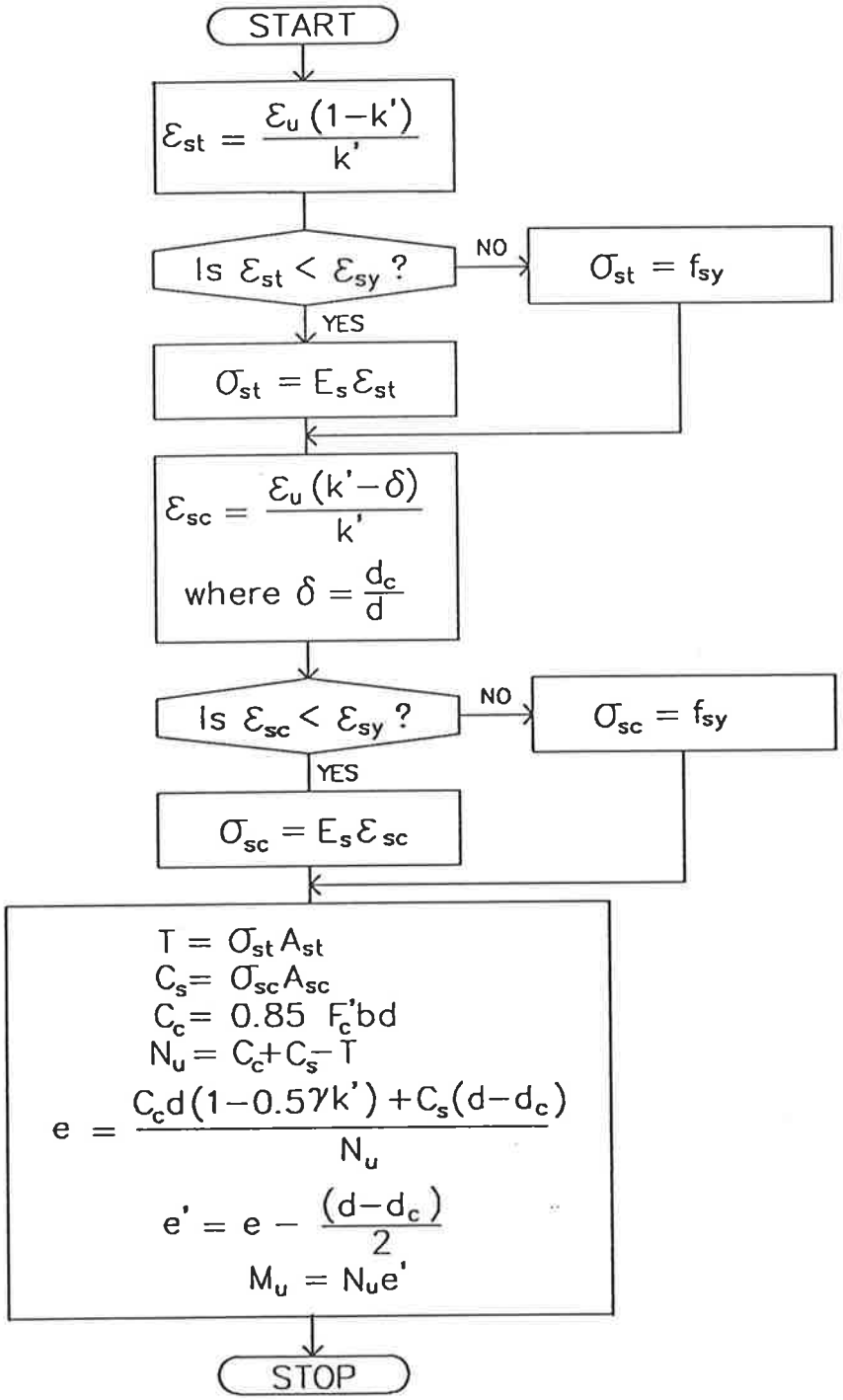

Figure D.2: Flow diagram for the determination of N-M points from given k' value

Appendix E

Derivation of Matrices for Analysis of Frames with Large Deformation

---

In developing the nonlinear equations relating forces and deformations, two separate co-ordinate systems are employed: a fixed global set of co-ordinates and a local convective system which rotates and translates with the element. The element deformations are thus separated from the joint displacements. The basic element force-deformation relations are derived in the local convective co-ordinates with element deformations assumed to be small relative to it, through the principle of minimum potential energy. This formulation of the equilibrium equation through an updated Lagrangian approach is thus applicable to analysing structures exhibiting large rotation small strain behaviour. The element forces and displacements in the various co-ordinate systems are illustrated in Figure E.1

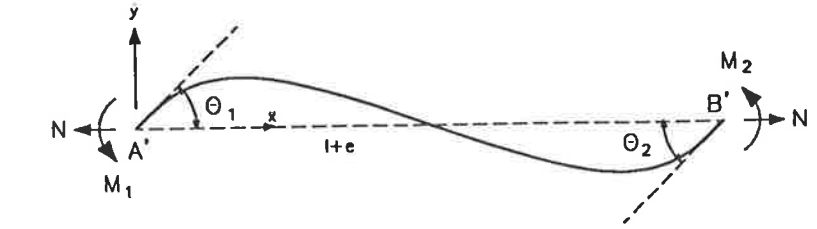

(a) Member basic displacements and forces

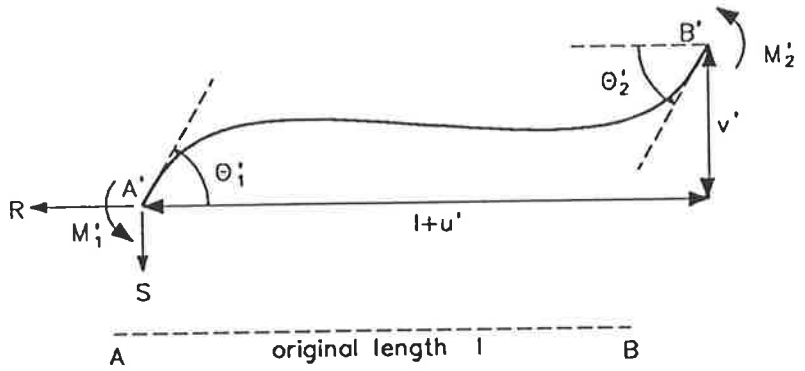

(b) Member intermediate displacements and forces

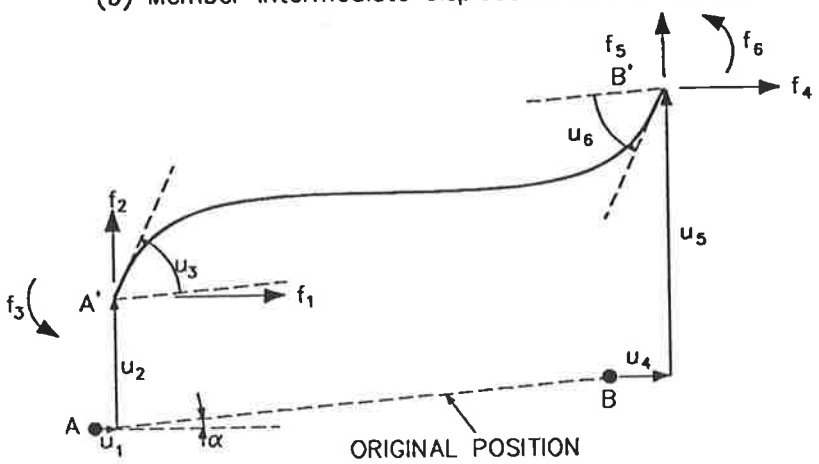

(c) Joints displacement and corresponding forces at ends of a typical member

Figure E.1: Element deformations and associated forces

E.1 Element Basic Force-Displacement Relation

On assuming a cubic lateral deflection curve and that the axial deformation, e is small compared to the original element length, l

$$y = \theta_1 \left(x - \frac{2x^2}{l} + \frac{x^3}{l^2} \right) + \theta_2 \left(-\frac{x^2}{l} + \frac{x^3}{l^2} \right) \tag{E.1}$$

and the axial length due to bowing is

$$u_b = \frac{1}{2} \int_0^l \left(\frac{dy}{dx} \right)^2 dx \tag{E.2}$$

$$= \frac{l}{30} \left(2\theta_1^2 - \theta_1 \theta_2 + 2\theta_2^2 \right) \tag{E.3}$$

The axial load, N is thus

$$N = EA \left[\frac{e}{l} + \frac{1}{30} \left(2\theta_1^2 - \theta_1 \theta_2 + 2\theta_2^2 \right) \right] \tag{E.4}$$

where EA is the axial rigidity. Neglecting the shear strain energy, the potential energy due to lateral deflection along the principal axis is:

$$\psi = \frac{1}{2} \int_0^l EI \left(\frac{d^2y}{dx^2} \right)^2 dx - M_1\theta_1 - M_2\theta_2 + N \left(\frac{1}{2} \int_0^l \left(\frac{d^2y}{dx^2} \right)^2 dx \right) \tag{E.5}$$

Through the principle of minimum potential energy, the element forces are thus:

$$M_1 = \left(\frac{4EI}{l} + \frac{4Nl}{30} \right) \theta_1 + \left(\frac{2EI}{l} - \frac{Nl}{30} \right) \theta_2 \tag{E.6}$$

$$M_2 = \left(\frac{2EI}{l} - \frac{Nl}{30} \right) \theta_1 + \left(\frac{4EI}{l} + \frac{4Nl}{30} \right) \theta_2 \tag{E.7}$$

where EI is the flexural rigidity.

The basic incremental stiffness is obtained by partial differentiating Equations E.4, E.6 and E.7 with respect to the element basic deformations. Hence

$$\begin{bmatrix} dN \\ dM_1 \\ dM_2 \end{bmatrix} = \begin{bmatrix} \frac{EA}{l} & \frac{EA}{30}(4\theta_1 - \theta_2) & \frac{EA}{30}(-\theta_1 + 4\theta_2) \\ SYMME- & k_{22} & k_{23} \\ TRIC & & k_{33} \end{bmatrix} \begin{bmatrix} de \\ d\theta_1 \\ d\theta_2 \end{bmatrix} \tag{E.8}$$

where

$$k_{22} = \frac{4EI}{l} + \frac{4EAe}{30} + \frac{EAl}{300}\left(8\theta_1^2 - 4\theta_1\theta_2 + 3\theta_2^2\right) \quad \text{(E.9)}$$

$$k_{23} = \frac{2EI}{l} - \frac{EAe}{30} + \frac{EAl}{300}\left(-2\theta_1^2 + 6\theta_1\theta_2 - 2\theta_2^2\right) \quad \text{(E.10)}$$

$$k_{33} = \frac{4EI}{l} + \frac{4EAe}{30} + \frac{EAl}{300}\left(3\theta_1^2 - 4\theta_1\theta_2 + 8\theta_2^2\right) \quad \text{(E.11)}$$

Equation E.8 can be written as:

$$\Delta \mathbf{s} = \mathbf{k}\,\Delta \mathbf{v} \quad \text{(E.12)}$$

E.2 Transformation from Element Basic Co-ordinates System to Element Intermediate Co-ordinates System

Considering gross deformation:

$$e = \sqrt{(l+u')^2 + v'^2} - l \quad \text{(E.13)}$$

$$\theta_1 = \theta_1' - tan^{-1}\left(\frac{v'}{l+u'}\right) \quad \text{(E.14)}$$

$$\theta_2 = \theta_2' - tan^{-1}\left(\frac{v'}{l+u'}\right) \quad \text{(E.15)}$$

On partial differentiating:

$$de = \left\{\frac{1}{2}\left[(l+u')^2 + v'^2\right]^{\frac{1}{2}} 2\,(l+u')\right\} du' + \left\{\frac{1}{2}\left[(l+u')^2 + v'^2\right]^{-\frac{1}{2}} 2v'\right\} dv' + (0)\,d\theta_1' + (0)\,d\theta_2' \quad \text{(E.16)}$$

$$d\theta_1 = \frac{v'}{(l+e)^2}du' - \frac{l+u'}{(l+e)^2}dv' + (1)\,d\theta_1' + (0)\,d\theta_2' \quad \text{(E.17)}$$

$$d\theta_2 = \frac{v'}{(l+e)^2}du' - \frac{l+u'}{(l+e)^2}dv' + (0)\,d\theta_1' + (1)\,d\theta_2' \quad \text{(E.18)}$$

Thus:

$$\begin{bmatrix} de \\ d\theta_1 \\ d\theta_2 \end{bmatrix} = \begin{bmatrix} \frac{l+u'}{l+e} & \frac{v'}{l+e} & 0 & 0 \\ \frac{v'}{(l+e)^2} & -\frac{l+u'}{(l+e)^2} & 1 & 0 \\ \frac{v'}{(l+e)^2} & -\frac{l+u'}{(l+e)^2} & 0 & 1 \end{bmatrix} \begin{bmatrix} du' \\ dv' \\ d\theta_1' \\ d\theta_2' \end{bmatrix} \tag{E.19}$$

Equation E.19 can be written as:

$$\Delta \mathbf{v} = \mathbf{A}\, \Delta \mathbf{u}' \tag{E.20}$$

By the contragrediant principle:

$$\mathbf{f}' = \mathbf{A}^T\, \mathbf{s} \tag{E.21}$$

where

$$\mathbf{f}' = \begin{bmatrix} R \\ S \\ M_1' \\ M_2' \end{bmatrix} \tag{E.22}$$

and

$$\mathbf{s} = \begin{bmatrix} N \\ M_1 \\ M_2 \end{bmatrix} \tag{E.23}$$

On differentiating Equation E.21:

$$\Delta \mathbf{f} = \mathbf{A}^T\, \Delta \mathbf{s} + \mathbf{D}\, \Delta \mathbf{u}' \tag{E.24}$$

where

$$\mathbf{D} = \begin{bmatrix} d_{11} & d_{12} & 0 & 0 \\ d_{21} & d_{22} & 0 & 0 \\ 0 & 0 & 0 & 0 \\ 0 & 0 & 0 & 0 \end{bmatrix} \tag{E.25}$$

and

$$d_{11} = \frac{1}{(l+e)^4} \left[-v'^2 (l+u')\, T + \left(2(l+u')^2 + v'^2 \right) v' S \right] \tag{E.26}$$

$$d_{12} = d_{21} = \frac{1}{(l+e)^4}\left[-v'^3 T - (l+u')^3 S\right] \tag{E.27}$$

$$d_{22} = \frac{1}{(l+e)^4}\left[(l+u')\left((l+u')^2 + 2v'^2\right) T - (l+u')^2 v' S\right] \tag{E.28}$$

E.3 Transformation from Element Intermediate Co-ordinates System to Nodal Global Co-ordinates System

The element intermediate displacements are related to the noadal displacements by:

$$\begin{bmatrix} u' \\ v' \\ \theta'_1 \\ \theta'_2 \end{bmatrix} = \begin{bmatrix} -\cos\alpha & -\sin\alpha & 0 & \cos\alpha & \sin\alpha & 0 \\ \sin\alpha & -\cos\alpha & 0 & -\sin\alpha & \cos\alpha & 0 \\ 0 & 0 & 1 & 0 & 0 & 0 \\ 0 & 0 & 0 & 0 & 0 & 1 \end{bmatrix} \begin{bmatrix} u_1 \\ u_2 \\ u_3 \\ u_4 \\ u_5 \\ u_6 \end{bmatrix} \tag{E.29}$$

Therefore

$$\mathbf{u}' = \mathbf{T}\,\mathbf{u} \tag{E.30}$$

and

$$\Delta\mathbf{u}' = \mathbf{T}\,\Delta\mathbf{u} \tag{E.31}$$

By the contragrediant principle,

$$\Delta\mathbf{f} = \mathbf{T}^T\left(\mathbf{A}^T\,\Delta\mathbf{s} + \mathbf{D}\,\Delta\mathbf{u}'\right) \tag{E.32}$$

$$= \mathbf{T}^T\left(\mathbf{A}^T\,\mathbf{k}\,\Delta\mathbf{v} + \mathbf{D}\,\Delta\mathbf{u}'\right) \tag{E.33}$$

$$= \mathbf{T}^T\left(\mathbf{A}^T\,\mathbf{k}\,\mathbf{A}\,\Delta\mathbf{u}' + \mathbf{D}\,\Delta\mathbf{u}'\right) \tag{E.34}$$

$$= \mathbf{T}^T\left(\mathbf{A}^T\,\mathbf{k}\,\mathbf{A} + \mathbf{D}\right)\mathbf{T}\,\Delta\mathbf{u} \tag{E.35}$$

$$= \mathbf{k}_g\,\Delta\mathbf{u} \tag{E.36}$$

Appendix F

Derivation of Geometric Stiffness Matrix

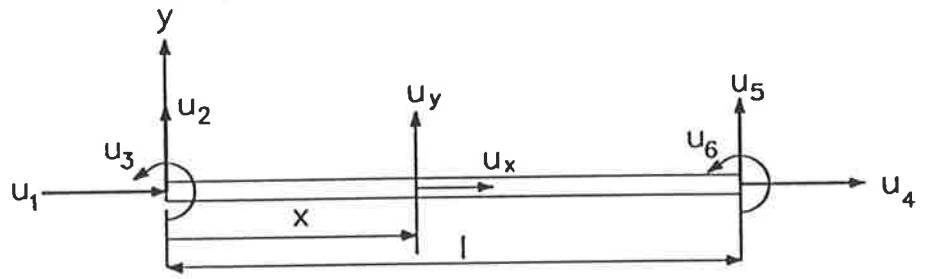

Figure F.1: Beam element with end displacements

The conventional displacement distribution on a uniform cross-section beam element is (Przemienski, 1968):

$$\begin{Bmatrix} u_z \\ u_y \end{Bmatrix} = \begin{bmatrix} 1-\xi & 6(\xi-\xi^2)\eta & (-1+4\xi-3\xi^2)l\eta \\ 0 & 1-3\xi^2+2\xi^3 & (\xi-2\xi^2+\xi^3)l \end{bmatrix}$$

$$\begin{bmatrix} \xi & 6(-\xi+\xi^2)\eta & (2\xi-3\xi^2)l\eta \\ 0 & 3\xi^2-2\xi^3 & (-\xi^2+\xi^3)l \end{bmatrix} \begin{Bmatrix} u_1 \\ u_2 \\ u_3 \\ u_4 \\ u_5 \\ u_6 \end{Bmatrix} \qquad \text{(F.1)}$$

where

$u_1, \ldots, u_6$ are the element displacements
shown in Figure F.1.

In calculating the strain energy U_i we neglect the contributions from the shearing strains. Thus only the normal strain ϵ_{xx} will be included. These strains for large deflections on a beam in bending are determined from :

$$\epsilon_{xx} = \frac{\partial u_0}{\partial x} - \frac{\partial^2 u_y}{\partial x^2} y + \frac{1}{2}(\partial u_y \partial x)^2 \qquad \text{(F.2)}$$

where

y is measured from the neutral axis of the beam; and
u_0 denotes the u_x displacement at $y = 0$.

We use Equation F.2, and the strain energy U_i is given by:

$$U_i = \frac{E}{2} \int_v \epsilon_{xx}^2 dV \qquad \text{(F.3)}$$

$$= \frac{E}{2}\int_v \left[\frac{\partial u_0}{\partial x} - \frac{\partial^2 u_y}{\partial x^2}y + \frac{1}{2}\left(\frac{\partial u_y}{\partial x}\right)^2\right]^2 dV \tag{F.4}$$

$$= \frac{E}{2}\int_{x=0}^{l}\int_A \left[\left(\frac{\partial u_0}{\partial x}\right)^2 + \left(\frac{\partial^2 u_y}{\partial x^2}\right)^2 y^2 + \frac{1}{4}\left(\frac{\partial u_y}{\partial x}\right)^4 - 2\frac{\partial u_0}{\partial x}\frac{\partial^2 u_y}{\partial x^2}y - \frac{\partial^2 u_y}{\partial x^2}\left(\frac{\partial u_y}{\partial x}\right)^2 y + \frac{\partial u_0}{\partial x}\left(\frac{\partial u_y}{\partial x}\right)^2\right] dx dA \tag{F.5}$$

The higher-order term $\frac{1}{4}\left(\frac{\partial u_y}{\partial x}\right)^4$ can be neglected in the above expression. Integrating over the cross-sectional area A and noting that since y is measured from the neutral axis, all integrals of the form $\int y dA$ must vanish, we have that:

$$U_i = \frac{EA}{2}\int_0^l \left(\frac{\partial u_0}{\partial x}\right)^2 dx + \frac{EI}{2}\int_0^l \left(\frac{\partial^2 u_y}{\partial x^2}\right)^2 dx + \frac{EA}{2}\int_0^l \frac{\partial u_0}{\partial x}\left(\frac{\partial u_y}{\partial x}\right)^2 dx \tag{F.6}$$

where

I denotes the moment of inertia of the cross-section.

We may note that the first two integrals in Equation F.6 represent the linear strain energy while the third integral is the contribution from the nonlinear component of the strain. From Equation F.1 we obtain:

$$\frac{\partial u_0}{\partial x} = \frac{1}{l}(-u_1 + u_4) \tag{F.7}$$

$$\frac{\partial u_y}{\partial x} = \frac{1}{l}\left[6\left(-\xi + \xi^2\right)u_2 + \left(1 - 4\xi + 3\xi^2\right)lu_3 + 6\left(\xi - \xi^2\right)u_5 + \left(-2\xi + 3\xi^2\right)lu_6\right] \tag{F.8}$$

$$\frac{\partial^2 u_y}{\partial x^2} = \frac{1}{l^2}\left[6\left(-1 + 2\xi\right)u_2 + 2\left(-2 + 3\xi\right)lu_3 + 6\left(1 - 2\xi\right)u_5 + \left(-1 + 3\xi\right)lu_6\right] \tag{F.9}$$

Substitution of Equations F.7 to F.8 into F.6 and integrating leads to:

$$
\begin{aligned}
U_i \;=\; & \frac{EA}{2l}\left(u_1^2 - 2u_1u_4 + u_4^2\right) + \\
& \frac{2EI}{l^3}\left(3u_2^2 + l^2u_3^2 + 3u_5^2 + l^2u_6^2 + 3lu_2u_3 - 6u_2u_5 + 3lu_2u_6 - \right. \\
& \left. 3lu_3u_5 + l^2u_3u_6 - 3lu_5u_6\right) + \\
& \frac{EA}{l^2}(u_4 - u_1)\left(\frac{3}{5}u_2^2 + \frac{1}{15}l^2u_3^2 + \frac{3}{5}u_5^2 + \frac{1}{15}l^2u_6^2 + \frac{1}{10}lu_2u_3 - \right. \\
& \left. \frac{6}{5}u_2u_5 + \frac{1}{10}lu_2u_6 - \frac{1}{10}lu_3u_5 - \frac{1}{30}l^2u_3u_6 - \frac{1}{10}u_5u_6\right)
\end{aligned}
\tag{F.10}
$$

We may note that even for relatively large deflections the quantity $EA(u_4 - u_1)/l$ may be treated as a constant equal to the axial tensile force in the beam. Hence we may introduce

$$
F = \frac{EA}{l}(u_4 - u_1) \approx const \tag{F.11}
$$

and apply Castigliano's theorem to the strain energy expression (Equation F.10). This results in the following element force-displacement equation:

$$
\begin{Bmatrix} S_1 \\ S_2 \\ S_3 \\ S_4 \\ S_5 \\ S_6 \end{Bmatrix} = \frac{EI}{l^3}
\begin{bmatrix}
\frac{Al^2}{I} & & & & & \\
0 & 12 & & & SYMME- & \\
0 & 6l & 4l^2 & & TRIC & \\
-\frac{Al^2}{I} & 0 & 0 & \frac{Al^2}{I} & & \\
0 & -12 & -6l & 0 & 12 & \\
0 & 6l & 2l^2 & 0 & -6l & 4l^2
\end{bmatrix}
\begin{Bmatrix} u_1 \\ u_2 \\ u_3 \\ u_4 \\ u_5 \\ u_6 \end{Bmatrix}
+ \frac{F}{l}
\begin{bmatrix}
0 & & & & & \\
0 & \frac{6}{5} & & & SYMME- & \\
0 & \frac{l}{10} & \frac{2}{15}l^2 & & TRIC & \\
0 & 0 & 0 & 0 & & \\
0 & -\frac{6}{5} & -\frac{l}{10} & 0 & \frac{6}{5} & \\
0 & \frac{l}{10} & -\frac{l}{30} & 0 & -\frac{l}{10} & \frac{2}{15}l^2
\end{bmatrix}
\begin{Bmatrix} u_1 \\ u_2 \\ u_3 \\ u_4 \\ u_5 \\ u_6 \end{Bmatrix}
\tag{F.12}
$$

which may be written symbolically as:

$$\mathbf{k} = (\mathbf{k}_e + \mathbf{k}_g)\,\mathbf{u} \tag{F.13}$$

Appendix G

Testing of Program NEWTONR

The testing of program NEWTONR is carried out by comparing results obtained using the program with published analytical solutions for a cantilevered beam and a portal frame.

The matrices given by Jennings(1968) have been used previously by other researchers and found to give accurate predictions of the non-linear behaviour of structures with geometrical nonlinearities. As the matrices given by Jennings have to be used together with Newton-Raphson procedure for solving non-linear equations, care has to be taken to ensure successful implementation into a computer program. Therefore, the testing of the program is not only to confirm the accuracy of using Jennings's matrices, but also to act as a check to ensure that the program NEWTONR has been coded correctly.

The matrices of Jennings have been used by Meek and Tan(1983) for post-buckling analysis of elastic frames. Meek and Tan compared results obtained

using this analytical approach with analytic solution to a cantilever beam with a vertical point load at its free end. This structure was chosen as its simple configuration allows 'exact' solutions to be obtained analytically. The analytic solution is obtained by Frisch-Fay(1962) using elliptic integrals. Meek and Tan observed that the solution using Jenning's algorithm agrees closely with that obtained by Frisch-Fay. Results obtained from these two analytical approaches are shown in Figure G.1 reproduced from the report by Meek and Tan.

The same beam is also analysed using program `NEWTONR`. The solutions for the beam modelled by one, two and four elements, given in Table G.1, Table G.2 and Table G.3 confirm Meek and Tan's observation that Jenning's algorithms can model accurately geometrical nonlinearities effect in elastic structures. In these tables, u is the horizontal displacement, v is the vertical displacement and θ is the rotation as indicated in Figure G.1.

A portal frame analysed by Lee, Manual and Rossow(1968) is also chosen for analysis using program `NEWTONR`. Results obtained are plotted as a series of points in Figure G.2. Those obtained by Lee et al are shown as a continuous curve. The plots show close agreement between the two solutions. The deformed shape of this frame at a load factor of 14.9 is obtained by Lee et al; the shape is shown in Figure G.3

It is not possible to obtain solution point closer to the plateau of the curve using a load control technique. Although the program `CRISFIEL` has been developed to trace the entire curve caused by geometrical nonlinearities, it is not used in the present study. The load control program `NEWTONR` is sufficient for the purpose of the present study which is to carry out a middle-tier strength analysis of frames.

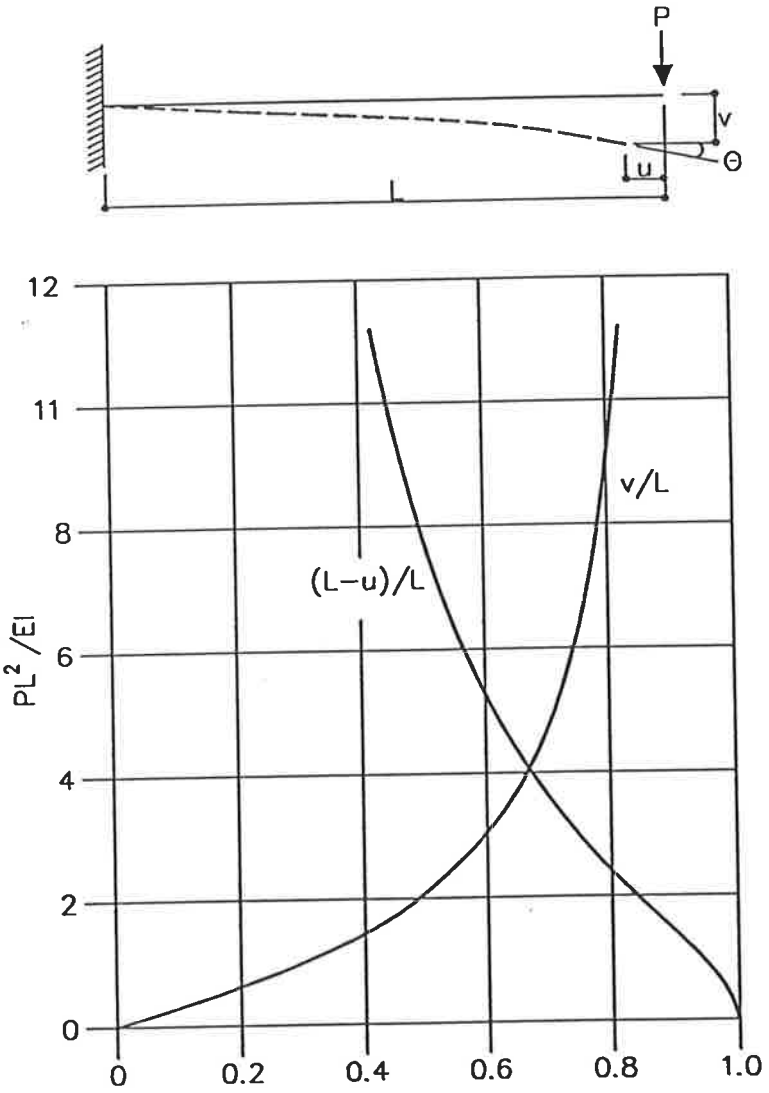

Figure G.1: Results for analysis of cantilevered beam (Meek and Tan,1983)

Table G.1: Results from analysis of cantilevered beam (vertical deflection)

	$(L-u)/L$			
PL^2/EI	1 ELEMENT	2 ELEMENTS	4 ELEMENTS	FRISH-FAY'S SOLUTION
0.0	1.0000	1.0000	1.0000	1.0000
1.0	0.9441	0.9438	0.9438	0.9436
2.0	0.8420	0.8401	0.8399	0.8394
3.0	0.7515	0.7468	0.7463	0.7456
4.0	0.6805	0.6728	0.6720	0.6711
5.0	0.6275	0.6150	0.6133	0.6124
6.0	0.5813	0.5683	0.5665	0.5654
7.0	0.5460	0.5305	0.5283	0.5271
8.0	0.5170	0.4990	0.4965	0.4952
9.0	0.4925	0.4728	0.4695	0.4682
10.0	0.4715	0.4500	0.4465	0.4450

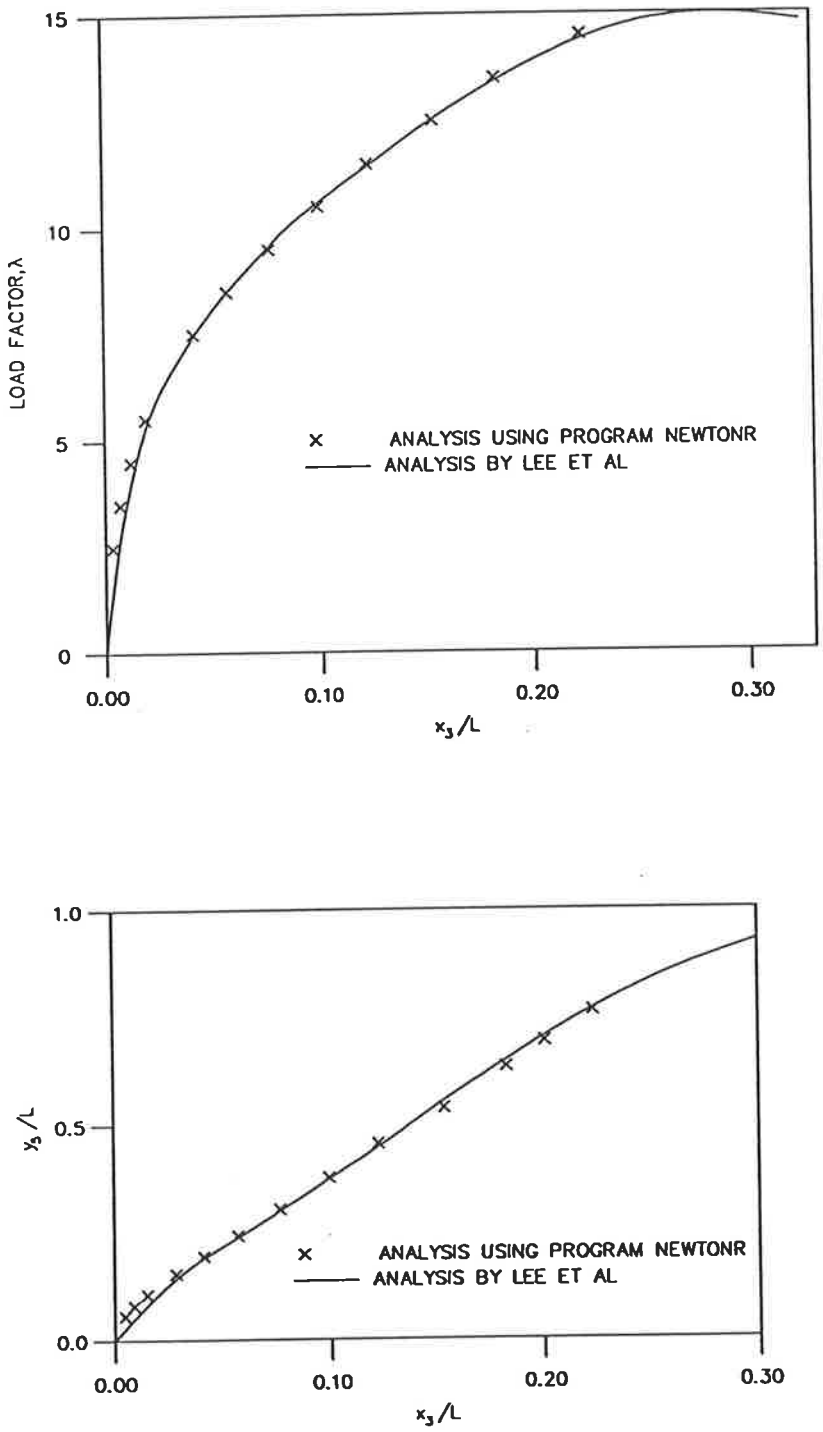

Figure G.2: Results for analysis of portal frame

Table G.2: Results from analysis of cantilevered beam (horizontal deflection)

	v/L			
PL^2/EI	1 ELEMENT	2 ELEMENTS	4 ELEMENTS	FRISH-FAY'S SOLUTION
0.0	0.0000	0.0000	0.0000	0.0000
1.0	0.3008	0.3018	0.3020	0.3017
2.0	0.4895	0.4938	0.4943	0.4935
3.0	0.5955	0.6040	0.6048	0.6033
4.0	0.6588	0.6708	0.6725	0.6700
5.0	0.6998	0.7150	0.7170	0.7138
6.0	0.7280	0.7460	0.7485	0.7446
7.0	0.7488	0.7690	0.7723	0.7674
8.0	0.7645	0.7870	0.7905	0.7850
9.0	0.7770	0.8013	0.8055	0.7991
10.0	0.7873	0.8133	0.8177	0.8106

Table G.3: Results from analysis of cantilevered beam (rotation)

	θ(radian)			
PL^2/EI	1 ELEMENT	2 ELEMENTS	4 ELEMENTS	FRISH-FAY'S SOLUTION
0.0	0.000	0.000	0.000	0.000
1.0	0.460	0.461	0.462	0.461
2.0	0.777	0.782	0.782	0.782
3.0	0.976	0.986	0.987	0.986
4.0	1.105	1.121	1.123	1.121
5.0	1.193	1.215	1.217	1.215
6.0	1.254	1.283	1.285	1.284
7.0	1.299	1.335	1.337	1.335
8.0	1.332	1.374	1.376	1.374
9.0	1.356	1.405	1.407	1.405
10.0	1.375	1.429	1.432	1.430

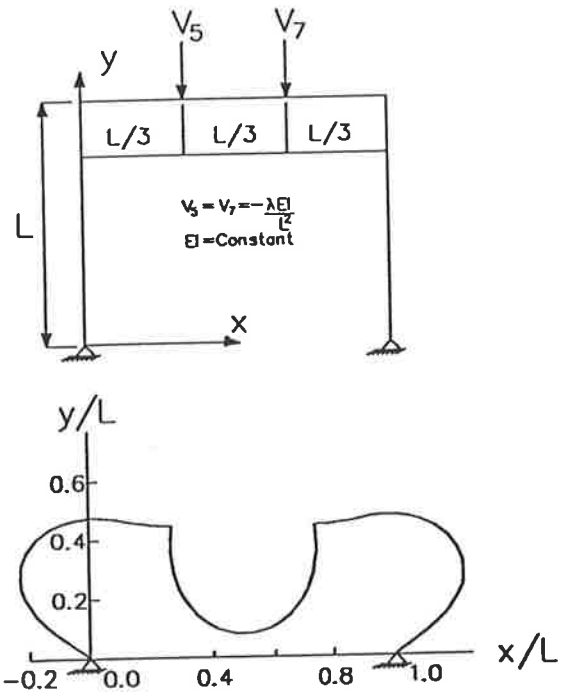

Figure G.3: Deflected shape at load factor = 14.9 (Lee et al,1968)

Appendix H

User Manual for Program SAFRAME

H.1 Scope of the Program

The program SAFRAME numerically simulates the behaviour of reinforced skeletal plane frames as they are progressively loaded up to and beyond the peak load, into the softening range.

The program takes into consideration the effect of geometric nonlinearity caused by the movement of the nodes under loading, but does not include the effect of geometric nonlinearity caused by the movement of the element away from the line joining its ends. Therefore to accurately simulate the behaviour of members in compression, such members are modelled using a few elements. This results in placing more nodes along a member and, therefore, enables the geometric nonlinearity effect along the member to be included in

Table H.1: Typical units for input data

length	m
curvature	m^{-1}
point load	kN
distributed load	kNm^{-1}
bending moment	kNm
Young's modulus	kNm^{-2}
yield stress	kNm^{-2}

the numerical model.

Program SAFRAME was developed using standard FORTRAN77 language to run in a UNIX-based operating environment.

H.2 Data Preparation

Input data are in consistent units. The set of units used by the program is given in Table H.2. An exception to the above is that the width and depth relating to the section are in millimetres.

H.3 Numbering of Nodes and Elements

The numbering of nodes is in sequence starting from unity up to the total number of nodes. Each element is assigned a number, starting from one up to the total number of elements. For each element, the connectivity detail is

declared. This connectivity detail specifies the initial position of the element in relation with the position of the nodes. The specification of the connectivity detail assists the interpretation of the directions of output forces in relation to the element.

H.4 Fixity of Nodes

The support condition of each node is defined by using a group of three integers. The first indicates the condition of the restraint along the x-axis, the second, along the y-axis, and the third, rotation about the z-axis. The input required for each of the integers is either unity (for no restraint) or null (for full restraint). Inputs required for nodes with different conditions of restraint are shown in Figure H.1.

H.5 Loading

The loading data are divided into two sets; the first defines the loading at the nodes, and the second defines loading along the elements.

Loading at a node is defined by specifying each of the point loads for the three possible degrees of movement. Even though a particular degree of movement is restrained, a value of null is still required for the corresponding point load.

Two different types of loading are allowed along an element. These are: (1) transverse uniformly distributed load (UDL) along the entire element and (2) a transverse point load anywhere along the element. An integer of 1 is required to specify the former load type, and an integer of 2 is required for the latter. Two further variables are required; for the UDL case, the first of these two variables specified both its magnitude (in force per unit length) and direction,

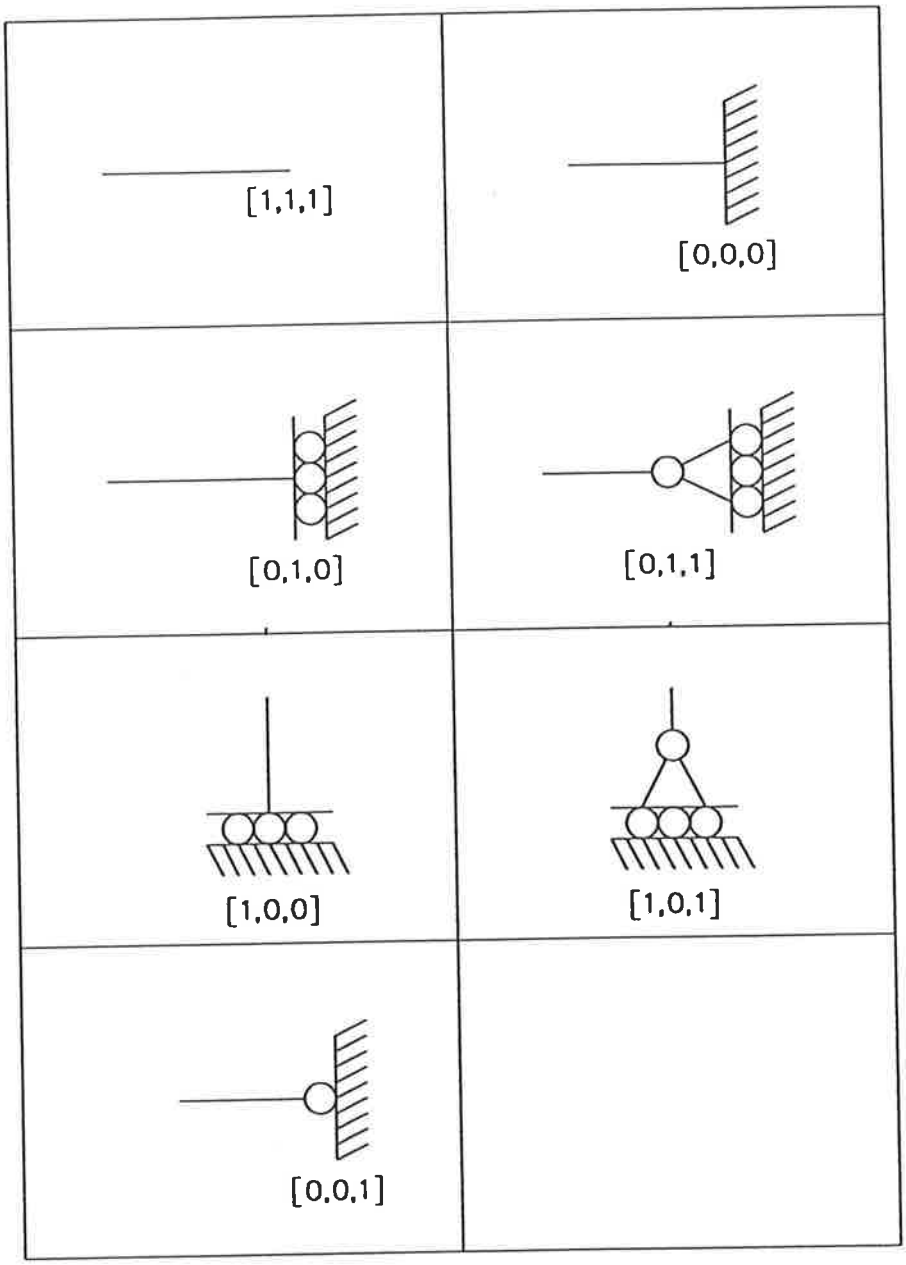

Figure H.1: Constraints of joints and supports

and the second is not used by the program, but a value of zero is required; for the second case, the first variable specifies the magnitude and direction, and the second variable specifies the distant of this load from the left end of the element. Up to four different sets of loading can be applied simultaneously to a particular element. This enables a combination of different basic loading patterns within an element, e.g., UDL together with a few point loads.

H.6 Dividing Elements into Segments

For each element, the program requires the input of the number of segments. As a guide, the number of segment should be chosen such that the segment length to depth ratio is between $0.5D$ to $1.0D$, where D is the depth of the element.

Material properties are defined for each segment. The program limits the number of layers of reinforcing steel to two.

H.7 Input Files

Input files are normal text files. No predefined format is used to read in the input, and therefore input data within the same line are separated by commas. For easy identification such files should have filenames with a suffix of "`inp`".

The various data required are listed below in the order in which they should be placed:

- `FILENAME` (type:string): For easy identification the output filename should has a prefix of "`t_`". An example for the name to be placed in first line for the input file with filename of "`t_test.inp`" is "`t_test`".

- `TITLE` (type:string): This is a one line description of the run. An example is "`Testing frame : 9 metre tall column`".

- `IPDEL` (type:integer): If `IPDEL` = 1 then include geometrical nonlinearity effect. If `IPDEL` = 0 then do not include this effect.

- `IPRINM` (type:integer): If `IPRINM` =1 then print detailed output for all the segments in output file with suffix "`out`". If `IPRINM` = 0 then print only partial output.

- `IDEGFRE` (type:integer): This gives the degree of freedom to be used for printing out the deflections in the output file with suffix "`pdl`".

- `IPMEM, IPSEG` (type:integer, integer): These specify the segment to be used for printing out the deflections in the output file with suffix "`pdl`".

- `ITO, JTO` (type:integer, integer): These specify the segment to be used as the key segment for controlling curvature. If they are zeros, then the program will locate the segment that has the largest curvature during the first step, and subsequently use this segment as the key segment.

- `NHSECT` (type:integer): This specify the number of concrete layers to be used to model the sections.

- `CURMAX` (type:real): This specify the maximum curvature to be used for the key segment to trace the behaviour of the structure.

- `NPOINT`(type:integer); This specifies the number of incremental curvature steps to reach peak curvature `CURMAX`.

- `TOLSTR, TOLMEM` (type:real, real): The first specifies the tolerance to be applied to the structure for the measure of convergency. The second specifies the tolerance to be applied to the section for the measure of convergency.

- `NODE, ELEMENT` (type:real, real): Number of nodes and number of elements.

- `J, X, Y, ND1, ND2, ND3` (type:integer, real, real, integer, integer, integer): `J` specifies the node number. `(X, Y)` is the co-ordinates of the node. The last three integers specifies the restraints of the node. This input is to be specified for all the nodes.

- `J, N1, N2, NSEG, GAMMA1, GAMMA2, FCPEAK, ECPEAK` (type:integer, integer, integer, real, real, real, real): where

  - `J` is the element number
  - `N1, N2` are the node numbers of the ends of the element
  - `NSEG` is the number of segments to be used for this element
  - `GAMMA1` is the material parameter γ_1 for this element
  - `GAMMA2` is the material parameter γ_2 for this element
  - `FCPEAK` is the peak concrete strength f_{cmax}
  - `ECPEAK` is the strain at peak concrete strength ϵ_{cmax}

  This input is to be specified for all the elements.

- `ESTEL, FSY` (type:real, real): `ESTEL` specifies the Young's Modulus and `FSY` specifies the yield stress of the reinforcing steel.

- `WIDTH, DEPTH, NST, AST(1), DT(1), AST(2), DT(2)` (type:real, real, integer, real, real, real, real): where

  - `WIDTH` and `DEPTH` are the width and depth of the segment
  - `NST` is the number of layer of reinforcing bars
  - `AST(1)` is the cross-sectional area of the top reinforcing layer
  - `DT(1)` is the distance from the centre of the top layer to the top concrete fibre

- `AST(2)` is the cross-sectional area of the bottom reinforcing layer
- `DT(2)` is the distance from the centre of the bottom layer to the top concrete fibre

This input is to be specified for all segments starting from the first segment of the first element to the last segment of the last element.

- `NN` (type:integer): this specifies the number of nodes with loads.
- `NN, PX(NN), PY(NN), PM(NN)` (type: integer, real, real, real): `NN` specifies the node number, and `PX`, `PY` and `PM` specify the loads acting on the node along X axis, the Y axis and Z direction. This input is to be specified for all the loaded nodes.
- `NL` (type:integer): For each element, the number of element loads `NL` is to be specified. If `NL` is not equal to zero, input lines following this line is required to specified the loading within the element. The additional lines for non zero `NL` have the following formats:
  - `LT, VL, A` (type:integer, real, real): `LT` =1 for UDL and `LT` =2 for point load. If `LT` =1 then `VL` specifies the magnitude and direction of the load in load per unit length, and `A` is to be zero. If `LT` =2 then `VL` specifies the magnitude and direction of the point load, and `A` specifies the distance of this point load from the left end of the element. Direction is positive upward along an element.

H.8 Output Files

All the output files have the first part of their names set equal to the input character string of the first line of the input file. The suffix of each file is assign a unique three-character string by the program. This enables output files to be easily located.

The name of the input can be of any form, but for easy identification, it should have a meaningful suffix such as "`dat`" or "`inp`". If the first line of the data file has a string "`test`", the output files created by the program are "`test.out`","`test.pdl`", "`test.map`" and "`test.mkt`". The output file with the suffix "`out`" consists of the complete information of the input and output data. The output file with the suffix of "`pdl`" is in a form suitable for plotting of the load versus deflection curves. The file with a suffix of "`map`" consists of information about the states of the segments. The file with the suffix of "`mkt`" consists of the complete moment-curvature information of all the segments. Another program BREAK is required to process this file to extract M-κ information and to create data files for segments selected by the users. The data files created are suitable for input into standard plotting programs.

Program PSPLOT has been developed using FORTRAN77 to create corresponding POSTSCRIPT test files from the individual moment-curvature file of the segment. The POSTSCRIPT file can then be sent to laser printers supporting the POSTSCRIPT language to create a hard copy of the plot. POSTSCRIPT (see Adobe System Incoporated,1985) is a device-independent graphic description language. Printer supporting this language has a built-in interpreter to process incoming file with POSTSCRIPT instructions, and translates these instructions to give hard copy plots.

To illustrate the input required for a typical frame using program SAFRAME, a portal frame shown in Figure H.2 is analysed. To reduce the amount of output only three elements are used, one for each member. Each of these element is modelled using nine segments only. The number of segments is also kept small to reduce the amount of output.

The input and output files are printed out onto the Apple LaserWriter. The input data are shown in Figure H.3.

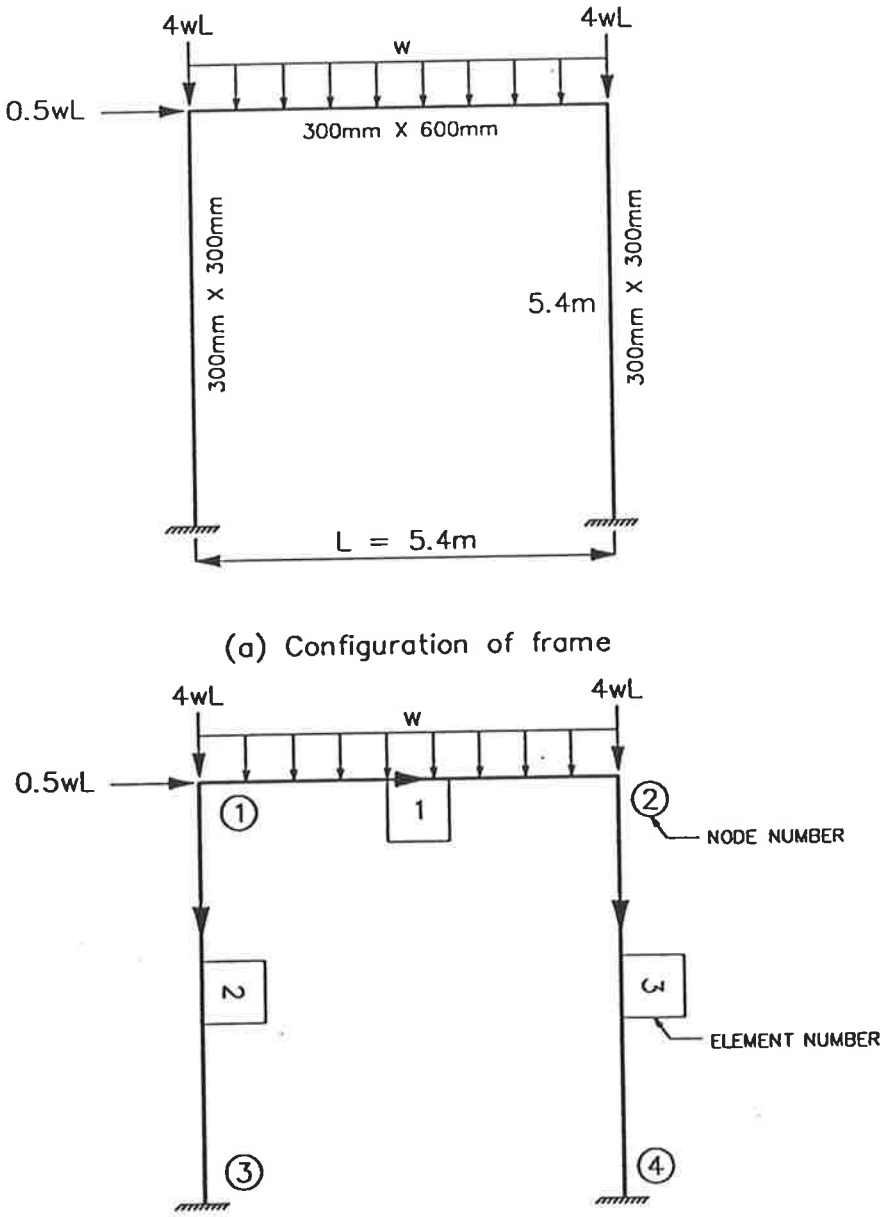

Figure H.2: Configuration of portal frame G

```
saframe                                          rem:output filename(no suffix!)
sample input for saframe.f                       rem:TITLE; notes.
1                                                rem:IPDEL (1 or 0).
0                                  rem:IPRINM (1 =complete, 0 =partial printout).
1                                  rem:IDEFGRE; DEGREE OF FREEDOM TO PRINT.
1,5                                rem:IPMEM,IPSEG; DEFLECTION OF SEGMENT TO PRINT.
3,1                                rem:ITO,JTO; CONTROL SEGMENT.
15                                 rem:NHSECT; NO OF LAYERS.
0.04                               rem:CURMAX; MAX CURVATURE FOR CONTROL SEGMENT.
15                                 rem:NPOINT; NO OF STEPS TO REACH MAX CURVATURE.
0.01,0.001                         rem:TOLSTR,TOLMEM; TOL.STRUCT, TOL.SECTION.
4,3                                rem:NODE, ELEM; NO OF NODES, NO OF ELEMENTS.
1,0.0,5.4,1,1,1                    rem1:J,       X,     Y,     ND1,  ND2  ,ND3.
2,5.4,5.4,1,1,1                    rem2:(NODE NO,X-ORD.,Y-ORD.,RES-X,RES-Y,RES-Z).
3,0.0,0.0,0,0,0
4,5.4,0.0,0,0,0
1,1,2,9,1.99,3.0,29.75,0.002     rem1:J,N1,N2,GAMMA1,GAMMA2,FCPEAK,ECPEAK.
2,1,3,9,1.99,3.0,29.75,0.002     rem2:(ELEM,FR,TO,GAMMA1,GAMMA2,FCPEAK,ECPEAK).
3,2,4,9,1.99,3.0,29.75,0.002     rem3:          <-----CONCRETE----------->.
2.0E+05,460.0                          rem1: ESTEEL,FSY;MODULUS, YIELD STRESS.
300.0,600.0,2,1800.0,50.0,1800.0,550.0    rem:WIDTH,
300.0,600.0,2,1800.0,50.0,1800.0,550.0         DEPTH,
300.0,600.0,2,1800.0,50.0,1800.0,550.0              NST,
300.0,600.0,2,1800.0,50.0,1800.0,550.0                AST(1),
300.0,600.0,2,1800.0,50.0,1800.0,550.0                    DT(1),
300.0,600.0,2,1800.0,50.0,1800.0,550.0                     AST(2),
300.0,600.0,2,1800.0,50.0,1800.0,550.0                         DT(2).
300.0,600.0,2,1800.0,50.0,1800.0,550.0
300.0,600.0,2,1800.0,50.0,1800.0,550.0
300.0,300.0,2,900.0,50.0,900.0,250.0
300.0,300.0,2,900.0,50.0,900.0,250.0
300.0,300.0,2,900.0,50.0,900.0,250.0
300.0,300.0,2,900.0,50.0,900.0,250.0
300.0,300.0,2,900.0,50.0,900.0,250.0
300.0,300.0,2,900.0,50.0,900.0,250.0
300.0,300.0,2,900.0,50.0,900.0,250.0
300.0,300.0,2,900.0,50.0,900.0,250.0
300.0,300.0,2,900.0,50.0,900.0,250.0
300.0,300.0,2,900.0,50.0,900.0,250.0
300.0,300.0,2,900.0,50.0,900.0,250.0
300.0,300.0,2,900.0,50.0,900.0,250.0
300.0,300.0,2,900.0,50.0,900.0,250.0
300.0,300.0,2,900.0,50.0,900.0,250.0
300.0,300.0,2,900.0,50.0,900.0,250.0
300.0,300.0,2,900.0,50.0,900.0,250.0
2                                  rem:NN; NO OF NODES WITH LOADS.
1,270.0,-2160.0,0.0                rem:NN,PX(NN),PY(NN),PM(NN);
2,0.000,-2160.0,0.0                          NODE NO,LOAD-X,LOAD-Y,MOM-Z.
1                                  rem:NL;NO OF LOADS FOR ELEMENT 1.
1,-100.0,0.0                       rem:LT,VL,A; LOADTYPE,VALUE,VARIABLE A.
0                                  rem:NO OF LOADS FOR ELEMENT 2.
0                                  rem:NO OF LOADS FOR ELEMENT 3.
rem:************************************************************
rem:*     THIS IS A SAMPLE INPUT FILE FOR PROGRAM SAFRAME       *
rem:************************************************************
```

Figure H.3: Input data for portal frame G

The output data from the file "`test.pdl`" are shown in Figure H.4. The output data from the file "`test.map`" are shown in Figure H.5. The output data from the file "`test.mkt`" are shown in Figure H.6 and Figure H.7. Owing to the large number of pages of printout, only the first page and the last page are shown. The output data from the file "`test.out`" are shown in Figure H.8 to Figure H.11. Owing to the large number of pages of printout, only the first four pages are listed.

The listings of output files, though not completely in a few cases, are sufficient to give an idea of the output expected from the program.

```
!FILENAME OF THIS FILE : saframe.pdl
!FILENAME OF PROGRAM USED : saframe.exe
!   CURTAR(1/m) SF(x100)   DELDF(mm)    MOMTAR(kNm)   DELSEG(mm)  ICYCLE
    0.00000      0.00000     0.00000      0.00000      0.00000       0
    0.00267      7.80978    11.66745     31.16089     -0.93588      19
    0.00533     15.22972    23.09885     60.15959     -2.37660       4
    0.00800     21.25901    34.41877     85.33136     -3.52100       5
    0.01067     26.08938    46.20701    107.22133     -4.48458       5
    0.01333     29.88170    58.04067    125.81378     -5.31807       5
    0.01600     32.76773    69.65690    141.16955     -6.05987       5
    0.01867     34.95599    81.00170    153.98021     -6.74462       5
    0.02133     36.63934    92.18530    165.07696     -7.39810       5
    0.02400     37.20830   101.33322    169.09291     -7.85576       6
    0.02667     36.95387   108.51307    168.78061     -8.10069       6
    0.02933     36.45671   115.13228    166.86218     -8.34741       6
    0.03200     35.80833   121.97652    164.24329     -8.52735       5
    0.03467     34.95486   128.65622    160.95389     -8.65805       5
    0.03733     34.01932   135.10124    156.77189     -8.75446       5
    0.04000     32.79293   140.86952    151.65450     -8.81839       7
```

Figure H.4: Printout of file "`test.pdl`"

```
FILENAME OF THIS FILE : saframe.map
      ********************************************************
      * L = LOADING,  U = UNLOADING, H = HINGE               *
      * S = SOFTENING : A HINGE IS DEFINED WHEN THE ABS.     *
      * OF THE SLOPE OF THE MOMENT-CURVATURE RELATION AT     *
      * THE PRESENT STEP IS LESS THAN 0.05 THAT OF THE       *
      * FIRST STEP. SOFTENING IS WHEN THE PRESENT SLOPE IS   *
      * NEGATIVE AND THE RATIO OF THE ABS. SLOPES DESCRIBED  *
      * ABOVE IS GREATER THAN 0.05.                          *
      * NOTE THAT THIS OUTPUT IS JUST TO GIVE SOME           *
      * INDICATIONS OF THE BEHAVIOUR OF THE SEGMENTS---      *
      * FOR MORE ACCURATE DETERMINATION OF BEHAVIOUR,        *
      * MOMENT CURVATURE RELATIONS OF SEGMENTS HAVE TO BE    *
      * PLOTTED.                                             *
      ********************************************************
 STEP NO    0000000001111111111222222222233333333334444444444555555555556
 ********   1234567890123456789012345678901234567890123456789012345678901
E= 1   S= 1 LLLLLLLLLLLLLUU
E= 1   S= 2 LLLLLLLLLLLLHUU
E= 1   S= 3 LLLLLLLLLLLLUUU
E= 1   S= 4 LLLLLLLLLLLLUUU
E= 1   S= 5 LLLLLLLLLLLLUUU
E= 1   S= 6 LLLLLLLLLLLLHUU
E= 1   S= 7 LLLLLLLULLLLLLL
E= 1   S= 8 LLLLLLLLLUUUUUU
E= 1   S= 9 LLLLLLLLLUUUUUU
 STEP NO    0000000001111111111222222222233333333334444444444555555555556
 ********   1234567890123456789012345678901234567890123456789012345678901
E= 2   S= 1 LLLLLLLLLLLLHHH
E= 2   S= 2 LLLLLLLLLLLLLLU
E= 2   S= 3 LLLLLLLLLLLLLLH
E= 2   S= 4 LLLLLLLLLLLLLLU
E= 2   S= 5 LLLLLLLLUUUUUUU
E= 2   S= 6 LLLLLLLLLUUUUUU
E= 2   S= 7 LLLLLLLLLLUHUUU
E= 2   S= 8 LLLLLLLLLLHHUUU
E= 2   S= 9 LLLLLLLLLHHHHHH
 STEP NO    0000000001111111111222222222233333333334444444444555555555556
 ********   1234567890123456789012345678901234567890123456789012345678901
E= 3   S= 1 LLLLLLLLLHHHHHH
E= 3   S= 2 LLLLLLLLLHUUUUU
E= 3   S= 3 LLLLLLLLLUUUUUU
E= 3   S= 4 LLLLLLLLLUUUUUU
E= 3   S= 5 LLLLLUUUUULLLLL
E= 3   S= 6 LLLLLLLLLLUUULL
E= 3   S= 7 LLLLLLLLLLUHUHH
E= 3   S= 8 LLLLLLLLLLUUUUU
E= 3   S= 9 LLLLLLLLLHHHHHH
```

Figure H.5: Printout of file "`test.map`"

FILENAME OF THIS FILE : saframe.mkt

ELEMENT= 1 SEGMENT= 1

KEYCUR[1/m]	MOM[kNm]	CUR[1/m]	EI[kNm^2]	SF(x100)	THRUST[kN]
0.267E-02	-0.253E+02	-0.358E-03	70621.8172	7.8098	12.3858
0.533E-02	-0.538E+02	-0.754E-03	71309.5238	15.2297	23.1805
0.800E-02	-0.792E+02	-0.110E-02	71971.8178	21.2590	31.8704
0.107E-01	-0.102E+03	-0.140E-02	72429.2946	26.0894	38.6847
0.133E-01	-0.121E+03	-0.167E-02	72747.5412	29.8817	43.8476
0.160E-01	-0.139E+03	-0.190E-02	72994.9851	32.7677	47.5866
0.187E-01	-0.154E+03	-0.210E-02	73021.0074	34.9560	50.2540
0.213E-01	-0.166E+03	-0.229E-02	72794.2255	36.6393	52.1840
0.240E-01	-0.175E+03	-0.241E-02	72579.0142	37.2083	52.1623
0.267E-01	-0.180E+03	-0.248E-02	72350.4227	36.9539	50.9778
0.293E-01	-0.183E+03	-0.254E-02	72177.4630	36.4567	49.3892
0.320E-01	-0.186E+03	-0.259E-02	72073.7346	35.8083	47.6781
0.347E-01	-0.187E+03	-0.260E-02	71948.2139	34.9549	45.8686
0.373E-01	-0.186E+03	-0.259E-02	71886.3365	34.0193	44.0518
0.400E-01	-0.183E+03	-0.255E-02	71785.2798	32.7929	41.9048

ELEMENT= 1 SEGMENT= 2

KEYCUR[1/m]	MOM[kNm]	CUR[1/m]	EI[kNm^2]	SF(x100)	THRUST[kN]
0.267E-02	-0.288E+02	-0.407E-03	70621.8172	7.8098	12.3858
0.533E-02	-0.600E+02	-0.841E-03	71309.5238	15.2297	23.1805
0.800E-02	-0.872E+02	-0.121E-02	71971.8178	21.2590	31.8704
0.107E-01	-0.111E+03	-0.153E-02	72429.2946	26.0894	38.6847
0.133E-01	-0.131E+03	-0.180E-02	72747.5412	29.8817	43.8476
0.160E-01	-0.148E+03	-0.203E-02	72998.6707	32.7677	47.5866
0.187E-01	-0.162E+03	-0.223E-02	72737.5678	34.9560	50.2540
0.213E-01	-0.174E+03	-0.240E-02	72543.8432	36.6393	52.1840
0.240E-01	-0.182E+03	-0.251E-02	72398.4860	37.2083	52.1623
0.267E-01	-0.186E+03	-0.257E-02	72215.7184	36.9539	50.9778
0.293E-01	-0.189E+03	-0.262E-02	72085.5014	36.4567	49.3892
0.320E-01	-0.191E+03	-0.265E-02	71963.7315	35.8083	47.6781
0.347E-01	-0.191E+03	-0.265E-02	71833.7765	34.9549	45.8686
0.373E-01	-0.189E+03	-0.263E-02	71746.1492	34.0193	44.0518
0.400E-01	-0.186E+03	-0.259E-02	71708.7295	32.7929	41.9048

ELEMENT= 1 SEGMENT= 3

KEYCUR[1/m]	MOM[kNm]	CUR[1/m]	EI[kNm^2]	SF(x100)	THRUST[kN]
0.267E-02	-0.294E+02	-0.416E-03	70621.8172	7.8098	12.3858
0.533E-02	-0.607E+02	-0.852E-03	71309.5238	15.2297	23.1805
0.800E-02	-0.875E+02	-0.122E-02	71971.8178	21.2590	31.8704
0.107E-01	-0.110E+03	-0.152E-02	72429.2946	26.0894	38.6847
0.133E-01	-0.129E+03	-0.178E-02	72747.5412	29.8817	43.8476
0.160E-01	-0.145E+03	-0.199E-02	73002.5026	32.7677	47.5866
0.187E-01	-0.158E+03	-0.217E-02	72879.0224	34.9560	50.2540
0.213E-01	-0.169E+03	-0.233E-02	72684.8698	36.6393	52.1840
0.240E-01	-0.176E+03	-0.242E-02	72524.1642	37.2083	52.1623
0.267E-01	-0.179E+03	-0.247E-02	72369.8556	36.9539	50.9778
0.293E-01	-0.181E+03	-0.251E-02	72223.2322	36.4567	49.3892
0.320E-01	-0.182E+03	-0.253E-02	72115.9132	35.8083	47.6781
0.347E-01	-0.182E+03	-0.253E-02	71999.7779	34.9549	45.8686
0.373E-01	-0.180E+03	-0.250E-02	71912.8189	34.0193	44.0518
0.400E-01	-0.177E+03	-0.246E-02	71807.0827	32.7929	41.9048

ELEMENT= 1 SEGMENT= 4

KEYCUR[1/m]	MOM[kNm]	CUR[1/m]	EI[kNm^2]	SF(x100)	THRUST[kN]
0.267E-02	-0.272E+02	-0.385E-03	70621.8172	7.8098	12.3858
0.533E-02	-0.560E+02	-0.785E-03	71309.5238	15.2297	23.1805
0.800E-02	-0.802E+02	-0.111E-02	71971.8178	21.2590	31.8704
0.107E-01	-0.100E+03	-0.139E-02	72429.2946	26.0894	38.6847
0.133E-01	-0.117E+03	-0.161E-02	72747.5412	29.8817	43.8476
0.160E-01	-0.131E+03	-0.179E-02	72994.9851	32.7677	47.5866
0.187E-01	-0.142E+03	-0.193E-02	73234.6804	34.9560	50.2540
0.213E-01	-0.151E+03	-0.206E-02	73195.4274	36.6393	52.1840
0.240E-01	-0.156E+03	-0.214E-02	73048.3814	37.2083	52.1623
0.267E-01	-0.159E+03	-0.218E-02	72895.0103	36.9539	50.9778
0.293E-01	-0.161E+03	-0.221E-02	72743.8245	36.4567	49.3892
0.320E-01	-0.161E+03	-0.222E-02	72638.2499	35.8083	47.6781

Figure H.6: First page printout of file "`test.mkt`"

```
 0.800E-02 -0.206E+02   -0.106E-02   19364.5479    21.2590   547.6600
 0.107E-01 -0.260E+02   -0.129E-02   20174.0187    26.0894   673.4535
 0.133E-01 -0.306E+02   -0.151E-02   20244.8691    29.8817   772.8702
 0.160E-01 -0.345E+02   -0.173E-02   19964.8845    32.7677   849.1439
 0.187E-01 -0.377E+02   -0.191E-02   19742.2071    34.9560   907.5519
 0.213E-01 -0.406E+02   -0.207E-02   19566.5320    36.6393   952.9878
 0.240E-01 -0.420E+02   -0.215E-02   19503.5294    37.2083   969.1373
 0.267E-01 -0.424E+02   -0.217E-02   19524.3974    36.9539   963.7824
 0.293E-01 -0.423E+02   -0.217E-02   19520.6446    36.4567   952.0370
 0.320E-01 -0.423E+02   -0.217E-02   19519.1527    35.8083   936.3591
 0.347E-01 -0.421E+02   -0.216E-02   19508.8932    34.9549   915.0494
 0.373E-01 -0.422E+02   -0.216E-02   19514.2031    34.0193   891.3314
 0.400E-01 -0.428E+02   -0.219E-02   19553.1897    32.7929   859.9407
ELEMENT=      3SEGMENT=      7
KEYCUR[1/m]   MOM[kNm]     CUR[1/m]     EI[kNm^2]     SF(x100)  THRUST[kN]
 0.267E-02 -0.152E+02   -0.115E-02   13173.1133     7.8098   200.4025
 0.533E-02 -0.304E+02   -0.175E-02   17380.1961    15.2297   391.5657
 0.800E-02 -0.423E+02   -0.228E-02   18519.0794    21.2590   547.6600
 0.107E-01 -0.525E+02   -0.294E-02   17874.7442    26.0894   673.4535
 0.133E-01 -0.617E+02   -0.360E-02   17128.0237    29.8817   772.8702
 0.160E-01 -0.695E+02   -0.421E-02   16497.8379    32.7677   849.1439
 0.187E-01 -0.760E+02   -0.477E-02   15951.7031    34.9560   907.5519
 0.213E-01 -0.816E+02   -0.527E-02   15483.8925    36.6393   952.9878
 0.240E-01 -0.846E+02   -0.557E-02   15191.6651    37.2083   969.1373
 0.267E-01 -0.851E+02   -0.565E-02   15067.3183    36.9539   963.7824
 0.293E-01 -0.845E+02   -0.564E-02   14964.0596    36.4567   952.0370
 0.320E-01 -0.840E+02   -0.565E-02   14859.2272    35.8083   936.3591
 0.347E-01 -0.829E+02   -0.564E-02   14699.0522    34.9549   915.0494
 0.373E-01 -0.821E+02   -0.565E-02   14520.0014    34.0193   891.3314
 0.400E-01 -0.813E+02   -0.571E-02   14248.8857    32.7929   859.9407
ELEMENT=      3SEGMENT=      8
KEYCUR[1/m]   MOM[kNm]     CUR[1/m]     EI[kNm^2]     SF(x100)  THRUST[kN]
 0.267E-02 -0.229E+02   -0.174E-02   13173.1133     7.8098   200.4025
 0.533E-02 -0.451E+02   -0.321E-02   14072.9554    15.2297   391.5657
 0.800E-02 -0.628E+02   -0.462E-02   13596.1206    21.2590   547.6600
 0.107E-01 -0.789E+02   -0.611E-02   12912.4415    26.0894   673.4535
 0.133E-01 -0.928E+02   -0.758E-02   12237.7191    29.8817   772.8702
 0.160E-01 -0.104E+03   -0.898E-02   11623.9437    32.7677   849.1439
 0.187E-01 -0.114E+03   -0.103E-01   11088.3065    34.9560   907.5519
 0.213E-01 -0.123E+03   -0.116E-01   10604.3598    36.6393   952.9878
 0.240E-01 -0.127E+03   -0.123E-01   10297.0396    37.2083   969.1373
 0.267E-01 -0.128E+03   -0.125E-01   10208.1474    36.9539   963.7824
 0.293E-01 -0.127E+03   -0.125E-01   10182.5180    36.4567   952.0370
 0.320E-01 -0.126E+03   -0.124E-01   10110.4793    35.8083   936.3591
 0.347E-01 -0.124E+03   -0.123E-01   10018.7675    34.9549   915.0494
 0.373E-01 -0.122E+03   -0.123E-01    9942.9907    34.0193   891.3314
 0.400E-01 -0.120E+03   -0.123E-01    9789.4623    32.7929   859.9407
ELEMENT=      3SEGMENT=      9
KEYCUR[1/m]   MOM[kNm]     CUR[1/m]     EI[kNm^2]     SF(x100)  THRUST[kN]
 0.267E-02 -0.306E+02   -0.260E-02   11794.3127     7.8098   200.4025
 0.533E-02 -0.589E+02   -0.516E-02   11431.7134    15.2297   391.5657
 0.800E-02 -0.838E+02   -0.774E-02   10825.0561    21.2590   547.6600
 0.107E-01 -0.105E+03   -0.103E-01   10185.1418    26.0894   673.4535
 0.133E-01 -0.124E+03   -0.130E-01    9551.0752    29.8817   772.8702
 0.160E-01 -0.139E+03   -0.156E-01    8927.0285    32.7677   849.1439
 0.187E-01 -0.152E+03   -0.182E-01    8346.1166    34.9560   907.5519
 0.213E-01 -0.164E+03   -0.209E-01    7822.5637    36.6393   952.9878
 0.240E-01 -0.169E+03   -0.233E-01    7251.6915    37.2083   969.1373
 0.267E-01 -0.169E+03   -0.256E-01    6624.0890    36.9539   963.7824
 0.293E-01 -0.168E+03   -0.279E-01    6027.4325    36.4567   952.0370
 0.320E-01 -0.166E+03   -0.302E-01    5497.7563    35.8083   936.3591
 0.347E-01 -0.164E+03   -0.325E-01    5037.0752    34.9549   915.0494
 0.373E-01 -0.161E+03   -0.347E-01    4655.6340    34.0193   891.3314
 0.400E-01 -0.159E+03   -0.364E-01    4373.7314    32.7929   859.9407
```

Figure H.7: Last page printout of file "`test.mkt`"

```
FILENAME OF THIS FILE : saframe.out
TITLE :sample input for saframe.f


IPDEL =    1

IPRINM =    0

DEGREE OF MOVEMENT OF NODE TO PRINT:      1
DEFLN OF ELEM,SEG TO PRINT:     1,     5
KEY ELEMENT =     3
KEY SEGMENT =     1
NO OF LAYERS FOR SECTION =    15

MAXIMUM CURVATURE =  0.040000
NO OF DIVISION FOR CURVATURE =   15

TOLERANCE=    0.010000

TOLERENCE(SECTION)=    0.001000

NODE          X-VALUE      Y-VALUE       ND1          ND2          ND3
    1         0.000000     5.400000        1            1            1
    2         5.400000     5.400000        1            1            1
    3         0.000000     0.000000        0            0            0
    4         5.400000     0.000000        0            0            0

ELEMENT    FROM TO  NSEG      GAMMA1     GAMMA2     FCMAX      ECMAX
      1     1    2     9       1.9900     3.0000    29.7500     0.0020
      2     1    3     9       1.9900     3.0000    29.7500     0.0020
      3     2    4     9       1.9900     3.0000    29.7500     0.0020

STEEL DATA
MODULUS OF ELASTICITY =0.2000E+06
YIELD STRESS =  460.0000

SEGMENTS DETAIL
***************

ELEMENT  NO =      1
NSEG    WIDTH      DEPTH    NBARS AST-TOP     DST-TOP   AST-BOT     DST-BOT
  1     300.00     600.00     2   1800.00      50.00    1800.00     550.00
  2     300.00     600.00     2   1800.00      50.00    1800.00     550.00
  3     300.00     600.00     2   1800.00      50.00    1800.00     550.00
  4     300.00     600.00     2   1800.00      50.00    1800.00     550.00
  5     300.00     600.00     2   1800.00      50.00    1800.00     550.00
  6     300.00     600.00     2   1800.00      50.00    1800.00     550.00
  7     300.00     600.00     2   1800.00      50.00    1800.00     550.00
  8     300.00     600.00     2   1800.00      50.00    1800.00     550.00
  9     300.00     600.00     2   1800.00      50.00    1800.00     550.00

ELEMENT  NO =      2
NSEG    WIDTH      DEPTH    NBARS AST-TOP     DST-TOP   AST-BOT     DST-BOT
  1     300.00     300.00     2    900.00      50.00     900.00     250.00
  2     300.00     300.00     2    900.00      50.00     900.00     250.00
  3     300.00     300.00     2    900.00      50.00     900.00     250.00
  4     300.00     300.00     2    900.00      50.00     900.00     250.00
  5     300.00     300.00     2    900.00      50.00     900.00     250.00
  6     300.00     300.00     2    900.00      50.00     900.00     250.00
  7     300.00     300.00     2    900.00      50.00     900.00     250.00
  8     300.00     300.00     2    900.00      50.00     900.00     250.00
  9     300.00     300.00     2    900.00      50.00     900.00     250.00

ELEMENT  NO =      3
NSEG    WIDTH      DEPTH    NBARS AST-TOP     DST-TOP   AST-BOT     DST-BOT
  1     300.00     300.00     2    900.00      50.00     900.00     250.00
```

Figure H.8: First page printout of file "`test.out`"

```
  2    300.00    300.00    2    900.00    50.00    900.00    250.00
  3    300.00    300.00    2    900.00    50.00    900.00    250.00
  4    300.00    300.00    2    900.00    50.00    900.00    250.00
  5    300.00    300.00    2    900.00    50.00    900.00    250.00
  6    300.00    300.00    2    900.00    50.00    900.00    250.00
  7    300.00    300.00    2    900.00    50.00    900.00    250.00
  8    300.00    300.00    2    900.00    50.00    900.00    250.00
  9    300.00    300.00    2    900.00    50.00    900.00    250.00

NODAL LOAD
----------
  NODE          PX           PY           PZ
    1         270.00     -2160.00        0.00
    2           0.00     -2160.00        0.00
 MEM     LT         VL           A
 ---     --         --           -
  1      1       -100.00        0.00
-------------------------------------------------------------------------------

TARGETED ELEMENT NUMBER =      3
TARGETED SEGMENT NUMBER =      1
    TARGETED CURVATURE =     0.0027
    SCALE FACTOR=      0.1359  ICONGE =      0
TARGETED ELEMENT NUMBER =      3
TARGETED SEGMENT NUMBER =      1
    TARGETED CURVATURE =     0.0027
    SCALE FACTOR=      0.1111  ICONGE =      0
TARGETED ELEMENT NUMBER =      3
TARGETED SEGMENT NUMBER =      1
    TARGETED CURVATURE =     0.0027
    SCALE FACTOR=      0.0996  ICONGE =      0
TARGETED ELEMENT NUMBER =      3
TARGETED SEGMENT NUMBER =      1
    TARGETED CURVATURE =     0.0027
    SCALE FACTOR=      0.0925  ICONGE =      0
TARGETED ELEMENT NUMBER =      3
TARGETED SEGMENT NUMBER =      1
    TARGETED CURVATURE =     0.0027
    SCALE FACTOR=      0.0877  ICONGE =      0
TARGETED ELEMENT NUMBER =      3
TARGETED SEGMENT NUMBER =      1
    TARGETED CURVATURE =     0.0027
    SCALE FACTOR=      0.0846  ICONGE =      0
TARGETED ELEMENT NUMBER =      3
TARGETED SEGMENT NUMBER =      1
    TARGETED CURVATURE =     0.0027
    SCALE FACTOR=      0.0824  ICONGE =      0
TARGETED ELEMENT NUMBER =      3
TARGETED SEGMENT NUMBER =      1
    TARGETED CURVATURE =     0.0027
    SCALE FACTOR=      0.0810  ICONGE =      0
TARGETED ELEMENT NUMBER =      3
TARGETED SEGMENT NUMBER =      1
    TARGETED CURVATURE =     0.0027
    SCALE FACTOR=      0.0801  ICONGE =      0
TARGETED ELEMENT NUMBER =      3
TARGETED SEGMENT NUMBER =      1
    TARGETED CURVATURE =     0.0027
    SCALE FACTOR=      0.0794  ICONGE =      0
TARGETED ELEMENT NUMBER =      3
TARGETED SEGMENT NUMBER =      1
    TARGETED CURVATURE =     0.0027
    SCALE FACTOR=      0.0790  ICONGE =      0
TARGETED ELEMENT NUMBER =      3
TARGETED SEGMENT NUMBER =      1
    TARGETED CURVATURE =     0.0027
```

Figure H.9: Second page printout of file "`test.out`"

```
    SCALE FACTOR=      0.0787  ICONGE =      0
TARGETED ELEMENT NUMBER =      3
TARGETED SEGMENT NUMBER =      1
    TARGETED CURVATURE =      0.0027
    SCALE FACTOR=      0.0785  ICONGE =      0
TARGETED ELEMENT NUMBER =      3
TARGETED SEGMENT NUMBER =      1
    TARGETED CURVATURE =      0.0027
    SCALE FACTOR=      0.0784  ICONGE =      0
TARGETED ELEMENT NUMBER =      3
TARGETED SEGMENT NUMBER =      1
    TARGETED CURVATURE =      0.0027
    SCALE FACTOR=      0.0783  ICONGE =      0
TARGETED ELEMENT NUMBER =      3
TARGETED SEGMENT NUMBER =      1
    TARGETED CURVATURE =      0.0027
    SCALE FACTOR=      0.0782  ICONGE =      0
TARGETED ELEMENT NUMBER =      3
TARGETED SEGMENT NUMBER =      1
    TARGETED CURVATURE =      0.0027
    SCALE FACTOR=      0.0781  ICONGE =      0
TARGETED ELEMENT NUMBER =      3
TARGETED SEGMENT NUMBER =      1
    TARGETED CURVATURE =      0.0027
    SCALE FACTOR=      0.0781  ICONGE =      0
TARGETED ELEMENT NUMBER =      3
TARGETED SEGMENT NUMBER =      1
    TARGETED CURVATURE =      0.0027
    SCALE FACTOR=      0.0781  ICONGE =      1
-------------------------------------------------------------------------------
TARGETED CURVATURE =      0.0027
LOAD FACTOR =      0.0781

ELEMENT DEFORMATIONS
 MEM   DEL1X       DEL1Y        ROT1       DEL2X       DEL2Y        ROT2
  1   0.0117      0.0000      -.0009      0.0132      0.0000      0.0001
  2   0.0000      0.0117      -.0009         0.          0.          0.
  3   0.0000      0.0132      0.0001         0.          0.          0.

ELEMENT FORCES
 MEM   F1X         F1Y          M1         F2X         F2Y          M2
  1    12.39       10.43      -22.53      -12.39       31.74      -35.01
  2    179.1       9.088       22.53      -179.1      -9.088       26.54
  3    200.4       12.87       35.01      -200.4      -12.87       34.51

NODAL DEFORMATION
   NODE    DELX          DELY          ROT
     1    0.0117        0.0000        -.0009
     2    0.0132        0.0000        0.0001
     3       0.            0.            0.
     4       0.            0.            0.

ELEMENT NO =      1
DIST(m)  MOM(kNm)   ROT(rad)   DEFN(m)   CUR(1/m)   EI(kNm^2)  STR-TOP    STR-BOT
 0.300    -25.32   -0.65D-03 -0.27D-03 -.36D-03   0.71D+05   0.32D-03   0.11D-03
 2.700    -22.23    0.27D-03 -0.94D-03 -.31D-03   0.71D+05   0.32D-03   0.14D-03
 5.100     25.86    0.12D-03 -0.79D-04 0.37D-03   0.71D+05  -0.87D-03  -0.66D-03

ELEMENT NO =      2
DIST(m)  MOM(kNm)   ROT(rad)   DEFN(m)   CUR(1/m)   EI(kNm^2)  STR-TOP    STR-BOT
 0.300     19.78   -0.18D-02  0.11D-01 0.16D-02   0.13D+05  -0.30D-03   0.17D-03
 5.100    -23.80   -0.14D-17 -0.35D-17 -.19D-02   0.13D+05   0.30D-03  -0.27D-03

ELEMENT NO =      3
DIST(m)  MOM(kNm)   ROT(rad)   DEFN(m)   CUR(1/m)   EI(kNm^2)  STR-TOP    STR-BOT
 0.300     31.16   -0.15D-02  0.13D-01 0.27D-02   0.12D+05  -0.43D-03   0.37D-03
```

Figure H.10: Third page printout of file "`test.out`"

```
5.100  -30.62     0.81D-18  0.24D-17 -.26D-02  0.12D+05  0.37D-03 -0.41D-03
-------------------------------------------------------------------------------
    SCALE FACTOR=      0.1562  ICONGE =     0
    SCALE FACTOR=      0.1540  ICONGE =     0
    SCALE FACTOR=      0.1528  ICONGE =     0
    SCALE FACTOR=      0.1523  ICONGE =     1
-------------------------------------------------------------------------------
TARGETED CURVATURE =      0.0053
LOAD FACTOR =      0.1523

ELEMENT DEFORMATIONS
 MEM   DEL1X       DEL1Y       ROT1       DEL2X       DEL2Y       ROT2
  1   0.0231      -.0005      -.0018      0.0245      -.0005      0.0003
  2   0.0004      0.0231      -.0018        0.          0.          0.
  3   0.0004      0.0245      0.0003        0.          0.          0.

ELEMENT FORCES
 MEM   F1X         F1Y         M1          F2X         F2Y         M2
  1    23.18       19.53      -48.56      -23.18       62.71      -68.04
  2    348.4       19.43       48.56      -348.4      -19.43       56.35
  3    391.6       24.96       68.04      -391.6      -24.96       66.76

NODAL DEFORMATION
   NODE    DELX          DELY          ROT
    1    0.0231        -.0005        -.0018
    2    0.0245        -.0005        0.0003
    3      0.            0.            0.
    4      0.            0.            0.

ELEMENT NO =      1
DIST(m)  MOM(kNm)   ROT(rad)    DEFN(m)    CUR(1/m)   EI(kNm^2)  E-TOP       E-BOT
 0.300    -53.75   -0.13D-02  -0.10D-02  -.75D-03   0.71D+05  0.33D-03  -0.12D-03
 2.700    -45.79    0.56D-03  -0.24D-02  -.64D-03   0.71D+05  0.33D-03  -0.55D-04
 5.100     50.01    0.31D-03  -0.59D-03   0.70D-03  0.71D+05 -0.87D-03  -0.45D-03

ELEMENT NO =      2
DIST(m)  MOM(kNm)   ROT(rad)    DEFN(m)    CUR(1/m)   EI(kNm^2)  E-TOP       E-BOT
 0.300     43.05   -0.37D-02   0.23D-01   0.32D-02   0.13D+05 -0.44D-03   0.52D-03
 5.100    -49.71    0.69D-17   0.15D-16  -.41D-02   0.12D+05  0.61D-03  -0.63D-03

ELEMENT NO =      3
DIST(m)  MOM(kNm)   ROT(rad)    DEFN(m)    CUR(1/m)   EI(kNm^2)  E-TOP       E-BOT
 0.300     60.16   -0.29D-02   0.25D-01   0.53D-02   0.11D+05 -0.84D-03   0.76D-03
 5.100    -58.93    0.48D-17   0.29D-16  -.52D-02   0.11D+05  0.74D-03  -0.81D-03
-------------------------------------------------------------------------------
    SCALE FACTOR=      0.2272  ICONGE =     0
    SCALE FACTOR=      0.2195  ICONGE =     0
    SCALE FACTOR=      0.2154  ICONGE =     0
    SCALE FACTOR=      0.2138  ICONGE =     0
    SCALE FACTOR=      0.2126  ICONGE =     1
-------------------------------------------------------------------------------
TARGETED CURVATURE =      0.0080
LOAD FACTOR =      0.2126

ELEMENT DEFORMATIONS
 MEM   DEL1X       DEL1Y       ROT1       DEL2X       DEL2Y       ROT2
  1   0.0344      -.0008      -.0025      0.0358      -.0009      0.0004
  2   0.0006      0.0344      -.0025        0.          0.          0.
  3   0.0006      0.0358      0.0004        0.          0.          0.

ELEMENT FORCES
 MEM   F1X         F1Y         M1          F2X         F2Y         M2
  1    31.87       26.11      -72.24      -31.87       88.69      -96.74
  2    485.1       28.64       72.24      -485.1      -28.64       82.44
  3    547.7       35.53       96.74      -547.7      -35.53       95.14
```

Figure H.11: Fourth page printout of file "`test.out`"

Appendix I

Programs for Bottom-tier Method of Analysis

A suite of computer programs has been developed to facilitate design and ultimate strength calculations for slender reinforced concrete frames based on the moment magnifier method of the Australian concrete standard AS3600.

All the programs were developed using Fortran77 language to run in a UNIX operating environment. The advantage of having all the programs within one operating system is that users can execute the programs without having to change over to another system. This also enables all the input and output files to be kept together, therefore, easing the task of interpreting the results.

The programs developed to carry out the moment magnifier method of analysis are listed below:

`LINFRAME` : A standard first-order, linear elastic frame analysis program using a stiffness approach.

`NMAUSTD` and `NMAUST` : Programs to generate data points used to define the strength column interaction diagram. Program `NMAUST` produces N-M points for the ultimate strength condition, whereby the strength reduction factor ϕ is assumed to be unity. Program `NMAUSTD` produces N-M points for the design strength condition, whereby all strength reduction factors are included.

`LOADCURVD` and `LOADCURV` : Programs to generate data points used to define the loading curves for individual column and for the column taking into consideration storey stability effect. Program `LOADCURV` generates loading curves for ultimate strength condition and program `LOADCURVD` generates loading curves for design strength condition.

`INTERSECB` : A program to locate the intersection point between the linearised curve fitted to data produced by program `NMAUST` and that fitted to data produced by program `LOADCURV`, or between the curve fitted to data produced by program `NMAUSTD` and that fitted to data produced by program `LOADCURVD`.

Program `LINFRAME` is a standard first-order elastic analysis program. Algorithms used in this program can be obtained from numerous texts on structural analysis(Hall and Kabaila, 1977; Cheung and Yeo, 1979).

Programs `NMAUST` and program `NMAUSTD` are used to generate the strength interaction diagrams of reinforced concrete columns with symmetrically placed reinforcement. The section analysis is based on the use of the rectangular stress block as outlined in AS3600. A description of program `NMAUST` is given in Appendix D.

Programs `LOADCURV` and `LOADCURVD` generate output files consisting of N-M values which define the loading curves based on the "braced" moment magnifier of braced column, δ_b, and on the "sway" moment magnifier, δ_s. The former file

is automatically assigned a filename with suffix "nmc" and the latter a filename with suffix "nms". The equations used to generate these files are Equation 7.11 for the former and Equation 7.13 for the latter.

Program INTERSECB first reads in the M-N points defining the interaction curve for the column section generated by program NMAUST(or NMAUSTD). The loading curve data, in the form of M-N points, stored in the file with suffix "nmc" is then read in. To obtain complete curves from individual data points, straight lines are used to connect neighbouring data points. The error brought about by this approximation is small provided the data points are not too far apart. An intersection point between the two linearised curves is obtained. The eccentricity of the solution point is then checked to see if it is greater then eccentricity e_2. If it is less than e_2, the intersection point does not satisfy the minimum moment magnifier of unity as stipulated by AS3600. If this is the case, a revised intersection point is chosen to be that between the loading line with a constant eccentricity value of e_2 (which is the loading line with a moment magnifier of unity) and the interaction curve. The loading curve with suffix "nms" is then read in, and another intersection point with the interaction curve is obtained. Of the two intersection points, the one with the lower N value gives the ultimate strength of the column. The N value of the lowest intersection points is obtained from the output of this program, which is automatically given the same file name as the input file but with the suffix changed to "met".

The suite of programs has been developed to enable maximum interaction between the different programs. Therefore, in some cases, the output files generated by some programs are in turn being used as input files for other programs. The users, therefore, need not reproduce these data, hence eliminating human errors caused by keying in incorrect data. For proper documentation of the output data files, input data are printed out in the output files. The printing of lines of input data in the output files enables ease of checking by the

users. These lines are ignored by those programs which use these files as input data files. In order to keep tab of the numerous input and output files produced during analysis, each of them is identifiable by using a filename with an identifiable prefix (eg. "`t`", "`m`" and "`b`" where `t`=top-tier, `m`=middle-tier and `b`=bottom-tier) and an identifiable suffix at the end (eg. "`inp`", "`out`", "`pdl`", "`nmc`", "`nms`", "`int`", etc.). An example of the filename for the input file of run "run1" using the bottom-tier method is "`b_run1.inp`". The automatic assignment of suffix for names of output files prevents the users from keying in the wrong suffix which can create confusion later in locating the output files. This also safeguard against the possibility of accidental deletion of existing files cause by not using the correct suffix.

The inter-relation between different input and output files, and their relationships with the programs listed earlier, are illustrated in the schematic diagram in Figure I.1.

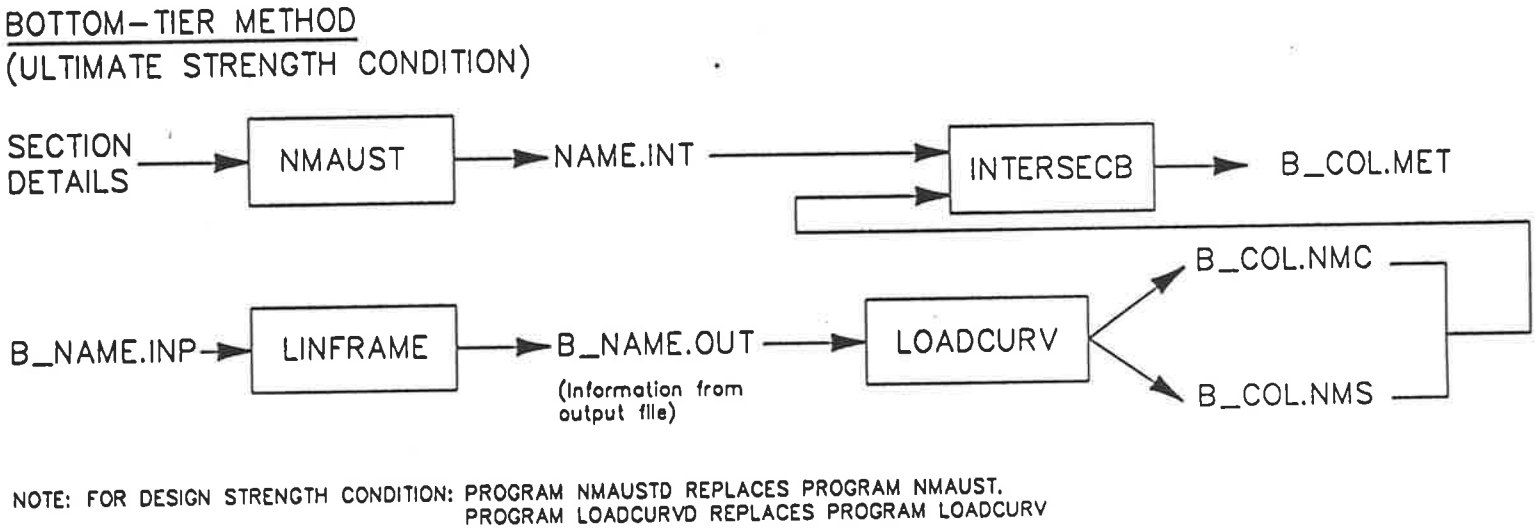

Figure I.1: Schematic diagram showing the relationship of files and programs for the bottom-tier method

Appendix J

Programs for Middle-tier Method of Analysis

A suite of computer programs was developed to allow the determination of ultimate and design strengths of slender reinforced concrete frames based on the middle-tier method of the Australian standard AS3600.

The programs developed to carry out the middle-tier method of analysis are listed below:

`NEWTONR` : A complete second-order elastic frame program using the nonlinear equilibrium equations proposed by Jennings(1968), and using the Newton-Raphson technique to solve these equations.

`CRISFIEL` : A complete second-order elastic frame analysis program using the nonlinear equilibrium equations proposed by Jennings(1968), and using the Newton-Raphson limit-point traversal technique of Crisfield(1980).

`NMAUSTD` and `NMAUST` : Programs to generate data points used to obtain strength column interaction diagrams, as described in Appendix I.

`INTERSECM` : A program to locate the intersection point between the linearised curve fitted to data produced by program `NMAUST` and that fitted to data produced by program `NEWTONR`.

Program `NEWTONR` is a nonlinear elastic analysis program which takes account of all geometrical nonlinearities present in a framed structure. The matrices to account for second-order effects are those proposed by Jennings(1968) described in Chapter 3. The program uses a Newton-Raphson technique, also described in Chapter 3, to solve the nonlinear equilibrium equations proposed by Jennings. The behaviour of the structure is obtained by controlling the load. The accuracy of this program has been checked by comparing analytical results obtained for a simple cantilever and a portal frame (see Appendix G).

Even though a more advanced program `CRISFIEL` was developed to allow traversing of limit points, it was not used as program `NEWTONR` was found to be sufficient to carry the present study.

The inter-relation between different input and output files, and their relationships with the programs listed earlier, are illustrated in the schematic diagram in Figure J.1.

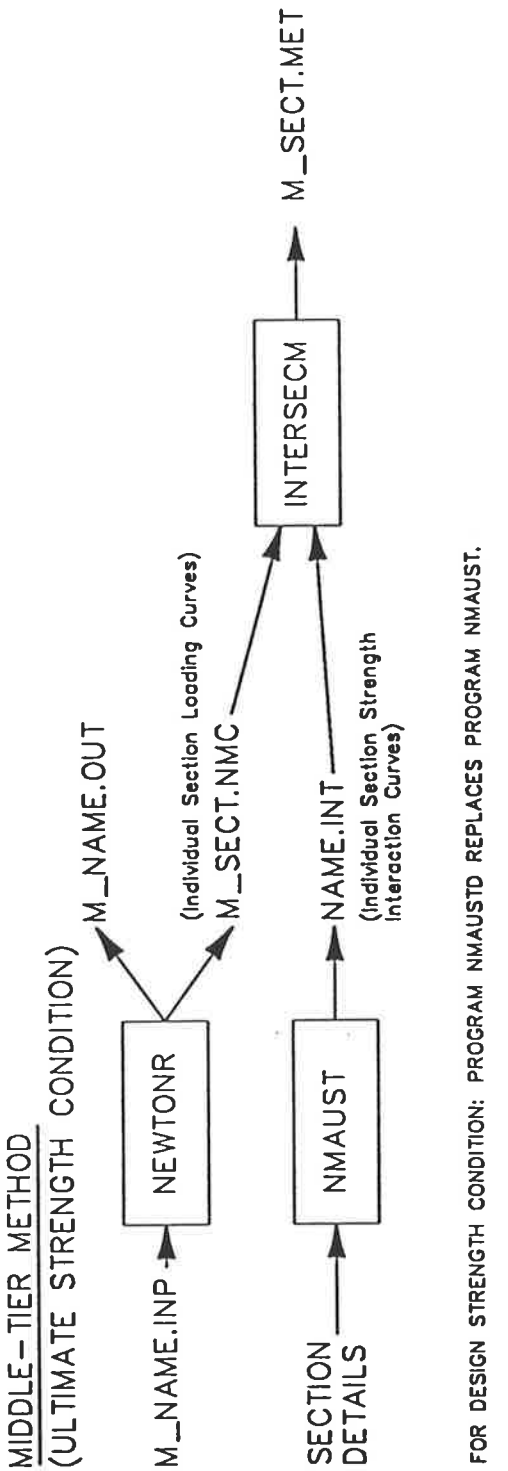

Figure J.1: Schematic diagram showing the relationship of files and programs for the middle-tier method

Bibliography

[1] Aas-Jakobsen, A. and Grenacher, M.(1974), "Analysis of Slender Reinforced Concrete Frames," *Publications, IABSE,* Vol.34-1, Zurich, pp.1-17.

[2] ACI Committee 318 (1983), "Building Code Requirements for Reinforced Concrete (ACI 318-83)," *American Concrete Institute,* Detroit, 111 pp.

[3] Adobe System Incoporated (1985), *Postscript Language Reference Manual,* Addison-Wesley Publishing Inc.

[4] Aguado, A., Murcia, J. and Mari, A.(1981), "Nonlinear Analysis of Concrete Structures by the Imposed Deformations Method Comparison with Experimental Results," *Report, IABSE Colloguim,* Delft, pp.255-262.

[5] Ahmad, A. and Warner, R.F.(1984), "Ductility Requirements for Continuous Reinforced Concrete Structures," *Research Report No. R62, Dept. of Civil Engineering, Univ. of Adelaide,* January, 23 pp.

[6] Ahmad, S.H. and Shah, S.P.(1979), "Complete Stress-Strain Curve of Concrete and Nonlinear Design," *CSCE-ASCE-ACI-CEB Int. Symp. on Nonlinear Design of Concrete Structures, Univ. of Waterloo, Ontario, Canada,* August, pp.61-80.

[7] American Institute of Steel Construction(1963), *Specification for the Design, Fabrication and Erection of Structural Steel for Buildings,* New York.

[8] Aldstedt, E. and Bergen, P.G.(1974), "Large Deformation and Stability Analysis of Reinforced Concrete Frames Considering Material Nonlinearities," *IABSE Symposium on Design and Safety of Reinforced Conc. Compression Members, Quebec,* pp.21-28.

[9] AS3600-1988 (1988), *SAA Concrete Structures Code,* Standard Association of Australia, 108 pp.

[10] Baker, A.L.L and Amarakone, A.M.N.(1964) "Inelastic Hyperstatic Frame Analysis," *Proceedinds of the International Symposium on the Flexural Mechanics of Reinforced Concrete, Maimi,* ACI SP-12, pp.501-520.

[11] Bakoss, S.L.(1985), "Non-linear and Time-dependent Behaviour of Reinforced Concrete Skeletal Structures," *Ph.D. Thesis, University of New South Wales,* April, 348 pp.

[12] Bakoss, S.L. and Corderoy, H.J.B.(1983), "Analysis of Non-Linear Behaviour of Reinforced Concrete Frames," *Conference on Computers and Engineering, Sydney, Inst. Engrs Aust.,* August-September, pp.84-89.

[13] Barnard, P.R.(1964), "Discussion of Paper Titled - Instability Consideration on Limit Design of Concrete Frames by E. Rosenblueth and R. Diaz De Cossio," *Proceedings International Symposium on The Flexural Mechanics of Reinforced Concrete, Miami, ACI Special Publication SP-12,* pp.439-464.

[14] Batoz, J. and Dhatt, G.(1979), "Incremental Displacement Algorithms for Nonlinear Problems," *International Journal for Numerical Methods in Engineering,* Vol.14, pp.1262-1267.

[15] Bažant, Z.P.(1976) "Instability, Ductility and Size Effect in Strain-softening Concrete," *Journal of the Engineering Mechanics Division,* ASCE, Vol.102, No.EM2, April, pp.331-344.

[16] Bažant, Z.P.(1984) "Continuum Theory for Strain-Softening," *Journal of the Engineering Mechanics Division,* ASCE, Vol.110, No.EM12, December, pp.1666-1692.

[17] Bažant, Z.P. and Oh, B.H.(1984), "Deformation of Progressively Cracking Reinforced Concrete Beam," *ACI Journal,* Vol. 81, No.3, May-June, pp.268-278.

[18] Bažant, Z.P., Pan, J. and Pijaudier-Cabot, G.(1987a), "Softening in Reinforced Concrete Beams and Frames," *Journal of the Structural Division,* Vol.113, No.12, December, pp.2333-2347.

[19] Bažant, Z.P., Pijaudier-Cabot, G. and Pan, J.(1987b), "Ductility, Snapback, Size Effect, and Redistribution in Softening Beams or Frames," *Journal of Structural Division,* Vol.113, No.12, December, pp.2348-2364.

[20] Beal, A.N.(1986), "The Design of Slender Columns," *Proc. Instn Civil Engrs (London),* Vol.81, Part 2, September, pp.379-414.

[21] Becker, J.M.(1967), "Inelastic Analysis of Reinforced Concrete Frames," *Master of Science Thesis, Lehigh University at Bethlehem, Pa.*

[22] Bennett, E.(1964), "Flexural Rigidity, Curvature and Rotation and their Significance in Reinforced Concrete Design," *Magazine of Concrete Research,* Vol.16, No. 47, June, pp.67-72.

[23] Bergan, P.G.(1980a), "Automated Incremental-Iterative Solution Schemes," *Numerical Methods for Nonlinear Problems, Vol.1 (Eds. Taylor, C., Hinton, E. and Owen, D.R.J.), Pine Ridge Press, Swansea,* pp.291-305.

[24] Bergan, P.G.(1980b) "Solution Algorithms for Nonlinear Structural Problems," *Computers and Structures,* Volume 12, pp.497-509.

[25] Bergan, P.G. and Clough, R.W.(1972), "Convergence Criteria for Iterative Processes," *AIAA Journal,* Vol.10, No.8, August, pp.1107-1109.

[26] Bertero, V.V. and Felippa, C.(1964), "Discussion of paper titled - Ductility of Concrete by Roy, H.E.H. and Sozen, M.A.," *Proceedings of the International Symposium on Flexural Mechanics of Reinforced Concrete, ASCE-ACI, Miami,* November, pp.227-234.

[27] Blaauwendraad, J.(1972), "Realistic Analysis of Reinforced Concrete Framed Structures," *Heron,* Volume 18, No.4, 31pp.

[28] Blaauwendraad, J. and De Groot, A.K.(1983), "Progress in Research on Concrete Plane Frames," *Heron,* Volume 28, No.2, 59 pp.

[29] Borges, J.F. and Arantes E Oliveira, E.R.(1963), "Non-linear Analysis of Reinforced Concrete Structures," *IABSE Publications,* Vol.23, pp.51-69.

[30] Breen, J.E.(1964) "Computer Use in Studies of Frames with Long Columns," *Proceedings International Symposium on the Flexural Mechanics of Reinforced Concrete, Miami, ACI Special Publication SP-12,* pp.535-556.

[31] Breen, J.E. and Ferguson, P.M.(1964), "The Restrained Long Concrete Column as Part of a Rectangular Frame," *ACI Journal,* Vol.61, No.5, May, pp.563-585.

[32] Breen, J.E., Macgregor, J.G. and Pfrang, E.O.(1972), "Determination of Effective Length Factors for Slender Concrete Columns," *ACI Journal,* Vol.69, No.11, November, pp.669-672.

[33] Bridge, R.Q. and Smith, R.G.(1982), "Tension Stiffening Model for Reinforced Concrete Members," *Australasian Conference on the Mechanics*

of Structures and Materials, University of New South Wales, August, pp.4-1,4-6.

[34] Broms, B and Viest, I. M.(1958), "Ultimate Strength of Long Hinged Reinforced Concrete Columns," *Journal of the Structural Division, ASCE, Vol.84, No.ST1, Proc. Paper 1510,* January.

[35] Bull, F.B. and Sved, G.(1965), *Moment Distribution in Theory and Pratice,* Pergamon Press, United Kingdom.

[36] Burnett, R.F.P and Yu C.W.(1964), "Reinforced Concrete Linear Structures At Ultimate Load," *Proc. Int. Symp. on the Flexural Mechanics of Reinforced Concrete, Miami, ACI Special Publication SP-12,* pp.29-52.

[37] Burns, N.H. and Siess, C.P.(1966), "Plastic Hinging in Reinforced Concrete," *Journal of the Structural Division, ASCE,* Vol.92, No.ST5, October, pp.45-64.

[38] CEB-FIP(1970), *International Recommendations for the Design and Construction of Concrete Structures, Principles and Recommendations,* FIP Sixth Congress, Prague, June.

[39] Chajes, A. and Churchill, J.E.(1987), "Nonlinear Frame Analysis by Finite Element Methods," *Journal of Structural Engineering,* ASCE, Vol.113, No.6, June, pp.1221-1235.

[40] Chan, W.W.L.(1955), "The Ultimate Strength and Deformation of Plastic Hinges in Reinforced Concrete Frameworks," *Magazine of Concrete Research,* Vol.7, No.21, November, pp.121-132.

[41] Chang, W.F.(1967), "Inelastic Buckling and Sidesway of Concrete Frames," *Journal of the Structural Division,* ASCE, Vol.93, No.ST2, April, pp.287-300.

[42] Cheung, Y.K. and Yeo, M.F.(1979), *A Practical Introduction to Finite Element Analysis,* Pitman, London, 188 pp.

[43] Clark, L.A. and Spiers, D.M.(1978) "Tension Stiffneing in Reinforced Concrete Beams and Slabs under Short Term Load," *Technical Report 42-521, Cement & Concrete Association, London,* July, 19 pp.

[44] Cohn, M.Z.(1968), "Limit Design of Reinforced Concrete Frames," *Journal of the Structural Division, ASCE,* Vol.94, ST10, October, pp.2467-2483.

[45] Cohn, M.Z.(1979), "Inelasticity of Reinforced Concrete and Structural Standards," *Journal of the Structural Division,* ASCE, Vol.105, No.ST11, November, pp.2221-2241.

[46] Cohn, M.Z.(1964), "Rotation Compatibility in the Limit Design of Reinforced Concrete Continuous Beams," *Proceedings Int. Symp. on the Flexural Mechanics of Reinforced Concrete, Miami, ACI Special Publication SP-12,* pp.359-382.

[47] Cohn, M.Z. and Ghosh, S.K.(1972), "The Flexural Ductility of Reinforced Concrete Sections," *IABSE Publications,* Vol. 32, Part II, Zurich , pp.53-83.

[48] Cohn, M.Z. and Petcu, V.A.(1963), "Moment Redistribution and Rotation Capacity of Plastic Hinges in Redundant Reinforced Concrete Beams," *Indian Concrete Journal,* Vol. 37, No.8, August, pp.282-290.

[49] Colville, James(1975), "Slenderness Effects in Reinforced Concrete Square Columns," *ACI Special Publication SP-50,* Detriot, pp.165-191.

[50] Committee ICE(1962), "Reply to Discussion on 'Ultimate load Design of Concrete Structure'," *Proc. Inst. Civil Engrs (London),* Vol.23, October, pp.532-537.

[51] Connor, J.J., Logcher, R.D. and Chan, S.C.(1968), "Nonlinear Analysis of Elastic Frame Structures," *Journal of the Structural Division, ASCE,* Vol.94, No.ST6, June, pp.1525-1547.

[52] Corley, W.G.(1966), "Rotational Capacity of Reinforced Concrete Beams," *Journal of the Structural Division, ASCE,* Vol.92, No.ST5, October, pp.121-146.

[53] Corley, W.G. and Sozen, M.A.(1966), "Time-dependent Deflections of reinforced Concrete Beams," *ACI Journal,* Vol.63, March, pp.373-385.

[54] Corradi, L., De Donato, O. and Maier, G.(1974), "Inelastic Analysis of Reinforced Concrete Frames," *Journal of the Structural Division, ASCE,* Vol.100, No.ST9, September, pp.1925-1942.

[55] Council on Tall Buildings & Urban Habitat (1978), *Structural Design of Tall Concrete and Masonry Buildings, ASCE,* Vol.CB of the Monograph on Planning and Design of Tall Building, 938 pp.

[56] Cranston, W.B.(1965a), "A Computer Method for Inelastic Analysis of Plane Frames," *Technical Report TRA 386, Cement and Concrete Association, London,* March, 38pp.

[57] Cranston, W.B.(1965b), "Tests on Reinforced Concrete Frames 1: Pinned Portal Frames," *Technical Report TRA 392, Cement and Concrete Association, London,* August, 38 pp.

[58] Cranston, W.B. and Cracknell, J.A.(1969), "Tests on Reinforced Concrete Frames 2: Portal Frames with Fixed Feet," *Technical Report TRA 420, Cement and Concrete Association, London,* December 35 pp.

[59] Crawley, D.B., Sved, G. and Warner, R.F.(1987) "Structural Design Aspects for Very High Strength Concrete," *XIII Biennial Conference, Brisbane, Concrete Institute of Australia,* May.

[60] Crisfield, M.A.(1980) "The Automatic Non-Linear Analysis of Stiffened Plates and Shallow Shells Using Finite Elements," *Proc. Instn Civil Engrs (London), Vol.69, Part 2,* December, pp.891-909.

[61] Crisfield, M.A.(1981) "A Fast Incremental/iterative Solution Procedure that Handles 'Snap Through'," *Computers and Structures,* Vol.13, pp.55-62.

[62] Crisfield, M.A.(1983), "An Arc-Length Method Including Line Searches and Accelerations," *International Journal for Numerical Methods in Engineering,* Vol.19, pp.1269-1289.

[63] Crisfield, M.A.(1986), "Snap-Through and Snap-Back Response in Concrete Structures and the Dangers of Under-Integration," *International Journal for Numerical Methods in Engineering,* Vol.22, pp.751-767.

[64] Darvall, P.LeP.(1983), "Critical Softening of Hinges in Indeterminate Beams and Portal Frames," *Civil Engineering Transactions, Inst. Engrs Aust.,* Vol.CE25 , No.3 , pp.199-210.

[65] Darvall, P.LeP.(1984) "Critical Softening of Hinges in Portal Frames," *Journal of the Structural Division, ASCE,* Vol.110, No.ST1, January, pp.157-162.

[66] Darvall, P.LeP. and Mendis, P.A.(1985), "Elastic-Plastic-Softening Analysis of Plane Frames," *Journal of Structural Engineering, ASCE,* Vol.111, No.4, April, pp.871-888.

[67] Desayi, P. and Krishnan, S.(1964), "Equation for Stress-Strain Curve of Concrete," *ACI Journal,* Vol.61, No.3, March, pp.345-350.

[68] Duncan, W. and Johnarry, T.(1979), "Further Studies on the Constant Stiffness Method of Non-linear Analysis of Concrete Structures," *Proc. Instn Civil Engrs (London),* Part 2, Vol.67, December, pp.951-969.

[69] Ehsani, M.R.(1987), "Discussion of Paper Titled -Evaluation of Approximate Slenderness Procedures for Nonlinear Analysis of Concrete Frames by M.A. Diaz and J.M. Roesset," *ACI Structural Journal,* January-February, pp.111.

[70] Ehsani, M.R. and Alameddine, F.(1987), "Refined Stiffness of Slender Circular Reinforced Concrete Columns," *ACI Structural Journal,* Vol.84, No.5, Sept.-Oct., pp.419-427.

[71] Espion, B.(1986), "Nonlinear Analysis of Framed Structures with a Plasticity Minded Beam Element," *Computers and Structures,* Vol.22, No.5, pp.831-839.

[72] Ferguson. P.M. and Breen, J.E.(1966), "Investigation of the Long Concrete Column in a Frame Subjected to Lateral Loads," *Symposium on Reinforced Concrete Columns, ACI Special Publication SP-13,* Detroit, Michigan, pp.75-119.

[73] Fey, T. (1966) "Approximate Second-order Analysis of Reiniforced Concrete Frames," *Bauingenieur,* June.

[74] Frish-Fay, R.(1962) *Flexible Bars,* Butterworths, London, pp.35-40.

[75] Ford, J.S., Chang, D.C. and Breen, J.E.(1981), "Behaviour of Concrete Columns under Controlled Lateral Deformation," *ACI Journal,* Vol.78, No.1, January - February, pp.3-20.

[76] Furlong, R.W. and Ferguson, P.M.(1966), "Tests of Frames with Columns in Single Curvature," *Symposium on Reinforced Concrete Columns, ACI Special Publication SP-13, Detroit, Michigan,* , pp.55-73.

[77] Gerlein, M.A. and Beaufait, F.W.(1979), "Nonlinear Analysis of Reinforced Concrete Frames," *CSCE-ASCE-ACI-CEB International Symposium on Nonlinear Design of Concrete Structures, Univ. of Waterloo, Ontario, Canada,* August, pp.173-193.

[78] Ghoneim, G.A.M., and Ghali, A.(1982), "Nonlinear Analysis of Concrete Structures," *Canadian Journal of Civil Engineering,* Vol.9, No.3, September, pp.489-501.

[79] Ghosh, S.K. and Cohn, M.Z.(1972), "Non-linear Analysis of Strain-softening Structures," *Symposium on Inelasticity and Non-linearity in Concrete Structure, University of Waterloo,* January-June, pp.315-332.

[80] Ghosh, S.K. and Cohn, M.Z.(1974), "Computer Analysis of Reinforced Concrete Sections Under Combined Bending and Compression," *Publication, IABSE,* Volume 34-I, pp.71-94.

[81] Ghosh, S.K.(1977), "Analysis of Concrete Structures Allowing for Strain-Softening," *Indian Concrete Journal,* Vol.51, No.4, April , pp.108-116.

[82] Gilbert, R.I. and Warner, R.F.(1978a), "Time-dependent Behaviour of Reinforced Concrete Slabs" *IABSE Proceedings, p-12/78,* Feburary

[83] Gilbert, R.I. and Warner, R.F.(1978b), "Tension Stiffening in Reinforced Concrete Slabs" *Journal of Structural Engineering,ASCE,* Vol.104, No.ST12, pp.1885-1900.

[84] Goto, Y.(1971), "Cracks formed in Concrete around Deformed Tension Bars," *ACI Journal,* Vol. 68, No. 4, April, pp.244-251.

[85] Goto, Y. and Chen, W.F.(1987), "Second-Order Elastic Analysis for Frame Design," *Journal of Structural Engineering,ASCE,* Vol.113, No.ST7, July, pp.1501-1519.

[86] Gouwens, A.J.(1985), "Simplified Design of Slender Unbraced Columns," *ACI Special Publication No. SP-97 on Analysis and Design of High-Rise Concrete Buildings.*

[87] Gunnin, B.L., Rad, F.N. and Furlong, R.W.(1977), "A General Nonlinear Analysis of Concrete Structures and Comparison with Frame Tests," *Computers and Structures,* Vol.7, pp.257-265.

[88] Gupta, B.K. and Edwards, A.D.(1972), "Moment-Curvature Characteristics of Prestressed Concrete Sections," *Magazine of Concrete Research,* Vol.24, No.81, December, pp.219-230.

[89] Haisler, W.E., Stricklin, J.A. and Key, J.E.(1977), "Displacement Incrementation in Non-linear Structural Analysis by the Self-Correcting Method," *International Journal for Numerical Methods in Engineering,* Vol.11, pp.3-10.

[90] Hall, A.S. and Kabaila, A.P.(1977) "Basic Concepts of Structural Analysis," *Pitman, London.*

[91] Harrison, H.B.(1976), "Interactive Nonlinear Structural Analysis," *Journal of the Structural Division,* ASCE, Vol. 102, No.ST 7, July, pp.1353-1364.

[92] Hays, C.O. and Matlock, H.(1973), "Nonlinear Discrete Element Analysis of Frames," *Journal of the Structural Division,* ASCE, Vol. 99, No.ST 10, October , pp. 2011-2030.

[93] Hays, C.O. and Santhanam, T.K.(1978), "Inelastic Section Response by Tangent Stiffness," *Conference on Computing in Civil Engineering,* Georgia, ASCE, June, pp.594-610.

[94] Hobbs, R.E. and Jowharzadeh, A.M.(1978), "An Incremental Analysis of Beam Columns and Frames Including Finite Deformations and Bilinear Elasticity," *Computers and Structures,* Vol.9, pp.323-330.

[95] Hognested, E.(1951), "A Study of Combined and Axial Load in Reinforced Concrete Members," *Bulletin Series No.399, University of Illinois, Engineering Experimental Station,* November, 128 pp.

[96] Hsu, C.T., Mirza, M.S. and Sea, C.S.S.(1981), "Nonlinear Analysis of Reinforced Concrete Frames," *Computers and Structures,* Vol. 13, pp.223-227.

[97] I.C.E. Research Committee(1962), "Ultimate Load Design of Concrete Structures," *Proc. I.C.E. (London),* Vol.21, No.2, February, pp 399-442.

[98] Iqbal, M. and Hatchar, D.S.(1975), "Post-Crushing Behaviour of Unbound Concrete Beams," *Journal of the Structural Division, ASCE,* Vol.101, No.ST11, November, pp.2303-2316.

[99] Jennings, A.(1968), "Frame Analysis Including Change of Geometry," *Journal of the Structural Division, ASCE,* Vol.94, No.ST3, March, pp.627-644.

[100] Kang, Y.J. and Scordelis, A.C.(1980), "Nonlinear Analysis of Prestressed Concrete Frames," *Journal of the Structural Division, ASCE,* Vol.106, No.ST2, February, pp.445-462.

[101] Kassimali, A.(1983), "Large Deformation Analysis of Elastic-Plastic Frames," *Journal of the Structural Division, ASCE,* Vol.109, NO.ST8, August , pp.1869-1886.

[102] Kayal, S.(1984), "Finite Element Analysis of RC Frames," *Journal of Structural Division, ASCE,* Vol. 110, No.12, December, pp.2891-2908.

[103] Kgoboko, K.(1987), "Collapse Behaviour of Non-ductile Partially Prestressed Concrete Bridge Girders," *M.Eng.Sc. Thesis, University of Adelaide,* November, 338 pp.

[104] Kgoboko, K., Wyche, P.J. and Warner, R.F.(1988), "Collapse Behaviour and Ductility Requirements in Partially Prestressed Concrete Bridge Girders," *Research Report No.R79, Department of Civil Engineering, University of Adelaide,* March, 12pp.

[105] Kopal, Z.(1978), *Numerical Analysis*, McGraw-Hill, London.

[106] Kroenke, W.C., Gutzwiller, M.J. and Lee, R.H.(1973), "Finite Element for Reinforced Concrete Frame Study," *Journal of the Structural Division, ASCE,* Vol.99, No.ST7, July, pp.1371-1390.

[107] Kulicki, J.M. and Kostem, C.N.(1974), "Inelastic Analysis of Reinforced Concrete Beam Columns," *IABSE Symposium on the Design and Safety of Reinforced Concrete Compression Members, Quebec,* pp.71-78.

[108] Lai, R.K.L. and Warner, R.F.(1973), "Non-linear Time-varying Behaviout of Reinforced Concrete Structures," *4th Australasian Conference on the Mechanics of Structures and Materials,* Queenland, 22-22, August.

[109] Lai, K.L. and Warner, R.F.(1978), "Shrinkage and Creep in Indeterminate Structures," *Douglas McHenry International Symposium on Concrete and Concrete Structures, ACI Special Publication SP-55,* , pp.305-320.

[110] Lai, S.A. and Macgregor, J.G.(1983), "Geometric Nonlinearities in Unbraced Multistorey Frames," *Journal of Structural Engineering,* Vol. 109, No.11, Nov. , pp.2528-2545.

[111] Lai, S.A., Macgregor, J.G. and Hellesland, J.,(1983), "Geometric Nonlinearities in Nonsway Frames," *Journal of Structural Engineering, ASCE.* Vol.109, No.12, December , pp.2770-2785.

[112] Lazaro, A.L., III, and Richards, R.,Jr(1973), "Full-Range Analysis of Concrete Frames," *Journal of the Structural Division, ASCE,* Vol.99, No. ST8, August , pp.1761-1783.

[113] Lee, S.L., Manual, S.M. and Rossow, E.C.(1968), "Large Deflections and Stability of Elastic Frames", *Journal of the Enginnering Mechanics Division, ASCE,* Vol.94, No.EM2, April, 1968, pp.521-547.

[114] Liebenberg, A.C.(1962), "A Stress-strain Function for Concrete Subjected to Short-term Loading," *Magazine of Concrete Research,* Vol.14, No.41, July, pp.85-99.

[115] Lin, C.S. and Scordelis, A.C.(1975), "Nonlinear Analysis of RC Shells of General Form," *Journal of the Structural Division, ASCE,* Vol.101, No. ST3, March, pp.523-538.

[116] Livesley, R.K. (1975) *Matrix Methods of Structural Analysis,* 2nd Edition, Pergamon Press.

[117] Livesley, R.K. and Chandler, D.B.(1956), *Stability Functions for Structural Frameworks,* Manchester University Press.

[118] Macchi G.(1964), "Elastic Distribution of Moments on Continuous Beams," *Proceedings of the International Symp. on Flexural Mechanics of Reinforced Concrete, Miami, ACI Special Publication SP-12,* November, pp.237-257.

[119] Macchi, G.(1979), "Nonlinear Analysis and Design in the CEB Model Code," *CSCE-ASCE-ACI-CEB Int. Symp. on Nonlinear Design of Concrete Structures, Univ. of Waterloo, Ontario, Canada,* August , pp.293-302.

[120] Macgregor, J.G.(1972), "Stability of Reinforced Concrete Concrete Building Frames," *State-of-Art Report 1, Technical Committee 23, ASCE-IABSE International Conference on Tall Buildings, Lehigh University, Bethlehem, Pennsylvania,* August, pp.19-35.

[121] Macgregor, J.G. and Barter, S.L.(1966), "Long Eccentrically Loaded Concrete Columns Bent in Double Curvature," *Symposium on Reinforced Concrete Columns, ACI Special Publication SP-13, Detroit, Michigan,* , pp.139-156.

[122] Macgregor, J.G., Breen, J.E. and Prang, E.O.(1970), "Design of Slender Concrete Column,", ACI Journal, January, pp.6-28.

[123] Macgregor, J.G. and Hage, S.E.(1977), "Stability Analysis and Design of Concrete Frames," *Journal of the Structural Division, ASCE,* Vol.103, No.ST10, October , pp.1953-1970.

[124] Macgregor, J.G., Oelhafen, U.H. and Hage, S.E.(1975), "A Re-Examination of the EI Value for Slender Columns," *ACI Special Publication SP-50,* Detriot, USA.

[125] Massett, D.A. and Stricklin, J.A.(1971), "Self-Correcting Incremental Approach in Nonlinear Structural Mechanics," *AIAA Journal,* Vol.9, No.12, December, pp.2464-2466.

[126] Mattiasson, K.(1981), "Numerical Results from Large Deflection Beam and Frame Problems Analysed by means of elliptic Integrals," *International Journal of Numerical Methods in Engineering,* Vol.16, pp.145-153.

[127] Mattock, A.H.(1967), "Discussion of Paper Titled - Rotational Capacity of Reinforced Concrete Beams by W.G. Corley," *Journal of the Structural Division, ASCE,* Vol.93, No.ST2, April, pp.519-522.

[128] McAdie, R.L., Resende, L. and Martin, J.B.(1987), "Nonlinear Stability Analysis of Framed Structures by Finite Elements," *The Civil Engineer in South Africa,* May, pp.165-174.

[129] Meek, J.L. and Tan, H.S.(1983), "Large Deflection and Post-Buckling Analysis of Two and Three Dimensional Elastic Spatial Frames," *Research Report No.CE49, University of Queensland,* December, 62 pp.

[130] Mendis, P.A.(1986), "Softening of Reinforced Concrete Structures" *Ph.D. Thesis, Monash University,* pp.358.

[131] Mendis, P.A. and Darvall, P.LeP.(1987), "Computer Program for Stability Analysis of Softening Frames," Civil Engineering Research Report, No.3/1987, Monash University, 35 pp.

[132] Menegotto, M. and Pinto, P.E.(1973), "Method of Analysis for Cyclically Loaded R.C. Frames Including Changes in Geometry and Non-elastic Behaviour of Elements Under Combined Normal Force and bending" *IABSE Reports,* Vol. 13, pp.15-21.

[133] Menegotto, M. and Pinto, P.E.(1974), "Exact Analysis of Reinforced Concrete Building Frames," *Technical Report, Ist. Scienza e Tecnica d. Costruzioni - Univ. of Rome Rep.,* n41, March, 18pp.

[134] Menn, C.(1974), "Symposium on Design and Safety of Reinforced Concrete Compression Members," *IABSE, Quebec.*

[135] Meyer, C. and Bathe, K.(1982), "Nonlinear Analysis of Reinforced Concrete Structures in Practice," *Journal of The Structural Division, ASCE,* Vol.108, No.ST7, July.

[136] Mirza, M.S. and McCutcheon, J.O.(1974), "Effect of Axial Compression on Flexural Hinge Rotation Capacity," *IABSE Symposium on the Design and Safety of Reinforced Concrete Compression Members, Quebec* pp.255-265.

[137] Mohr, G.A. and Milner, H.R.(1981), "Finite Element Analysis of Large Displacements in Flexural Systems," *Computers and Structures,* Vol.13, pp.533-536.

[138] Monnier, Th.(1970), "The Moment Curvature Relation of Reinforced Concrete," *Heron,* Volume 17, No.2, 101pp.

[139] Nahnas, U. and Yu, C.W.(1972), "The Elastic-Plastic Design of Reinforced Concrete Sway Frames Against Instability," *Proc. Instn Civil Engrs (London),* Vol.53, Part 2, June, pp.41-56.

[140] Noor, F.A.(1976), "Inelastic Behaviour of Reinforced Concrete Frames," *Magazine of Concrete Research,* Vol. 28, No.97, December, pp.209-224.

[141] Oran, C.(1973), "Tangent Stiffness in Plane Frames," *Journal of the Structural Division, ACSE,* Vol.99, No.ST6, June, pp.973-985.

[142] Oran. C. and Kassimali, A.(1976) "Large Deformations of Framed Structures under Static and Dynamic Loads," *International Journal of Computers and Structures,* Vol.6, Dec., pp.539-547.

[143] Oelhafen, Urs.H.(1974), "Accuracy of Simple Design Procedures for Concrete Columns," *IABSE Symposium on The Design and Safety of Reinforced Concrete Compression Member, Quebec,* pp.93-115.

[144] Pagay, S.N., Ferguson, P.M. and Breen, J.E.(1970), "Importance of Beam Properties on Concrete Column Behaviour," *ACI Journal,* October, pp.808-815.

[145] Park, R. Priestly, M.J.N. and Gill, W.D.(1982), "Ductility of Square-Confined Concrete Columns," *Journal of the Structural Division, ASCE,* Vol.108, No.ST4, April, pp.929-950.

[146] Park, R. and Sampson, R.A.(1972), "Ductility of Reinforced Concrete Sections in Seismic Design," *ACI Journal, Proceedings,* Vol.69, No.9, September, pp.543-550.

[147] Parme, A.L.(1966) "Capacity of Restrained Eccentrically Loaded Long Columns," *ACI Special Publication SP-13,* pp.355-360.

[148] Pfrang, E.O., Siess, C.P. and Sozen, M.A.(1964), "Load-Moment-Curvature Chracteristic of Reinforced Concrete Cross Sections," *ACI Journal,* Vol.61, No.7, July , pp.763-778.

[149] Pozzo, E.(1987), "The Influence of Axial Load and Rate of Loading on Experimental Post-Elastic Behaviour and Ductility of Reinforced Concrete Members," *Materials and Structures,* Vol.20, No. 118, July, pp.303-314.

[150] Przemieniecki, J.S.(1968), "Theory of Matrix Structural Analysis," *Dover Publications, Inc., New York,* 468pp.

[151] Ramu, P., Grenacher, M., Baumann, M., and Thürlimann, B.(1969), "Versuche an Gelenkig Gelagerten Stahbetonstützen unter Dauerlast" *Intitut für Baustatic, ETH, Zürich,* Bericht Nr. 6418-1, Mai (Tests on Pin-ended Columns under Sustained Load).

[152] Ramm, E.(1981), "Strategies for Tracing the Nonlinear Response Near Limit Points," *Nonlinear Finite Element Analysis in Structural Mechanics, editors: Wunderlich, W., Stein, E. and Bathe, K.J.*, Springer-Verlag, Berlin, pp.63-69.

[153] Richard, R, Jr. and Lazaro, A.L, III(1971), "Limit Analysis of a Reinforced Concrete Frame," *ACI Journal,* October, pp.748-755.

[154] Riks, E.(1979), "An Incremental Approach to the Solution of Snapping and Buckling Porblems," *International Journal of Solids and Structures,* Vol.15, pp.529-551.

[155] Rosenblueth, E.(1965), "Slenderness Effects in Building," *Journal of the Structural Division, ASCE,* Vol.91, No.ST1, February, pp.229-252.

[156] Rossi, M. and Bazzi, G.(1981), "Two Simple Reinforced Concrete Beam Elements for Static and Dynamic Analysis," *Inst. fur Baustatik und Konstruktion,* Bericht Nr.118, ETH, Zurich, Oktober, pp.377-392.

[157] Roy, H.E.H. and Sozen, M.A.(1964), "Ductility of Concrete," *Proceedings of International Symposium on the Flexural Mechanics of Reinforced Concrete, Miami, ACI Special Publication SP-12,* pp.213-235.

[158] Rüsch, H.(1960), "Researches Toward a General Flexural Theory for Structural Concrete," *ACI Journal,* Volume 57, No.1, July, pp.1-28.

[159] Saafan, S.A. and Brotton, D.M.(1962), "Elastic Finite Deflection Analysis of Finite Frameworks by Digital Computer," *Symposium on the Use of Computers in Civil Engineering,*.

[160] Sawyer, H.A.(1964), "Design of Concrete for Two Failure Stages," *Proceedings of International Symposium on the flexural Mechanics of Reinforced Concrete, Miami, ACI Special Publication SP-12,* pp.405-437.

[161] Sawyer, H.A. and Stephen, J.E.(1957), "Under-Reinforced Concrete Beams Under Long-Term Loads," *ACI Journal,* Vol.54, July, pp.21-30.

[162] Scanlon, A. and Murray, D.W.(1974), "Time-Dependent Reinforced Concrete Slab Deflections," *Journal of the Structural Division, ASCE,* Vol.100, No.ST9, September, pp.1911-1925.

[163] Scordelis, A. C.(1984), "Computer Models for Nonlinear Analysis of Reinforced and Prestressed Concrete Structures," *PCI Journal,* Vol.29, No.6, November-December, pp.116-132.

[164] Shah, S.P. and Rangan, B.V.(1970), "Effects of Reinforcements on Ductility of Concrete," *Journal of the Structural Division, ASCE,* Vol.96, No.ST6, June, pp.1167-1184.

[165] Smith, R.G. and Bridge, R.Q.(1984), "Slender Braced Reinforced and Prestressed Concrete Columns- a Comparative Study," *Research Report No.R472, School of Civil and Mining Engineering, University of Sydney,* April, 15pp.

[166] Smith, G.M. and Young, L.E.(1956), "Ultimate Flexural Analysis Based on Stress-Strain Curve of Cylinders," *ACI Journal,* Vol.28, No.6, December, pp.597-609.

[167] Somes, N.F.(1966), "Moment Rotation Characteristics of Prestressed Concrete Members. Stage 1 : Rectangular Sections," *Technical Report TRA/398, Cement & Concrete Association,* September, 80pp.

[168] Stevens, L.K.(1967), "Elastic Stability of Practical Multi-Storey Frames," *Proceedings, Institution of Civil Engineers,* Vol.36, pp.99-117.

[169] Stockl, S.(1964), "Discussion of paper titled - Ductility of Concrete by Roy, H.E.H. and Sozen, M.A.", *Proceedings of the International Symposium on Flexural Mechanics of Reinforced Concrete, ASCE-ACI, Miami,* November, pp.225-227.

[170] Stricklin, J.A., Haisler, W.E. and Von Riesemann, W.A.(1973), "Evaluation of Solution Procedures for Material and/or Geometrically Nonlinear Structural Analysis," *AIAA Journal,* Vol.11, No.3, March , pp.292-299.

[171] Sved, G.(1988) "A Non-iterative Solution of the Axial Force-Moment-Curvature Problem for Rectangular Reinforced Concrete Sections," *11th Australasian Conference on the Mechanics of Structures and Materials, University of Auckland,* pp.105-107.

[172] Tse, David and Darvall, P. LeP.(1986), "Analysis of Reinforced Concrete Frames With Four Stage Behaviour," *10th Australasian Conference on the Mechanics of Structures and Materials," University of Adelaide,* pp.81-85.

[173] Vecchio, F.J.(1987) "Nonlinear Analysis of Reinforced Concrete Frames Subjected to Thermal and Mechanical Loads",*ACI Structural Journal,* November-December, pp.492-501.

[174] Virdi, K.S.(1977) "A New Technique for Moment-Thrust-Curvature Calculations for Columns in Biaxial Bending",*Sixth Australasian Conference on Mechanics of Structures and Materials*, University of Canterbury, New Zealand, pp.307-313.

[175] Virdi, K.S. and Dowling, P.J.(1976), "The Ultimate Strength of Biaxially Retrained Columns," *Proc. Instn Civil Engrs (London),* Vol.61, Part 2, Mar, pp.41-58.

[176] Warner, R.F.(1975), "Segmental Analysis for Non-linear Concrete Frames," *Fifth Australasian Conference on Mechanics of Structures and Materials, University of Melbourne,* pp.535-548.

[177] Warner, R.F.(1969), "Biaxial Moment Thrust Curvature Relations," *Journal of the Structural Division, ASCE,* Vol ,No.ST56, pp.923-940.

[178] Warner, R.F.(1984), "Computer Simulation of the Collapse Behaviour of Concrete Structures with Limited Ductility," *Proceedings, Int. Conf. on Computer Aided Analysis and Design of Concrete Structure, Ed. Damjanic et al, Part II, Pine Ridge Press, Swansea, U.K.,* September, pp.1257-1270.

[179] Warner, R.F. and Lambert, J.H.(1974), "Moment-Curvature-Time Relations for Reinforced Concrete Beams," *IABSE Publication,* Vol. 34-I, Zürich, pp.181-203.

[180] Warner, R.F., Rangan, B.V. and Hall, A.S.(1982), *Reinforced Concrete,* 2nd Edition, Pitman, 477pp.

[181] Warner, R.F., Rangan, B.V. and Hall, A.S.(1989), *Reinforced Concrete,* 3nd Edition, Pitman, 553pp.

[182] Warner, R.F. and Yeo, M.F.(1984a), "Collapse Behaviour of Concrete Structures with Limited Ductility," *Research Report No.R61, Department of Civil Engineering, Univ. of Adelaide,* January, 23pp.

[183] Warner, R.F. and Yeo, M.F.(1984b), "Ductility Requirements for Partially Prestressed Concrete ," *Proceedings of the NATO Advanced Research Workshop on ' Partially Prestressing, From Theory to Practice', Paris, France,* June, pp.315-326.

[184] Warner, R.F. and Yeo, M.F.(1984c), "Discussion of Paper Titled - Critical Softening of Hinges in Indeterminate Beams and Portal Frames by

P.LeP. Darvall," *Civil Engineering Transactions, Instn Engrs Aust.,* Vol. CE26, No.2, May, pp.148-149.

[185] Wempner, G.A.(1971), "Discrete Approximations Related to Non-linear Theories of Solids," *International Journal of Solids and Structures,* Vol.15, pp.1581-1599.

[186] Winter, G.(1964), "Whither Inelastic Concrete Design?" *Proceedings International Symposium on the Flexerul Mechanics of Reinforced Concrete, Miami, ACI Special Publication SP-12,* pp.581-594.

[187] Wong, K.W., Yeo, M.F. and Warner, R.F.(1987a), "Analysis of Non-linear Structures by Deformation Control," *First National Structural Conference, Melbourne, Instn Engrs Aust.,* August, pp.181-185.

[188] Wong, K.W., Yeo, M.F. and Warner, R.F.(1987b), "Collapse Behaviour of Reinforced Concrete Frames," *Research Report No.78A, Department of Civil Engineering, University of Adelaide,* August, 34pp.

[189] Wong, K.W., Yeo, M.F. and Warner, R.F.(1988a), "Discussion of Paper Titled -Evaluation of Approximate Slenderness Procedures for Nonlinear Analysis of Concrete Frames by M.A. Diaz and J.M. Roesset," *ACI Structural Journal,* January-February, pp.111-115.

[190] Wong, K.W. and Warner, R.F.(1988b), "Analysis and Design of Slender Concrete Frames by Computer," *The Second International Conference on Computer Applications in Concrete*, Singapore Concrete Institute, March 1988, pp.I58-I66.

[191] Wong, K.W., Yeo, M.F. and Warner, R.F.(1988c), "Non-linear Behaviour of Reinforced Concrete Frames," *Civil Engineering Transactions, Instn Engrs Aust.,* Vol.CE30, No.2, July 1988, pp.57-65.

[192] Yang, T.Y. and Saigal, S.(1984), "A Simple Element for Static and Dynamic Response of Beams with Material and Geometric Nonlinearities,"

International Journal for Numerical Methods in Engineering, Vol.20, pp.851-867.

[193] Young, Dana (1973), "Stiffness Matrix for a Beam with an Axial Force," *AIAA Journal,* Vol.11, No.2, February, pp.240-241.

[194] Yu, W.W. and Winter, G.(1960), "Instantaneous and Long-term Deflections of Reinforced Concrete Beams Under Working Loads", *ACI Journal,* Vol.57, No.1, July, pp.29-50.

[195] Zienkiewicz, O.C.(1967), *The Finite Element Method,* McGraw Hill, London.